Spatial and temporal dynamics of biogeochemical processes in the
Fraser River, Canada: A coupled organic-inorganic perspective

by

Britta Marie Voss

B.S., University of Washington, 2009

Submitted in partial fulfillment of the requirements for the degree of

Doctor of Philosophy

at the

MASSACHUSETTS INSTITUTE OF TECHNOLOGY

and the

WOODS HOLE OCEANOGRAPHIC INSTITUTION

September 2014

Author…………………………………………………………………………………………

Department of Earth, Atmospheric, and Planetary Sciences, MIT &

Department of Marine Chemistry and Geochemistry, WHOI

August 25, 2014

Certified by…………………………………………………………………………………

Bernhard Peucker-Ehrenbrink

Thesis Co-Supervisor

Certified by…………………………………………………………………………………

Timothy I. Eglinton

Thesis Co-Supervisor

Accepted by…………………………………………………………………………………...

Elizabeth B. Kujawinski

Chair, Joint Committee for Chemical Oceanography

Spatial and temporal dynamics of biogeochemical processes in the Fraser River, Canada: A coupled organic-inorganic perspective

by

Britta Marie Voss

Submitted to the Department of Marine Chemistry and Geochemistry,
MIT/WHOI Joint Program in Oceanography/Applied Ocean Science and
Engineering on August 25, 2014 in partial fulfillment of the requirements
for the degree of Doctor of Philosophy

ABSTRACT

The great geologic and climatic diversity of the Fraser River basin in southwestern Canada render it an excellent location for understanding biogeochemical cycling of sediments and terrigenous organic carbon in a relatively pristine, large, temperate watershed. Sediments delivered by all tributaries have the potential to reach the ocean due to a lack of main stem lakes or impoundments, a unique feature for a river of its size. This study documents the concentrations of a suite of dissolved and particulate organic and inorganic constituents, which elucidate spatial and temporal variations in chemical weathering (including carbonate weathering in certain areas) as well as organic carbon mobilization, export, and biogeochemical transformation. Radiogenic strontium isotopes are employed as a tracer of sediment provenance based on the wide variation in bedrock age and lithology in the Fraser basin. The influence of sediments derived from the headwaters is detectable at the river mouth, however more downstream sediment sources predominate, particularly during high discharge conditions. Bulk radiocarbon analyses are used to quantify terrestrial storage timescales of organic carbon and distinguish between petrogenic and biospheric organic carbon, which is critical to assessing the role of rivers in long-term atmospheric CO_2 consumption. The estimated terrestrial residence time of biospheric organic carbon in the Fraser basin is 650 years, which is relatively short compared to other larger rivers (Amazon, Ganges-Brahmaputra) in which this assessment has been performed, and is likely related to the limited floodplain storage capacity and non-steady-state post-glacial erosion state of the Fraser River. A large portion of the dissolved inorganic carbon load of the Fraser River (>80%) is estimated to derive from remineralization of dissolved organic carbon, particularly during the annual spring freshet when organic carbon concentrations increase rapidly. This thesis establishes a baseline for carbon cycling in a largely unperturbed modern mid-latitude river system and establishes a framework for future process studies on the mechanisms of organic carbon turnover and organic matter-mineral associations in river systems.

Thesis Supervisors:

Bernhard Peucker-Ehrenbrink
Senior Scientist, WHOI

Timothy Eglinton
Adjunct Scientist, WHOI
Professor, ETH-Zürich

friends. A number of ETH graduate students also made significant analytical contributions to this thesis. Franziska Lechleitner and Stefanie Wirth provided generous guidance with lab techniques and Thomas Blattmann and Bao Rui performed important radiocarbon analyses. Numerous other members of the Biogeoscience group and beyond provided analytical assistance, good humor, and advice in navigating Zürich, including Marilu Tavagna, Alysia Cox, Maarten Lupker, Nora Ernst, Hongyan Bao, Lisa Bröder, Chase LeCroy, Chantal Freymond, Clayton Magill, Björn Buggle, Roland Zech, Lydia Zehnder, and Stewart Bishop. Finally, Kathrin Fehr and Regula Schälchli provided critical logistical support for my ETH visits, and even tolerated my attempts to practice German. I hope that my dreadful American accent is now augmented with a Swiss German twang.

Outreach activities were a rewarding aspect of this project. I thank Kathleen Bertrand and Shannon King at the Fraser River Discovery Centre for making the My River, My Home exhibit a reality. I feel honored to have had the opportunity to participate in this endeavor. This exhibit was also largely based on the photography of Chris Linder, who has created stunning collections of photos and videos of scientists at work on rivers around the world, including the Fraser. I was extremely fortunate to accompany Chris and Bernhard on a flight over the Fraser Valley, provided by LightHawk and flown by volunteer pilot Hunter Handsfield. I also wish to thank journalist Anne Casselman for the opportunity to communicate our Fraser River research to the public. Finally, the Graphics department at WHOI provided tremendous support in helping me produce an article about my research for *Oceanus*. I thank Lonny Lippsett and Chris Reddy for teaching the writing course, Jeffrey Brodeur at Woods Hole Sea Grant for writing guidance, Eric Taylor for producing wonderful animations, and Lonny and Kate Madin for shepherding me through the publication process. Tom Kleindienst in Graphics also provided media support throughout this project.

Countless folks at WHOI and MIT provided administrative support and institutional wisdom for navigating research and the Joint Program. Special thanks to Sheila Clifford, Donna Mortimer, Mary Zawoysky, Mary Murphy, Julia Westwater, Lea Fraser, Tricia Gebbie, Marsha Gomes, Christine Charette, Mark Kurz, Liz Kujawinski, Ronni Schwartz, Ed Boyle, and Kristen Barilaro for all the big and small things you've helped us students with over the years, especially the things I didn't even realize!

I have been extremely fortunate to spend the past five years in the company of some truly wonderful people. To Liz, Kristen, and Amalia, thanks for keeping me sane and well-fed at home for the past four years. Liz in particular has tolerated my sarcasm and unusual tv obsessions, and orchestrated some unforgettable celebrations over the years. Thanks for all the awesome adventures around the Cape (not all of which ended at the ER), and hopefully there are more to come around the world! Jill has been my chemistry compatriot since before day 1, always ready to talk science, fix my bike, or offer a ride home. Meagan is a font of wisdom and a supportive friend. Life in Woods Hole was infinitely better thanks to kayak adventures, homemade pizza, Landfall gossip, quahog stuffing, gardening, almost-cruises, DIY pH indicator experiments, bike

journeys, trailer decorations, golf course sledding, and ridiculous costume parties with Mary, Kalina, Jason, Elise, Liz B, Wilken, Abby, Dan, Alec, Santiago, Kyrstin, Evan, Carly, Marilena, Kim, Karin, Sophie, Sam, and John. Thanks to Jess and Paty for making me feel at home at MIT. To all the amazing folks at Fossil Free MIT, thank you for affirming my faith in humanity, and keep fighting the good fight! And to my friends back home—Helen, Jared, Stephanie, Shannon, and Jessica—memories of spending time with you in Seattle got me through the bleakest points of the New England winters.

Finally, words can't express how important the support of my parents, my sister, and my grandma has been throughout my grad school adventure. Between skype chats and care packages, you always reminded me of the goal at the end of the road and kept me abreast of the goings on in the PNW. Your dedication to education is what got me here, and I can't thank you enough.

for Celia

"All the changes are of no concern to the Fraser. It lives as it has always lived, ignoring man's recent and brief presence, sure of his final departure, ceaselessly expanding its substance from a placid glacial brook to an untamable torrent, moving relentlessly and forever to its destined goal and grave in the distant sea."

—Bruce Hutchinson

CONTENTS

CHAPTER 1. INTRODUCTION

1.1 Biogeochemical cycling in river systems

Rivers bridge elemental cycles in the atmosphere, land plants, and soils through the constant flow of material draining off the continents into the coastal ocean. The geochemical signatures preserved in river-influenced margin sediments can be used to quantify the influence of terrigenous organic carbon (OC) on marine ecosystems and reconstruct past changes in terrestrial climate, vegetation, and continental erosion (Bader, 1956; Hedges and Mann, 1979; Hinrichs and Rullkötter, 1997; Holtvoeth et al., 2003; Schefuß et al., 2003; Pancost and Boot, 2004; Eglinton and Eglinton, 2008; Bianchi and Allison, 2009; Drenzek et al., 2009; Weijers et al., 2009; Ponton et al., 2012; Agrawal et al., 2014; Carpentier et al., 2014; Goodbred et al., 2014). The terrigenous OC associated with river sediments ("particulate organic carbon," POC) is an important transport pathway of atmospheric CO_2 through land plants to marine sediments, where its gradual accumulation over millions of years exerts a control on global climate (Ebelmen, 1845; Chamberlin, 1899; Berner, 1982; Schlünz and Schneider, 2000; Blair et al., 2004; Burdige, 2007; Galy et al., 2007; Kao et al., 2014). Dissolved organic carbon (DOC) from rivers may also persist for centuries in the global ocean, representing another terrestrially derived sink of atmospheric CO_2 (Meyers-Schulte and Hedges, 1986; Opsahl and Benner, 1997; Bauer et al., 2001; Hernes and Benner, 2003; Benner et al., 2005); although the exact fate of terrigenous DOC in the ocean is a matter of ongoing debate (Nelson and Siegel, 2013; Dittmar and Stubbins, 2014). The third major riverine carbon pool is dissolved inorganic carbon (DIC), which in most rivers exists primarily in the form of HCO_3^-. Depending on environmental conditions, DIC in rivers can be produced primarily by chemical weathering (particularly if carbonates are present), exchange with atmospheric CO_2, or respiration by soil and aquatic heterotrophs. There is tremendous variability in the fluxes and relative proportions of each of these three pools in particular rivers globally; however, in total, the annual fluxes from rivers to the ocean are 216 Tg C (POC), 246 Tg C (DOC), and 407 Tg C (DIC) (Tg = 10^{12} g) (Cai, 2011).

Yet before terrigenous OC ever reaches a river mouth, biogeochemical processing through microbial degradation, autotrophic productivity, and photochemical oxidation can significantly alter the OC initially mobilized in soils and headwater streams. Pools of DOC,

POC, and DIC may all exchange with one another to yield geochemical compositions in downstream areas that do not represent source materials upstream. If rivers are to be used as past recorders or present-day integrators of weathering and biogeochemical processes across a river basin, the impacts of such alterations must be understood and, ideally, quantified. Such an understanding requires a holistic approach, incorporating information on physical and chemical weathering, sediment transport, sediment mineralogy, and organic and inorganic carbon composition. Studies spanning organic and inorganic and sedimentary and dissolved geochemical approaches are rare, largely due to traditional disciplinary and analytical divides. Furthermore, appropriate research settings are necessary to answer questions pertaining to *natural* biogeochemical processes, as many river basins are significantly perturbed by anthropogenic activities affecting fluxes of water (Vörösmarty et al., 2010; Grafton et al., 2012), sediment (Vörösmarty et al., 2003; Syvitski et al., 2005; Walling, 2006), nutrients (Boyer et al., 2006; Laruelle et al., 2009), trace elements (Poulton and Raiswell, 2000; Rauch, 2010), radionuclides (Moran et al., 2002; Sansone et al., 2008), and carbon (Stallard, 1998; Raymond et al., 2008; Hossler and Bauer, 2013). While no single field site can satisfy all of these goals, the Fraser River basin in British Columbia has many key features (including limited artificial sediment impoundments, diverse terrain, geology, and climate, and low human population density) that make it a valuable window into natural biogeochemical processes within large temperate river systems.

1.2 Geochemical tools for river biogeochemistry

This study incorporates a range of analytical approaches to characterize riverine material. Each chapter provides a detailed introduction to the techniques used for each study within this project, but the primary methods employed in this thesis are briefly outlined here. One traditional tool for characterizing the chemical composition of rivers is to quantify the relative abundance of dissolved major and trace elements, such as Ca, Mg, Na, K, Sr, Cl, SO_4, and HCO_3. Ratios of these elements can be indicative of the lithologies undergoing chemical weathering, allowing quantification of the relative contributions of carbonate-, silicate-, and evaporite-derived material (e.g. Mackenzie and Garrels, 1966; Reeder et al., 1972; Stallard and Edmond, 1983; Meybeck, 1987; Négrel et al., 1993; Bluth and Kump, 1994; Gíslason et al., 1996; Blum et al., 1998;

Gaillardet et al., 1999; Jacobsen et al., 2002; Dürr et al., 2005; Moon et al., 2014). The relative importance of carbonate versus silicate weathering in a river basin determines the strength of atmospheric CO_2 drawdown by chemical weathering, which can be demonstrated with these simplified weathering reactions:

$$(Ca, Mg)SiO_3 + 2CO_2 + H_2O \longrightarrow Ca^{2+} + SiO_2 + 2HCO_3^- \longrightarrow CaCO_3 + SiO_2 + CO_2 + H_2O$$
$$CaCO_3 + CO_2 + H_2O \longrightarrow Ca^{2+} + 2HCO_3^- \longrightarrow CaCO_3 + CO_2 + H_2O$$
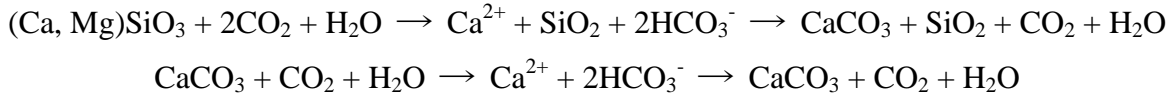
In the first reaction, the primary silicate mineral ($[Ca, Mg]SiO_3$) reacts with 2 moles of atmospheric CO_2, which transforms into dissolved HCO_3 in river water, and may be reprecipitated as $CaCO_3$ by calcareous organisms in the ocean, releasing 1 mole of CO_2. This $CaCO_3$ sinks to marine sediments and may remain buried for millions of years, sequestered in the cycle of crustal recycling and volcanism for hundreds of millions of years before returning to the atmosphere as CO_2. The influence of this process takes a minimum of thousands of years to exert a change in atmospheric CO_2 concentration due to the long residence time of HCO_3 in the global ocean (~3000 years) (François and Goddéris, 1998; Beaulieu et al., 2012). In the second reaction, only 1 mole of atmospheric CO_2 is consumed, hence when $CaCO_3$ is formed in the ocean, the mole of CO_2 returns to the atmosphere and no net draw-down of CO_2 occurs. Distinguishing between these two weathering sources is therefore critical to quantifying the influence of chemical weathering on atmospheric CO_2 cycling and long-term climate changes.

Another method for quantifying the contributions of various weathering sources to the dissolved load of rivers is with radioisotope tracers influenced by the age and composition of rocks. The radiogenic Rb-Sr isotope system is a classic tool used to distinguish rocks on account of the variable Rb/Sr content of different minerals and the age of the rock due to the β^- decay $^{87}Rb \longrightarrow {}^{87}Sr$ (half-life 49.6 Gyr; Rotenberg et al., 2012). In a river basin such as the Fraser, with large variations in bedrock lithology and age, the dissolved $^{87}Sr/^{86}Sr$ composition can be quantitatively exploited to estimate contributions of upstream inputs draining distinct lithologies.

Organic matter in this study has been characterized in terms of its abundance as well as its bulk isotope composition ($\delta^{13}C$, $\Delta^{14}C$) and molecular (POC) or chromophoric (DOC) composition. Bulk $\delta^{13}C$ composition is a useful tracer for identifying OC sources, such as land plant- versus aquatic production-derived OC. In the Fraser basin, where vegetation is composed almost entirely of C_3 plants, plant-derived, or "allochthonous," OC is expected to have $\delta^{13}C$

values of -26 to -28‰; aquatic production, while potentially variable depending on the isotopic composition of dissolved inorganic carbon, is expected to have values of -15 to -25‰ (Deines, 1980). Thus $\delta^{13}C$ values above ~-26‰ may be indicative of contributions from *in situ* production, or "autochthonous" OC. The radiocarbon content of OC is informative of the length of time since carbon was part of the living biosphere (Libby et al., 1949). Since bulk ages of POC are presumably the product of a mixture of components with different ages, bulk ^{14}C content can be used in concert with other properties to quantify specific components. For instance, by calculating the amount of modern OC in a suite of samples, a petrogenic (i.e. ^{14}C-dead) contribution can be estimated, as well as an average age for non-petrogenic OC (Galy et al., 2008; Galy and Eglinton, 2011; Bouchez et al., 2014). As the non-petrogenic component is the portion of POC that, when sequestered in marine sediments, represents a net sink of atmospheric CO_2, this distinction is vital to quantifying the importance of riverine POC flux to long-term global climate cycles.

The molecular composition of POC can be used to distinguish different types of vegetation sources across the river basin. Vegetation biomarkers such as long-chain *n*-alkanes and *n*-alkanoic acids (derived from leaf epicuticular waxes) and branched glycerol dialkyl glycerol tetraethers (produced by soil bacteria) can vary in their distributions depending on environmental factors such as temperature and precipitation, which influence the plant types growing in different areas (e.g. Peterse et al., 2009; Weijers et al., 2009; Luo et al., 2012; Sarkar et al., 2014). Furthermore, these markers are diagnostic of terrigenous OC, so their presence in marine environments can be used to trace terrestrial influence in river-influenced sedimentary deposits (e.g. Hopmans et al., 2004). The ^{14}C content of these individual compounds can also be analyzed in order to probe transport timescales of more refined portions of the POC pool (Galy and Eglinton, 2011; Vonk et al., 2012; Feng et al., 2013).

Due to its macromolecular structure, DOC is less amenable to compound-level characterization than POC; however, bulk optical properties provide a way of comparing structural features of DOC in different samples (Helms et al., 2008). The chromophoric nature of terrigenous DOC results in different absorbance depending on the molecular weight and aromaticity of the structures making up the complex macromolecules within DOC. DOC freshly leached from living plant material is generally higher in molecular weight and aromaticity than DOC which has been subjected to photobleaching or extensive microbial degradation (Spencer et

al., 2009). Hence DOC optical properties provide information about the biogeochemical history of DOC.

Finally, physical characteristics of sediments can influence how OC is mobilized into aquatic systems. The type of bedrock and intensity of weathering determine the grain size and surface area of soil particles. Fine-grained soils and sediments with high specific surface area tend to associate with higher concentrations of OC (Mayer, 1994). Hence, patterns of POC flux may be due in part to variations in the capacity of mineral particles to associate with OC, as opposed to the amount of OC available or microbial degradation. In this study, relationships between grain size and surface area of sediments and OC content and composition are explored to assess the importance of sedimentological controls on POC transport.

A key approach taken in this study is the use of basin-wide samples of numerous tributary inputs and points along the main stem, along with time series observations near the river mouth. The basin-wide samples provide the context of spatial variability across the basin, which is a critical framework for interpreting seasonal changes in the basin-integrated signals near the mouth. Time series sampling is needed to account for seasonal variations due to annual cycles of discharge and water temperature, which influence concentrations of sediment and dissolved weathering products, flowpaths of surface runoff through soils, and biological activity.

1.3 Fraser River basin environmental setting

The main stem of the Fraser River follows a course of approximately 1375 km from its headwaters in Jasper National Park at Fraser Pass in the Canadian Rocky Mountains to the Pacific Ocean (Fig. 1). For the first 500 km, the river flows northwestward through the Rocky Mountain Trench, a fault zone which divides the Rocky Mountains from the Cariboo Mountains and forms the boundary between the Foreland and Omineca belts. Near the city of Prince George, the river enters a flat peneplain region of the Intermontane belt. Here the Fraser receives its second-largest tributary, the Nechako, as it makes its first major bend to flow south. The Nechako River is the first tributary to enter the main stem draining the Coast Range. It is the only tributary of the Fraser bearing a large man-made impoundment, the Kenney Dam, built in 1954 to power the Alcan aluminum smelter 100 km to the west. The Nechako basin also lies in

the heart of the mountain pine beetle outbreak of British Columbia (Safranyik and Wilson, 2006).

Approximately 200 km downstream of Prince George begins the Fraser Canyon. For the remainder of its southward flow, until the city of Hope, the Fraser carves a narrow gorge between the Omineca and Intermontane belts, flowing along the Fraser Fault. Due to the rain shadow effect of the Coast Range, the canyon region is exceptionally dry. Areas in the Fraser Canyon experience some of the hottest, driest summer conditions in Canada with average temperatures >20°C and ~20 mm of rainfall per month. The Thompson River, the largest tributary of the Fraser, draining 55,600 km^2 of the Omineca and Intermontane belts, enters the main stem near the base of the Canyon, 100 km upstream of Hope.

At the city of Hope, the Fraser bends west, breaking through the Coast Range and entering the floodplain of the Fraser Valley for its remaining 130 km route to the ocean. Its last major tributary, the Harrison River, drains the western flank of the Coast Range, a region of temperate rain forest. In contrast to the dry interior, the western Coast Range receives >300 mm per month of precipitation in winter and 70-100 mm per month in summer.

The present configuration of the Fraser River is geologically relatively young. Recent analysis of volcanic dams in the interior plateau reveals that prior to 1.06 Ma, the upper Fraser River averted a substantial portion of the basin downstream of the Fraser Canyon, flowing northward rather than south (Andrews et al., 2012). The reversal to the modern configuration resulted in a massive increase in the delivery of terrigenous sediment to the North American continental shelf, leading to the creation of the deep sea Nitinat Fan (Underwood et al., 2005; Andrews et al., 2012). The temperate rain forest of the Coast Range became established around 9-6.5 ka while the Aleutian Low pressure system dominated over the Pacific High, creating a pattern of relatively cool and wet weather in the region (Hallett et al., 2003). Human habitation in the Fraser basin has existed throughout the postglacial period; European settlement began in the early 19th century following westward expansion of the North American fur trade, and accelerated beginning in 1858, initially spurred by discoveries of gold in the Fraser Canyon and Cariboo regions.

During the retreat of the Late Wisconsinan Cordilleran ice sheet 10-12 ka (Clague and James, 2002; Margold et al., 2013), several glacial lakes formed in the valleys of the Fraser River and its tributaries behind ice dams (Ryder et al., 1991; Johnsen and Brennand, 2004). The

sediment load of the Fraser River continues to be dominated by the ongoing mobilization of these deposits rather than primary denudation (Church and Slaymaker, 1989). The Fraser Valley has accumulated significant amounts of these sediments (Clague et al., 1991; Luternauer et al., 1993), causing consolidation-driven subsidence in the delta region today (Mazzotti et al., 2009).

Since glacial retreat, the Fraser basin has developed several distinct forest ecosystem zones. These zones, codified by the Biogeoclimatic Ecosystem Classification system, are defined by an area's vegetation and soil types and climatic conditions, and are generally named according to the topography and dominant tree or vegetation type (Pojar et al., 1987; Klinka et al., 1991; MacKinnon et al., 1992) (Fig. 2). Diverse soil types (Valentine et al., 1978) developed through weathering of the basin's varied bedrock geology, which ranges from old (>500 Myr) sedimentary rocks, which dominate the Rocky Mountain headwater areas, to young (<100 Myr) volcanic and intrusive rocks, which dominate the Coast Range in the western portion of the basin (Fig. 3). The influence of bedrock source material is modulated by precipitation, which is also extremely variable due to the mountainous topography of the region. The main source of precipitation in the basin is moisture from the North Pacific Ocean (Gimeno et al., 2012); as moisture travels inland, the orographic effect of the Coast Range results in significant precipitation (1500-4000 mm a^{-1}) in the lower portions of the Fraser basin. The interior of the basin between the Coast Range and Rocky Mountains is significantly drier with annual precipitation of <1000 mm, and <300 mm in some areas. A second orographic effect occurs as air masses pass over the Rocky Mountains, and precipitation in the northeastern portion of the basin is ~1000 mm a^{-1}.

Hydrology in the Fraser River is dominated by the annual melting of mountain snowpack in spring (March-June); the associated peak in river discharge is known as the freshet. The spring freshet builds over a period of weeks, tapers off throughout the summer, and is often followed by a secondary fall peak driven by rain storms. In the fall and winter months, baseflow runoff is fed by rainfall and, to some extent, groundwater flow. The influence of snowmelt, rainfall, and groundwater to different tributary basins is variable, with Coast Range tributaries significantly impacted by fall and winter rain events and headwater streams in the Rockies almost exclusively fed by snowmelt, but the spring freshet discharge pulse is a prominent feature of the annual hydrograph in all major tributaries (Fig. 4). Total Fraser River discharge during the spring freshet typically reaches 6,000-10,000 m^3 s^{-1}, versus winter base flow of 800-2,000 m^3 s^{-1}.

The most significant human impacts in the Fraser basin come from industrial activities (mining and forestry) and urban expansion in the Vancouver metropolitan area. The most extensive mining operations exist in the Thompson, Nechako, and Bridge drainage basins, and primarily include excavation for copper, gold, molybdenum, silver, and rare earth elements (Fredericks et al., 2009). Industrial-scale logging has been active in the Fraser basin since the 1960s, and today British Columbia produces over 40% of Canada's total timber volume (Nealis and Peter, 2008). The dominant tree type in the interior forests of the Fraser basin is lodgepole pine (*Pinus contorta* var. *latifolia*), which is highly susceptible to infestation by the mountain pine beetle (*Dendroctonus ponderosae* Hopkins). Higher winter temperatures and the maturation of single-aged pine stands (following logging and re-planting) are key contributors to the recent mountain pine beetle outbreak, which is the most extensive of the 100-year period of record (Taylor and Carroll, 2004). The outbreak, which began in the late 1990s, reached its peak in 2007 with >100,000 km^2 infested across British Columbia (Westfall and Ebata, 2010) (Fig. 5). Given that deforestation is generally associated with increased soil erosion (Syvitski et al., 2005; Gregory, 2006), the loss of significant areas of forest in the Fraser basin to pine beetle attack is likely to increase riverine sediment fluxes in the coming decades.

Direct impacts on the Fraser River due to global warming are likely to cause a shift towards an earlier and weaker spring freshet, with mean summer water temperatures increased by up to 2°C, by the year 2100 (Morrison et al., 2002; Shrestha et al., 2012). Such an increase in water temperature and decrease in late summer discharge are vital threats to the iconic salmon runs of the Fraser basin (Hague et al., 2011; Healey and Bradford, 2011). Changes in air temperature and precipitation will also have impacts on forest ecosystems and vegetation distributions (Carroll et al., 2004; Hamann and Wang, 2006; Woods et al., 2010). Many mountain glaciers of southern British Columbia are already retreating due to rising global air temperatures (Koch et al., 2009; Bolch et al., 2010), and average global temperatures by 2100 are likely to rise an additional 2°C assuming current trends in CO_2 emissions (IPCC, 2013). Therefore, hydrologic effects in the Fraser River due to global warming will likely become increasingly apparent in coming decades.

1.4 Thesis Objectives & Outline

This thesis provides a case study of coupled inorganic and organic tracers of chemical weathering and OC dynamics in a modern river system. Linking the characteristics of terrigenous OC to its associated mineral particles offers unique insight into the sources and geochemical evolution of dissolved and sedimentary material carried by the river. The objectives of this thesis are to (1) establish the OC and mineralogical properties of sediment sources within the Fraser basin; (2) quantify seasonal variability in these signals; and (3) identify evidence of biogeochemical processing of dissolved and sedimentary OC during riverine transport.

Chapter 2 presents a study of seasonal and spatial variability in dissolved inorganic constituents in the Fraser River. Building on the work of Cameron et al. (1995), Cameron (1996), Cameron and Hattori (1997), and Spence and Telmer (2005), this study investigates the lithological controls on major and trace element fluxes from different source regions in the Fraser basin, with an emphasis on dissolved $^{87}Sr/^{86}Sr$ as a tracer of weathering sources. In addition to spatial variations, a two-year time series record of dissolved $^{87}Sr/^{86}Sr$, as well as stable isotopes of water (δD, $\delta^{18}O$) and nutrient concentrations, reveals significant seasonal variations in the relative contributions of different portions of the basin to the total flux of dissolved weathering products. A mixing model, calculating a flux-weighted average $^{87}Sr/^{86}Sr$ based on discharge and $^{87}Sr/^{86}Sr$ composition of the major tributaries, predicts the seasonal cycle of basin-integrated $^{87}Sr/^{86}Sr$ observed in the time series. The model is improved by adding a component to account for discharge not accounted for by the major tributaries, which is assumed to be similar to relatively unradiogenic Coast Range tributaries in $^{87}Sr/^{86}Sr$ composition.

Chapter 3 investigates seasonal and spatial patterns in carbon cycling across the Fraser basin. By comparing the concentrations of DIC, DOC, and POC at different sites and under different flow conditions, the spatial heterogeneity of different components of the total carbon flux become apparent. For instance, the majority of DOC flux originates in the peneplain region of the upper Fraser basin, whereas POC flux is dominated by tributaries draining the central canyon region. In addition, suspended sediments exported during low flow conditions are finer-grained and more OC-rich relative to sediments mobilized during the spring freshet. The ^{14}C content of these sediments indicates that petrogenic OC content varies throughout the basin, likely as a result of the diverse bedrock lithology, affecting both the OC content and weatherability of source materials. The contribution of DOC respiration to DIC concentration is

estimated using major element compositions as an indicator of the influence of carbonate weathering. Using this approach, it is estimated that DOC respiration constitutes the main source of DIC throughout most of the basin, particularly during the spring freshet when DOC concentrations are high. By comparing the OC loading (relative to mineral surface area) of bank sediments with that of suspended sediments, it appears that significant loss of soil OC occurs in some areas before sediments are mobilized into river channels. This study demonstrates the importance of observations across multiple seasons, and the value of a diverse suite of techniques in elucidating the biogeochemical processes driving carbon export in river systems.

Chapter 4 is a detailed investigation of geochemical changes which take place during the early portion of the spring freshet, when discharge increases dramatically as a result of melting snowpack. In advance of the peak water discharge, a pulse of DOC begins as soon as water levels rise to the point where surface soils begin to flush with meltwater. The shift in water sources, from precipitation and groundwater which dominate baseflow runoff to snow and icemelt, is evident in the rapid shift in the stable isotope composition of water. The chemical composition of DOC also changes during this period, with pre-freshet DOC having optical properties indicative of relatively low molecular weight and aromaticity. A full two-year record of DOC concentration and optical properties reveals that throughout the summer, DOC optical properties return to pre-freshet values while DOC concentration declines. A second shift in DOC composition occurs in the fall, likely due to precipitation-driven runoff pulses associated with storm events. Dissolved and particulate Hg dynamics were also investigated in order to determine whether the freshet DOC pulse is associated with a pulse of dissolved Hg, as has been observed in other systems (Dittman et al., 2010; Schuster et al., 2011). The link between dissolved Hg and DOC in the Fraser River is less clear than was anticipated, thus interactions between dissolved and particulate Hg and OC in this basin warrant further study.

Chapter 5 exploits depth profiles of suspended sediments collected under freshet and low discharge conditions to assess seasonal variations in sources of sediment and OC. The large difference in $^{87}Sr/^{86}Sr$ composition of sediments collected during the freshet versus the low flow period demonstrate that sediment provenance is highly dependent on flow regime. The relatively radiogenic composition of low flow sediments appears to be diluted by unradiogenic material, which is derived preferentially from more proximal Coast Range sources. This dilution behavior is also evident in the bulk OC composition, as relatively high concentrations of young OC in low

flow sediments are diluted by old OC in freshet sediments. Using the approach of Galy et al. (2008), these sediments predict a constant petrogenic OC contribution of 0.12 wt% in Fraser River sediments under both freshet and low flow conditions, and an average terrestrial residence time for non-petrogenic OC in the basin of 650 years. In addition, compound-specific ^{14}C analysis of a bank sediment sample which integrates a large portion of the Fraser basin shows a wide range in ages for terrestrial OC (likely due to mixed-age sources of biomarker compounds) and a contribution from significantly pre-aged material. This old (>8000 yr) OC is likely the result of post-glacial mobilization of Holocene sediments in the Pacific Northwest region (Smittenberg et al., 2006).

Chapter 6 synthesizes the conclusions of this work, placing the results obtained in the Fraser basin in a broader context, and proposes future research avenues.
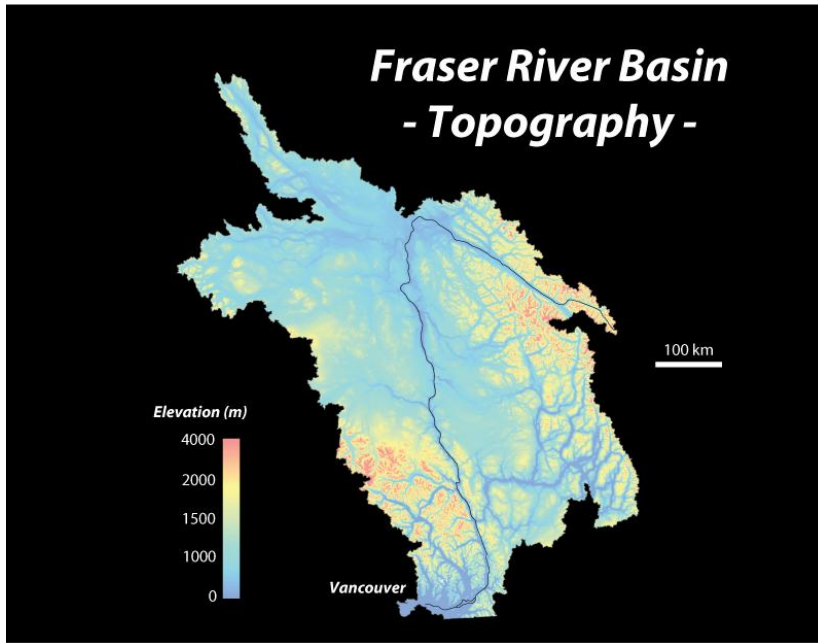
Figure 1. Topographic map of the Fraser River basin (courtesy S. Adam Soule, WHOI).
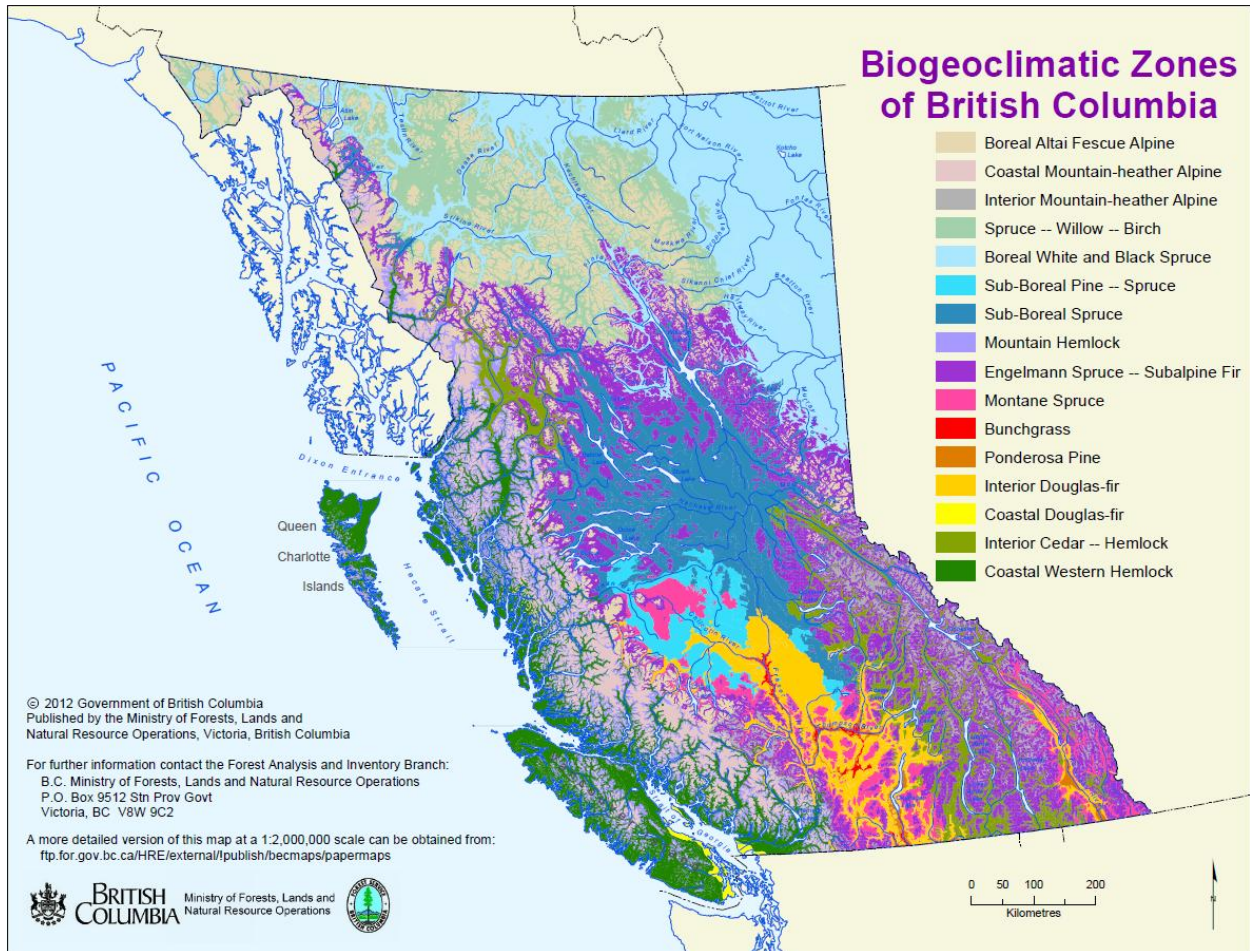
Figure 2. Biogeoclimatic ecosystem classifications of British Columbia (source: British Columbia Ministry of Forests, Lands, and Natural Resource Operations, 2012; http://www.for.gov.bc.ca/hre/resources/maps/index.html).
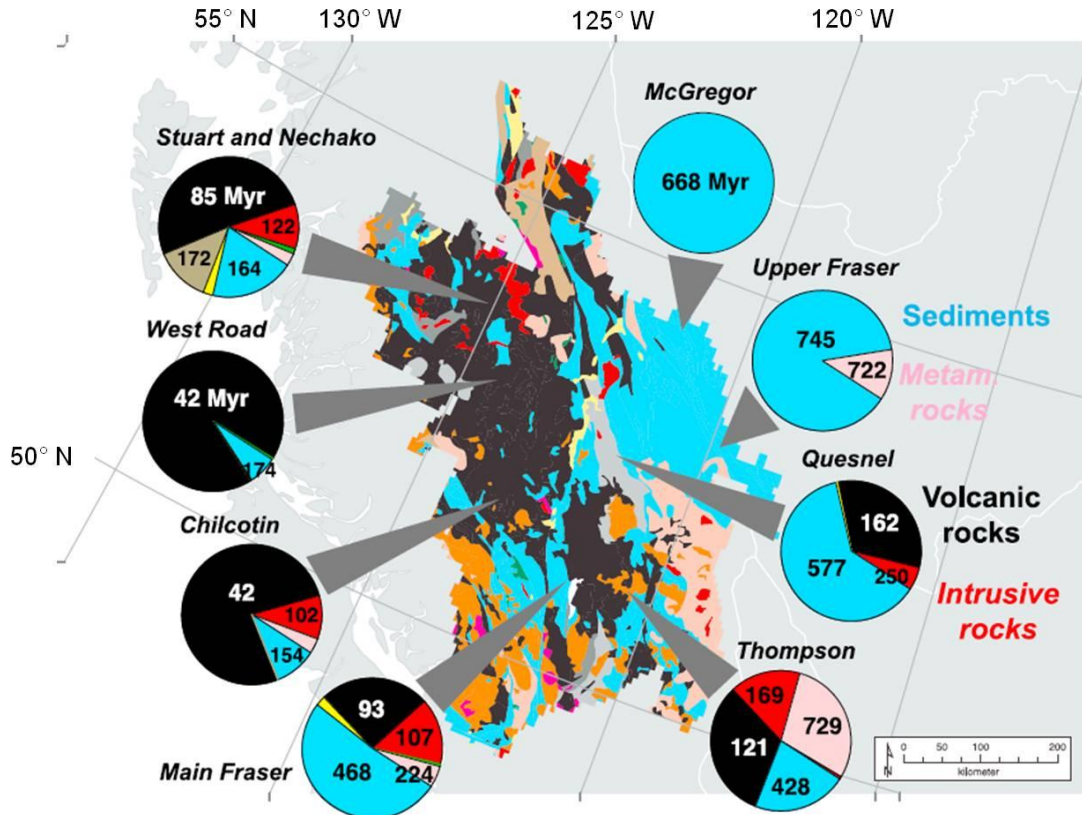
Figure 3. Bedrock geology of the Fraser River basin (modified from Peucker-Ehrenbrink et al., 2010). Each pie chart indicates the portion of a particular tributary subbasin composed of each lithological category, and the average age (in million years) of each lithology within the subbasin is shown within each pie wedge. Map colors are: yellow, continental sediments; blue, marine sediments; black, mafic volcanic rocks; pink, metamorphic rocks; red, felsic intrusive rocks; orange, intermediate intrusive rocks; dark green, ultramafic rocks; light gray, felsic volcanic rocks; dark gray, intermediate volcanic rocks; brown, sediments and volcanic rocks.

1. Fraser River at Red Pass
2. McGregor River
3. Willow River
4. Nechako River
5. Blackwater River
6. Quesnel River
7. Chilcotin River
8. Thompson River
9. Harrison River
10. Fraser River at Mission
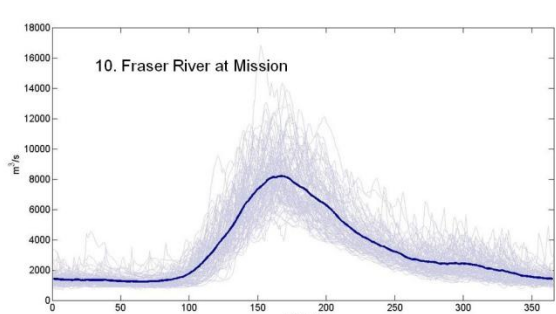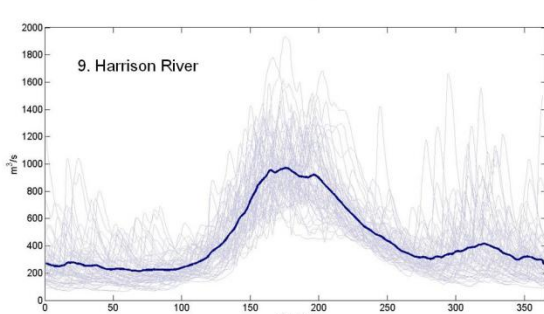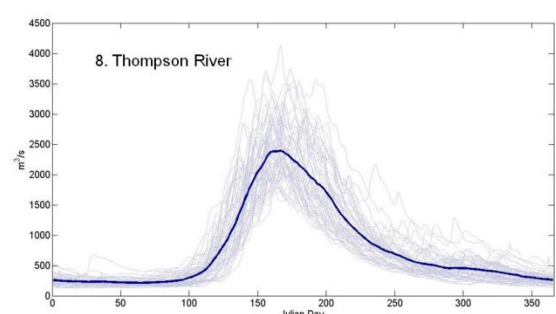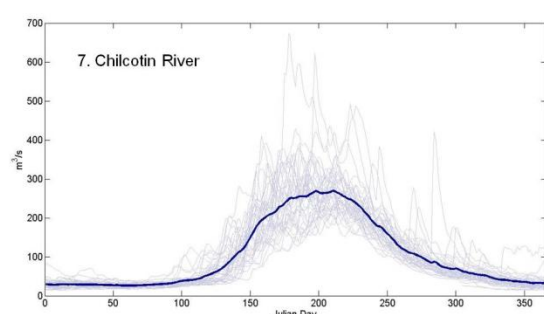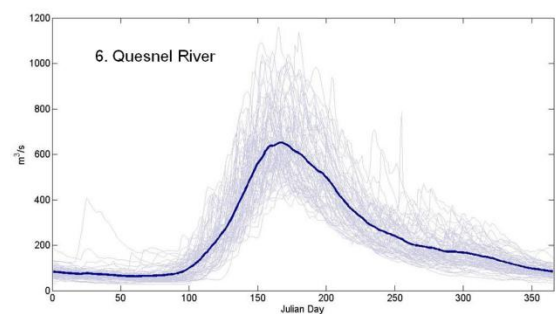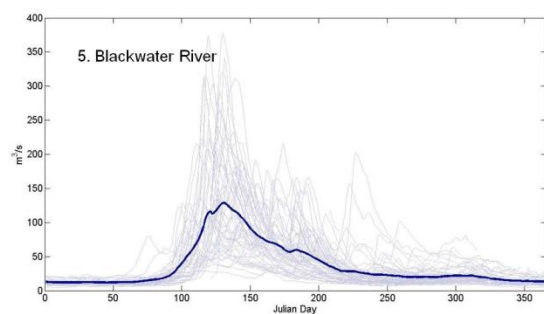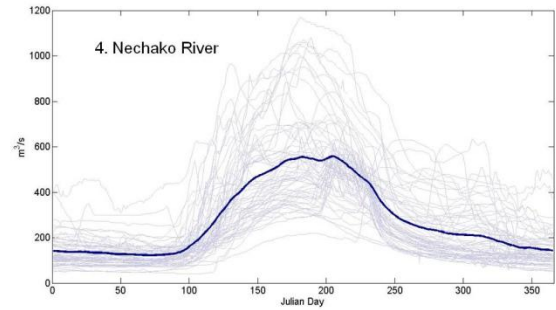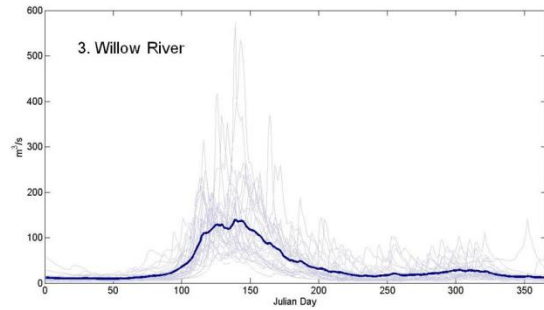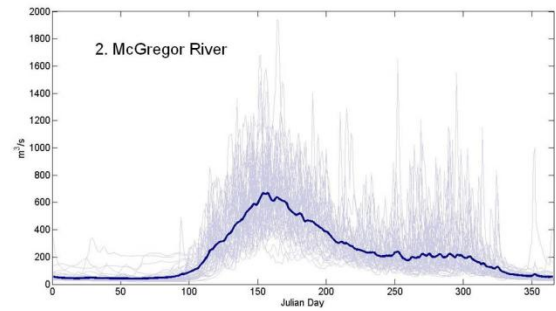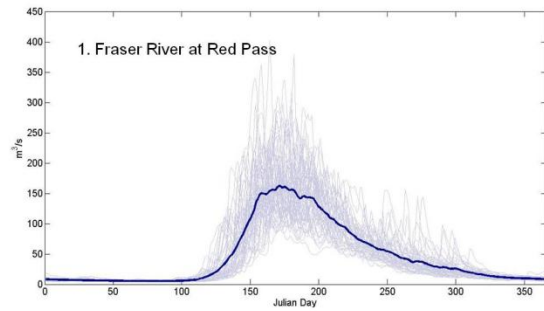
Figure 4. Annual hydrographs of all major tributaries of the Fraser River. Panels are ordered in a downstream direction based on where the tributary flows into the main stem Fraser, and the Fraser at Mission is the total discharge of the Fraser River. Grey lines are single annual hydrographs; thick lines are the mean of all years of record.
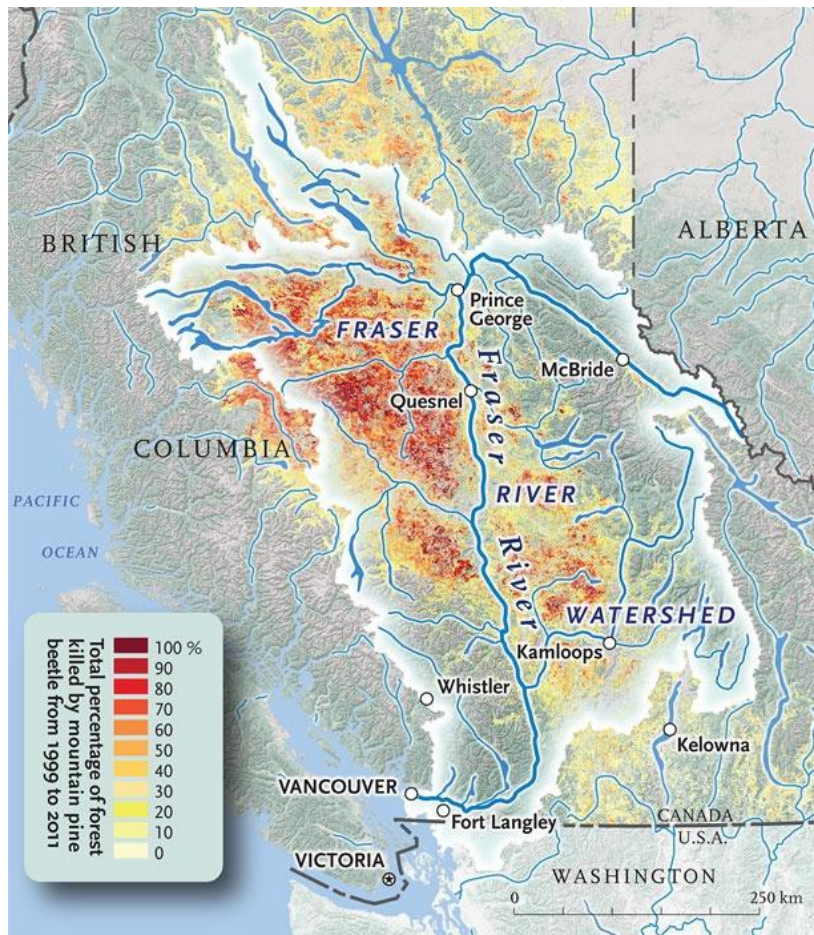
Figure 5. Extent of the mountain pine beetle infestation in forests of the Fraser River basin (Casselman and Linder, 2013).

References

Agrawal S., Galy V., Sanyal P., and Eglinton T. (2014) C$_4$ plant expansion in the Ganga Plain during the last glacial cycle: Insights from isotopic composition of vascular plant biomarkers. *Org. Geochem.* **67**, 58-71. doi:10.1016/j.orggeochem.2013.12.007.

Andrews G. D. M., Russell J. K., Brown S. R., and Randolph J. E. (2012) Pleistocene reversal of the Fraser River, British Columbia. *Geology* **40**, 111-114. doi:10.1130/g32488.1.

Bader R. G. (1956) The lignin fraction of marine sediments. *Deep Sea Res.* **4**, 15-22.

Bauer J. E., Druffel E. R. M., Wolgast D. M., and Griffin S. (2001) Sources and cycling of dissolved and particulate organic radiocarbon in the Northwest Atlantic Continental Margin. *Global Biogeochem. Cycles* **15**, 615-636. doi:10.1029/2000gb001314.

Beaulieu E., Goddéris Y., Donnadieu Y., Labat D., and Roelandt C. (2012) High sensitivity of the continental-weathering carbon dioxide sink to future climate change. *Nat. Clim. Change* **2**, 346-349. doi:10.1038/nclimate1419.

Benner R., Louchouarn P., and Amon R. M. W. (2005) Terrigenous dissolved organic matter in the Arctic Ocean and its transport to surface and deep waters of the North Atlantic. *Global Biogeochem. Cycles* **19**. doi:10.1029/2004gb002398.

Berner R. A. (1982) Burial of organic carbon and pyrite sulfur in the modern ocean: its geochemical and environmental significance. *Am. J. Sci.* **282**, 451-473. doi:10.2475/ajs.282.4.451.

Bianchi T. S. and Allison M. A. (2009) Large-river delta-front estuaries as natural "recorders" of global environmental change. *Proc. Natl. Acad. Sci.* **106**, 8085-8092. doi:10.1073/pnas.0812878106.

Blair N. E., Leithold E. L., and Aller R. C. (2004) From bedrock to burial: the evolution of particulate organic carbon across coupled watershed-continental margin systems. *Mar. Chem* **92**, 141-156. doi:10.1016/j.marchem.2004.06.023.

Blum J. D., Gazis C. A., Jacobsen A. D., and Chamberlain C. P. (1998) Carbonate versus silicate weathering in the Raikhot watershed within the High Himalayan crystalline series. *Geology* **26**, 411-414.

Bluth G. J. S. and Kump L. R. (1994) Lithologic and climatologic controls of river chemistry. *Geochim. Cosmochim. Acta* **58**, 2341-2359.

Bolch T., Menounos B., and Wheate R. (2010) Landsat-based inventory of glaciers in western Canada, 1985–2005. *Remote Sens. Environ.* **114**, 127-137. doi:10.1016/j.rse.2009.08.015.

Bouchez J., Galy V., Hilton R. G., Gaillardet J., Moreira-Turcq P., Pérez M. A., France-Lanord C., and Maurice L. (2014) Source, transport and fluxes of Amazon River particulate organic carbon: Insights from river sediment depth-profiles. *Geochim. Cosmochim. Acta* **133**, 280-298. doi:10.1016/j.gca.2014.02.032.

Boyer E. W., Howarth R. W., Galloway J. N., Dentener F. J., Green P. A., and Vörösmarty C. J. (2006) Riverine nitrogen export from the continents to the coasts. *Global Biogeochem. Cycles* **20**. doi:10.1029/2005gb002537.

Burdige D. J. (2007) Preservation of organic matter in marine sediments: Controls, mechanisms, and an imbalance in sediment organic carbon budgets? *Chem. Rev.* **107**, 467-485.

Cai W.-J. (2011) Estuarine and coastal ocean carbon paradox: CO$_2$ sinks or sites of terrestrial carbon incineration? *Annu. Rev. Mar. Sci.* **3**, 123-145. doi:10.1146/annurev-marine-120709-142723.

Cameron E. M. (1996) Hydrogeochemistry of the Fraser River, British Columbia: seasonal variation in major and minor components. *J. Hydrol.* **182**, 209-225.

Cameron E. M., Hall G. E. M., Veizer J., and Krouse H. R. (1995) Isotopic and elemental hydrogeochemistry of a major river system: Fraser River, British Columbia, Canada. *Chem. Geol.* **122**, 149-169.

Cameron E. M. and Hattori K. (1997) Strontium and neodymium isotope ratios in the Fraser River: a riverine transect across the Cordilleran orogen. *Chem. Geol.* **137**, 243-253.

Carpentier M., Weis D., and Chauvel C. (2014) Fractionation of Sr and Hf isotopes by mineral sorting in Cascadia Basin terrigenous sediments. *Chem. Geol.* **382**, 67-82. doi:10.1016/j.chemgeo.2014.05.028.

Carroll A. L., Taylor S. W., Régnière J., and Safranyik L. (2004) Effects of climate change on range expansion by the mountain pine beetle in British Columbia. (eds. T. L. Shore, J. E. Brooks, and J. E. Stone) Mountain Pine Beetle Symposium: Challenges and Solutions, 30-31 October 2003, Kelowna, BC. 223-232.

Casselman A. and Linder C. (2013) The health of the Fraser River. *Canadian Geographic*. **133**(3). http://www.canadiangeographic.ca/magazine/jun13/british_columbia_fraser_river.asp.

Chamberlin T. C. (1899) An Attempt to Frame a Working Hypothesis of the Cause of Glacial Periods on an Atmospheric Basis. *J. Geol.* **7**, 545-584.

Church M. and Slaymaker O. (1989) Disequilibrium of Holocene sediment yield in glaciated British Columbia. *Nature* **337**, 452-454.

Clague J. J. and James T. S. (2002) History and isostatic effects of the last ice sheet in southern British Columbia. *Quat. Sci. Rev.* **21**, 71-87.

Clague J. J., Luternauer J. L., Pullan S. E., and Hunter J. A. (1991) Postglacial deltaic sediments, southern Fraser River delta, British Columbia. *Can. J. Earth Sci.* **28**, 1386-1393.

Deines P. (1980) The isotopic composition of reduced organic carbon. In *Handbook of Environmental Isotope Geochemistry* (eds. P. Fritz and J. C. Fontes). Elsevier. 329-406.

Dittman J. A., Shanley J. B., Driscoll C. T., Aiken G. R., Chalmers A. T., Towse J. E., and Selvendiran P. (2010) Mercury dynamics in relation to dissolved organic carbon concentration and quality during high flow events in three northeastern U.S. streams. *Water Resour. Res.* **46**. doi:10.1029/2009wr008351.

Dittmar T. and Stubbins A. (2014) Dissolved Organic Matter in Aquatic Systems. In *Treatise on Geochemistry* (ed. H. H. a. K. Turekian). Elsevier. 125-156.

Drenzek N. J., Hughen K. A., Montlucon D. B., Southon J. R., dos Santos G. M., Druffel E. R. M., Giosan L., and Eglinton T. I. (2009) A new look at old carbon in active margin sediments. *Geology* **37**, 239-242. doi:10.1130/g25351a.1.

Dürr H. H., Meybeck M., and Dürr S. H. (2005) Lithologic composition of the Earth's continental surfaces derived from a new digital map emphasizing riverine material transfer. *Global Biogeochem. Cycles* **19**. doi:10.1029/2005gb002515.

Ebelmen J. J. (1845) Sur les produits de la decomposition des espèces minérales de la famille des silicates. *Annales des Mines* **7**, 3-66.

Eglinton T. I. and Eglinton G. (2008) Molecular proxies for paleoclimatology. *Earth Planet. Sci. Lett.* **275**, 1-16. doi:10.1016/j.epsl.2008.07.012.

Feng X., Vonk J. E., van Dongen B. E., Gustafsson O., Semiletov I. P., Dudarev O. V., Wang Z., Montlucon D. B., Wacker L., and Eglinton T. I. (2013) Differential mobilization of

terrestrial carbon pools in Eurasian Arctic river basins. *Proc. Natl. Acad. Sci.* **110**, 14168-14173. doi:10.1073/pnas.1307031110.

François L. M. and Goddéris Y. (1998) Isotopic constraints on the Cenozoic evolution of the carbon cycle. *Chem. Geol.* **145**, 177-212.

Fredericks J., Grieve D., Lefebure D., Madu B., Northcote B., and Wojdak P. (2009) British Columbia mining and mineral exploration overview. Ministry of Energy, Mines, and Petroleum Resources. 1-36.

Gaillardet J., Dupré B., Louvat P., and Allègre C. J. (1999) Global silicate weathering and CO_2 consumption rates deduced from the chemistry of large rivers. *Chem. Geol.* **159**, 3-30.

Galy V., Beyssac O., France-Lanord C., and Eglinton T. (2008) Recycling of graphite during Himalayan erosion: A geological stabilization of carbon in the crust. *Science* **322**, 943-945. doi:10.1126/science.1161408.

Galy V. and Eglinton T. (2011) Protracted storage of biospheric carbon in the Ganges–Brahmaputra basin. *Nat. Geosci.* **4**, 843-847. doi:10.1038/ngeo1293.

Galy V., France-Lanord C., Beyssac O., Faure P., Kudrass H., and Palhol F. (2007) Efficient organic carbon burial in the Bengal fan sustained by the Himalayan erosional system. *Nature* **450**, 407-410. doi:10.1038/nature06273.

Gimeno L., Stohl A., Trigo R. M., Dominguez F., Yoshimura K., Yu L., Drumond A., Durán-Quesada A. M., and Nieto R. (2012) Oceanic and terrestrial sources of continental precipitation. *Rev. Geophys.* **50**. doi:10.1029/2012rg000389.

Gíslason S. R., Arnórsson S., and Ármannsson H. (1996) Chemical weathering of basalt in southwest Iceland: Effects of runoff, age of rocks and vegetative/glacial cover. *Am. J. Sci.* **296**, 837-907.

Goodbred S. L., Paolo P. M., Ullah M. S., Pate R. D., Khan S. R., Kuehl S. A., Singh S. K., and Rahaman W. (2014) Piecing together the Ganges-Brahmaputra-Meghna River delta: Use of sediment provenance to reconstruct the history and interaction of multiple fluvial systems during Holocene delta evolution. *Geol. Soc. Am. Bull.* doi:10.1130/b30965.1.

Grafton R. Q., Pittock J., Davis R., Williams J., Fu G., Warburton M., Udall B., McKenzie R., Yu X., Che N., Connell D., Jiang Q., Kompas T., Lynch A., Norris R., Possingham H., and Quiggin J. (2012) Global insights into water resources, climate change and governance. *Nat. Clim. Change* **3**, 315-321. doi:10.1038/nclimate1746.

Gregory K. J. (2006) The human role in changing river channels. *Geomorphol.* **79**, 172-191. doi:10.1016/j.geomorph.2006.06.018.

Hague M. J., Ferrari M. R., Miller J. R., Patterson D. A., Russell G. L., Farrell A. P., and Hinch S. G. (2011) Modelling the future hydroclimatology of the lower Fraser River and its impacts on the spawning migration survival of sockeye salmon. *Global Change Biol.* **17**, 87-98. doi:10.1111/j.1365-2486.2010.02225.x.

Hallett D., Lepofsky D. S., Mathewes R. W., and Lertzman K. P. (2003) 11 000 years of fire history and climate in the mountain hemlock rain forests of southwestern British Columbia based on sedimentary charcoal. *Can. J. Forest Res.* **33**, 292-312. doi:10.1139/X02-177.

Hamann A. and Wang T. (2006) Potential effects of climate change on ecosystem and tree species distribution in British Columbia. *Ecology* **87**, 2773-2786.

Healey M. and Bradford M. (2011) The cumulative impacts of climate change on Fraser River sockeye salmon (*Oncorhynchus nerka*) and implications for management. *Can. J. Fish. Aquat. Sci.* **68**, 718-737. doi:10.1139/f2011-010.

Hedges J. I. and Mann D. C. (1979) The lignin geochemistry of marine sediments from the southern Washington coast. *Geochim. Cosmochim. Acta* **43**, 1809-1818.

Helms J. R., Stubbins A., Ritchie J. D., Minor E. C., Kieber D. J., and Mopper K. (2008) Absorption spectral slopes and slope ratios as indicators of molecular weight, source, and photobleaching of chromophoric dissolved organic matter. *Limnol. Oceanogr.* **53**, 955-969.

Hernes P. J. and Benner R. (2003) Photochemical and microbial degradation of dissolved lignin phenols: Implications for the fate of terrigenous dissolved organic matter in marine environments. *J. Geophys. Res.* **108**. doi:10.1029/2002jc001421.

Hinrichs K.-U. and Rullkötter J. (1997) Terrigenous and marine lipids in Amazon fan sediments: Implications for sedimentological reconstructions. In *Proceedings of the Ocean Drilling Program, Scientific Results* (eds. R. D. Flood, D. J. W. Piper, A. Klaus, and L. C. Peterson). 539-553.

Holtvoeth J., Wagner T., and Schubert C. J. (2003) Organic matter in river-influenced continental margin sediments: The land-ocean and climate linkage at the Late Quaternary Congo fan (ODP Site 1075). *Geochem., Geophys., Geosyst.* **4**. doi:10.1029/2003gc000590.

Hopmans E. C., Weijers J. W. H., Schefuß E., Herfort L., Sinninghe Damsté J. S., and Schouten S. (2004) A novel proxy for terrestrial organic matter in sediments based on branched and isoprenoid tetraether lipids. *Earth Planet. Sci. Lett.* **224**, 107-116. doi:10.1016/j.epsl.2004.05.012.

Hossler K. and Bauer J. E. (2013) Amounts, isotopic character, and ages of organic and inorganic carbon exported from rivers to ocean margins: 2. Assessment of natural and anthropogenic controls. *Global Biogeochem. Cycles* **27**, 347-362. doi:10.1002/gbc.20034.

IPCC (2013) Climate change 2013: The physical science basis. Contribution of Working Group I to the Fifth Assessment Report of the Intergovernmental Panel on Climate Change. (eds. T. F. Stocker, D. Qin, G.-K. Plattner, M. Tignor, S. K. Allen, J. Boschung, A. Nauels, Y. Xia, V. Bex, and P. M. Midgley). Cambridge, United Kingdom and New York, NY, USA. 1535 pp.

Jacobsen A. D., Blum J. D., Chamberlain C. P., Poage M. A., and Sloan V. F. (2002) Ca/Sr and Sr isotope systematics of a Himalayan glacial chronosequence: Carbonate versus silicate weathering rates as a function of landscape surface age. *Geochim. Cosmochim. Acta* **66**, 13-27.

Johnsen T. F. and Brennand T. A. (2004) Late-glacial lakes in the Thompson Basin, British Columbia: paleogeography and evolution. *Can. J. Earth Sci.* **41**, 1367-1383. doi:10.1139/e04-074.

Kao S. J., Hilton R. G., Selvaraj K., Dai M., Zehetner F., Huang J. C., Hsu S. C., Sparkes R., Liu J. T., Lee T. Y., Yang J. Y. T., Galy A., Xu X., and Hovius N. (2014) Preservation of terrestrial organic carbon in marine sediments offshore Taiwan: mountain building and atmospheric carbon dioxide sequestration. *Earth Surf. Dyn.* **2**, 127-139. doi:10.5194/esurf-2-127-2014.

Klinka K., Pojar J., and Meidinger D. V. (1991) Revision of biogeoclimatic units of coastal British Columbia. *Northwest Sci.* **65**, 32-47.

Koch J., Menounos B., and Clague J. J. (2009) Glacier change in Garibaldi Provincial Park, southern Coast Mountains, British Columbia, since the Little Ice Age. *Global Planet. Change* **66**, 161-178. doi:10.1016/j.gloplacha.2008.11.006.

Laruelle G. G., Roubeix V., Sferratore A., Brodherr B., Ciuffa D., Conley D. J., Dürr H. H., Garnier J., Lancelot C., Le Thi Phuong Q., Meunier J. D., Meybeck M., Michalopoulos P., Moriceau B., Ní Longphuirt S., Loucaides S., Papush L., Presti M., Ragueneau O., Regnier P., Saccone L., Slomp C. P., Spiteri C., and Van Cappellen P. (2009) Anthropogenic perturbations of the silicon cycle at the global scale: Key role of the land-ocean transition. *Global Biogeochem. Cycles* **23**, n/a-n/a. doi:10.1029/2008gb003267.

Libby W. F., Anderson E. C., and Arnold J. R. (1949) Age Determination by Radiocarbon Content- World-Wide Assay of Natural Radiocarbon. *Science* **109**, 227-228. doi:10.1126/science.109.2827.227.

Luo P., Peng P. A., Lü H. Y., Zheng Z., and Wang X. (2012) Latitudinal variations of CPI values of long-chain *n*-alkanes in surface soils: Evidence for CPI as a proxy of aridity. *Sci. China* **55**, 1134-1146.

Luternauer J. L., Clague J. J., Hunter J. A. M., Pullan S. E., Roberts M. C., Woeller D. J., Kostaschuk R. A., Moslow T. F., Monahan P. A., and Hart B. S. (1993) The Fraser River delta, British Columbia: architecture, geological dynamics and human impacts. (eds. R. Kay and O. T. Magoon), New Orleans, Louisiana, USA.

Mackenzie F. T. and Garrels R. M. (1966) Chemical mass balance between rivers and oceans. *Am. J. Sci.* **264**, 507-525.

MacKinnon A., Meidinger D., and Klinka K. (1992) Use of the biogeoclimatic ecosystem classification system in British Columbia. *For. Chron.* **68**, 100-120.

Margold M., Jansson K. N., Kleman J., Stroeven A. P., and Clague J. J. (2013) Retreat pattern of the Cordilleran Ice Sheet in central British Columbia at the end of the last glaciation reconstructed from glacial meltwater landforms. *Boreas* **42**, 830-847. doi:10.1111/bor.12007.

Mayer L. M. (1994) Relationships between mineral surfaces and organic carbon concentrations in soils and sediments. *Chem. Geol.* **114**, 347-363.

Mazzotti S., Lambert A., Van der Kooij M., and Mainville A. (2009) Impact of anthropogenic subsidence on relative sea-level rise in the Fraser River delta. *Geology* **37**, 771-774. doi:10.1130/g25640a.1.

Meybeck M. (1987) Global chemical weathering from surficial rocks estimated from river dissolved loads. *Am. J. Sci.* **287**, 401-428.

Meyers-Schulte K. J. and Hedges J. I. (1986) Molecular evidence for a terrestrial component of organic matter dissolved in ocean water. *Nature* **321**, 61-63.

Moon S., Chamberlain C. P., and Hilley G. E. (2014) New estimates of silicate weathering rates and their uncertainties in global rivers. *Geochim. Cosmochim. Acta* **134**, 257-274. doi:10.1016/j.gca.2014.02.033.

Moran J. E., Oktay S. D., and Santschi P. H. (2002) Sources of iodine and iodine 129 in rivers. *Water Resour. Res.* **38**, 24-1-24-10. doi:10.1029/2001wr000622.

Morrison J., Quick M. C., and Foreman M. G. G. (2002) Climate change in the Fraser River watershed: flow and temperature projections. *J. Hydrol.* **263**, 230-244.

Nealis V. and Peter B. (2008) Risk assessment of the threat of mountain pine beetle to Canada's boreal and eastern pine forests. Canadian Forest Service Pacific Forestry Center, BC-X-417, Victoria, B.C. 1-31.

Négrel P., Allègre C. J., Dupré B., and Lewin E. (1993) Erosion sources determined by inversion of major and trace element ratios and strontium isotopic ratios in river water. *Earth Planet. Sci. Lett.* **120**, 59-76.

Nelson N. B. and Siegel D. A. (2013) The Global Distribution and Dynamics of Chromophoric Dissolved Organic Matter. *Annu. Rev. Mar. Sci.* **5**, 447-476. doi:10.1146/annurev-marine-120710-100751.

Opsahl S. and Benner R. (1997) Distribution and cycling of terrigenous dissolved organic matter in the ocean. *Nature* **386**, 480-482.

Pancost R. D. and Boot C. S. (2004) The palaeoclimatic utility of terrestrial biomarkers in marine sediments. *Mar. Chem* **92**, 239-261. doi:10.1016/j.marchem.2004.06.029.

Peterse F., Schouten S., van der Meer J., van der Meer M. T. J., and Sinninghe Damsté J. S. (2009) Distribution of branched tetraether lipids in geothermally heated soils: Implications for the MBT/CBT temperature proxy. *Org. Geochem.* **40**, 201-205. doi:10.1016/j.orggeochem.2008.10.010.

Peucker-Ehrenbrink B., Miller M. W., Arsouze T., and Jeandel C. (2010) Continental bedrock and riverine fluxes of strontium and neodymium isotopes to the oceans. *Geochem., Geophys., Geosyst.* **11**. doi:10.1029/2009gc002869.

Pojar J., Klinka K., and Meidinger D. V. (1987) Biogeoclimatic ecosystem classification in British Columbia. *For. Ecol. Manage.* **22**, 119-154.

Ponton C., Giosan L., Eglinton T. I., Fuller D. Q., Johnson J. E., Kumar P., and Collett T. S. (2012) Holocene aridification of India. *Geophys. Res. Lett.* **39**. doi:10.1029/2011gl050722.

Poulton S. W. and Raiswell R. (2000) Solid phase associations, oceanic fluxes and the anthropogenic perturbation of transition metals in world river particulates. *Mar. Chem* **72**, 17-31.

Rauch J. N. (2010) Global spatial indexing of the human impact on Al, Cu, Fe, and Zn mobilization. *Environ. Sci. Technol.* **44**, 5728-5734.

Raymond P. A., Oh N.-H., Turner R. E., and Broussard W. (2008) Anthropogenically enhanced fluxes of water and carbon from the Mississippi River. *Nature* **451**, 449-452. doi:10.1038/nature06505.

Reeder S. W., Hitcheon B., and Levinson A. A. (1972) Hydrogeochemistry of the surface waters of the Mackenzie River drainage basin, Canada—I. Factors controlling inorganic composition. *Geochim. Cosmochim. Acta* **36**, 825-865.

Rotenberg E., Davis D. W., Amelin Y., Ghosh S., and Bergquist B. A. (2012) Determination of the decay-constant of ^{87}Rb by laboratory accumulation of ^{87}Sr. *Geochim. Cosmochim. Acta* **85**, 41-57. doi:10.1016/j.gca.2012.01.016.

Ryder J. M., Fulton R. J., and Clague J. J. (1991) The Cordilleran ice sheet and the glacial geomorphology of southern and central British Columbia. *Géogr. phys. Quat.* **45**, 365-377.

Safranyik L. and Wilson B. (2006) The mountain pine beetle: A synthesis of biology, management, and impacts on lodgepole pine. Natural Resources Canada, Victoria, B.C. 1-304.

Sansone U., Kim C. K., Kis-Benedek G., Schorn R., Zeiller E., Qaribov A., Huseynov V., and Chupov A. (2008) Natural and anthropogenic radionuclides in the rivers of Azerbaijan. *J. Radioanal. Nucl. Chem.* **277**, 357-364. doi:10.1007/s10967-007-7027-0.

Sarkar S., Wilkes H., Prasad S., Brauer A., Riedel N., Stebich M., Basavaiah N., and Sachse D. (2014) Spatial heterogeneity in lipid biomarker distributions in the catchment and sediments of a crater lake in central India. *Org. Geochem.* **66**, 125-136. doi:10.1016/j.orggeochem.2013.11.009.

Schefuß E., Ratmeyer V., Stuut J.-B. W., Jansen J. H. F., and Sinninghe Damsté J. S. (2003) Carbon isotope analyses of n-alkanes in dust from the lower atmosphere over the central eastern Atlantic. *Geochim. Cosmochim. Acta* **67**, 1757-1767. doi:10.1016/s0016-7037(02)01414-x.

Schlünz B. and Schneider R. R. (2000) Transport of terrestrial organic carbon to the oceans by rivers: re-estimating flux and burial rates. *Int. J. Earth Sci.* **88**, 599-606.

Schuster P. F., Striegl R. G., Aiken G. R., Krabbenhoft D. P., Dewild J. F., Butler K., Kamark B., and Dornblaser M. (2011) Mercury export from the Yukon River Basin and potential response to a changing climate. *Environ. Sci. Technol.* **45**, 9262-9267. doi:10.1021/es202068b.

Shrestha R. R., Schnorbus M. A., Werner A. T., and Berland A. J. (2012) Modelling spatial and temporal variability of hydrologic impacts of climate change in the Fraser River basin, British Columbia, Canada. *Hydrol. Processes* **26**, 1840-1860. doi:10.1002/hyp.9283.

Smittenberg R. H., Eglinton T. I., Schouten S., and Damsté J. S. S. (2006) Ongoing buildup of refractory organic carbon in boreal soils during the Holocene. *Science* **314**, 1283-1286. doi:10.1126/science.1129376.

Spence J. and Telmer K. (2005) The role of sulfur in chemical weathering and atmospheric CO_2 fluxes: Evidence from major ions, $d^{13}C_{DIC}$, and $d^{34}S_{SO4}$ in rivers of the Canadian Cordillera. *Geochim. Cosmochim. Acta* **69**, 5441-5458. doi:10.1016/j.gca.2005.07.011.

Spencer R. G. M., Stubbins A., Hernes P. J., Baker A., Mopper K., Aufdenkampe A. K., Dyda R. Y., Mwamba V. L., Mangangu A. M., Wabakanghanzi J. N., and Six J. (2009) Photochemical degradation of dissolved organic matter and dissolved lignin phenols from the Congo River. *J. Geophys. Res.* **114**. doi:10.1029/2009jg000968.

Stallard R. F. (1998) Terrestrial sedimentation and the carbon cycle: Coupling weathering and erosion to carbon burial. *Global Biogeochem. Cycles* **12**, 231-257. doi:10.1029/98gb00741.

Stallard R. F. and Edmond J. M. (1983) Geochemistry of the Amazon: 2. The influence of geology and weathering environment on the dissolved load. *J. Geophys. Res.* **88**, 9671. doi:10.1029/JC088iC14p09671.

Syvitski J. P. M., Vörösmarty C. J., Kettner A. J., and Green P. (2005) Impact of humans on the flux of terrestrial sediment to the global coastal ocean. *Science* **308**, 376-380. doi:10.1126/science.1109454.

Taylor S. W. and Carroll A. L. (2004) Disturbance, forest age, and mountain pine beetle outbreak dynamics in B.C.: A historical perspective. Mountain Pine Beetle Symposium: Challenges and Solutions, 30-31October 2003, Kelowna, B.C. 41-51.

Underwood M. B., Hoke K. D., Fisher A. T., Davis E. E., Giambalvo E., Zuhlsdorff L., and Spinelli G. A. (2005) Provenance, stratigraphic architecture, and hydrogeologic influence of turbidites on the mid-ocean Ridge flank of northwestern Cascadia Basin, Pacific Ocean. *J. Sediment. Res.* **75**, 149-164. doi:10.2110/jsr.2005.012.

Valentine K. W. G., Sprout P. N., Baker T. E., and Lawkulich L. M. E. (1978) *The Soil Landscapes of British Columbia*. BC Ministry of Environment, Resource Analysis Branch.

Vonk J. E., Sánchez-García L., van Dongen B. E., Alling V., Kosmach D., Charkin A., Semiletov I. P., Dudarev O. V., Shakhova N., Roos P., Eglinton T. I., Andersson A., and Gustafsson Ö. (2012) Activation of old carbon by erosion of coastal and subsea permafrost in Arctic Siberia. *Nature* **489**, 137-140. doi:10.1038/nature11392.

Vörösmarty C. J., McIntyre P. B., Gessner M. O., Dudgeon D., Prusevich A., Green P., Glidden S., Bunn S. E., Sullivan C. A., Liermann C. R., and Davies P. M. (2010) Global threats to human water security and river biodiversity. *Nature* **467**, 555-561. doi:10.1038/nature09440.

Vörösmarty C. J., Meybeck M., Fekete B., Sharma K., Green P., and Syvitski J. P. M. (2003) Anthropogenic sediment retention: major global impact from registered river impoundments. *Global Planet. Change* **39**, 169-190. doi:10.1016/s0921-8181(03)00023-7.

Walling D. E. (2006) Human impact on land–ocean sediment transfer by the world's rivers. *Geomorphol.* **79**, 192-216. doi:10.1016/j.geomorph.2006.06.019.

Weijers J. W. H., Schouten S., Schefuß E., Schneider R. R., and Sinninghe Damsté J. S. (2009) Disentangling marine, soil and plant organic carbon contributions to continental margin sediments: A multi-proxy approach in a 20,000 year sediment record from the Congo deep-sea fan. *Geochim. Cosmochim. Acta* **73**, 119-132. doi:10.1016/j.gca.2008.10.016.

Westfall J. and Ebata T. (2010) Summary of forest health conditions in British Columbia. B.C. Ministry of Forests, Mines and Lands. 1-70.

Woods A. J., Heppner D., Kope H. H., Burleigh J., and Maclauchlan L. (2010) Forest health and climate change: A British Columbia perspective. *For. Chron.* **86**, 412-422.

CHAPTER 2.

TRACING RIVER CHEMISTRY IN SPACE AND TIME: DISSOLVED INORGANIC
CONSTITUENTS OF THE FRASER RIVER, CANADA

2.1 Abstract

The Fraser River basin in southwestern Canada bears unique geologic and climatic
features which make it an ideal setting for investigating the origins, transformations and delivery
to the coast of dissolved riverine loads under relatively pristine conditions. We present results
from sampling campaigns over three years which demonstrate the lithologic and hydrologic
controls on fluxes and isotope compositions of major dissolved inorganic runoff constituents
(dissolved nutrients, major and trace elements, $^{87}Sr/^{86}Sr$, δD). A time series record near the
Fraser mouth allows us to generate new estimates of discharge-weighted concentrations and
fluxes, and an overall chemical weathering rate of 32 t km^{-2} y^{-1}. The seasonal variations in
dissolved inorganic species are driven by changes in hydrology, which vary in timing across the
basin. The time series record of dissolved $^{87}Sr/^{86}Sr$ is of particular interest, as a consistent shift
between higher ("more radiogenic") values during spring and summer and less radiogenic values

in fall and winter demonstrates the seasonal variability in source contributions throughout the basin. This seasonal shift is also quite large (0.709 – 0.714), with a discharge-weighted annual average of 0.7120 (2 s.d. = 0.0003). We present a mixing model which predicts the seasonal evolution of dissolved ^{87}Sr/^{86}Sr based on tributary compositions and water discharge. This model highlights the importance of chemical weathering fluxes from the old sedimentary bedrock of headwater drainage regions, despite their relatively small contribution to the total water flux.

2.2 Introduction

2.2.1 Tracing river geochemistry across space and time

Elemental and isotope tracers have tremendous utility in elucidating the sources and biogeochemical history of material dissolved in river waters (e.g. Livingstone, 1963; Mackenzie and Garrels, 1966; Palmer and Edmond, 1989; Gaillardet et al., 1999; Schulte et al., 2011). Time series observations are critical in order to accurately quantify annual fluxes and understand the processes controlling the properties of chemical species in rivers (Walling and Foster, 1975; Christophersen et al., 1990; Scanlon et al., 2001; Raymond and Cole, 2003; Tipper et al., 2006; Cooper et al., 2008; Bagard et al., 2011; Kirchner and Neal, 2013). In addition, basin-integrated signals often do not represent the entire drainage region equally, but rather are significantly biased by specific, sometimes geographically small, areas (Edmond, 1992; Blum et al., 1998; Hartmann et al., 2009; Wolff-Boenisch et al., 2009). Only by sampling for both spatial variability across a basin and temporal variability near a river mouth can the dynamics of source contributions and seasonal dynamics be understood.

The Fraser River basin (Fig. 1) was chosen as the focus for this work because of its large variability in bedrock geology across a relatively small area, which has been shown to impart stark contrasts to the characteristics of its chemical load (Armstrong, 1988; Cameron et al., 1995; Cameron, 1996; Cameron and Hattori, 1997). In addition, the large seasonal variability in discharge of the Fraser, typical of temperate mountainous and subarctic regions, is expected to lead to time-varying changes in the relative contributions of material derived from different portions of the basin. These properties make the Fraser basin an excellent candidate for quantitatively tracing the sources of dissolved material over time.

Studies such as this are necessary in order to (1) accurately quantify annual fluxes of terrestrial material to the coastal ocean; (2) determine the relative importance of different portions of the drainage basin to the total chemical load; (3) accurately interpret records of past fluvial drainage basin history; and (4) establish seasonal and interannual variability in natural systems under increasing anthropogenic and environmental stress. In recent centuries and decades, river basins have emerged as some of the areas most acutely affected by human influence in the forms of global warming, resource extraction, land use change, and ecosystem disturbance (Nilsson, 2005; Peterson, 2006; Chao et al., 2008; Milliman et al., 2008; Syvitski, 2008; Coggins et al., 2011). Research on large, relatively pristine systems such as the Fraser River, which are rare, is critical to the fundamental understanding of how river geochemistry evolves under natural conditions, and for projections of how this behavior may change in the future.

2.2.2 Fraser River basin environmental setting

A detailed description of the geological composition of the Foreland, Omineca, Intermontane, and Coast belts comprising the bedrock of the Fraser basin is given by Cameron and Hattori (1997) and references therein. The hydrology of the Fraser River is characterized by a spring freshet fed by a mixture of snowmelt and rainfall, which typically begins in April and tapers off throughout the summer, and is often followed by a secondary fall peak driven by rain storms (Fig. 2; Dorcey, 1991). Discharge during the spring freshet peaks at approximately 8000 $m^3\ s^{-1}$, while winter base flow is ~1800 $m^3\ s^{-1}$. The hydrology of subbasins within the watershed is complex due to mountainous topography and variable climatic regimes (Thorne and Woo,

2011), resulting in large differences in the timing of the spring freshet in various tributary basins (Déry et al., 2012).

This study combines spatial and temporal observations of river chemistry in order to interpret seasonal patterns at the river mouth in the context of upstream inputs. We present results from three basin-wide surveys of the main stem and multiple tributaries at different hydrologic stages, as well as a two-year time series near the river mouth with samples collected approximately twice per month. Our results show how seasonal variations in hydrology coincide with changes in the flux and composition of dissolved inorganic material carried by the Fraser River. Basin-wide sampling campaigns (Table 1), probing multiple points along the main stem and at confluences of major tributaries, create a framework for interpreting the trends observed in the time series. The source-specificity of isotope tracers, particularly dissolved ^{87}Sr/^{86}Sr, allows for quantitative provenance analysis of the time-varying contributions from different sub-basins. The focus here on dissolved inorganic components lays the foundation for a holistic understanding of biogeochemical processes in rivers extending to organic matter and suspended sediments, which are the subjects of forthcoming publications.

2.3 Methods

2.3.1 Sample collection

All samples were collected from river banks by extending collection devices as far as possible into the stream (typically ~3 m). Exceptions to this are main stem samples in the delta, which were collected mid-channel from on board a small boat, and samples collected at Fort Langley and New Westminster, which were collected off of a dock ~50 m from the bank. The data presented in Table 2 represent the basin-wide sampling campaigns which took place in

2009, 2010, and 2011. Table 3 presents data for the time series samples collected approximately every other week from July 2009 to October 2011 at Fort Langley and New Westminster.

Water samples were collected at each site using a combination of filtration techniques. Material remaining in water passed through these filter types is hereafter defined as "dissolved." Water samples for nutrient and trace and major element concentrations collected in summer 2009 and as part of the time series were collected with a 0.5 L high-density polyethylene (HDPE) "dipper" (Bel-Art Scienceware), subsampled with an all-plastic (polypropylene [PP] and polyethylene [PE]) syringe, and filtered through Sterivex cartridges (Millipore, pore size 0.22 μm). Samples collected in fall 2010 and spring 2011 were filtered with a membrane cartridge filter (Pall AcroPak 500 Supor Membrane, 0.8/0.2 μm pore size). All major and trace element concentration samples were collected, unacidified, in HDPE bottles (pre-cleaned with certification by the U.S. Environmental Protection Agency). This sampling protocol has been described previously (Miller, 2009; Miller et al., 2011). Nutrient concentration samples were collected in PE scintillation vials, pre-cleaned first with laboratory soap solution, then soaked for 3 days in 10% HCl, followed by 3 rinses with Milli-Q (Millipore) water. Nutrient samples were frozen in the field and stored in the dark. Total alkalinity (TA) samples were collected by pumping water through a 0.45 μm cartridge filter into 250 mL borosilicate glass bottles; samples were immediately poisoned with 60 μL of saturated $HgCl_2$ solution and sealed with a greased ground-glass stopper (Dickson et al., 2007).

In order to make the results and sample archives of this work accessible to the broader community, all samples have been registered in the online System for Earth Sample Registration database (www.geosamples.org). Each sample is assigned a unique International Geo Sample

Number (IGSN) code beginning with "GRO" (Global Rivers Observatory). Registered users can search the database to retrieve sample metadata and information about archived material.

2.3.2 Laboratory analyses

Nutrient samples were thawed in the dark immediately prior to analysis on a four-channel AutoAnalyzer (Lachat QuickChem 8000) with standard spectrophotometric methods certified by the U.S. Environmental Protection Agency. Briefly, nitrate and nitrite (NO_3+NO_2) were measured together as azo dye after reduction in a Cu-Cd column. Phosphate (orthophosphorus) was measured as a chromophoric antimony-phosphomolybdate complex. Soluble silica (hereafter denoted SiO_2) was measured as a heteropoly blue complex. Ammonium was measured as indophenol blue via the Berthelot reaction. All samples were analyzed in duplicate and concentrations were calculated from 6-point dilution curves of standard MOOS-2 (National Research Council Canada) prepared on the day of analysis. One standard dilution was analyzed for every 5 samples. No international reference standard is available for NH_4, hence these values are calibrated to an artificial standard prepared on the day of analysis. Instrumental detection is generally <0.05 µmol L^{-1} for all analytes. This limit represents the lowest detectable standard dilution, which is at least 5 times higher than the blank value.

Anion concentrations (Cl, SO_4) were measured on a Dionex ion chromatography system. Approximately 5 mL of undiluted sample was injected three times on an anion column (AS15, 4 mm, with ASRS suppressor) in 65% 50 mM NaOH and 35% H_2O eluents. Standards were prepared by gravimetric dilution of SpecPure ion chromatography standards (Alfa Aesar). One Milli-Q H_2O blank and one standard dilution were injected for every 3 samples. Concentrations were calculated based on 3-point standard calibration curves using Chromeleon software,

followed by blank correction. Concentrations of Br and F were also analyzed, but results were too low to be reliably quantified.

Total alkalinity (TA) measurements were made following the methods described by Wang et al. (2013). Briefly, TA was measured with an automated titrator (AS-ALK2, Apollo SciTech) using a modified Gran titration procedure (Wang and Cai, 2004); this titration includes weak acids and anions (such as HCO_3^-, CO_2^{3-}, and deprotonated organic acids) (Morel and Hering, 1993). Sample analyses were calibrated with certified reference material from Dr. A.G. Dickson at the Scripps Institution of Oceanography. Bicarbonate (HCO_3^-) is the dominant component of alkalinity in Fraser River water, representing ~98% of the total concentration (Wang et al., in prep), so we assume here that $TA = HCO_3^-$.

Water samples for cation concentrations were prepared in a clean laboratory. An indium tracer solution and sub-boiling distilled HNO_3 (to achieve 5% acidity) were added to 1 mL of undiluted sample. Blanks were prepared in the same manner with Milli-Q H_2O (18.2 MΩ cm^{-1}) instead of river water. Standards were prepared from dilutions of natural river water standard reference material SLRS-5 (National Research Council Canada). Samples were analyzed interspersed with blanks and standard dilutions on a Thermo Scientific Element2 single collector inductively-coupled plasma mass spectrometer (ICPMS). An argon flow nebulizer and quartz double pass (cyclonic, coupled to a Scott-type) spray chamber were used to introduce the sample to the plasma source by means of self-aspiration and the ion beam was tuned scanning U, In, and Sc. The following isotopes were analyzed and reported in this manuscript: ^{82}Kr, ^{83}Kr, ^{85}Rb, ^{86}Sr, ^{87}Sr, ^{88}Sr, ^{137}Ba, and ^{138}Ba at low mass resolution (m/Δm ~300); ^{42}Ca, ^{43}Ca, ^{44}Ca, and ^{48}Ca at medium mass resolution (m/Δm ~3000); and ^{23}Na, ^{24}Mg, ^{25}Mg, ^{26}Mg, and ^{39}K at high mass resolution (m/Δm ~10,000). Multiple isotopes were measured for each element whenever

possible to check for isobaric interferences; such interferences were corrected when appropriate. Concentrations were calculated based on 7-point calibration curves of standard dilutions for each element.

Major and trace element concentration samples were subsampled for strontium separation in a PicoTrace® clean laboratory at WHOI. Target volumes were transferred to acid-cleaned Teflon beakers, dried down, and resuspended in 3.5 N distilled HNO_3. Strontium was isolated by ion chromatography using ~300 µL of Sr Spec resin (Eichrom, 100-150 µm) and eluted with 7 mL Milli-Q water. Column eluents were refluxed at 80°C overnight in distilled sub-boiling concentrated HNO_3 and a few drops of 30% H_2O_2 (to remove residual organics from the resin), dried down and resuspended in 5% HNO_3. Eluents were analyzed on a Thermo Scientific Neptune multicollector (MC) ICPMS by static measurement of ^{82}Kr, ^{83}Kr, ^{84}Sr, ^{85}Rb, ^{86}Sr, ^{87}Sr, and ^{88}Sr. Raw $^{87}Sr/^{86}Sr$ for all samples and standards was corrected for instrumental mass bias with a power law and corrected for ^{86}Kr and ^{87}Rb interferences. Sample results were normalized to repeated measurements of international standard SRM 987 (U.S. National Institute of Standards and Technology), analyzed once for every 5 samples. The certified value of the standard is $^{87}Sr/^{86}Sr = 0.710240$; the average measured value was 0.71028 (n = 52, 2 s.d. = 0.00007). Although greater precision for this measurement is possible, the instrument was tuned to achieve the best precision for our measurements given the amount of analyte.

Stable isotope compositions of hydrogen (δD) and oxygen ($\delta^{18}O$) in filtered water samples were measured on a Picarro L2120-I cavity ring-down spectrometer at the ETH in Zürich, Switzerland. Each sample was injected six times, with the results of the first three injections discarded to eliminate instrumental memory effects. Results were also rejected if the concentration of H_2O was outside 20,000 ± 2,000 ppm. Aliquots of standard reference materials

SLAP2, GISP, and VSMOW2 (International Atomic Energy Agency) were analyzed to bracket sets of 5 samples, with standard calibration corrections and interfering contamination from dissolved organic matter assessed using Picarro ChemCorrect software.

Statistics on analytical precision and accuracy for all of the above measurements are summarized under the corresponding results at the bottom of Table 2.

2.3.3 Discharge data and flux calculations

Daily water flux (discharge) data were obtained online from the Environment Canada Water Office (http://www.wateroffice.ec.gc.ca). Discharge at the city of Mission is considered the total Fraser River discharge, as this site is only 75 km from the Strait of Georgia and includes all major tributaries. A continuous record of discharge at Mission from Environment Canada (station 08MH024) is not available. Various linear correlations between reported daily discharge (Q_w) at Mission and Hope (station 08MF005) have been developed, as the station at Hope integrates discharge from the Fraser River basin above the floodplain and has a record extending back to 1912.   A published calibration based only on peak flows between 1965 and 2008 (Northwest Hydraulic Consultants, 2008) reported the correlation: $Q_w^{Mission} = 1.142 * Q_w^{Hope} - 135$ (m^3 s^{-1}). A calibration including the full period of overlap for Hope and Mission records yields the correlation ($r^2 = 0.983$, n = 10,598):

$$Q_w^{Mission} = 1.086 * Q_w^{Hope} + 344 \ (m^3 \ s^{-1}) \tag{1}$$

Total Fraser River discharge can alternatively be estimated by summing measured discharge at Hope with measured discharge from the Harrison River (station 08MG013). This summation estimate shows good overall agreement with the correlation estimate of Eq. 1 ($r^2 = 0.998$, n =

21,991). Because the correlation estimates tend to overestimate baseflow discharge, the

summation estimate of total Fraser discharge has been applied for flux calculations in this study.

Environment Canada gauging data are reported online in real-time and published

annually as historical data after quality control measures—necessary adjustments to rating curves

based on occasional discharge measurements—have been made. Historical data for our Fraser

River sites were only available through 2010. Therefore, discharge data presented here for 2011

are based on real-time data, which have been quality-checked by the authors to ensure that

records do not exhibit discontinuities and are consistent with historical trends. No such issues

were identified, except in the cases of the McGregor River and the Fraser River at McBride. For

these sites, real-time values for 1 January through ~25 April 2011 are erroneously high (2 – 5x

greater than historical average flows during this period). The McGregor and McBride sites

exhibit consistent winter base flow in historical records; therefore, in these cases, an average

base flow value has been applied. This issue is discussed in section 4.4 regarding the modeled

time series.

2.3.4 Load and average concentration estimates

Annual fluxes and discharge-weighted average concentrations of dissolved species were

calculated using the Load Estimator (LoadEst) program developed by the United States

Geological Survey (Runkel et al., 2004). Time series measurements ("quality data") at Fort

Langley and New Westminster between September 2009 and October 2011 were used with

discharge data at Mission ("flow data") as a calibration set. Data files were manipulated using

the LoadRunner program (Booth et al., 2007). Dissolved inorganic elements and isotopes are

characterized with ~80 observations spanning the entire sampling period. Nutrient

concentrations are represented by 66 measurements between March 2010 and October 2011. A smaller number (n = 13) of TA measurements were also made on time series samples, primarily in 2011.

Annual fluxes (loads) of each constituent are presented with uncertainties of one standard deviation for the result of the three annual estimates (2009, 2010, 2011) using the maximum likelihood estimation model. This statistic thus represents a combination of year-to-year variability in fluxes and the uncertainty of calibrating the estimates from uneven sampling distributions (as samples were not collected at regular intervals of time or discharge). Variability in flux from one year to the next is expected, given differences in discharge volume. Though imperfect, the values obtained by weighting a time series record in this manner are much more robust than extrapolations based on the single or seasonal measurements commonly available for river systems.

Average river nutrient concentrations were also calculated from the Global Nutrient Export from WaterSheds (NEWS 2) model dataset (Mayorga et al., 2010). Global dissolved silicon, nitrogen, and phosphorus loads were calculated from the sum of the 5,917 exorheic basins in the dataset (version 1.0, Aug. 2011), yielding fluxes of 143×10^{12} g Si a^{-1}, 22.8×10^{12} g N a^{-1}, and 1.64×10^{12} g P a^{-1}. Actual global exorheic water discharge was calculated from the dataset in the same manner, resulting in a total of 37.9×10^3 km^3 a^{-1}, which is consistent with other literature estimates, e.g. 38.3×10^3 (Fekete et al., 2002), 38.9×10^3 (Peucker-Ehrenbrink et al., 2010). Inorganic nutrient fluxes estimated by the NEWS 2 model for the Fraser River are 68.7×10^9 g Si a^{-1}, 20.5×10^9 g N a^{-1}, and 0.777×10^9 g P a^{-1} for a water flux of 102 km^3 a^{-1}.

2.4 Results

2.4.1 Major and trace elements and nutrients

Concentrations of all dissolved species varied significantly at different sites across the basin, as well as at individual sites at different flow stages (Table 2). Concentrations of dissolved major (HCO_3, Ca, Mg, SO_4, Na, Cl, K) and trace (Sr, Ba) constituents measured at low discharge (fall 2010) are generally slightly higher than those measured at medium (summer 2009) and high (spring 2011) discharge.

Dissolved concentrations and isotope compositions of time series samples are shown in Table 3. This record demonstrates the kinetic-limited weathering behavior of most dissolved elements on the basin-scale (West et al., 2005), with only modest dilution occurring when discharge exceeds base flow (Fig. 3). Discharge-weighted average concentrations and annual fluxes of major and trace elements estimated using LoadEst are shown in Table 4. Differences in total water flux for the three years analyzed (87, 84, and 117 km^3 in 2009, 2010, and 2011, respectively) drive the observed variation in estimated fluxes of dissolved species from year to year. Concentrations reported elsewhere for the Fraser River, and for world average river water, are presented in Table 4 for comparison.

The major element concentrations in Table 4 sum to give an average total dissolved solids concentration of 74 mg L^{-1}. Scaled to the basin area and average annual discharge, this yields a chemical weathering rate of 32 t km^{-2} y^{-1} for the Fraser basin. This is a minimum estimate, as the total Fraser basin area includes the entire Nechako River basin, and a significant portion of the flow of the Nechako is diverted to a different watershed for hydropower production. This diversion causes a ~3% reduction in the total natural Fraser River discharge at Hope (Dorcey, 1991).

A charge balance of major ions (HCO_3, Ca, Mg, SO_4, Na, Cl, K) in Table 2 indicates a slight surplus of positively charged species in nearly all samples (average +4%). The "missing" negative charge ($\sum^{net} > 0$) in most samples is likely derived from organic acids, as proposed by Spence and Telmer (2005). This is especially likely as the most positive $\sum^{net}$ values generally occur in samples collected during the 2011 freshet, when dissolved organic carbon concentrations are likely highest. Missing positive charge ($\sum^{net} < 0$) in some tributary samples during low discharge conditions may result from unaccounted-for cations from hydrothermal (Bridge and Chilcotin rivers) or industrial (Bridge, Quesnel, and Thompson rivers) sources.

In general, concentrations of dissolved nutrients (NO_3+NO_2, NH_4, SiO_2, and PO_4) were highest during the freshet sampling of spring 2011 and lowest during the low-flow sampling of fall 2010 (Table 2). Also striking are variations between different sites within the basin. The Blackwater River, for instance, exhibited consistently higher concentrations of dissolved SiO_2 than all other tributaries during any of the sampling expeditions (>2 times higher than any other site). Tributaries in the upper canyon area (Nechako, Blackwater, Chilcotin) have generally higher dissolved SiO_2 concentrations than the rest of the basin. The upper canyon region also exhibits lower NO_3+NO_2 concentrations than the rest of the basin. The time series records of nutrients show generally counterclockwise hysteresis behavior at discharge conditions above base flow (Fig. 4), cycling between relatively low concentrations during the rising limb of the freshet, followed by higher concentrations during the falling limb.

2.4.2 Isotope composition of spatial tracers

The geologic diversity and hydrologic regime of the Fraser basin lead to such distinct isotope signatures in material carried by the river, that these constituents can be viewed as

"tracers" of particular regions or even specific tributaries. Here we focus on two such tracers: the deuterium composition of water (δD), as a qualitative indicator of the precipitation source of runoff, and the dissolved radiogenic strontium composition (^{87}Sr/^{86}Sr), as a quantitative indicator of the lithological source of dissolved weathering products.

To a first order, the δD composition of precipitation in the Fraser basin is affected by the cumulative fractionation between ^{1}H and ^{2}H (D) of precipitation as air masses originating over the Pacific Ocean migrate inland (Gimeno et al., 2012). Year-to-year variations in the sources of air masses lead to modest variability in the average annual δD composition of precipitation in this region (Liu et al., 2011). The δD composition of precipitation approaching the Fraser basin from the west is approximately −71 ± 9‰, based on monitoring at Victoria, B.C. (48.65 °N, 123.43 °W; IAEA/WMO, 2006). The result of the inland movement of Pacific Ocean moisture is a progressive decrease in the δD values of regions draining the Coast Range to the Cariboo Mountains to the Rocky Mountains, or, roughly, moving upstream. Evaporation may also generate higher δD values in river water relative to precipitation, particularly in relatively arid tributary basins such as the Nechako, Blackwater, Chilcotin, and Thompson Rivers.

The magnitude of the deuterium depletion in the Fraser headwaters relative to the mouth is large, >50‰ between the Pitt River (δD: −95‰) and the Fraser at Fitzwilliam (δD: −150‰) (Fig. 5A). As a larger portion of the basin-integrated runoff is sourced from headwater snowmelt during the spring freshet, the time series record of δD shows a shift towards more negative isotope values at this time of year, and less negative values in fall and winter (Fig. 5B). Large variability in tributary δD composition at different flow stages complicates the interpretation of this cycle. Time series observations of the δD composition of precipitation across the basin would be needed in order to quantitatively model time-varying trends in the basin-integrated

stable isotope composition of the river. The discharge-weighted average compositions of the

Fraser River based on our time series are -126.3 ± 3.7‰ (δD) and -16.63 ± 0.49‰ (δ^{18}O) (±1

s.d.).

Radiogenic ^{87}Sr/^{86}Sr in river systems is primarily influenced by bedrock age, lithology,

and weathering history (Goldstein and Jacobsen, 1987; Peucker-Ehrenbrink et al., 2010; Bataille

and Bowen, 2012). Lithology (with characteristic Rb/Sr composition) and bedrock age

(controlling ingrowth of radiogenic ^{87}Sr from decay of ^{87}Rb) determine the amount of radiogenic

^{87}Sr in the bedrock, and chemical weathering rates determine the specific flux (or yield) of

dissolved Sr from each lithology within a catchment. A basin with easily weathered sedimentary

rock of old age, such as the uppermost catchment of the Fraser in the Yellowhead Lake area, has

a high yield of radiogenic Sr; in contrast, a basin such as the Harrison, composed of young, more

weathering-resistant igneous rock, carries a relatively low yield of less radiogenic Sr.

The correlation between drainage basin bedrock age and riverine dissolved ^{87}Sr/^{86}Sr has

been described for many rivers; the Fraser shares with Himalayan rivers an unusually radiogenic

isotope composition for the average bedrock age of its drainage basin (Peucker-Ehrenbrink et al.,

2010). This likely reflects the strong influence of highly radiogenic lithologies in the headwater

region with Neoproterozoic and Paleozoic (250 – 1000 Ma) strata. The ages of these strata, and

not those of the Meso- and Paleoproterozoic (1000 – 2500 Ma) precursor materials (Armstrong,

1988; Cameron and Hattori, 1997), are used to calculate average bedrock ages. While the

bedrock ages record this rejuvenation, the radiogenic isotope systems were not fully reset

(Peucker-Ehrenbrink et al., 2010; their Fig. 7) and reflect—in part—the time-integrated history

of the older material. Alternatively, old, radiogenic source areas may contribute

disproportionately to the dissolved load, due to differences in mineralogy, hydrology, or other factors.

The diversity of bedrock lithology and spatial variations in precipitation patterns within individual tributary basins are small enough that the ^{87}Sr/^{86}Sr compositions of these basins do not change significantly on a seasonal basis (Fig. 6). Hence, changes in the basin-integrated ^{87}Sr/^{86}Sr signature measured at a downstream site can be interpreted as a response to changes in the relative contributions of constant end-members. The time series record of the basin-integrated ^{87}Sr/^{86}Sr of the Fraser River indicates such a seasonal cycle (Fig. 7). In fall and winter, the ^{87}Sr/^{86}Sr composition is less radiogenic (~0.709), but becomes more radiogenic (~0.714) at the onset of the spring freshet, and remains so through late summer, months after the water flux has returned to near base flow. A secondary discharge peak in early fall is evident in both years of the record, which appears to prolong the radiogenic signature after the freshet has ended.

In addition, the magnitude of the shift from less radiogenic fall/winter ^{87}Sr/^{86}Sr to more radiogenic spring/summer ^{87}Sr/^{86}Sr is not equivalent in both years of the record. The freshet of 2011 was larger with a more rapid onset than that of 2010; however, the change in ^{87}Sr/^{86}Sr was smaller during the 2011 freshet. On a finer temporal scale, this time series record also shows that the period when the balance of radiogenic versus unradiogenic contributions is shifted most strongly towards less radiogenic character is very short (on the order of two weeks). This point was captured by one or two samples in late fall each year; therefore, the true minimum value may have been even lower than what was observed.

Using the LoadEst program, a discharge-weighted ^{87}Sr/^{86}Sr value was calculated by translating the time series record of Sr concentrations and dissolved ^{87}Sr/^{86}Sr values to

concentrations of the individual isotopes [87]Sr and [86]Sr, accounting for changes in the atomic weight of Sr. The discharge-weighted flux of [87]Sr was divided by that of [86]Sr, resulting in a dissolved [87]Sr/[86]Sr value for the Fraser River of 0.7120 (2 s.d. = 0.0003).

2.5 Discussion

2.5.1 Seasonally-integrated flux estimates

The vast majority of flux or average concentration estimates for global rivers are based on very few measurements; many data are decades old and represent a single and often biased portion of the river's hydrograph. The oft-cited global compilation of major element concentrations of Meybeck (1979), for instance, includes discharge-weighted concentrations for only 10 of the world's largest rivers, while the remaining 18 rivers are represented by arithmetic means of 20 or fewer measurements. In the case of the Fraser, the values reported by Meybeck (1979) (which are reproduced in the compilation of Berner and Berner, 1996) derive from three samples during medium and low discharge collected at the city of Mission in 1958-59 (Durum et al., 1960). These data are also the ultimate source of Fraser values reported in a more recent well-known compilation by Gaillardet et al. (1999), based on the GEMS-GLORI database (Meybeck and Ragu, 2012), together with Sr concentration and isotope composition from the study of Cameron et al. (1995). However, the Sr data of Gaillardet et al. (1999) do not correspond to any of the values reported in the Cameron et al. (1995) work, nor to other previously published data (Wadleigh et al., 1985; Cameron, 1996; Cameron and Hattori, 1997). Thus reference to such global compilations should be made cautiously.

Another well-known global compilation from Livingstone (1963) includes major element concentrations for the Fraser and world average river water (Table 4). The Fraser values in this

collection are based on a single sample from December 1938, and correspondingly show higher concentrations of most solutes, as expected for low discharge conditions (winter). A more recent study of the Fraser River by Spence and Telmer (2005) extrapolates measurements at two flow stages to estimate annual fluxes by simply assuming that medium and low flow conditions represent 70% and 30% of total discharge, respectively.

The fact that the discharge-weighted fluxes of all dissolved elements in the Fraser considered here scale proportionally with discharge gives promise for the determination of more accurate flux estimates in rivers with only water flux monitoring, once this relationship has been calibrated. The time series presented here for the Fraser provides a template for the frequency of sampling necessary to capture the variability in a highly dynamic system, which may provide a benchmark for future work in other basins.

2.5.2 Sources of dissolved inorganic material

The predominance of HCO_3, Ca, Mg, and Si in the dissolved load point to the action of silicate and carbonate weathering within the Fraser basin (Fig. 8). Relatively low Na and Cl concentrations (compared to the global average, see Table 4) demonstrate a lack of significant pollution (e.g. pulp and sewage effluent, road salt), inputs from evaporite weathering, or hydrothermal sources. The ratios of major elements in tributaries of the Fraser all fall on a mixing line between carbonate- and silicate-dominated regimes. Main stem sites follow a path from the carbonate towards the silicate end-members moving from the headwaters to the delta. The influence of carbonates is mainly confined to headwater regions, and the silicate lithologies that dominate the remainder of the basin dilute the carbonate signal as water flows downstream. This observation is consistent with the regional geology. Fraser River waters are generally

slightly undersaturated with respect to calcite (Wang et al., in prep). The influence of pulp mill

effluent on Na and Cl concentrations in the Fraser near the confluence with the Nechako River

has been demonstrated (Cameron, 1996); however, this flux is not detectable as far downstream

as our time series location (Spence and Telmer, 2005).

The presence of Cl in unpolluted, evaporite-free river water unaffected by hydrothermal

springs is indicative of the incorporation of sea salt aerosols (so-called cyclic salts) (Meybeck,

1987; Meybeck and Helmer, 1989). The importance of this source of Cl to the Fraser River is

supported by the increase in concentration in the main stem moving from the inland,

mountainous headwaters towards the Pacific Ocean. There may be an additional source of Cl

and other dissolved species from hydrothermal springs in metamorphic lithologies of the Coast

Range, particularly in the Pitt and Harrison rivers (Friele and Clague, 2009), as has been shown

in some catchments of the Himalaya (Galy and France-Lanord, 1999; Becker et al., 2008) and

the Yellowstone River (Hurwitz et al., 2010). Assuming such hydrothermal inputs are negligible

and sea salt aerosols are the sole source of Cl measured at the time series sampling site, the sea

salt aerosol contribution to other dissolved concentrations can be calculated using seawater

elemental ratios to Cl. Applying this calculation to the discharge-weighted average

concentrations in Table 4 shows that sea salt aerosols contribute little ($<3\%$) to the observed

levels of most major ions, with the exception of Na, which is 26% sea salt-derived. The time

series samples show a peak in the sea salt contribution during fall and winter relative to spring

and summer, pointing to an increase in the relative importance of the precipitation source of

dissolved species during low discharge periods. Individual sites with a calculated sea salt

contribution $>100\%$ (such as SO_4 in the Pitt River) suggest additional sources of Cl, such as

hydrothermal springs.

One sample from January 2011 (GRO000117, Table 3) shows a sharp peak in absolute concentrations of most major and some trace solutes, notably excluding Ca, SiO_2, and Ba. Chloride and Na exhibited 157x and 43x enrichments, respectively, over their discharge-weighted average concentrations, while other solutes were 2 – 7x their average values. This is likely due to a pulse of concentrated fluid into the Fraser River near the sampling site (e.g. road salt runoff, sewage overflow, industrial release). The pulse was short-lived, as the following sample (9 days later) shows no elevated concentrations. A road salt source is most likely, as this sample was collected during a significant winter snow storm. Analysis of rainwaters from across the basin and records of road salting would further inform the importance and nature of sea salts to variability of the Fraser River dissolved load.

2.5.3 Global and historical context of current results

Comparing our discharge-weighted concentrations (Table 4) to those in global "average" river water, the Fraser is relatively dilute in many solutes (SiO_2, Na, Cl, NO_3+NO_2, PO_4, and Ba) and typical in others (Ca, Mg, SO_4, K, Sr). In addition to the global average river compilations described above, Table 4 also includes values from recent assessments by Peucker-Ehrenbrink et al. (2010) and Miller et al. (2011), which calculate average river water compositions from a database of observations spatially extrapolated using a large-scale drainage region approach (Graham et al., 1999).

To compare our results to the study of Cameron (1996), which is based on an Environment Canada time series record from 1984 – 1992, we focus on his most downstream main stem sampling site at Hope. It should be noted, however, that our estimates are based on samples collected 100 km further downstream and after the confluence of the Harrison River, a

large tributary (~15% of total discharge) with low concentrations of dissolved material. The

average values reported by Cameron (1996) for Hope are within ±30% of our discharge-

weighted average concentrations. Exceptions include Cl, which is 2 times higher than our

estimate, and NO_3+NO_2, for which our estimate is ~4 times higher. The apparent drop in Cl load

in the Fraser is likely due to changes in organohalide pollution standards for pulp mills in the

basin, which began in 1992. Our comparatively high NO_3+NO_2 concentrations are likely due to

the fact that our sampling site at Fort Langley includes runoff from the Fraser Valley agricultural

region. The variability in nutrient concentrations at different sites across the basin may be due to

a combination of hydrologic processes (surface runoff, groundwater discharge, flushing of soils,

and dilution) and biogeochemical effects (turbulence, light penetration, availability of

micronutrients, and temperature impacts on biological activity). For instance, Cameron (1996)

attributes the pulse of NO_3+NO_2 during the early freshet to mobilization of NO_x aerosols

accumulated in winter snowpack.

Although rich for its length, the Environment Canada record presented by Cameron

(1996) is complicated by the use of different methods over time. Prior to 1990, samples were

filtered (0.45 μm) and analyzed by atomic absorption spectrometry or flame photometry; later

samples were not filtered but subjected to a weak acid leach (termed "extractable") and analyzed

by ICP-emission spectroscopy. Quality analysis by the authors resulted in exclusion of SiO_2 data

predating the change, citing "substantially different results" (Cameron, 1996). Trace element

concentrations (Sr and P) were based on strong acid leaching of unfiltered samples, and also

underwent a change in analytical methods in 1990. It is therefore difficult to compare our data

(from 0.22 μm filtered, unacidified samples) with those that may have elevated solute

concentrations from acid-leaching of suspended sediments. Finally, average concentrations

reported by Cameron (1996) are mean values of regularly spaced samples, which will over-represent low-discharge periods (when concentrations are higher), resulting in higher concentrations than a true discharge-weighted average.

Also shown in Table 4 are concentrations calculated from annual fluxes generated by the global Nutrient Export from Watersheds (NEWS 2) model, developed to estimate regional- and continental-scale nutrient fluxes to the ocean (Dumont et al., 2005; Harrison et al., 2005; Seitzinger et al., 2005; Beusen et al., 2009; Mayorga et al., 2010). Compared to the NEWS-estimated global average concentrations, NEWS-estimated Fraser nutrient concentrations are very low in dissolved inorganic N, P, and Si. It is important to note, however, that the NEWS models are tuned to match large-scale flux estimates. Scaling down to a drainage area the size of the Fraser is likely to lead to large uncertainties. The NEWS nitrogen model also does not distinguish between NO_3/NO_2 and NH_4.

The NEWS-estimated Fraser nutrient concentrations agree rather poorly with our discharge-weighted estimates (showing lower SiO_2 and higher PO_4 and NO_3+NO_2). The NEWS model parameterizes nutrient fluxes based on land uses, including agricultural and urban sources. Our time series sampling location drains only ~60% of the agricultural lands in the Fraser floodplain (Brisbin, 1994), and, importantly, lies entirely upstream of any inputs from the Vancouver metropolitan area. Our measurements may exclude significant inputs of N and P from fertilizer and manure runoff and sewage and stormwater overflow, sources which rival or dwarf natural fluxes in many other rivers (Howarth et al., 1996; Boyer et al., 2006; Shen and Liu, 2008; Alvarez-Cobelas et al., 2009). If inputs in the Vancouver area downstream of Fort Langley account for the discrepancy between the NEWS model nutrient flux estimates and our

discharge-weighted estimates, then urban sources represent ~61% of the dissolved inorganic nitrogen and ~52% of the dissolved inorganic phosphorus fluxes of the Fraser River.

The influence of groundwater seepage on concentrations of dissolved solutes in the Fraser River is unknown and requires further study. However, the large seasonal variation in the δD time series record suggests that groundwater is not a significant source of water (and therefore dissolved material) to the river compared to surface runoff. More data are needed on the seasonal variability in precipitation composition across the basin in order to quantify the importance of this potential source (for example, as demonstrated by Calmels et al., 2011).

Literature values of $^{87}Sr/^{86}Sr$ available for the Fraser River (Table 5) are variable; however, the differences can be understood in the context of the time series presented here. Wadleigh et al. (1985) report a value of 0.71195 for a sample collected in May 1979, and Cameron and Hattori (1997) report 0.712707 for a sample collected in July 1993. These results align well with the values observed in our time series (Fig. 7): ~0.7115 in May, and ~0.7128 in July. A third Fraser River $^{87}Sr/^{86}Sr$ literature value, 0.7188 reported by Allègre et al. (2010), is significantly more radiogenic than all other reported values, and more radiogenic than any individual value observed in our time series record. This value, although cited as unpublished data, likely derives from the dissolved $^{87}Sr/^{86}Sr$ value of 0.718886 reported by both Millot et al. (2003) and Huh et al. (2004) for a Fraser main stem sample (CAN99-21) collected at the city of Prince George. This site is located between our main stem sampling sites of Hansard and Stoner, which exhibited $^{87}Sr/^{86}Sr$ of ~0.719 in our analyses. It therefore appears that the "Fraser" value reported by Allègre et al. (2010) reflects not the entire Fraser River, but merely the upper third of the basin. These observations highlight the danger of assigning single literature values as

representative averages for an entire system, and the importance of seasonal sampling for large river systems such as the Fraser.

2.5.4 *Modeling seasonal variability in dissolved load composition*

The seasonal trend observed in the time series $^{87}Sr/^{86}Sr$ record demonstrates that, although the total Fraser River hydrograph can serve as an indicator of when upstream portions of the drainage basin begin to exert a stronger influence on the composition of the dissolved load, it is not quantitatively informative about the duration or magnitude of this shift. To better elucidate the observed variability in $^{87}Sr/^{86}Sr$ composition in the time series record, we have constructed a model to predict the composition at the Fort Langley site based on chemical and hydrological inputs upstream. The model is an isotope mixing equation, which sums the contributions of eight major tributary basins (Thompson, Nechako, Harrison, Quesnel, Chilcotin, McGregor, Blackwater, and the Fraser upstream of McBride) to the main stem of the Fraser. For each basin, we applied a single value of Sr concentration, $^{87}Sr/^{86}Sr$ composition, and daily discharge from Environment Canada online real-time records. Discharge for each model day represents a 7-day running average, i.e. the mean of the daily discharge values for the 7 day period centered on a given model day. The equation has the form:

$$R_{mix} = \frac{\sum_i (R_i C_i Q_i)}{\sum_i (C_i Q_i)}$$

(2)

where R is the $^{87}Sr/^{86}Sr$ composition, C_i is the Sr concentration, and Q_i is the water flux of tributary *i*. We have assumed that the Sr concentration and $^{87}Sr/^{86}Sr$ composition for each tributary are invariant, and that changes in the atomic weight of strontium, groundwater

contributions (e.g. Calmels et al., 2011), and water abstractions can be neglected. Differences in Sr concentration for tributaries were somewhat variable during the three sampling campaigns (Fig. 9); however, the differences did not follow a pattern suggesting dilution at different flow stages. We therefore chose to use the average Sr concentration from the three flow stages. As shown earlier (Fig. 6), the $^{87}Sr/^{86}Sr$ composition of these tributaries was essentially constant at low, medium, and high flow. These approximations are appropriate for the purposes of this model; lacking time series measurements on individual tributaries, attempting to interpolate seasonality in these properties could lead to spurious results.

Due to irregularities in certain portions of Environment Canada real-time discharge records, we chose to adjust discharge values for specific periods. For the McGregor River and Fraser at McBride gauging stations (Environment Canada stations 08KB003 and 08KA005, respectively), real-time data for January – April 2011 are abruptly and extremely high, inconsistent with the ~60-year historical records at these sites. For the purposes of our model, we applied a constant discharge of 35 m^3 s^{-1} for both sites, which is consistent with historical winter base flow. The timing of the transition from base flow to freshet (which is rapid at both sites) is difficult to constrain, which may generate a discontinuity in modeled $^{87}Sr/^{86}Sr$ during the early freshet period in 2011.

The model clearly captures the observed seasonal shift between relatively radiogenic and unradiogenic $^{87}Sr/^{86}Sr$ composition, both in timing and magnitude (Fig. 10). Shorter timescale changes are also apparent, most notably the dip towards a less radiogenic signature in late summer, before the return to more radiogenic values during the secondary fall discharge peaks in 2009 and 2011. Overall the seasonal trends predicted by the model match the time series observations.

There are, however, notable divergences between the model and the measured ^{87}Sr/^{86}Sr

values. Two main disparities stand out: the model is at nearly all times more radiogenic than the

measured values, and the offset between the model and the observations is systematically larger

at certain times of year. The first issue, regarding a bias in the spatial representativeness of the

modeled tributaries is addressed in Figure 11, which shows the percentage of the total water flux

characterized by our modeled tributaries. The times of year when the model captures the greatest

fraction of the total discharge is during the spring freshet and summer, when ^{87}Sr/^{86}Sr is most

radiogenic. During late fall and winter, the model gradually loses predictive power as a smaller

portion of the discharge falls inside the window of the monitored gauging stations (as little as

40%). This is related to the second issue of the consistently radiogenic bias of the model, in that

upstream subdrainage basins exert more influence during the spring and summer months than

during late fall and winter; thus, the larger fraction of uncharacterized discharge during fall and

winter may also have a less radiogenic signature than that during spring and summer. In

addition, the model captures less of the actual discharge during the 2011 freshet than during the

2010 freshet, which may explain the greater offset between our model and observations in 2011

versus 2010.

To address these issues, we consider that the eight modeled tributaries do not constitute

the entire drainage basin, and appear to be consistently biased towards a more radiogenic subset

of the total discharge. Accounting for the hundreds of very small basins which comprise the

remaining 10 to 60% of the total discharge with additional measurements of ^{87}Sr/^{86}Sr and water

flux is an unrealistic goal. However, it is clear that the model tends to be biased towards more

radiogenic contributions. Assuming that the unradiogenic portions of the basin contribute the

entirety of the "missing" component in our model, we can add such a component to account for

the uncharacterized fraction of the total discharge. Tributaries contributing Sr with a less radiogenic signature are represented by basins draining the Coast Range: Nechako, Blackwater, Chilcotin, Bridge, Harrison, and Pitt Rivers. These tributaries have consistently less radiogenic $^{87}Sr/^{86}Sr$ (0.7043 – 0.7049) and low Sr concentration (0.13 – 0.81 µmol L^{-1}). Applying a Sr concentration of 0.45 µmol L^{-1} and $^{87}Sr/^{86}Sr$ composition of 0.7046 to the unmonitored basins results in a modified model shown in Figure 12. The discharge of the missing component is calculated as the difference between total Fraser River discharge and the sum of the discharges of each modeled tributary. The addition of this missing component aligns the model much more closely with the observed $^{87}Sr/^{86}Sr$ values throughout the record, suggesting that the Coast Range is the source of nearly all of the uncharacterized Sr flux in the basin. This conclusion is supported by the fact that tributary basins in the lower portions of the watershed (mainly draining the Coast Range) experience more significant secondary fall discharge peaks than basins draining the upper portions of the watershed.

There are still points where the modified model and the measured values diverge. In the first months of 2010, as the measured $^{87}Sr/^{86}Sr$ begins to rise after its fall 2009 minimum, the modified model predicts a longer persistence of less radiogenic values than is observed in the samples (Fig. 12). The points where the modified model predicts the least radiogenic values correspond to brief discharge peaks. This may be due to the fact that these winter peaks contain a significant flux from radiogenic portions of the basin in addition to the unradiogenic flux assumed for the missing component. In contrast, the recovery from the minimum $^{87}Sr/^{86}Sr$ in early 2011 shown by the modified model matches the observed values much more closely. There appear to have been fewer large discharge pulses during this period in 2011 than in 2010, and the assumption of a missing component made of exclusively unradiogenic Sr is more

appropriate for 2011. The divergence between the modified model and measured values at the onset of the 2011 freshet is likely related to our imprecise estimates of discharge for the McGregor and McBride drainages during the transition between base flow and freshet conditions.

An alternative approach to this type of analysis is to define the composition of end-members and solve for their relative contributions through time. For instance, Calmels et al. (2011) modeled the relative contributions of various reservoirs (slow and rapid surface runoff and deep groundwater) within the Liwu River in Taiwan during a typhoon event. Their analysis found a consistent offset to less radiogenic $^{87}Sr/^{86}Sr$ values of the model relative to measured values, attributed to unrepresentative characterization of deep groundwater. Our Sr model assumes that the contribution of each source (tributary flux) is known, and the ability of the modeled $^{87}Sr/^{86}Sr$ to predict the observed values indicates that these sources do represent the major contributors to the total dissolved load of the Fraser. The calculated composition of the uncharacterized portion of the discharge suggests additional sources with, on average, composition similar to that of Coast Range tributaries.

Despite the apparently better agreement between the modified model curve shown in Figure 12 and the original curve in Figure 10, assuming an entirely Coast Range-like composition for the missing discharge overcompensates for the radiogenic bias of the original model. Figure 13A compares the results of the two models to the measured time series values. The magnitude of the less radiogenic offset of the modified model is nearly as large as the more radiogenic offset of the original model. By adjusting the $^{87}Sr/^{86}Sr$ composition of the missing discharge component, we can estimate the composition necessary to bring the modified model closest to 1:1 agreement with the measured time series values. The best agreement (determined

as the minimum residual sum of squares, i.e. the sum of the squared difference between each measured time series value and the model estimate for the same day) occurs at $^{87}Sr/^{86}Sr = 0.7080$ with the residual sum of squares $= 5.5 \times 10^{-5}$ (Fig. 13B). Assuming this composition is the product of a binary mixture of a radiogenic Rocky Mountain endmember with $^{87}Sr/^{86}Sr = 0.7285$ and an unradiogenic Coast Range endmember with $^{87}Sr/^{86}Sr = 0.7046$ (based on our measurements of tributaries in these regions), we estimate that the missing strontium is derived of ~14% Rocky Mountain material and ~86% Coast Range material. In reality, these proportions represent sources from across the basin and likely fluctuate throughout the year. This complexity cannot be resolved without more detailed spatial and temporal discharge data.

2.5.5 Fraser River dissolved fluxes in global context

It is noteworthy that the effect of runoff in the Fraser basin is to bias the dissolved load towards contributions from older lithologies. Using the same construction as the model described above, an "area-based" prediction of the basin-integrated average bedrock age has the form:

$$BA_{basin} = \frac{\sum_i (BA_i A_i)}{\sum_i A_i} \tag{3}$$

where BA is the average bedrock age and A is the area of a given subdrainage basin. Since digital bedrock maps are available at reasonably high resolution (1:5,000,000) for this basin (Wheeler et al., 1997), the true average bedrock age of the Fraser basin is well constrained at 260 $\pm$ 39 Ma (Peucker-Ehrenbrink et al., 2010). Using only the eight modeled tributaries in Eq. 3, the area-based estimate is very similar: 280 Ma. If the true average bedrock age for the entire

basin is assumed to be 260 Ma, then the 24% of the drainage area not included in our model

(62,000 km^2) has an average bedrock age of 171 Ma. This supports the conclusion of the

^{87}Sr/^{86}Sr model, which shows a disproportionate contribution from portions of the basin draining

older, more radiogenic lithologies.

The area-based formulation can be modified to use discharge as follows:

$$BA_{basin} = \frac{\sum_i (BA_i Q_i)}{\sum_i Q_i}$$

(4)

where Q_i is the total annual average discharge for an individual tributary (Table 1). Applying

Eq. 4 to the eight modeled tributaries predicts a much older basin-integrated average bedrock age

of 356 Ma. Hence the runoff regime and weathering rates in the Fraser River have the effect of

drawing a disproportionate fraction of dissolved material from subbasins with older bedrock

lithologies. This is the opposite offset to what is observed for global exorheic continental runoff,

for which the area-average bedrock age is 453 Ma, while the discharge-weighted average age is

394 Ma (Peucker-Ehrenbrink et al., 2010). The headwater regions of the Fraser basin, with

bedrock composed mainly of old (>600 Ma) sedimentary rock, are distinct from global average

sedimentary rock, which is generally young, 246 ± 42 Ma; while global average volcanic rock is

slightly older, 331 ± 52 Ma (Peucker-Ehrenbrink and Miller, 2007). The offset between

discharge- and area-weighted bedrock age, both in the Fraser basin and globally, thus appears to

reflect the generally higher chemical weathering rate of sedimentary rocks compared to volcanic

rocks (Meybeck, 1987; Gaillardet et al., 1999). Given that the headwater regions with the oldest

lithologies in the Fraser basin also correspond to the most easily weathered rock types, this

portion of the Fraser basin also exerts the dominant control on atmospheric CO_2 consumption by

chemical weathering (Amiotte Suchet et al., 2003). The older discharge-weighted bedrock age

of the Fraser basin underscores the importance of headwater snowmelt and bedrock distribution to weathering processes in this river, despite year-round high runoff in regions draining the Coast Range. Large river basins such as the Fraser, which reach inland far past the young lithologies of active margins, have a fundamentally different impact on riverine fluxes to the ocean compared to small mountainous watersheds lining the periphery of active continental margins.

2.6 Conclusions

The exceptional diversity of bedrock lithology and seasonal hydrology in the Fraser River basin are reflected in the geochemical signatures of its tributaries and their variable admixtures. The basin-wide and time series characterizations of dissolved inorganic species in the Fraser River presented here show that:

- Concentrations of most dissolved elements derive from natural weathering processes, with the exception of Cl and Na, which are sourced largely from sea salt aerosols.

- Isotope tracers of water (δD) and dissolved weathering products ($^{87}Sr/^{86}Sr$) serve as source indicators for distinct portions of the drainage basin. The dynamic range of dissolved $^{87}Sr/^{86}Sr$ between tributaries allows this tracer to serve as a geochemical fingerprint of specific regions across the basin.

- A mixing model of $^{87}Sr/^{86}Sr$ demonstrates that the time series records a seasonal shift in source material. Less radiogenic-dominated runoff (representing the Coast Range tributaries) in fall and winter transitions to substantial radiogenic contributions (deriving from headwater subbasins) in spring and summer.

- The discharge-weighted average bedrock age of the Fraser River is significantly older than the basin area-weighted average, demonstrating the dominance of old sedimentary lithologies to the chemical weathering flux of this basin.

Since the bulk of water, and thus elemental, flux occurs during spring and summer snowmelt, the overall composition of material exported to the ocean by the Fraser River is weighted disproportionately to material derived from the most upstream portions of the drainage basin. This spatial bias has important implications for understanding signals recorded in the chemistry of large rivers and sedimentary deposits influenced by such systems. In modern settings, awareness of the relative importance of different portions of a drainage basin to the overall chemical load is necessary for identifying lithologic and biogeoclimatic zones driving weathering fluxes. Furthermore, when large river-dominated sedimentary records are probed for signs of past changes in weathering activity and terrestrial climate, a deeper knowledge of spatial heterogeneity in weathering across the river basin is critical.

Site	IGSN	Date (yyyy-mm-dd)	Lat (°N)	Lon (°W)	Distance from source (km)	Elevation (masl)	Average precipitation (mm a^{-1})	Upstream drainage area (km^2)	Average bedrock age (Ma)	Average discharge (km^3 a^{-1})
Fraser at Fitzwilliam	GRO000009	2009-08-03	52.8526	118.6063	50	1,085	594	672	764	1.4
	GRO000027	2010-10-14								
	GRO000073	2011-06-03								
Fraser at McBride	GRO000011	2009-08-04	53.3023	120.1411	230	713	679	6,907	738	6.2
	GRO000030	2010-10-14								
	GRO000070	2011-06-02								
Fraser at Hansard	GRO000012	2009-08-04	54.0817	121.8462	480	604	644	18,088	700	14.5
	GRO000038	2010-10-16								
	GRO000066	2011-06-01								
Fraser at Stoner	GRO000018	2009-08-08	53.6384	122.6652	615	550	641	80,731	345	
	GRO000041	2010-10-19								
Fraser at Lillooet	GRO000022	2009-08-10	50.7080	121.9132	1050	200	330	152,364	254	54.7
	GRO000045	2010-10-21								
	GRO000058	2011-05-28								
Fraser at Lytton	GRO000008	2009-08-01	50.2479	121.5910	1110	145	433	156,342	251	
	GRO000047	2010-10-22								
Fraser at Hope	GRO000048	2010-10-24	49.3893	121.4557	1210	34	2,008	216,561	281	85.6
	GRO000055	2011-05-27	49.3817	121.4486						
Fraser at Fort Langley	GRO000001	2009-07-30	49.1801	122.5672	1315	3	1,789	228,776	274	
	GRO000025	2009-08-13								
	GRO000051	2010-10-25								
	GRO000076	2011-06-07								
Fraser at Vancouver	GRO000002	2009-07-28	49.2145	122.7829	1336	1	1,708	228,993	274	99.6
	GRO000052	2010-10-27								
	GRO000075	2011-06-06								
Yellowhead Lake	GRO000028	2010-10-14	52.8515	118.6027	49	1,086	594	132	768	
Robson River	GRO000010	2009-08-03	53.0506	119.2138	125	835	594	181	556	
	GRO000029	2010-10-14								
	GRO000074	2011-06-03								
Small River	GRO000031	2010-10-15	53.0602	119.6139	185	756	631	252	732	
	GRO000072	2011-06-02								
Holmes River	GRO000032	2010-10-15	53.2518	120.0289	223	725	631	803	752	
	GRO000071	2011-06-02								
Dore River	GRO000033	2010-10-15	53.3221	120.2251	235	725	679	412	770	0.4
	GRO000069	2011-06-02								

River	ID	Date	Lat	Long						
Goat River	GRO000034	2010-10-15	53.4946	120.6060	265	717	679	658	770	
	GRO000068	2011-06-02								
Bowron River	GRO000014	2009-08-05	53.8971	121.9869	478	708	601	3,168	530	
	GRO000035	2010-10-15								
	GRO000062	2011-05-31								
McGregor River	GRO000013	2009-08-05	54.2202	121.9020	500	606	601	5,463	672	6.8
	GRO000037	2010-10-16								
	GRO000065	2011-06-01								
Willow River	GRO000015	2009-08-06	54.0678	122.4675	555	582	644	3,157	324	1.1
	GRO000036	2010-10-15								
	GRO000063	2011-05-31								
Nechako River	GRO000016	2009-08-06	53.9265	122.7379	575	570	496	47,148	183	8.8
	GRO000039	2010-10-17								
	GRO000064	2011-05-31								
Blackwater River	GRO000019	2009-08-08	53.2891	123.1380	705	624	511	11,865	49	1.1
	GRO000040	2010-10-18								
	GRO000061	2011-05-30								
Quesnel River	GRO000020	2009-08-09	52.9725	122.4935	770	472	693	12,100	429	7.4
	GRO000042	2010-10-19								
	GRO000060	2011-05-30								
Chilcotin River	GRO000021	2009-08-09	51.8307	122.5718	805	448	338	19,595	61	3.2
	GRO000043	2010-10-20								
	GRO000059	2011-05-29								
Bridge River	GRO000023	2009-08-10	50.7513	121.9339	1,045	208	519	4,748	155	
	GRO000044	2010-10-21								
	GRO000057	2011-05-28								
Thompson River	GRO000007	2009-08-01	50.2367	121.5315	1,111	145	279	55,616	381	24.4
	GRO000046	2010-10-22								
	GRO000056	2011-05-27	50.3461	121.3902						
Harrison River	GRO000006	2009-07-31	49.2361	121.9621	1,265	10	1,755	8,397	151	14.0
	GRO000049	2010-10-24								
	GRO000054	2011-05-26								
Pitt River	GRO000024	2009-08-13	49.3496	122.6162	1,335	5	2,253	1,134	127	
	GRO000050	2010-10-25								
	GRO000053	2011-05-26								

Table 1. Sampling campaigns of the Fraser River main stem and tributaries were carried out in summer 2009 (28 Jul – 13 Aug), fall 2010 (14 – 27 Oct), and spring 2011 (26 May – 7 Jun). International Geo Sample Number (IGSN) codes refer to an open online database of archived metadata (www.geosamples.org). Elevations are shown in meters above sea level (masl). Average precipitation is compiled from Environment Canada National Climate Data and Information Archive records for 1971 – 2000 (climate.weatheroffice.gc.ca) for weather stations corresponding to our sampling sites. Average discharge values for gauged tributaries represent the means for all years of Environment Canada records. These records range from 36 years (Willow River) to 100 years (Fraser at Hope). Site coordinates were determined in the field with a handheld GPS (Garmin, WGS 1984 datum). Note that, in some sources, the Blackwater River is referred to as the West Road River.

Site	IGSN	Flow Stage	NH_4	SiO_2	PO_4	NO_3+NO_2	TA	Ca	Mg	Na	SO_4	Cl	K	Sr	Ba	$\sum_{ex}^{+}$ (%)	$^{87}Sr/^{86}Sr$ diss.	δD (‰)	$δ^{18}O$ (‰)
Fraser at Fitzwilliam	GRO000027	low	0.41	58	0.11	2.2	813	362	308	34.5	255	6.8	5.75	0.789	0.071	1.9	0.75152	-146.4	-19.14
	GRO000009	med					537	229	211	21.9	176	2.9	4.70	0.547	0.051	0.8	0.75150	-145.1	-19.09
	GRO000073	high	0.14	46	0.19	2.9	679	256	209	30.1	148	8.5	4.17	0.541	0.038	-1.0	0.74884	-155.8	-20.55
Fraser at McBride	GRO000030	low	0.33	31	0.07	2.5	1104	495	205	37.4	208	8.1	15.13	1.606	0.066	-2.5	0.72686	-143.4	-18.77
	GRO000011	med					730	352	114	16.3	110	4.0	10.48	0.955	0.029	0.3	0.72480	-148.8	-19.70
	GRO000070	high	0.33	41	<0.05	8.4	867	462	173	30.8	121	4.8	10.72	1.383	0.049	8.3	0.72738	-153.6	-20.30
Fraser at Hansard	GRO000038	low	0.36	86	<0.05	1.1	1936	697	244	64.9	67	10.8	16.75	1.370	0.205	-2.9	0.71598	-132.2	-17.06
	GRO000012	med					1110	495	156	28.7	116	2.6	12.38	1.236	0.070	-0.1	0.72250	-145.5	-19.20
	GRO000066	high	0.31	51	<0.05	8.4	1033	551	163	31.5	80	4.4	9.21	1.337	0.070	10.2	0.71583	-147.8	-19.54
Fraser at Stoner	GRO000041	low	0.70	40	<0.05	2.9		538	197	140.7	131	28.5	14.04	1.317	0.108		0.71928	-135.3	-17.54
	GRO000018	med					977	410	140	79.0	78	14.1	12.96	0.909	0.083	-1.9	0.71704	-137.3	-17.68
Fraser at Lillooet	GRO000045	low	0.61	84	<0.05	3.3		465	179	148.2	135	22.2	16.05	1.257	0.097		0.71639	-120.7	-12.93
	GRO000022	med						426	137	92.7	86	13.0	15.20	0.998	0.084		0.71496	-137.9	-17.69
	GRO000058	high	0.47	99	0.11	5.9	1040	476	166	96.3	42	12.8	19.85	1.054	0.090	10.3	0.70440	-143.2	-18.61
Fraser at Lytton	GRO000047	low	0.38	48	<0.05	2.8		501	195	157.1	125	19.4	18.08	1.224	0.095		0.71529	-134.8	-17.35
	GRO000008	med					968	425	134	81.9	83	9.0	14.58	0.990	0.086	3.0	0.71530	-138.6	-17.91
Fraser at Hope	GRO000048	low	0.54	55	<0.05	2.9		459	171	144.8	111	22.0	18.83	1.132	0.092		0.71503	-132.9	-17.26
	GRO000055	high	0.30	97	0.15	6.3	755	362	114	91.4	41	20.9	16.80	0.769	0.083	10.5	0.71090	-129.5	-17.12
Fraser at Fort Langley	GRO000051	low	0.93	55	<0.05	5.5	983				102	21.8		1.029	0.090		0.71381	-128.5	-16.51
	GRO000001	med					832	486	147	110.0	78	18.5	21.88	0.897	0.092	16.3	0.71380	-133.7	-17.38
	GRO000076	high	0.29	95	0.13	4.9	849	344	113	80.6	49	15.5	16.92	0.852	0.100	2.5		-136.0	-17.83
Fraser at Vancouver	GRO000052	low	1.10	53	0.43	7.3											0.70467		
	GRO000002	med					693	420	116	94.7	66	15.1	18.74	0.751	0.082	17.2	0.71340	-125.1	-16.45
Yellowhead Lake	GRO000028	low	0.39	52	0.08	0.9		438	478	49.8	249	15.7	4.96	0.906	0.049		0.74540	-146.4	-18.92
Robson River	GRO000029	low	0.30	14	0.11	4.4	1411	535	245	15.9	117	4.6	4.70	2.373	0.159	-2.1	0.71144	-129.3	-14.67
	GRO000010	med					1219	515	183	9.5	71	43.3	3.94	1.834	0.121	0.1	0.71110	-142.4	-17.95
	GRO000074	high	0.18	24	<0.05	6.6	1593	661	318	19.0	108	5.7	5.06	2.757	0.182	4.4	0.71179	-150.8	-20.04
Small River	GRO000031	low	0.35	49	0.07	6.0		634	236	31.9	253	1.9	5.30	1.355	0.029		0.72865	-145.6	-19.15
	GRO000072	high	1.07	41	0.22	10.7		578	176	25.7	122	2.0	5.34	1.079	0.025		0.72877	-138.8	-15.72
Holmes River	GRO000032	low						488	217	48.1	205	5.5	4.80	1.790	0.054		0.73216	-141.5	-18.66
	GRO000071	high	0.32	41	0.05	4.3		374	148	31.4	92	2.5	4.49	1.189	0.031		0.73229	-153.7	-20.23
Dore River	GRO000033	low	0.35	44	0.07	6.8		575	199	29.8	233	1.3	4.43	2.535	0.012		0.73008	-138.5	-18.29
	GRO000069	high	0.44	34	<0.05	14.7		453	129	22.0	90	2.3	4.50	1.733	0.011		0.72960	-143.9	-17.62
Goat River	GRO000034	low	0.34	57	0.07	5.9		704	177	38.6	181	6.8	2.81	2.615	0.022		0.71766	-136.9	-17.82
	GRO000068	high	0.45	45	0.21	10.7		695	139	31.1	81	6.7	2.77	2.224	0.015		0.71620	-142.7	-18.51
Bowron River	GRO000035	low	0.34	69	0.06	<0.05		641	139	34.6	36	3.6	5.39	1.650	0.213		0.71343	-133.8	-17.24

River	Sample	Level																	
	GRO000014	med					1624	714	160	37.7	33	3.1	5.57	1.608	0.223	2.8	0.71350	-135.7	-17.58
	GRO000062	high	0.46	66	<0.05	2.2	1029	516	101	25.1	14	2.5	5.17	1.204	0.074	8.8	0.71293	-141.3	-18.26
McGregor River	GRO000037	low	0.32	49	0.08	5.0	1647	590	203	26.7	57	4.9	5.57	0.785	0.100	-4.3	0.71999	-129.7	-17.02
	GRO000013	med					1402	566	155	16.4	43	3.0	4.28	0.612	0.075	-0.9	0.71860	-141.1	-18.75
	GRO000065	high	0.27	30	0.22	8.4	1098	507	156	14.2	20	3.1	4.42	0.528	0.057	8.3	0.72161	-148.5	-19.65
Willow River	GRO000036	low	0.23	130	<0.05	<0.05	1019	365	129	56.1	33	9.7	8.02	0.793	0.142	-2.0	0.71434	-110.9	-10.83
	GRO000015	med					1161	443	161	72.2	29	7.9	11.92	0.908	0.152	2.6	0.71340	-133.7	-16.91
	GRO000063	high	0.08	88	0.17	0.4	462	262	86	40.9	13	5.0	9.62	0.500	0.063	20.4	0.70532	-142.8	-18.66
Nechako River	GRO000039	low	0.31	92	0.27	<0.05		349	169	109.3	49	8.5	17.84	0.873	0.130		0.70511	-130.4	-15.94
	GRO000016	med					779	287	113	83.6	34	6.0	13.13	0.644	0.094	2.4	0.70500	-130.0	-15.96
	GRO000064	high	0.06	97	0.11	0.1	819	355	168	140.3	34	10.5	26.46	0.920	0.118	14.9	0.72019	-134.5	-16.49
Blackwater River	GRO000040	low	0.33	295	0.24	2.3	1553	320	291	227.8	15	9.6	50.95	0.748	0.047	-3.0	0.70438	-135.5	-16.50
	GRO000019	med					1738	398	377	257.7	15	7.4	57.95	0.915	0.059	2.5	0.70446	-137.6	-16.75
	GRO000061	high	<0.05	269	0.15	0.8	948	284	242	177.2	10	9.8	52.46	0.615	0.073	13.5	0.71297	-144.7	-18.32
Quesnel River	GRO000042	low					1056	428	97	36.3	80	4.1	8.95	1.555	0.056	-5.4	0.71487	-135.5	-17.53
	GRO000020	med					986	456	93	35.7	73	3.1	9.83	1.533	0.050	0.4	0.71476	-138.0	-17.79
	GRO000060	high	0.14	52	<0.05	7.4	1093	557	132	49.3	53	16.6	11.77	1.575	0.074	8.4	0.70481	-141.0	-18.31
Chilcotin River	GRO000043	low	0.19	78	<0.05	<0.05	710	227	99	103.1	70	7.7	19.35	0.661	0.060	-5.0	0.70426	-138.5	-17.72
	GRO000021	med					525	218	58	66.8	63	4.9	18.10	0.538	0.047	-1.5	0.70416	-138.9	-17.82
	GRO000059	high	0.06	228	1.34	0.8	1365	392	349	274.0	48	10.4	55.78	1.010	0.079	10.4	0.71396	-147.0	-18.73
Bridge River	GRO000044	low	0.47	92	0.06	1.2	1688	428	412	120.8	179	16.5	15.04	1.427	0.098	-6.4	0.70482	-140.6	-18.44
	GRO000023	med					1315	381	350	103.8	132	15.5	16.47	1.094	0.080	-0.4	0.70481	-138.9	-18.24
	GRO000057	high	0.36	132	0.08	5.7		516	365	154.0	124	16.2	18.52	1.642	0.082		0.71225	-141.2	-18.61
Thompson River	GRO000046	low	0.35	70	0.06	4.1	721	287	81	88.9	94	19.4	20.09	0.853	0.065	-4.7	0.71267	-132.6	-17.17
	GRO000007	med					642	287	68	70.0	71	15.4	19.04	0.801	0.057	0.0	0.71290	-135.6	-17.76
	GRO000056	high	0.97	111	0.19	3.7	769	359	119	122.4	64	19.0	26.71	0.929	0.075	9.4	0.70448	-136.2	-17.68
Harrison River	GRO000049	low	8.19	57	0.18	2.2	371	156	35	54.8	45	13.8	16.66	0.334	0.072	-2.3	0.70437	-113.1	-15.16
	GRO000006	med					306	156	27	55.6	51	15.4	14.89	0.318	0.064	1.3	0.70410	-113.7	-15.39
	GRO000054	high	0.51	82	0.22	4.0	304	165	32	59.0	46	11.0	17.62	0.345	0.079	7.3	0.71068	-111.1	-15.11
Pitt River	GRO000050	low	0.82	11	<0.05	4.3		53	9	28.7	15	9.5	7.12	0.126	0.034		0.70483	-94.5	-13.07
	GRO000024	med						54	9	25.5	19	11.2	7.47	0.131	0.033		0.70465	-98.7	-13.44
	GRO000053	high	1.10	40	0.16	4.9	98	65	11	39.3	16	15.6	6.87	0.143	0.038	15.5	0.70424	-93.9	-13.14
Int. Precision			9.7%	1.5%	11.3%	2.4%	0.2%	2.1%	2.5%	2.6%	0.6%	1.4%	2.6%	2.0%	2.2%		0.000008	0.1	0.03
Ext. Precision				3.5%	6.3%	4.0%	0.03%	3.8%	6.3%	1.9%	0.5%	0.5%	4.3%	2.4%	3.6%		0.000020	0.3	0.02
Accuracy							0.3%	5.2%	4.1%	1.6%			0.8%	1.1%	5.7%		0.000042	1.0	0.07

Table 2. Samples were collected at three flow stages: low (fall 2010), medium (summer 2009), and high/freshet (spring 2011). All dissolved solute concentrations are defined as material passing through a 0.22 μm filter and shown in units of μmol L^{-1}. $\sum_{ex}^{+}$ is the excess positive charge as a percent of the total ionic charge of major ions. The final rows show the average precision and accuracy of each measurement. Internal precision indicates the average standard deviation of a single measurement; external precision indicates the uncertainty of certified values of international standard reference materials. Accuracy for cation concentrations (Ca, Mg, Na, K, Sr, Ba) indicates the difference between concentrations determined from dilution curves of two different standards: SLRS-5 (National Research Council Canada) and NIST 1640a (U.S. National Institute of Standards and Technology). For total alkalinity (TA), accuracy indicates the average error given a 2 μmol L^{-1} measurement uncertainty. For $^{87}Sr/^{86}Sr$, $\delta^{18}O$, and δD, accuracy indicates the average absolute difference between certified and measured values of standard reference materials.

IGSN	Date	Site	Discharge at Mission ($m^3\ s^{-1}$)	NH_4	SiO_2	PO_4	NO_3+NO_2	TA	Ca	Mg	Na	SO_4	Cl	K	Sr	Ba	$^{87}Sr/^{86}Sr$ diss.	δD (‰)	δ¹⁸O (‰)
GRO000001	2009-07-30	FL	4,694					832	486	147	110	78	18.5	21.9	0.897	0.092	0.71380	-133.7	-17.38
GRO000025	2009-08-13	FL	3,416					811	344	101	83	77	16.8	17.6	0.833	0.085	0.71284	-130.4	-17.15
GRO000077	2009-09-17	FL	2,034						382	124	102	90	19.1	19.1	0.893	0.088	0.71340	-128.5	-16.81
GRO000078	2009-10-17	FL	1,410						351	124	117	94	30.6	21.8	0.814	0.094	0.71223	-115.3	-15.21
GRO000079	2009-10-31	NW	1,926						220	81	106	61	45.4	17.6	0.528	0.061	0.71101	-101.9	-13.93
GRO000080	2009-11-29	NW	2,210						199	63	97	50	41.8	15.9	0.465	0.061	0.70929	-97.7	-13.51
GRO000081	2010-01-26	FL	1,338						405	146	156	93	46.6	22.2	0.921	0.104	0.71051	-120.8	-15.80
GRO000082	2010-02-23	FL	1,015						447	183	214	112	50.5	26.8	1.031	0.113	0.71039	-121.2	-15.99
GRO000083	2010-03-09	FL	1,122	2.16	122	0.17	10.0		454	177	195	114	52.0	24.5	1.062	0.114	0.71041	-121.4	-15.78
GRO000084	2010-03-30	FL	1,842	1.16	78	0.27	1.7		419	163	166	93	41.5	24.7	0.968	0.109	0.71090	-121.6	-15.80
GRO000085	2010-04-13	FL	1,474	2.14	118	0.18	6.6		435	167	165	88	42.8	24.0	0.995	0.112	0.71075	-124.3	-16.27
GRO000086	2010-05-07	FL	2,958	0.98	117	0.13	5.3		403	142	120	71	28.4	20.5	0.920	0.096	0.71201	-126.5	-16.42
GRO000087	2010-05-21	FL	5,053	0.76	97	0.08	6.9		349	118	107	63	18.7	18.1	0.806	0.090	0.71125	-126.7	-16.65
GRO000088	2010-05-21	NW	5,053						301	101	99	57	19.9	17.2	0.696	0.081			
GRO000089	2010-05-28	FL	5,089	0.91	99	0.06	7.6		368	113	90	64	16.0	17.5	0.855	0.085	0.71284	-131.1	-17.06
GRO000090	2010-06-04	FL	5,769	0.37	94	0.07	5.3		327	99	80	59	15.4	16.6	0.760	0.079	0.71167	-125.6	-16.12
GRO000091	2010-06-04	NW	5,769	0.82	88	0.09	6.3		301	95	82	57	17.7	16.0	0.699	0.075		-123.4	-16.25
GRO000092	2010-06-11	FL	6,143	0.28	92	0.05	1.9		307	86	67	53	11.0	13.5	0.747	0.076	0.71219	-129.1	-17.01
GRO000093	2010-06-11	NW	6,143	0.93	92	0.08	5.8		302	91	82	59	16.8	16.1	0.730	0.074		-125.2	-16.57
GRO000094	2010-06-18	FL	6,583	0.32	84	0.06	1.7		335	101	73	66	10.5	14.9	0.794	0.077	0.71268	-130.2	-17.05
GRO000095	2010-06-18	NW	6,583	0.41	84	0.06	3.7		314	97	75	58	10.8	15.7	0.756	0.076		-128.5	-16.84
GRO000097	2010-07-09	FL	5,491	0.44	84	0.06	2.4		327	95	105	70	31.1	35.4	0.805	0.080	0.71287	-122.8	-15.06
GRO000098	2010-07-09	NW	5,491	0.88	55	0.10	1.8		252	72	65	59	13.9	13.4	0.628	0.068		-122.3	-16.08
GRO000099	2010-07-14	FL	5,670	0.28	62	0.03	1.0		307	89	68	71	10.9	15.5	0.773	0.075	0.71271	-128.6	-16.71
GRO000100	2010-07-20	FL	4,700	0.29	82	0.04	2.7		310	91	70	76	12.5	15.9	0.776	0.077	0.71299	-129.6	-16.85
GRO000101	2010-07-26	FL	4,341	0.31	60	0.05	0.4		321	102	81	80	15.2	19.2	0.807	0.081	0.71284	-129.5	-16.69
GRO000102	2010-07-30	NW	4,153	0.48	55	<0.05	1.6		299	86	72	68	21.5	15.1	0.738	0.075	0.71287	-127.5	-16.73
GRO000103	2010-08-06	FL	3,797	0.18	75	0.05	1.1		317	98	83	79	13.9	19.4	0.784	0.079	0.71291	-130.7	-17.03
GRO000104	2010-08-13	FL	3,475	0.68	64	0.05	1.0		335	104	88	82	19.2	18.4	0.828	0.082	0.71286	-121.9	-14.60
GRO000105	2010-08-20	NW	3,107						263	76	72	60	8.5	14.2	0.643	0.070	0.71251	-122.0	-16.39
GRO000106	2010-08-27	FL	2,477	0.60	65	0.24	5.7		336	99	87	79	9.0	17.1	0.833	0.082	0.71340		
GRO000107	2010-09-11	NW	2,166						273	82	71	58	9.9	11.2	0.663	0.072	0.71343	-127.5	-16.95
GRO000108	2010-09-13	FL	2,068	0.59	47	<0.05	0.9		393	127	102	90	24.2	18.8	0.938	0.089	0.71377	-129.5	-17.08
GRO000109	2010-09-27	FL	2,402	1.48	67	0.12	5.5		372	126	113	91	17.9	21.5	0.914	0.091	0.71286	-125.6	-16.31
GRO000110	2010-10-18	FL	2,047	0.97	71	0.09	3.8		387	131	115	95	18.3	19.5	0.936	0.087	0.71353		
GRO000111	2010-10-21	NW	1,822	1.60	70	0.15	5.0		328	101	91	73	12.8	15.0	0.794	0.080	0.71380	-122.8	-16.19
GRO000051	2010-10-25	FL	2,189	0.93	55	<0.05	5.5	983				102	21.8		1.029	0.090	0.71381	-128.5	-16.51
GRO000112	2010-11-01	FL	1,949	2.37	88	0.20	7.1		399	136	115	88	28.9	19.8	0.938	0.091	0.71319	-124.2	-16.02

GRO000113	2010-11-04	NW	1,875	1.35	51	0.08	7.1		250	82	95	56	23.3	16.5	0.589	0.070	0.71203	-108.1	-14.47
GRO000114	2010-11-15	FL	1,865	2.19	85	0.24	5.8		392	135	122	88	23.4	19.9	0.923	0.093	0.71261		
GRO000115	2010-12-09	FL	1,310	2.37	88	0.20	7.1		423	157	161	97	45.2	23.6	1.003	0.104	0.71150	-121.5	-15.74
GRO000116	2010-12-16	FL	1,423	2.19	85	0.24	5.8		347	124	128	84	32.0	24.0	0.828	0.099	0.71041		
GRO000117	2011-01-11	NW	983	7.31	25	0.30	13.6		458	592	4761	301	4536	120.7	1.663	0.110	0.70978	-111.4	-15.07
GRO000118	2011-01-20	FL	1,258	2.94	58	<0.05	12.6		295	101	120	71	48.5	21.4	0.700	0.091	0.70870	-110.1	-14.74
GRO000119	2011-01-24	NW	1,214	2.86	34	<0.05	8.3		244	84	159	57	98.1	18.1	0.586	0.076	0.70888	-103.9	-14.18
GRO000121	2011-02-03	FL	1,150	2.62	104	0.24	10.3		413	150	179	100	39.0	22.7	0.969	0.107	0.71023	-119.4	-15.62
GRO000122	2011-02-08	NW	1,256	2.22	84	0.17	15.6		286	102	149	67	77.9	18.0	0.686	0.085	0.71028	-107.5	-14.51
GRO000123	2011-02-24	FL	1,022	3.21	99	0.17	9.4		418	150	175	99	52.1	22.7	0.983	0.111	0.71023	-120.7	-15.85
GRO000124	2011-03-03	FL	903						447	174	208	107	82.2	23.6	1.073	0.124	0.71036	-121.5	-15.66
GRO000125	2011-03-04	NW	883	3.68	102	0.20	13.0		392	149	273	94	176.9	21.1	0.936	0.111	0.71035	-114.7	-14.77
GRO000126	2011-03-25	NW	1,039	4.74	94	0.20	9.2		371	135	214	92	131.2	21.8	0.904	0.107	0.70984	-117.0	-15.43
GRO000127	2011-04-19	FL	1,601	1.83	105	0.26	8.6		440	168	176	88	43.7	25.4	1.036	0.126	0.71040	-127.8	-16.84
GRO000128	2011-04-21	FL	1,562						413	167	167	86	60.5	24.6	0.986	0.120	0.71042	-129.2	-16.87
GRO000129	2011-05-03	FL	2,535									68	50.7				0.71064	-134.0	-17.51
GRO000130	2011-05-10	FL	3,929	2.96	102	0.24	2.5		385	149	148	53	65.7	40.9	0.882	0.122	0.71056	-136.4	-17.70
GRO000131	2011-05-13	NW	4,888	1.22	97	0.20	5.6		307	108	99	42	40.8	17.7	0.707	0.090	0.71040	-127.0	-16.65
GRO000132	2011-05-20	FL	7,819	0.56	103	0.16	4.2		402	140	102	50	14.4	20.6	0.913	0.110	0.71123	-130.1	-15.94
GRO000133	2011-05-25	FL	8,590	<0.05	103	0.18	1.1	913	389	127	97	50	21.0	18.7	0.869	0.101	0.71144	-134.9	-17.52
GRO000134	2011-05-28	FL	9,461																-135.6	-17.78
GRO000135	2011-06-03	FL	9,904	0.19	90	0.19	1.8		369	122	87	49	17.1	18.8	0.869	0.094	0.71180	-137.3	-17.98
GRO000076	2011-06-07	FL	10,469	0.29	95	0.13	4.9	849	344	113	81	49	15.5	16.9	0.852	0.100		-136.0	-17.83
GRO000136	2011-06-10	NW	10,780	0.75	92	0.20	5.1		326	102	78	48	28.2	15.6	0.779	0.085	0.71141	-131.3	-17.17
GRO000137	2011-06-17	FL	10,010	0.44	84	0.05	5.3		349	106	75	54	14.6	15.7	0.838	0.086	0.71223	-133.1	-16.91
GRO000140	2011-06-28	FL	10,020	0.99	74	0.07	4.2	795	357	115	78	56	14.0	16.8	0.856	0.081	0.71264	-137.9	-18.02
GRO000141	2011-06-30	FL	9,780	0.15	85	0.22	4.6		327	99	68	54	14.3	14.2	0.804	0.080	0.71234	-135.6	-17.78
GRO000142	2011-07-08	FL	9,680	0.61	72	0.06	3.8	771	358	108	73	53	12.7	16.3	0.838	0.078	0.71265	-136.6	-17.95
GRO000143	2011-07-15	FL	9,750	0.73	70	0.07	3.7	878	370	112	66	51	12.6	15.8	0.872	0.085	0.71296	-138.2	-18.11
GRO000144	2011-07-19	FL	9,650	0.51	74	0.08	3.1	840	370	118	75	55	13.0	16.0	0.876	0.085	0.71295	-137.1	-18.04
GRO000145	2011-07-29	FL	7,520	0.96	79	0.09	3.3		359	120	83	56	14.8	17.3	0.865	0.090	0.71244	-135.1	-17.72
GRO000146	2011-08-05	NW	7,154	0.91	56	0.11	0.2		345	112	79	52	15.5	16.2	0.814	0.084	0.71243	-132.4	-17.45
GRO000147	2011-08-12	FL	5,291	0.35	76	0.09	3.1		366	122	89	63	15.8	17.5	0.883	0.091	0.71243	-134.2	-17.53
GRO000148	2011-08-16	FL	4,636	1.20	71	0.09	0.9		373	123	94	66	19.3	18.1	0.895	0.092	0.71232	-133.6	-17.46
GRO000149	2011-08-19	NW	4,264	0.35	67	0.09	1.5		315	105	88	56	19.9	17.0	0.757	0.083	0.71211	-128.0	-16.72
GRO000150	2011-08-26	FL	4,521	0.68	73	0.10	2.2		381	127	110	70	15.0	20.8	0.910	0.094	0.71229	-133.5	-17.41
GRO000152	2011-09-08	FL	2,855	2.20	67	0.08	1.2		412	138	101	76	18.9	19.0	0.975	0.100	0.71285	-102.8	-8.27
GRO000153	2011-09-13	FL	2,657	0.88	74	0.06	2.8		418	143	108	81	21.1	19.8	0.993	0.102	0.71268	-132.0	-17.19
GRO000154	2011-09-19	FL	2,406	1.42	68	0.08	1.2		415	144	116	81	27.4	20.3	0.986	0.101	0.71278	-131.9	-17.23
GRO000155	2011-09-26	FL	3,145	1.88	71	0.07	3.3		391	135	108	81	21.8	19.7	0.925	0.095	0.71243		

GRO000156	2011-10-14	FL	2,714	1.97	69	0.12	5.0	783	355	123	105	70	21.8	18.6	0.834	0.084	0.71232	-124.5	-16.42
GRO000157	2011-10-25	FL	2,255	1.40	60	0.11	1.4	893	395	143	124	75	26.2	19.3	0.923	0.093	0.71211	-127.5	-16.55
GRO000158	2011-10-26	FL	2,236	2.04	77	0.11	4.7	864	385	143	124	73	25.1	19.0	0.900	0.093	0.71218	-127.8	-16.75
GRO000159	2011-10-31	FL	2,156					900	398	147	124	74	27.5	20.1	0.923	0.091	0.71239	-128.3	-16.78

Table 3. Time series measurements of concentrations of dissolved nutrients and major and trace element concentrations (all values in µmol L^{-1}), and radiogenic Sr and stable H_2O isotope compositions, show seasonal trends in sources of dissolved material in the Fraser basin. Site abbreviations are FL for Fort Langley (see Table 1) and NW for New Westminster (49.2178 °N, -122.8923 °W), two nearby cities close to the mouth of the Fraser River. Discharge at Mission, the total water flux of the Fraser River, is calculated as the sum of discharge for the Fraser at Hope and the Harrison River. This record was used to calculate annual loads and discharge-weighted average concentrations (Table 4).

	Fraser Flux (mol a^{-1})	Discharge-Weighted Average Fraser Concentration (μmol L^{-1})	Fraser Literature Concentrations (μmol L^{-1})	Ref.	World Average River Concentration (μmol L^{-1})	Ref.
HCO$_3$	$82 \pm 13 \times 10^9$	851 ± 74	1016	1	957	5
			1145	2	852	8
			983	3		
			841	4		
			1000	4		
Ca	$35 \pm 8 \times 10^9$	365 ± 27	434	1	374	5
			470	2	367	7
			399	3	334	8
			442	4	470	9
			494	5		
Mg	$12.0 \pm 2.9 \times 10^9$	123 ± 13	139	1	169	5
			170	2	152	7
			118	3	138	8
			148	4	193	9
			185	5		
Na	$10.5 \pm 1.8 \times 10^9$	110 ± 12	133	1	274	5
			161	2	313	7
			68	3	224	8
			126	4	270	9
SiO$_2$	$8.2 \pm 2.0 \times 10^9$	81.23 ± 0.12	57.8	1	218	5
			87.4	2	402	6
			81.6	3	173	8
			90.9	4		
			121	5		
			71.4	6		
SO$_4$	$6.6 \pm 0.7 \times 10^9$	69 ± 6	88.2	1	117	5
			113	2	85.9	8
			83.3	3	190	9
			85.4	4		
			104	5		
Cl	$2.8 \pm 0.6 \times 10^9$	29 ± 6	67.7	1	220	5
			44.7	2	162	8
			1.9	3	190	9
			67.7	4		
			42.3	5		
K	$1.9 \pm 0.3 \times 10^9$	19.5 ± 1.7	18.4	1	58.8	5
			20.7	2	35.8	7
			18.8	3	33.2	8
			17.9	4	38.0	9
NO$_3$+ NO$_2$	$0.48 \pm 0.09 \times 10^9$	4.76 ± 0.28	1.45	1	16.1	5
			6.29	2	43.0	6
			3.23	3		
			7.07	4		
			14.3	6		
NH$_4$	$0.12 \pm 0.05 \times 10^9$	1.12 ± 0.19				
Sr	$83 \pm 19 \times 10^6$	0.85 ± 0.04	1.14	1	0.68	7
			1.10	2	0.70	9
			0.28	3	1.26	10
PO$_4$	$13 \pm 5 \times 10^6$	0.125 ± 0.016	1.61	4	1.39	6
			0.25	6		
Ba	$8.7 \pm 2.1 \times 10^6$	$90 \pm 4 \times 10^{-3}$	100×10^{-3}	2	167×10^{-3}	7
			134×10^{-3}	3	180×10^{-3}	9

Table 4. Elemental fluxes and discharge-weighted average concentrations for the Fraser River (first two columns) were calculated from time series measurements and Environment Canada discharge data at Mission using LoadEst (Runkel et al., 2004). Uncertainties for these estimates represent 1 s.d. for the average of three annual load estimates (2009, 2010, 2011; see text section 3.1). Numbered references are: (1) Cameron (1996); (2) Cameron et al. (1995); (3) Durum et al. (1960); (4) Meybeck and Ragu (2012); (5) Livingstone (1963); (6) Mayorga et al. (2010); (7) Gaillardet et al. (2003); (8) Meybeck (1979); (9) Miller et al. (2011); and (10) Peucker-Ehrenbrink et al. (2010). For discussion of comparisons, see text sections 4.1 and 4.3.

Reference	Sample Collection Date	Sampling Location	dissolved $^{87}Sr/^{86}Sr$
Wadleigh et al. (1985)	May 1979	not reported	0.71195
Cameron and Hattori (1997)	July 1993	Fraser at Vancouver	0.712707 ± 0.000008
Allègre et al. (2010)	not reported	not reported	0.7188
This study	discharge-weighted average	Fraser at Fort Langley	0.7120 ± 0.0003

Table 5. The dissolved $^{87}Sr/^{86}Sr$ composition of the Fraser River reported in the literature varies according to which portion of the hydrograph was sampled. The value reported by Allègre et al. (2010) likely represents only the upper third of the Fraser basin. The uncertainty shown for the value of Cameron and Hattori (1997) represents a 2σ analytical error, while the uncertainty given for our discharge-weighted average (2 s.d.) reflects a combination of LoadEst model calibration error and interannual variability.
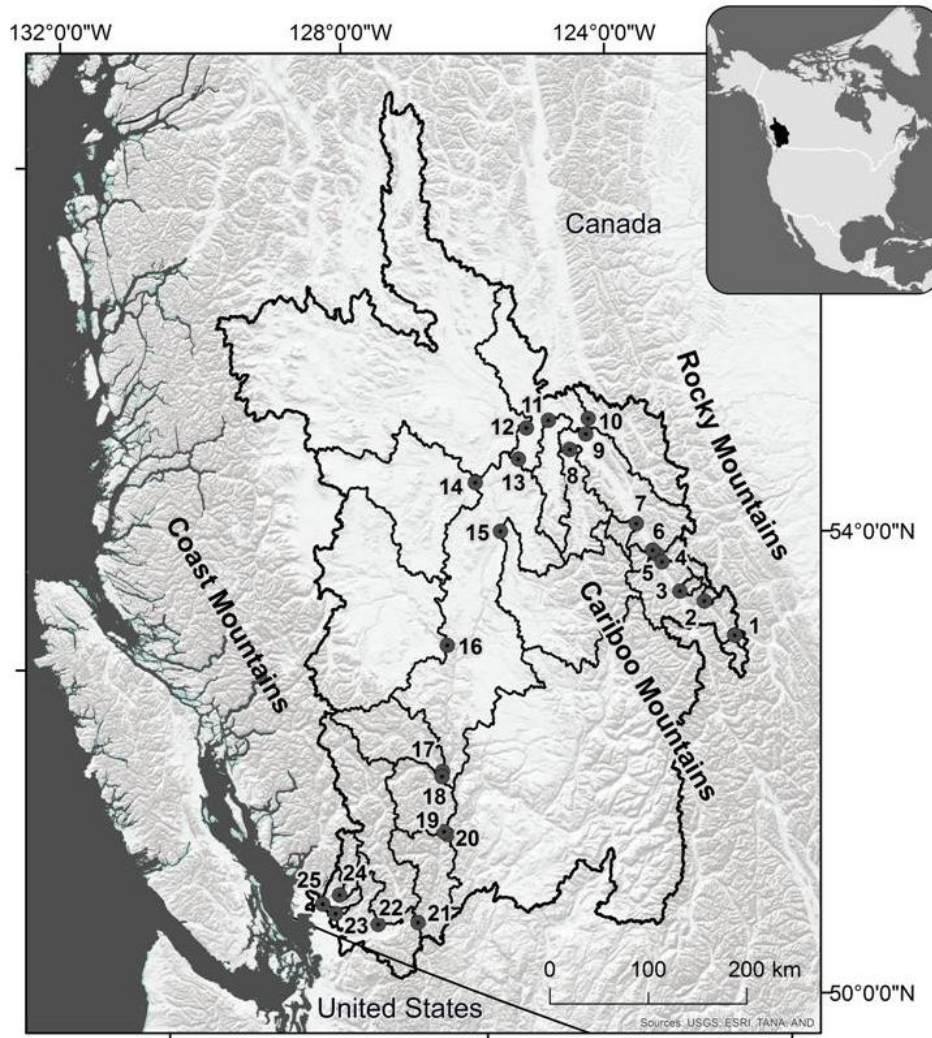
Figure 1. Topographic map of the Fraser River basin with large tributary subdrainage basins outlined. Sampling points are indicated by numbered circles: (1) Fraser at Fitzwilliam; (2) Robson River; (3) Small River; (4) Holmes River; (5) Fraser at McBride; (6) Dore River; (7) Goat River; (8) Bowron River; (9) Fraser at Hansard; (10) McGregor River; (11) Willow River; (12) Nechako River; (13) Fraser at Stoner; (14) Blackwater (West Road) River; (15) Quesnel River; (16) Chilcotin River; (17) Bridge River; (18) Fraser at Lillooet; (19) Fraser at Lytton; (20) Thompson River; (21) Fraser at Hope; (22) Harrison River; (23) Fraser at Fort Langley; (24) Pitt River; (25) Fraser at Vancouver. The Fraser at Mission lies between (22) and (23).
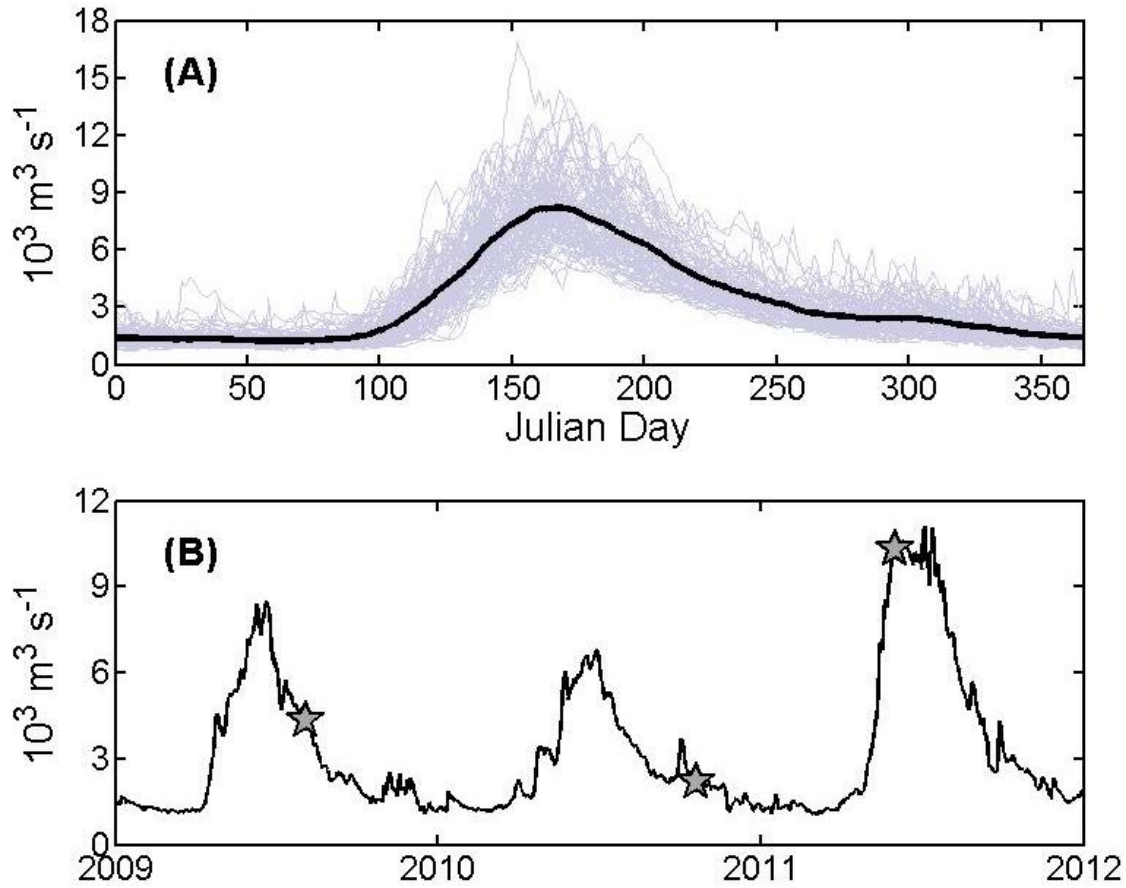
Figure 2. (A) The total Fraser River hydrograph at Mission is characterized by a spring freshet of ~8000 m^3 s^{-1} and winter base flow of ~1800 m^3 s^{-1}. Faint curves show individual hydrographs, whereas the bold curve is the average hydrograph for the period of record (1912 – 2011). (B) The recent hydrograph of the Fraser River at Mission shows the variability in the progression and magnitude of the spring freshet from one year to the next. Stars indicate the timing of basin-wide sampling campaigns in this study.
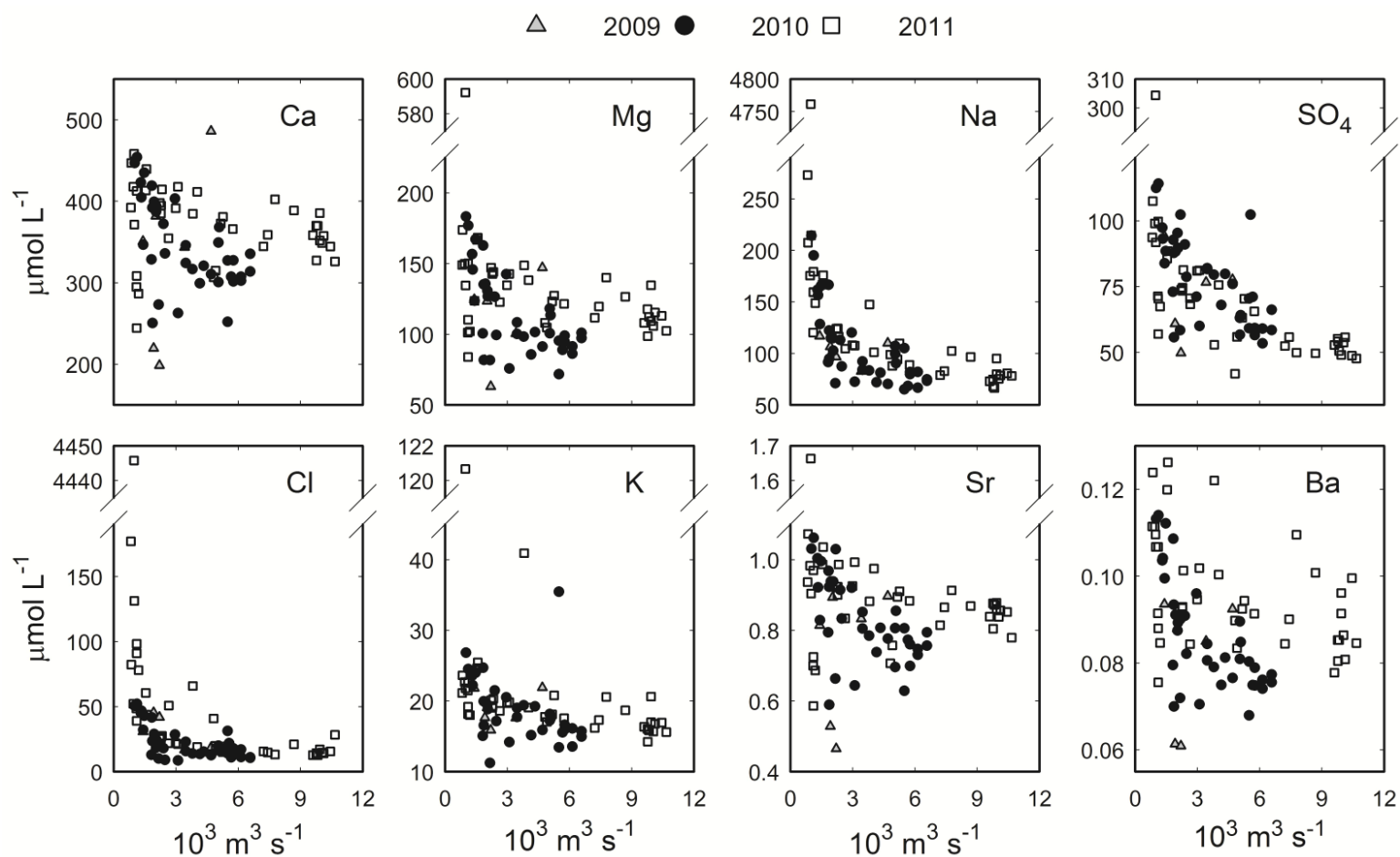
Figure 3. Plots of dissolved element concentrations versus total Fraser River discharge (at Mission) on the day of sampling generally show kinetic-limited chemical weathering behavior with modest dilution when discharge exceeds base flow (~1800 m^3 s^{-1}). The most extreme variability is seen in species strongly affected by sea salt aerosols (Cl, Na).
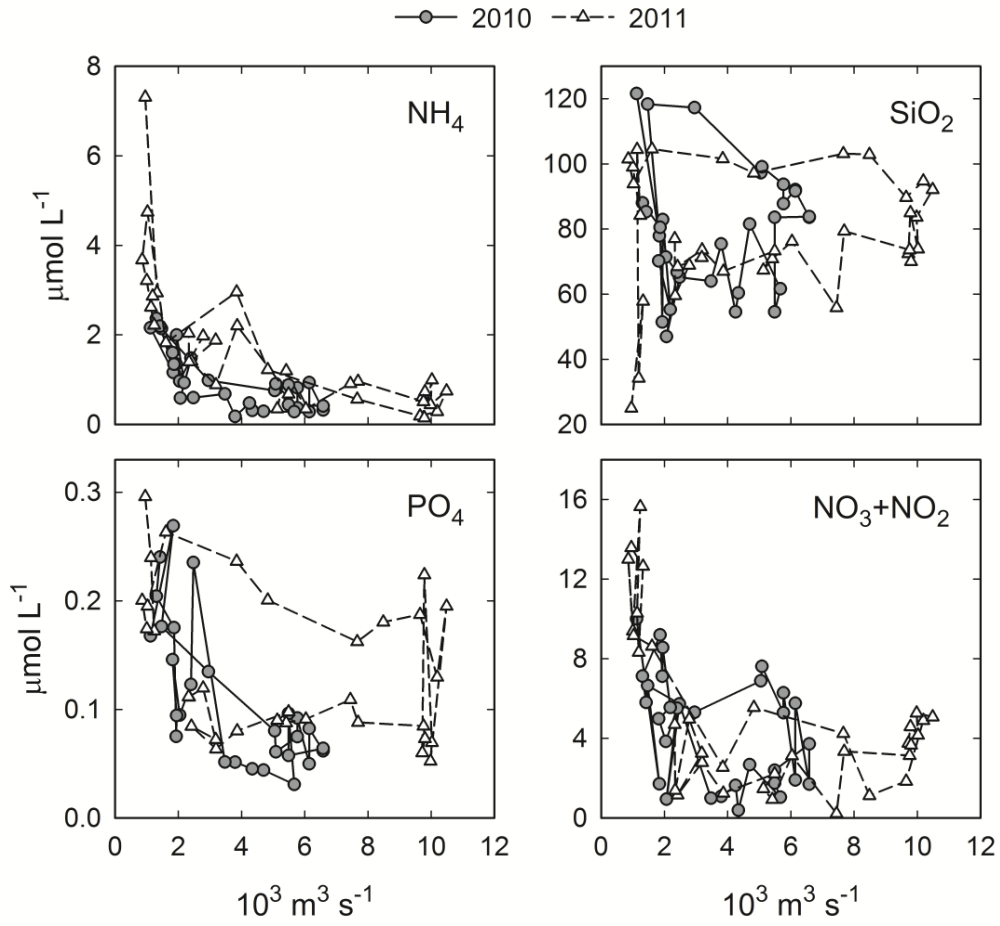
Figure 4. The time series records of inorganic nutrient concentrations exhibit hysteresis behavior (generally counterclockwise) with respect to discharge.
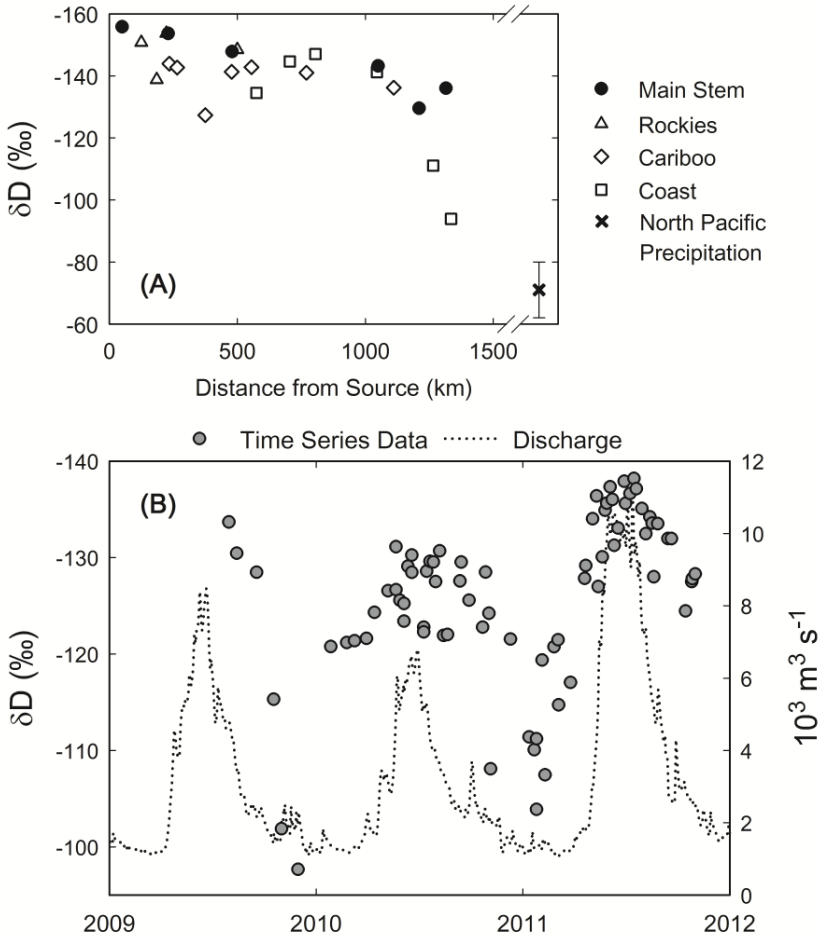
Figure 5. (A) The δD value of precipitation in the Fraser River basin decreases as Pacific Ocean air masses travel inland (right to left on *x*-axis). In this June 2011 transect, points represent main stem sites, as well as tributaries draining the Rocky Mountain headwaters, the Cariboo Range of the central basin, and the Coast Range of the western basin. The δD composition of precipitation near the Fraser mouth is also shown (error bars indicate ±1 s.d. of seven years of monthly sampling). (B) The basin-integrated δD composition of the Fraser River shows significant seasonal variability, with more negative spring and summer values indicating greater contributions from snowmelt in the headwaters.
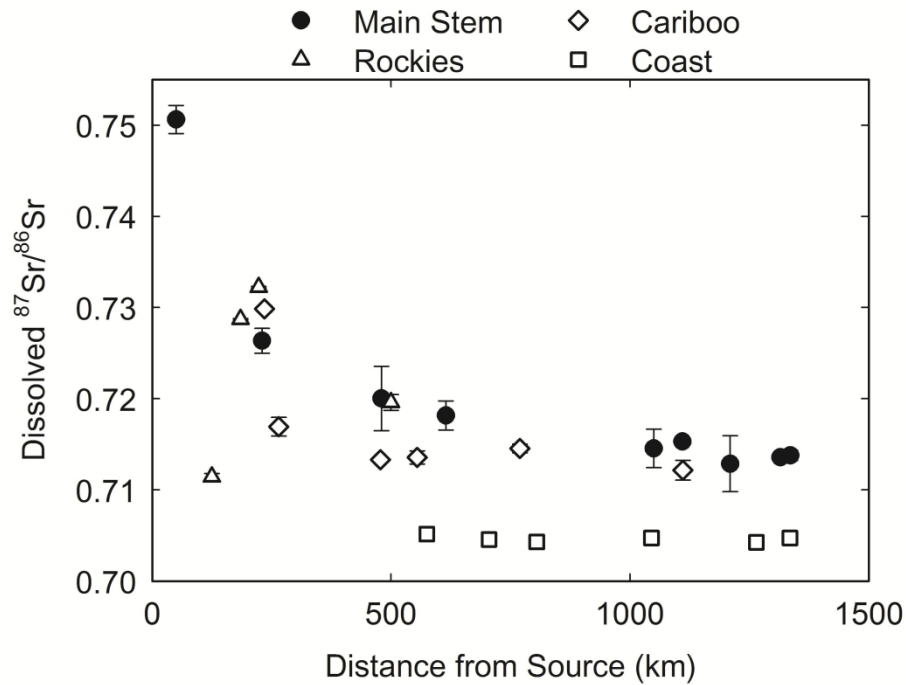
Figure 6. A downstream transect of dissolved $^{87}Sr/^{86}Sr$ in the Fraser River shows the abrupt transition between more radiogenic tributary basins in the Rocky and Cariboo Mountains to less radiogenic tributaries draining the Coast Range. Error bars indicate one standard deviation from the average of the three sampling campaigns. Our values for samples collected in summer 2009 (medium flow) are indistinguishable from those reported by Cameron and Hattori (1997) for samples collected in July 1993.
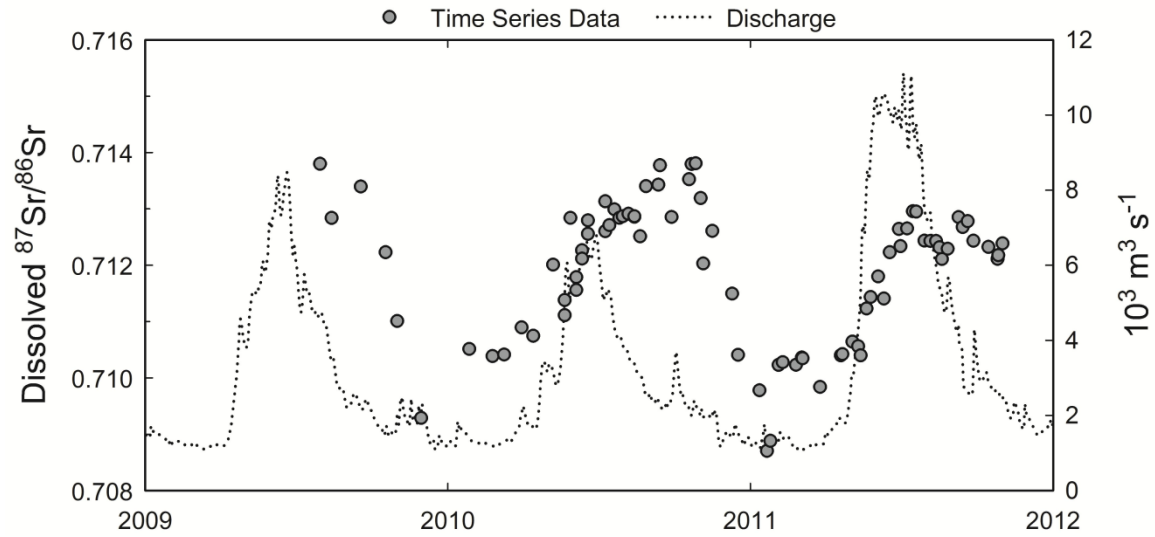
Figure 7. A time series record of dissolved ^{87}Sr/^{86}Sr in the Fraser River shows a seasonal shift in contributions to the dissolved load from more radiogenic portions of the drainage basin (stronger in spring and summer) to less radiogenic portions (stronger in fall and winter).
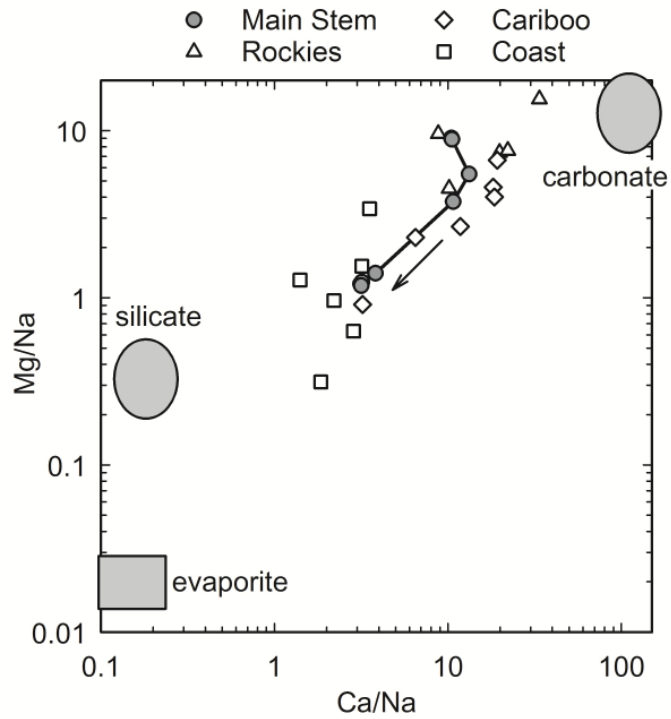
Figure 8. Major element ratios (mol mol^{-1}) of the Fraser River dissolved load indicate a dilution of carbonate-dominated weathering products by material bearing a silicate weathering signature moving downstream (data shown from fall 2010 samples). Main stem sites are connected with a line, and an arrow indicates the direction from headwaters to the delta. Large shapes show the compositions of endmembers for waters draining pure lithologies (Gaillardet et al., 1999).
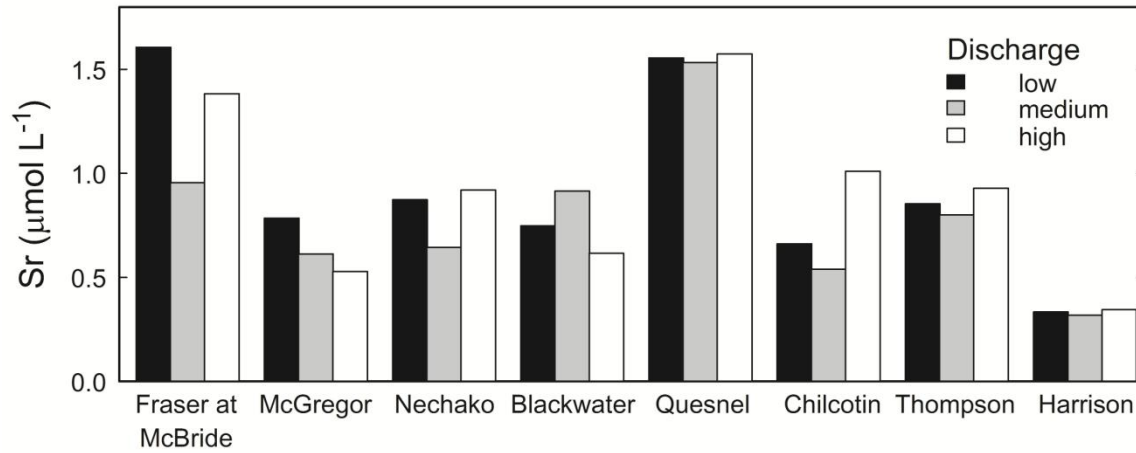
Figure 9. Tributaries included in the $^{87}Sr/^{86}Sr$ model do not show a systematic dilution of strontium concentration with discharge conditions at the time of sampling (low in fall 2010, medium in summer 2009, high in spring 2011). In the model, we chose to use average concentrations for each tributary.
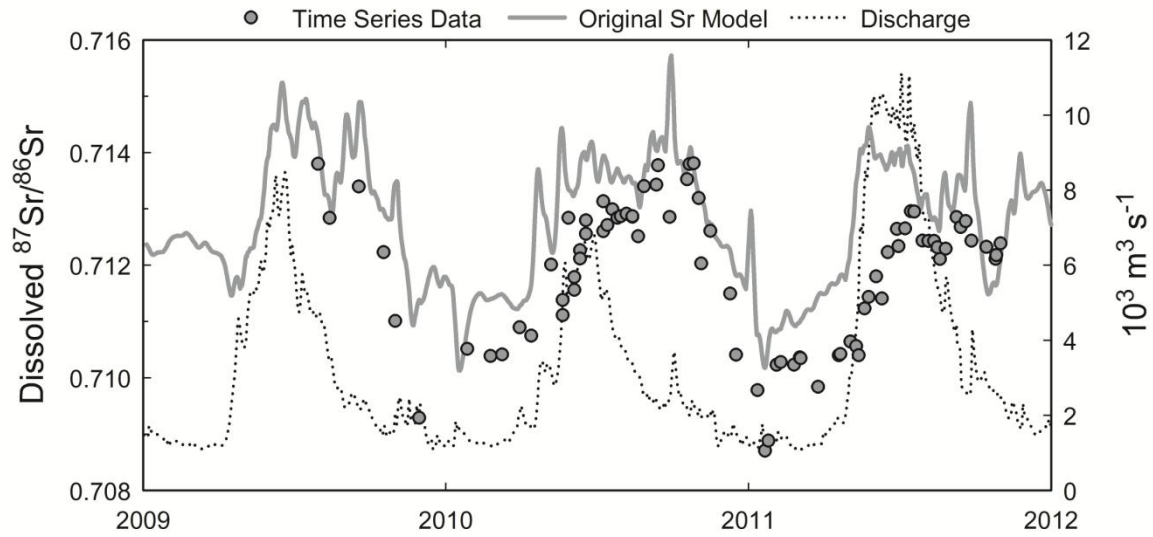
Figure 10. A model of the variability in basin-integrated ^{87}Sr/^{86}Sr using Sr flux and ^{87}Sr/^{86}Sr composition of eight subdrainage basins follows the seasonal pattern of the measured time series values.
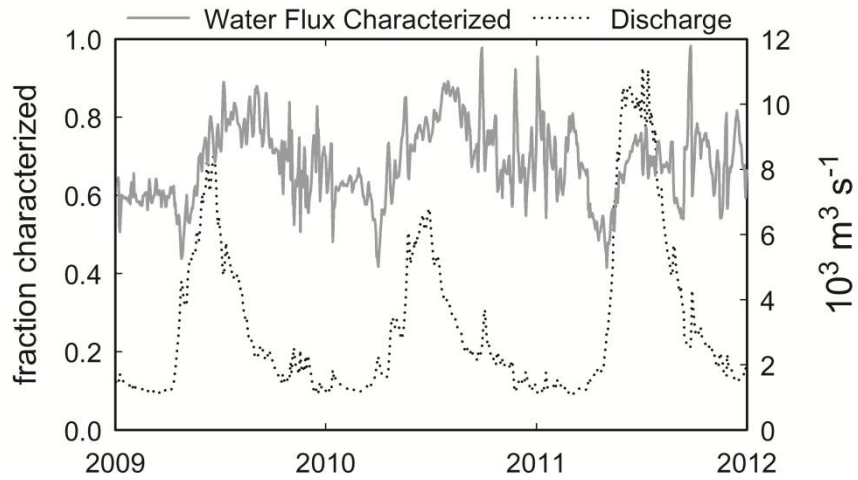
Figure 11. The fraction of total discharge characterized by the original ^{87}Sr/^{86}Sr model shows that the model characterizes a greater portion of the discharge during spring and summer.
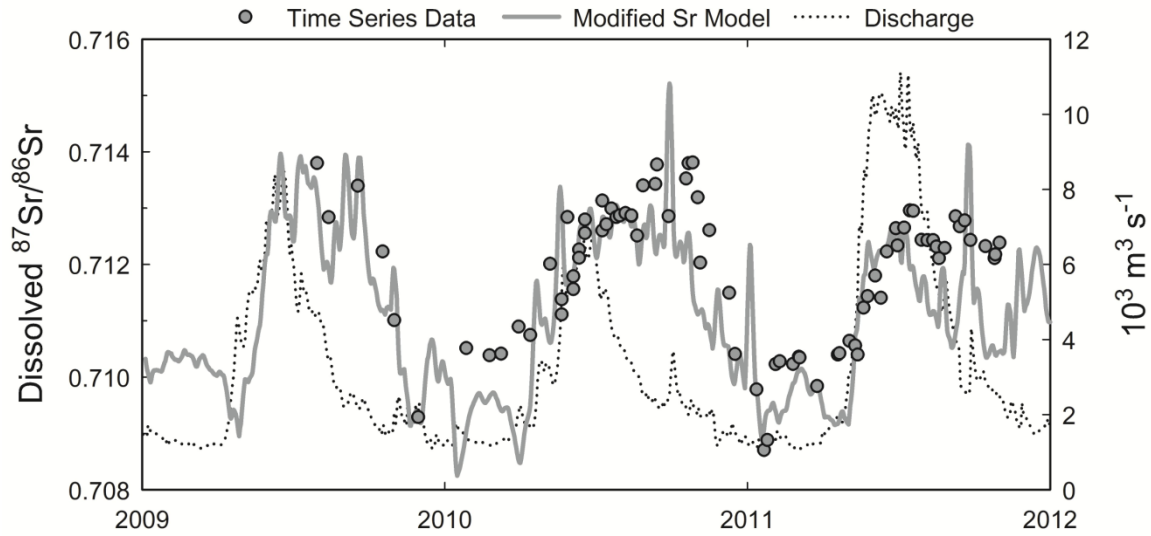
Figure 12. Addition of an unradiogenic (^{87}Sr/^{86}Sr = 0.7046) component with low Sr

concentration (0.45 µmol L^{-1}) to the ^{87}Sr/^{86}Sr model appears to resolve most of the offset

between the original model and measured time series values, suggesting that the majority of the

uncharacterized flux derives from basins draining the Coast Range.
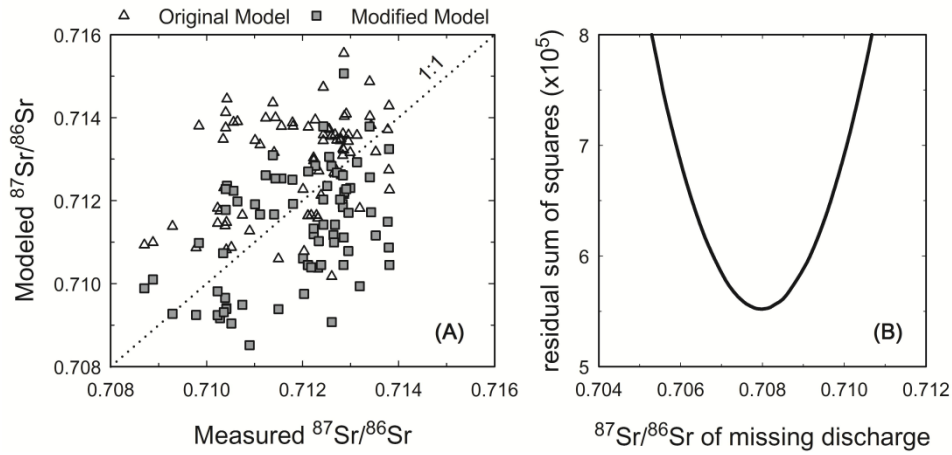
Figure 13. (A) Modeled $^{87}Sr/^{86}Sr$ for the original model exhibits, on average, a radiogenic bias when compared to time series measurements on the same day. The modified model with a Coast Range-like composition applied to uncharacterized discharge has, on average, a less radiogenic bias of similar magnitude. (B) Adjusting the $^{87}Sr/^{86}Sr$ composition of the uncharacterized discharge to 0.7080 minimizes the residual sum of squares between the time series measurements and the modified model.

Acknowledgements

References

Allègre C. J., Louvat P., Gaillardet J., Meynadier L., Rad S., and Capmas F. (2010) The fundamental role of island arc weathering in the oceanic Sr isotope budget. *Earth Planet. Sci. Lett.* **292**, 51-56. doi:10.1016/j.epsl.2010.01.019.

Alvarez-Cobelas M., Sánchez-Carrillo S., Angeler D. G., and Sánchez-Andrés R. (2009) Phosphorus export from catchments: a global view. *J. N. Am. Benthol. Soc.* **28**, 805-820. doi:10.1899/09-073.1.

Amiotte Suchet P., Probst J.-L., and Ludwig W. (2003) Worldwide distribution of continental rock lithology: Implications for the atmospheric/soil CO_2 uptake by continental weathering and alkalinity river transport to the oceans. *Global Biogeochem. Cycles* **17**. doi:10.1029/2002gb001891.

Armstrong R. L. (1988) Mesozoic and early Cenozoic magmatic evolution of the Canadian Cordillera. *Geol. Soc. Am. Spec. Pap.* **218**, 55-92. doi:10.1130/SPE218-p55.

Bagard M.-L., Chabaux F., Pokrovsky O. S., Viers J., Prokushkin A. S., Stille P., Rihs S., Schmitt A.-D., and Dupré B. (2011) Seasonal variability of element fluxes in two Central Siberian rivers draining high latitude permafrost dominated areas. *Geochim. Cosmochim. Acta* **75**, 3335-3357. doi:10.1016/j.gca.2011.03.024.

Bataille C. P. and Bowen G. J. (2012) Mapping $^{87}Sr/^{86}Sr$ variations in bedrock and water for large scale provenance studies. *Chem. Geol.* **304-305**, 39-52. doi:10.1016/j.chemgeo.2012.01.028.

Becker J. A., Bickle M. J., Galy A., and Holland T. J. B. (2008) Himalayan metamorphic CO_2 fluxes: Quantitative constraints from hydrothermal springs. *Earth Planet. Sci. Lett.* **265**, 616-629. doi:10.1016/j.epsl.2007.10.046.

Berner E. K. and Berner R. A. (1996) Global Environment: Water, Air, and Geochemical Cycles. Prentice Hall. pp. 172-235.

Beusen A. H. W., Bouwman A. F., Dürr H. H., Dekkers A. L. M., and Hartmann J. (2009) Global patterns of dissolved silica export to the coastal zone: Results from a spatially explicit global model. *Global Biogeochem. Cycles* **23**. doi:10.1029/2008gb003281.

Blum J. D., Gazis C. A., Jacobsen A. D., and Chamberlain C. P. (1998) Carbonate versus silicate weathering in the Raikhot watershed within the High Himalayan Crystalline Series. *Geology* **26**, 411-414.

Booth G., Raymond P., and Oh N.-H. (2007) LoadRunner. New Haven, CT. http://environment.yale.edu/raymond/loadrunner.

Boyer E. W., Howarth R. W., Galloway J. N., Dentener F. J., Green P. A., and Vörösmarty C. J. (2006) Riverine nitrogen export from the continents to the coasts. *Global Biogeochem. Cycles* **20**. doi:10.1029/2005gb002537.

Brisbin P. E. (1994) Agricultural inventory of the Lower Fraser Valley data summary report. Management of livestock and poultry manures in the Lower Fraser Valley. Charcoal Creek Projects Inc., Abbotsford, B. C.

Calmels D., Galy A., Hovius N., Bickle M., West A. J., Chen M.-C., and Chapman H. (2011) Contribution of deep groundwater to the weathering budget in a rapidly eroding mountain belt, Taiwan. *Earth Planet. Sci. Lett.* **303**, 48-58. doi:10.1016/j.epsl.2010.12.032.

Cameron E. M. (1996) Hydrogeochemistry of the Fraser River, British Columbia: seasonal variation in major and minor components. *J. Hydrol.* **182**, 209-225.

Cameron E. M., Hall G. E. M., Veizer J., and Krouse H. R. (1995) Isotopic and elemental hydrogeochemistry of a major river system: Fraser River, British Columbia, Canada. *Chem. Geol.* **122**, 149-169.

Cameron E. M. and Hattori K. (1997) Strontium and neodymium isotope ratios in the Fraser River, British Columbia: a riverine transect across the Cordilleran orogen. *Chem. Geol.* **137**, 243-253.

Chao B. F., Wu Y. H., and Li Y. S. (2008) Impact of artificial reservoir water impoundment on global sea level. *Science* **320**, 212-214. doi:10.1126/science.1154580.

Christophersen N., Neal C., Hooper R. P., Vogt R. D., and Andersen S. (1990) Modelling streamwater chemistry as a mixture of soilwater end-members — A step towards second-generation acidification models. *J. Hydrol.* **116**, 307-320.

Coggins S. B., Coops N. C., Wulder M. A., Bater C. W., and Ortlepp S. M. (2011) Comparing the impacts of mitigation and non-mitigation on mountain pine beetle populations. *J. Environ. Manage.* **92**, 112-120. doi:10.1016/j.jenvman.2010.08.016.

Cooper L. W., McClelland J. W., Holmes R. M., Raymond P. A., Gibson J. J., Guay C. K., and Peterson B. J. (2008) Flow-weighted values of runoff tracers (δ^{18}O, DOC, Ba, alkalinity) from the six largest Arctic rivers. *Geophys. Res. Lett.* **35**. doi:10.1029/2008gl035007.

Déry S. J., Hernández-Henríquez M. A., Owens P. N., Parkes M. W., and Petticrew E. L. (2012) A century of hydrological variability and trends in the Fraser River Basin. *Environ. Res. Lett.* **7**. doi:10.1088/1748-9326/7/2/024019.

Dickson A. G., Sabine C. L., and Christian J. R. (2007) Guide to best practices for ocean CO_2 measurements. PICES Special Publication. Sidney, British Columbia, Canada. 191 pp.

Dorcey A. H. J. (1991) Hydrology and water supply in the Fraser River basin. In *Water in Sustainable Development: Exploring Our Common Future in the Fraser River Basin* (eds. A. H. J. Dorcey and J. R. Griggs). Westwater Research Centre, Univ. of British Columbia, Vancouver, B.C. pp. 21-40.

Dumont E., Harrison J. A., Kroeze C., Bakker E. J., and Seitzinger S. P. (2005) Global distribution and sources of dissolved inorganic nitrogen export to the coastal zone: Results from a spatially explicit, global model. *Global Biogeochem. Cycles* **19**. doi:10.1029/2005gb002488.

Durum W. H., Heidel S. G., and Tison L. J. (1960) Worldwide run-off of dissolved solids. *IAHS-AISH Publ.* **51**, 618-628.

Edmond J. M. (1992) Himalayan tectonics, weathering processes, and the strontium isotope record in marine limestones. *Science* **258**, 1594-1597.

Fekete B. M., Vörösmarty C. J., and Grabs W. (2002) High-resolution fields of global runoff combining observed river discharge and simulated water balances. *Global Biogeochem. Cycles* **16**. doi:10.1029/1999GB001254.

Friele P. A. and Clague J. J. (2009) Paraglacial geomorphology of Quaternary volcanic landscapes in the southern Coast Mountains, British Columbia. *Geol. Soc., London, Spec. Publ.* **320**, 219-233. doi:10.1144/sp320.14.

Gaillardet J., Dupré B., Louvat P., and Allègre C. J. (1999) Global silicate weathering and CO_2 consumption rates deduced from the chemistry of large rivers. *Chem. Geol.* **159**, 3-30.

Gaillardet J., Viers J., and Dupré B. (2003) Trace elements in river waters. In *Treatise on Geochemistry* (eds. H. D. Holland and K. K. Turekian). Elsevier. pp. 225-272.

Galy A. and France-Lanord C. (1999) Weathering processes in the Ganges-Brahmaputra basin and the riverine alkalinity budget. *Chem. Geol.* **159**, 31-60.

Gimeno L., Stohl A., Trigo R. M., Dominguez F., Yoshimura K., Yu L., Drumond A., Durán-Quesada A. M., and Nieto R. (2012) Oceanic and terrestrial sources of continental precipitation. *Rev. Geophys.* **50**. doi:10.1029/2012rg000389.

Goldstein S. J. and Jacobsen S. B. (1987) The Nd and Sr isotopic systematics of river-water dissolved material: implications for the sources of Nd and Sr in seawater. *Chem. Geol.* **66**, 245-272.

Graham S. T., Famiglietti J. S., and Maidment D. R. (1999) Five-minute, 1/2°, and 1° data sets of continental watersheds and river networks for use in regional and global hydrologic and climate system modeling studies. *Water Resour. Res.* **35**, 583-587. doi:10.1029/1998wr900068.

Harrison J. A., Seitzinger S. P., Bouwman A. F., Caraco N. F., Beusen A. H. W., and Vörösmarty C. J. (2005) Dissolved inorganic phosphorus export to the coastal zone: Results from a spatially explicit, global model. *Global Biogeochem. Cycles* **19**. doi:10.1029/2004gb002357.

Hartmann J., Jansen N., Dürr H. H., Kempe S., and Köhler P. (2009) Global CO_2-consumption by chemical weathering: What is the contribution of highly active weathering regions? *Global Planet. Change* **69**, 185-194. doi:10.1016/j.gloplacha.2009.07.007.

Howarth R. W., Billen G., Swaney D., Townsend A., Jaworski N., Lajtha K., Downing J. A., Elmgren R., Caraco N., Jordan T., Berendse F., Freney J., Kudeyarov V., Murdoch P., and Zhao-Liang Z. (1996) Regional nitrogen budgets and riverine N & P fluxes for the drainages to the North Atlantic Ocean: Natural and human influences. *Biogeochemistry* **35**, 75-139.

Huh Y., Birck J.-L., and Allègre C. J. (2004) Osmium isotope geochemistry in the Mackenzie River basin. *Earth Planet. Sci. Lett.* **222**, 115-129. doi:10.1016/j.epsl.2004.02.026.

Hurwitz S., Evans W. C., and Lowenstern J. B. (2010) River solute fluxes reflecting active hydrothermal chemical weathering of the Yellowstone Plateau Volcanic Field, USA. *Chem. Geol.* **276**, 331-343. doi:10.1016/j.chemgeo.2010.07.001.

IAEA/WMO (2006) Global Network of Isotopes in Precipitation. The GNIP Database. http://www.iaea.org/water.

Kirchner J. W. and Neal C. (2013) Universal fractal scaling in stream chemistry and its implications for solute transport and water quality trend detection. *Proc. Natl. Acad. Sci.* **110**, 12213-12218. doi:10.1073/pnas.1304328110.

Liu Z., Kennedy C. D., and Bowen G. J. (2011) Pacific/North American teleconnection controls on precipitation isotope ratios across the contiguous United States. *Earth Planet. Sci. Lett.* **310**, 319-326. doi:10.1016/j.epsl.2011.08.037.

Livingstone D. A. (1963) Chemical composition of rivers and lakes. In *Data of Geochemistry* (ed. M. Fleischer). United States Geological Survey, Washington D.C. pp. 1-64.

Mackenzie F. T. and Garrels R. M. (1966) Chemical mass balance between rivers and oceans. *Am. J. Sci.* **264**, 507-525.

Mayorga E., Seitzinger S. P., Harrison J. A., Dumont E., Beusen A. H. W., Bouwman A. F., Fekete B. M., Kroeze C., and Van Drecht G. (2010) Global Nutrient Export from WaterSheds 2 (NEWS 2): Model development and implementation. *Environ. Modell. Softw.* **25**, 837-853. doi:10.1016/j.envsoft.2010.01.007.

Meybeck M. (1979) Concentrations des eaux fluviales en éléments majeurs et apports en solution aux océans. *Rev. Géol. Dyn. Géogr. Phys.* **21**, 215-246.

Meybeck M. (1987) Global chemical weathering from surficial rocks estimated from river dissolved loads. *Am. J. Sci.* **287**, 401-428.

Meybeck M. and Helmer R. (1989) The quality of rivers: from pristine stage to global pollution. *Palaeogeogr. Palaeoclimatol. Palaeoecol.* **75**, 283-309.

Meybeck M. and Ragu A. (2012) GEMS-GLORI world river discharge database. Laboratoire de Géologie Appliquée, Université Pierre et Marie Curie, Paris. doi:10.1594/PANGAEA.804574.

Miller C. A. (2009) Surface-cycling of rhenium and its isotopes. PhD Thesis, Woods Hole Oceanog. Inst.

Miller C. A., Peucker-Ehrenbrink B., Walker B. D., and Marcantonio F. (2011) Re-assessing the surface cycling of molybdenum and rhenium. *Geochim. Cosmochim. Acta* **75**, 7146-7179. doi:10.1016/j.gca.2011.09.005.

Milliman J. D., Farnsworth K. L., Jones P. D., Xu K. H., and Smith L. C. (2008) Climatic and anthropogenic factors affecting river discharge to the global ocean, 1951–2000. *Global Planet. Change* **62**, 187-194. doi:10.1016/j.gloplacha.2008.03.001.

Millot R., Gaillardet J., Dupré B., and Allègre C. J. (2003) Northern latitude chemical weathering rates: clues from the Mackenzie River Basin, Canada. *Geochim. Cosmochim. Acta* **67**, 1305-1329. doi:10.1016/s0016-7037(02)01207-3.

Morel F. M. M. and Hering J. G. (1993) *Principles and applications of aquatic chemistry*. John Wiley, Hoboken, N.J.

Nilsson C. (2005) Fragmentation and flow regulation of the world's large river systems. *Science* **308**, 405-408. doi:10.1126/science.1107887.

Northwest Hydraulic Consultants (2008) Comprehensive review of Fraser River at Hope flood hydrology and flows: scoping study. B.C. Ministry of Environment, North Vancouver, B.C. 1-25.

Palmer M. R. and Edmond J. M. (1989) The strontium isotope budget of the modern ocean. *Earth Planet. Sci. Lett.* **92**, 11-26.

Peterson B. J. (2006) Trajectory shifts in the Arctic and Subarctic freshwater cycle. *Science* **313**, 1061-1066. doi:10.1126/science.1122593.

Peucker-Ehrenbrink B. and Miller M. W. (2007) Quantitative bedrock geology of the continents and large-scale drainage regions. *Geochem. Geophys. Geosyst.* **8**. doi:10.1029/2006gc001544.

Peucker-Ehrenbrink B., Miller M. W., Arsouze T., and Jeandel C. (2010) Continental bedrock and riverine fluxes of strontium and neodymium isotopes to the oceans. *Geochem. Geophys. Geosyst.* **11**. doi:10.1029/2009gc002869.

Raymond P. A. and Cole J. J. (2003) Increase in the export of alkalinity from North America's largest river. *Science* **301**, 88-91. doi:10.1126/science.1083788.

Runkel R. L., Crawford C. G., and Cohn T. A. (2004) Load Estimator (LOADEST): A FORTRAN program for estimating constituent loads in streams and rivers. U.S. Geological Survey techniques and methods Book 4, chapter A5. Reston, VA. http://water.usgs.gov/software/loadest.

Scanlon T. M., Raffensperger J. P., and Hornberger G. M. (2001) Modeling transport of dissolved silica in a forested headwater catchment: Implications for defining the hydrochemical response of observed flow pathways. *Water Resour. Res.* **37**, 1071-1082.

Schulte P., van Geldern R., Freitag H., Karim A., Négrel P., Petelet-Giraud E., Probst A., Probst J.-L., Telmer K., Veizer J., and Barth J. A. C. (2011) Applications of stable water and

carbon isotopes in watershed research: Weathering, carbon cycling, and water balances. *Earth-Sci. Rev.* **109**, 20-31. doi:10.1016/j.earscirev.2011.07.003.

Seitzinger S. P., Harrison J. A., Dumont E., Beusen A. H. W., and Bouwman A. F. (2005) Sources and delivery of carbon, nitrogen, and phosphorus to the coastal zone: An overview of Global Nutrient Export from Watersheds (NEWS) models and their application. *Global Biogeochem. Cycles* **19**. doi:10.1029/2005gb002606.

Shen Z.-L. and Liu Q. (2008) Nutrients in the Changjiang River. *Environ. Monit. Assess.* **153**, 27-44. doi:10.1007/s10661-008-0334-2.

Spence J. and Telmer K. (2005) The role of sulfur in chemical weathering and atmospheric CO_2 fluxes: Evidence from major ions, $\delta^{13}C_{DIC}$, and $\delta^{34}S_{SO4}$ in rivers of the Canadian Cordillera. *Geochim. Cosmochim. Acta* **69**, 5441-5458. doi:10.1016/j.gca.2005.07.011.

Syvitski J. P. M. (2008) Deltas at risk. *Sustain. Sci.* **3**, 23-32. doi:10.1007/s11625-008-0043-3.

Thorne R. and Woo M.-k. (2011) Streamflow response to climatic variability in a complex mountainous environment: Fraser River Basin, British Columbia, Canada. *Hydrol. Processes* **25**, 3076-3085. doi:10.1002/hyp.8225.

Tipper E. T., Bickle M. J., Galy A., West A. J., Pomiès C., and Chapman H. J. (2006) The short term climatic sensitivity of carbonate and silicate weathering fluxes: Insight from seasonal variations in river chemistry. *Geochim. Cosmochim. Acta* **70**, 2737-2754. doi:10.1016/j.gca.2006.03.005.

Wadleigh M. A., Veizer J., and Brooks C. (1985) Strontium and its isotopes in Canadian rivers: Fluxes and global implications. *Geochim. Cosmochim. Acta* **49**, 1727-1736.

Walling D. E. and Foster I. D. L. (1975) Variations in the natural chemical concentration of river water during flood flows, and the lag effect: Some further comments. *J. Hydrol.* **26**, 237-244.

Wang Z. A., Bienvenu D. J., Mann P. J., Hoering K. A., Poulsen J. R., Spencer R. G. M., and Holmes R. M. (2013) Inorganic carbon speciation and fluxes in the Congo River. *Geophys. Res. Lett.* **40**, 511-516. doi:10.1002/grl.50160.

Wang Z. A. and Cai W.-J. (2004) Carbon dioxide degassing and inorganic carbon export from a marsh-dominated estuary (the Duplin River): A marsh CO_2 pump. *Limnol. Oceanogr.* **49**, 341-354.

Wang Z. A., Voss B. M., Peucker-Ehrenbrink B., Eglinton T. I., and Hoering K. (in prep) Carbon cycling in the Fraser River, Canada: Inorganic carbon systematics.

West A., Galy A., and Bickle M. (2005) Tectonic and climatic controls on silicate weathering. *Earth Planet. Sci. Lett.* **235**, 211-228. doi:10.1016/j.epsl.2005.03.020.

Wheeler J. O., Hoffman P. F., Card K. D., Davidson A., Stanford B. V., Okulitch A. V., and Roest W. R. (1997) Geologic map of Canada, Map D1860A, version 1.0, scale 1:5,000,000. Nat. Resour. Can., Ottawa, Ont., Canada.

Wolff-Boenisch D., Gabet E. J., Burbank D. W., Langner H., and Putkonen J. (2009) Spatial variations in chemical weathering and CO_2 consumption in Nepalese High Himalayan catchments during the monsoon season. *Geochim. Cosmochim. Acta* **73**, 3148-3170. doi:10.1016/j.gca.2009.03.012.

INSIGHTS ON CARBON CYCLING IN THE FRASER RIVER BASIN FROM ISOTOPIC, ELEMENTAL, AND MOLECULAR COMPOSITION OF SEDIMENTARY AND DISSOLVED ORGANIC CARBON

3.1 Abstract

Sources of dissolved and particulate organic carbon (OC) in the Fraser basin exhibit significant spatial and temporal bias. In addition to the annual basin-wide pulse of dissolved OC (DOC) which occurs during the spring freshet, tributaries in the northern interior of the basin (Blackwater, Nechako, and Willow rivers) consistently deliver higher concentrations of DOC to the main stem Fraser. Particulate OC (POC) concentrations, in contrast, are highest in tributaries draining the central canyon region of the basin (Blackwater, Chilcotin, Bridge and Thompson rivers). Dissolved inorganic carbon (DIC) concentrations are generally highest in the Rocky Mountain headwater region where carbonate weathering is evident, but also in tributaries with high DOC concentrations, indicating that DOC respiration is responsible for a large portion of DIC in this basin. It is estimated that throughout the year, >80% of DIC delivered by the Fraser River to the coastal ocean is derived from DOC respiration. The bulk elemental and isotopic composition of POC is variable between high and low discharge conditions, with high discharge periods characterized by low %OC (0.3-2.2), high C:N (9.4-13.7), low δ^{13}C (-30.2 to -25.8‰), and high ^{14}C content (fraction modern, Fm, 0.58-1.00) relative to low discharge conditions (0.6-10.5 %OC, 6.3-13.8 C:N, -28.4 to -21.8‰ δ^{13}C, and Fm 0.66-0.95). The composition of OC

associated with fine (<63 μm) flood sediments is similar to that of suspended POC, but less variable between flow conditions for a given site. Elevated POC δ^{13}C values (-21.8 and -23.2‰) in the Chilcotin and Thompson rivers during low discharge conditions suggest the influence of autotrophic production which may be related to the presence of lakes in tributary basins, however this is not a universal feature of tributaries containing lakes. The relationship between mineral surface area and sediment ^{14}C content indicates that lower OC:surface area (OC:SA) sediments (<0.6 mg m^{-2}) are associated with a wide range of mostly modern to largely petrogenic OC (Fm 0.48-1.10), however higher OC:SA sediments (>0.6 mg m^{-2}) are associated with relatively modern OC (Fm 0.82-1.10). The spatial and temporal heterogeneity in OC sources across the Fraser basin must be taken into account when interpreting Fraser River-influenced sedimentary deposits (e.g. Saanich Inlet) or assessing sources of dissolved and sedimentary OC delivered to the river mouth.

3.2 Introduction

The delivery of terrestrial material from the land to the ocean via rivers is one of the fundamental processes regulating Earth's long-term climate, as well as an important source of nutrients supporting marine ecosystems. Rivers fuel the most productive coastal marine biomes on Earth and transfer a portion of the atmospheric CO_2 consumed by weathering and photosynthesis to sediments, exerting a major long-term control on Earth surface temperature (Ebelmen, 1845; Rubey, 1951; Garrels et al., 1976; Walker et al., 1981; Berner et al., 1983; France-Lanord and Derry, 1997; Hayes and Waldbauer, 2006). The organic matter released into rivers interacts with microbes and sunlight as it travels downstream, and sediments suspended in river water are deposited and remobilized along the way. Quantifying the extent of this in-transit degradation of riverine organic matter is critical to assessing the role of watersheds in the consumption versus release of atmospheric CO_2 (Richey et al., 1980; Cole and Caraco, 2001; Battin et al., 2009; Tranvik et al., 2009; Aufdenkampe et al., 2011). Observing the processes of transport and transformation of riverine organic matter is challenging due to seasonal changes in temperature and hydrology, which affect the amount and type of material mobilized in river channels over the course of a year.

The present study aims to link the organic and inorganic biogeochemical characteristics of material in both dissolved and particulate forms in order to present a holistic perspective on source materials and processes of biogeochemical alteration during riverine transport. The study area, the Fraser River basin in southwestern Canada, provides a unique setting for such a study due to three main features: its modest size (250,000 km^2) allows for a detailed characterization of the majority of its subdrainage basins; its variety of bedrock lithology—including carbonate outcrops in certain tributary basins—and spatial and temporal precipitation gradients impart

naturally large variability in biogeoclimatic zones, and thus potentially in geochemical parameters; and its lack of lakes and dams in the main stem allows sediments from all tributaries to influence the composition of material exported to the coastal ocean, an unusual quality for a modern river of any size. Previous work on the impact of bedrock diversity and seasonal hydrology on dissolved and particulate inorganic constituents in the Fraser basin (Cameron et al., 1995; Cameron, 1996; Cameron and Hattori, 1997; Voss et al., 2014) has documented the importance of detailed basin-wide characterizations of source compositions and seasonal sampling to understand the provenance and variability of material reaching the river mouth. This study extends this approach to carbon dynamics. The use of a broad suite of tracers, including bulk concentration and isotope characterizations, elemental and molecular composition, and sedimentological properties, reveals the influence of chemical weathering, sediment transport processes, and biogeochemical cycling on the integrated geochemical composition of Fraser River carbon pools.

3.3 Methods

3.3.1 Sample collection and processing

Surface suspended sediment samples were obtained by pumping 10-20 L of river water with a peristaltic pump from a distance of ~3 m from the river bank through silicone tubing and into plastic carboys. Carboys were rinsed three times with sample water before filling. Samples were filtered on the same day as they were collected (typically within ~4 hours). Water was passed over 90 mm polyethersulfone (PES) membrane filters (pore size 0.22 µm) in pressurized Teflon-lined aluminum filtration units. Filters were folded and placed inside plastic sample bags and frozen. In the lab, filters were thawed and sediment was rinsed into pre-combusted (450°C, 5

hours) glass jars using purified water (18.2 MΩ cm^{-1}, MilliQ system). The residue was freeze dried in a freeze drier with an in-line cold trap to prevent contamination from pump oil, and transferred to pre-combusted glass vials. Suspended sediments collected in summer 2009 (medium flow) were collected on pre-combusted 142 mm glass fiber filters (GFF; nominal pore size: 0.7 μm) in a stainless steel manifold rather than PES membrane filters. These sediments were not recovered from the filters (as was the case of those collected on PES membranes), but rather analyzed with the filter material.

Sediment was collected from river banks just above the water line, which is presumed to derive largely from material recently mobile within the river channel, either as suspended material or mobile bed sediment, and deposited on the banks as water levels declined. This material is hereafter referred to as "flood sediment." Flood sediment samples were collected using a plastic shovel, pre-rinsed with river water before each collection. placed in plastic sample bags, and frozen immediately. In the lab, sediments were freeze dried and subsamples were taken using a microsplitter. Grain size fractions were generated by dry sieving using stainless steel sieves, rinsed with MilliQ water and organic solvents (methanol, dichloromethane, and acetone; reagent-grade) between samples. The majority of flood sediment data are for the <63 μm fraction; data are also presented for selected larger grain size fractions (63-150 μm, 150-250 μm, 250-1000 μm). Where indicated, "ground" samples were ground to a fine powder using an agate mortar and pestle.

3.3.2 Sediment organic carbon and nitrogen content and stable isotopes

Sediments were weighed in triplicate into combusted silver capsules and acidified in concentrated HCl vapor under partial vacuum at 65°C to remove inorganic carbonate. Organic

carbon and nitrogen concentrations (%OC and %N, by weight) and isotope values (δ^{13}C and δ^{15}N) were measured by Carl Johnson at WHOI on an Elemental Analyzer (Carlo Erba 1107) coupled via a Finnigan-MAT Conflo II open split interface to a stable isotope ratio mass spectrometer (Delta^{Plus}) for measurement of ^{13}C/^{12}C (referenced to Pee Dee Belemnite) and ^{15}N/^{14}N (referenced to N$_2$ air) (IAEA, 1995). Sample %OC, %N, δ^{13}C, and δ^{15}N values were determined from standard reference materials NBS-19 limestone (Coplen et al., 2006), IAEA-N-1 ammonium sulfate (Böhlke et al., 1993), USGS-40 glutamic acid (Qi et al., 2003), and a laboratory glycine standard. Analytical accuracy and precision of these measurements are 0.1 wt% for C and N abundance, 0.3‰ for δ^{13}C, and 0.4‰ for δ^{15}N.

Suspended sediment samples collected in 2009 on GFF filters were analyzed by subsampling the filter itself (using a circular stainless steel punch, cleaned with methanol and dichloromethane between samples), as sediments were embedded in the filter material. Representative subsampling of GFF filters was challenging, thus the uncertainties associated with bulk POC results for 2009 samples are larger than those for samples collected on PES membranes in 2010 and 2011. Furthermore, though the POC composition and the amount of POC collected for a given volume of water was determined, the %OC of these sediments cannot be determined.

3.3.3 Grain size and mineral surface area

Bulk sediments were pre-treated for grain size and surface area analyses with repeated applications of 30% H$_2$O$_2$ and mild heating (50°C) to remove organic matter. Grain size samples were then resuspended in 5% sodium pyrophosphate solution to ensure dispersion. Grain size distributions were measured using a laser diffraction grain size analyzer (Malvern Mastersizer

2000) at ETH-Zürich. Sample treatment procedures and technical details of this method are

described by Sperazza et al. (2004) and Jonkers et al. (2009).

Specific surface area measurements were made on a Nova 4000e surface area analyzer

with Quantachrome software using the Brunauer-Emmett-Teller (BET) method (Brunauer et al.,

1938) in the lab of Timothy Eglinton at ETH-Zürich. Samples were degassed for 3 hours at

300°C (mass lost during degassing was typically <5%). Surface area measurements are based on

five-point N_2 adsorption isotherms at 77 K. Data quality was controlled by ensuring five-point

isotherms had a linear $r^2 > 0.9975$. Absolute instrumental error is 0.1 m^2 g^{-1}. Accuracy was tested

by analysis of Quantachrome surface area reference materials 2009 (certified value: 31.18 ± 4.21

m^2 g^{-1}) and 2007 (certified value: 2.85 m^2 g^{-1} $\pm$ 0.20 m^2 g^{-1}) (measured values: 28.2 m^2 g^{-1} and

2.5 m^2 g^{-1}, respectively). The average standard deviation for independently analyzed sample

aliquots was ~2%.

3.3.4 X-ray fluorescence elemental abundances

Approximately 2 g of sediment (<63 μm flood sediment or bulk suspended sediment) was

prepared for x-ray fluorescence analysis (XRF) by drying 6 hours at 105°C then heating at

1050°C for 2 hours to eliminate water, carbonate, and other volatiles. Sediments were then

homogenized with dilithium tetraborate flux at a sample:flux mass ratio of 1:5, transferred to Pt-

Au crucibles, and melted to form a pill using a Claisse M4 automated glass bead casting

machine. Pills were analyzed by Lydia Zehnder on a Panalytical Axios wave-length dispersive

XRF spectrometer at the ETH-Zürich Institute for Geochemistry and Petrology. Precision of

weight abundances of most major elements (TiO_2, Al_2O_3, Fe_2O_3, MnO, CaO, MgO, Na_2O, K_2O,

P_2O_5, Cr_2O_3, NiO) is better than 0.1 wt%, 0.2 wt% for SiO_2, 5 wt% or better for most trace

elements (Ba, Sr, Zr, Cr, V, Th), up to 10 wt% for trace elements at 10-100 ppm (most Rb, Nb, Hf, Y, Ga, Zn, Cu, Ni, Co, Sc, La, Ce, Nd, and Pb values), and up to 50 wt% for trace elements <10 ppm (most Th and all U values). Selected element ratios are presented in Table 3; the full dataset is presented in Tables S1 and S2.

3.3.5 Biomarker concentrations

Biomarker compounds (including n-alkanes and n-alkanoic acids) were extracted from <63 um flood sediment samples in 9:1 dichloromethane (DCM):methanol using a microwave accelerated reaction system (MARS-X). Compound classes were separated using aminopropyl silica gel column chromatography. The fatty acid fraction was saponified, transesterified (generating fatty acid methyl esters, or FAMEs), and purified with a second silica gel column. Alkane and FAMEs fractions were analyzed on a gas chromatography system with flame ionization detector (HP Agilent 5890 series II) and quantified with an external standard matrix of alkanes (n-C_{17}, C_{25}, C_{29}, and C_{33}) and FAMEs (n-C_{16}, C_{20}, C_{23}, and C_{28}). Overall precision for concentration determination (including extraction and analysis) is ~5% (Galy et al., 2011).

3.3.6 DIC and DOC concentrations, optical properties

Samples for dissolved inorganic carbon (DIC) were collected by pumping bubble-free water in-line over membrane filters (0.45 μm pore size used for 2009 and 2010 samples; 0.2 μm pore size for 2011 samples) into pre-cleaned 250 mL borosilicate glass bottles (pre-cleaned with mild Liquinox soap solution and rinsed thoroughly with purified water). Bottles were overfilled with 3x the sample volume and poisoned immediately with 60 μL saturated $HgCl_2$ solution. Glass stoppers were sealed with vacuum grease (Apiezon M) and secured with rubber bands.

DIC concentration was measured on a LICOR CO_2 analyzer by Katherine Hoering in Dr. Zhaohui Aleck Wang's lab at WHOI. Concentrations were quantified by standard curves of DIC reference material provided by Dr. A.G. Dickson at the Scripps Institution of Oceanography (Dickson et al., 2007; Dickson, 2010).

Samples for DOC were filtered in the same manner as DIC samples and collected in 20-60 mL low-density polyethylene bottles (precleaned with 10% HCl). Samples were acidified to pH 2 in the field and stored refrigerated until analysis. DOC and total dissolved nitrogen concentrations were analyzed by high temperature combustion on a Shimadzu TOC analyzer by Ekaterina Bulygina in Dr. Robert Max Holmes' lab at the Woods Hole Research Center.

3.3.7 DOC, DIC, and POC [14]C

DOC and DIC isotope samples were filtered in the same manner as the samples for concentration analysis. DOC ^{14}C samples were collected in combusted (450°C, 5 hours) amber glass bottles and acidified immediately with H_3PO_4 (Certified ACS grade) to pH 2. DIC ^{14}C samples were collected in combusted (450°C, 5 hours) 500 mL borosilicate glass bottles, poisoned immediately with 100 μL of saturated $HgCl_2$ solution, and sealed with greased (Apiezon M) ground glass stoppers and rubber bands. Both DOC and DIC ^{14}C samples were submitted to the National Ocean Science Accelerator Mass Spectrometry (NOSAMS) facility in Woods Hole, USA. Briefly, DOC samples were sparged to remove DIC, then UV-irradiated for 4 hours and sparged on an in-line vacuum line cryo-trap. Evolved CO_2 was converted to graphite and analyzed by accelerator mass spectrometry (AMS). DIC samples were sparged, CO_2 converted to graphite, and analyzed by AMS (Roberts et al., 2010). Analytical precision for NOSAMS DOC and DIC [14]C Fm values was better than 0.005.

POC ^{14}C samples were acidified by fumigation at 60-65°C under partial vacuum for at least 24 hours to remove inorganic carbonate. Sediments were transferred to pre-combusted quartz tubes with a small amount of pre-combusted CuO grains and evacuated on a vacuum line. Tubes were flame-sealed and combusted at 850°C for 5 hours to convert all OC to CO_2, was cryogenically purified, manometrically quantified and transferred to glass tubes on a vacuum line. Samples were either submitted to NOSAMS as CO_2, where they were converted to graphite and analyzed by AMS, or analyzed as CO_2 on the Micadas gas ion source AMS at ETH-Zürich (Christl et al., 2013; Wacker et al., 2013). Analytical precision for POC [14]C Fm values (NOSAMS or ETH-Zürich) was better than 0.01.

3.4 Results

3.4.1 Effect of sample treatment on sediment nitrogen and mineral surface area analyses

Acidification of sediment (a necessary step in order to remove carbonate minerals for organic carbon analysis) can affect measured values of nitrogen content and stable isotope composition (Kennedy et al., 2005; Brearley, 2009; Mazumder et al., 2010; Brodie et al., 2011; Schlacher and Connolly, 2014). A subset of samples (n = 25) was analyzed both with and without the acidification step to test the effect of acidification on nitrogen content and composition in Fraser River sediment samples, and allow for inorganic carbon content estimates (by difference: unacidified %C – acidified %C). Acidification was found to have very little effect on N content over a range of 0.01-0.23 wt% N. Isotope composition, however, was influenced by acidification (Fig. S1). The majority of samples (n = 17) showed lower δ^{15}N in acidified samples. Nitrogen isotope results are presented here, but not interpreted.

The effect of sample pre-treatment on measured surface area was tested by analyzing a subset of samples (n = 40) before and after H_2O_2 treatment. Pretreatment was not found to bias measured surface area, except in samples with very low total measured surface area (<5 m^2), which did show generally higher results for H_2O_2-treated samples than untreated samples (Fig. S2); however, such samples lie below the desired sample size.

3.4.2 Organic and inorganic carbon distribution of the Fraser River

The total carbon budget of the Fraser River is dominated by dissolved inorganic carbon (DIC). At nearly every site and all times of year, the concentration of DIC is the largest component of total carbon species (DIC+DOC+POC), constituting 80% on average (Table 1, Fig. 1). Notably high concentrations of DIC are found in particular tributaries (Robson, McGregor, Blackwater, Willow, and Bridge rivers), which span a wide swath of the Fraser basin and are not restricted to particular lithological zones. Tributaries with especially low DIC concentrations (Harrison and Pitt rivers), however, represent areas with highly weathering-resistant igneous lithologies, and presumably contain negligible carbonate-rich lithologies, and possibly only disseminated carbonate minerals.

Among OC pools, DOC is generally dominant over POC. Most sites have 80% or more of their OC as DOC regardless of season and flow conditions. The largest contribution of POC to the total OC load occurs in samples collected at medium discharge (summer 2009), with some sites bearing 30-60% of OC as POC. DOC is most dominant (85% to 99% of total OC) over POC in low discharge (fall 2010) samples, when DOC and suspended sediment concentrations are at the lowest. DOC concentrations are highest during the freshet (spring 2011 samples). A comparison of peak freshet DOC concentrations at different sites is complicated by the fact that

the freshet DOC pulse is very rapid, and each tributary was likely not sampled at the point of

maximum DOC load. DOC concentrations are higher in tributaries draining the peneplain region

upstream of Prince George (Nechako and Willow Rivers), and one Coast Range tributary, the

Blackwater River, stands out as having an especially high DOC concentration relative to all other

tributaries (466, 546, and 1479 µmol L^{-1} during low, medium, and high discharge, respectively)

relative to other sites under all flow conditions. Another group of tributaries (the Bridge,

McGregor, Robson, Pitt, and Harrison rivers) are notable for their very low DOC concentrations.

POC concentration is a function of both sediment concentration and the OC content of

the sediments, which can vary independently. Suspended sediment concentrations in the Fraser

River are highest during the spring freshet, however discharge events of shorter duration can

rapidly increase the sediment concentration throughout the year (Fig. 2). The organic carbon

content of suspended sediments is significantly higher under low discharge conditions relative to

freshet conditions at nearly all sites in this study (Fig. 3). However, the higher sediment

concentrations during the spring freshet compensate for the low OC content, resulting in much

higher freshet POC concentrations than during the low and medium discharge sampling periods.

POC concentrations were lowest in low discharge (fall 2010) samples.

3.4.3 Isotopic signatures of dissolved and suspended carbon pools

Downstream trends in POC composition are largely consistent between different flow

conditions (Fig. 4, Table 1). The C:N ratio is highest (basin-wide mean: 7.9 mol/mol) during

freshet conditions and lowest (basin-wide mean: 12.1 mol/mol) in summer (medium discharge).

Stable carbon isotope composition ($\delta^{13}C$) of POC is highest (basin-wide mean: -26.7‰) during

high flow conditions and lowest (basin-wide mean: -28.2‰) during medium flow, with the

significant exceptions of the Chilcotin, Thompson, and Robson rivers, which have their lowest

δ^{13}C values (-26.6, -26.4, and -30.2‰, respectively) during high flow. Radiocarbon contents,

expressed as fraction modern (^{14}C Fm), are highest (basin-wide mean: 0.88) during low flow and

lowest (basin-wide mean: 0.80) during medium flow conditions. In other words, the OC exported

during the late summer is significantly older (~700 ^{14}C years) than that exported during the

fall/winter low flow period. These patterns are summarized in Table 2.

3.4.4 Bulk OC composition of fine flood deposit sediments

The majority of flood deposit sediment analyses were made on the <63 μm fraction of

bulk sediments (hereafter referred to as "fine flood sediments") in order to compare these

deposits with the suspended sedimentary load, and to minimize potential bias due to

heterogeneous deposition at a particular site. Data for flood sediment OC composition (%OC,

C:N, δ^{13}C, δ^{15}N, Fm, and long-chain *n*-alkanoic acid and *n*-alkane concentrations) are presented

in Table 3. In comparison to suspended sediments collected at the same time and place, fine

flood sediments were generally leaner in OC (SPM 4.4x higher %OC), higher in C:N (fine flood

sediments on average 52% higher C:N than SPM for low and medium discharge conditions), and

higher in δ^{13}C (fine flood sediments on average ~1.6‰ higher than SPM; Table 2). A notable

exception to these patterns is the C:N composition of fine flood sediments collected during the

spring freshet, which were on average 7% lower in C:N than the corresponding SPM. Unlike

suspended sediments, fine flood sediments did not vary consistently in %OC, C:N, or δ^{13}C

between flow conditions, although individual sites did exhibit some variability between sampling

times.

Bulk OC composition was also analyzed on multiple size fractions for a subset of samples from the 2011 high flow conditions. Although different grain size fractions typically exhibited significantly different %OC, C:N, and δ^{13}C compositions, the differences were not generally a systematic function of grain size (Fig. 5).

3.4.5 Sediment grain size, mineral surface area, and mineralogy

Sediment grain size, specific surface area, elemental composition, and inorganic carbon content (for selected samples) data are presented in Table 4. Bulk grain size distributions of flood sediments were in many cases bimodal, with distinct peaks in both a coarser region (>250 μm) and a finer region (<100 μm). This behavior complicates comparisons between samples using single values, such as the median (D_{50}) or D_{84} grain size. Suspended sediments were more homogeneous and generally finer-grained (flood sediment average ± 1 s.d. D_{84}: 458 ± 347 μm, n = 61; suspended sediment average D_{84}: 89 ± 86 μm, n = 19).

Mineral surface area of fine flood sediments of the main stem Fraser generally increased moving downstream under all flow conditions. Under medium and low discharge conditions, tributary fine flood sediments had higher surface area than the main stem; however, at high flow, this relationship was not consistent across the basin. Surface area measurements were only possible on a small number of suspended sediment samples due to limited sample material. In the one case for which both a fine flood and a suspended sediment sample were analyzed (Blackwater River, spring 2011), the suspended sediment surface area was much greater than that of the flood sediment (19.7 and 4.5 m^2 g^{-1}, respectively). Bulk flood sediment grain size metrics (D_{50}, D_{84}) do not correlate with surface area, whereas those of suspended sediment grain size do (Fig. 6).

Sediment chemical composition (determined by XRF) exhibits considerable variability across the Fraser basin, as indicated by the range in molar ratios of Fe/Si (0.036-0.108) and Al/Si (0.13-0.33) (Fig. 7). For the fine flood sediments, these parameters did not correlate with grain size (which is logical considering that they represent only a portion of the grain size distribution) or mineral surface area. The Al/Si and Fe/Si composition of suspended sediments collected during the spring freshet (n = 6) did correlate strongly with D_{84} grain size ($r^2 = 0.94$ and 0.90, respectively). Particular sites in the Rocky Mountains exhibit elevated Ca/Na (>3) and Mg/Na (>2) composition (Robson, McGregor, and Willow rivers), indicating significant weathering of carbonates in these basins. A subset of fine flood sediments which were also analyzed for both total (unacidified) and organic (acidified) carbon content indicate that these high Ca/Na and Mg/Na values are associated with relatively high inorganic carbon content (McGregor: 2.5%, Robson: 5.9%; all other samples [n = 23] were <0.6%).

While the majority of Fraser River sediments describe a coherent trend in Ca/Na versus Mg/Na space, samples from the Bridge River (Coast Range) and the Fraser at Fitzwilliam (Rocky Mountains) fall off the trend with higher Mg/Ca composition. This is likely due to the weathering of sulfate minerals (in the sedimentary Rocky Mountains) and sulfide minerals (in the Coast Range; Cameron et al., 1995; Spence and Telmer, 2005).

3.5 Discussion

3.5.1 Flow-dependence and spatial patterns of DOC, POC, and DIC

Concentrations of all major carbon species in the Fraser River main stem exhibit similar downstream trends. In general, concentrations are relatively low in the Rocky Mountain headwaters, elevated in the central portion of the basin, and gradually decline for roughly the

second half of the river's length. The tributary inputs of each of these pools, however, are distinct in their contribution to spatial variability and in their response to seasonal changes in discharge.

Inputs of relatively OC-rich POC from tributaries in the central part of the Fraser basin (Blackwater and Chilcotin rivers) cause a slight rise in the OC content of suspended sediments moving downstream (between roughly Hansard and Lillooet). Despite OC-rich sediments delivered by the Thompson and Bridge rivers, main stem Fraser POC becomes leaner in OC in the lower reaches around Hope and in the floodplain between Hope and the river mouth. Although the OC content of lower basin tributaries such as the Harrison and Pitt was not determined in this study, the contribution of these rivers to the total Fraser POC load is certainly minor. These tributaries flow into the Fraser immediately downstream of large lakes, which effectively strip their entire sediment load.

The downstream trends in POC concentration, however, are likely the product of not only distinct source contributions, but also the different suspended sediment concentrations in different portions of the basin. Particularly during medium and low flow conditions, the POC concentration of the main stem Fraser is higher than that of all of the tributaries. The reason for this is likely the presence of lakes in many tributary basins, which lead to lower suspended sediment concentrations, and therefore lower POC concentration even if the %OC is relatively high. The main stem Fraser, in contrast, has no such sediment impoundments, and is therefore able to maintain higher sediment and POC concentrations, for instance, by mobilizing bank material from the main channel. This dichotomy is somewhat obscured in the samples from the freshet campaign, during which certain tributaries (particularly the Blackwater and Chilcotin rivers) had such high sediment loads that their POC concentrations far exceeded that of the main

stem Fraser. Other tributaries sampled during this campaign, however, did not carry sufficiently high suspended sediment concentrations to reach the POC concentrations of the main stem Fraser.

The downstream pattern of DOC concentrations is similar to that of POC, with low concentrations in tributaries draining the Rocky Mountains and the lower Coast Range, and high concentrations in those draining the central portion of the basin (Cariboo and upper Coast Range). The main stem Fraser reflects this in a rising DOC concentration from the headwaters until Hansard/Stoner, and then a slight decrease for the remainder of its length. While this spatial pattern is quite consistent between the different flow regimes, the absolute concentrations vary substantially. DOC concentrations are lowest in the samples collected during medium discharge, somewhat higher during low discharge, and highest during the spring freshet. This freshet DOC pulse is a common feature of many high-latitude rivers (Cooper et al., 2008; Holmes et al., 2008; Guo et al., 2012), and likely results from changing hydrologic flowpaths as surface soils across the basin become inundated, releasing DOC accumulated throughout the previous year. Chapter 4 investigates this transition in more detail.

The seasonal variations in DIC concentrations are notably distinct from those of DOC and POC. DIC is the single largest component of the dissolved load of the Fraser River and its concentration at most sites varies only modestly between high, medium, and low discharge conditions (1 s.d. average 23% for all sites; average 1 s.d. DOC variability, in contrast, is 59%).

3.5.2 Carbon composition evidence of sources and biogeochemical interactions

The geochemical compositions of sediments and dissolved material provide multiple indicators of the influence of carbonate weathering in particular portions of the Fraser basin. As

noted above, the exceptionally high DIC concentrations in certain tributaries reveal a contribution from carbonate-rich lithologies. The dissolved inorganic load of the Fraser River is essentially a binary mixture between carbonate- and silicate-derived weathering products (Voss et al., 2014), although sulfate and sulfide weathering also occur in certain regions (Cameron et al., 1995; Spence and Telmer, 2005). The major cation composition of the Robson River in particular resembles that of runoff from carbonate-dominated lithologies (Meybeck, 1986; Gaillardet et al., 1999). However, if DIC were derived entirely from carbonate weathering, a strong linear correlation would be expected between DIC concentration and (Ca+Mg)/Na (as a combined proxy for carbonate influence, corrected for precipitation contributions assuming all dissolved chloride derives from sea salt aerosols). In the Fraser River, this is clearly not the case (Fig. 8).

The estimate of non-carbonate DIC uses this equation:

$$DIC_{non-carb} = DIC_{meas} - \left(\frac{Ca + Mg}{Na}\right)_i \times \left(\frac{DIC}{(Ca + Mg)/Na}\right)_{Robson}$$

where (Ca+Mg)/Na$_i$ is the ratio of sea salt-corrected concentrations for sample i and DIC/[(Ca+Mg)/Na]$_{Robson}$ is the slope of the DIC-(Ca+Mg)/Na relationship for the Robson River under medium discharge conditions. The reason for this choice is that this sample exhibits the highest Ca+Mg/Na value, which should correspond the closest to a geochemical composition reflecting only carbonate weathering in the Fraser basin. It should be noted that the sea salt aerosol correction is complicated for the Robson River medium discharge sample, as the very high dissolved Cl value of 43 µmol L^{-1} reported by Voss et al. (2014) is likely influenced by sources other than aerosols. Robson River Cl concentrations at low and high discharge are 4.6 and 5.7 µmol L^{-1}. Cl concentrations for other Rocky Mountain tributaries, i.e. McGregor, Holmes, and Small Rivers, under all discharge conditions do not exceed 5.5 µmol L^{-1}, and all

other Fraser basin samples under medium discharge conditions do not exceed 18.5 µmol L^{-1}. A lower Robson River Cl concentration results in a lower estimated non-carbonate DIC concentration. We therefore chose to correct the sea salt contribution to the medium discharge Robson River sample using a Cl concentration of 3 µmol L^{-1}, which represents the lower range of Cl concentrations for Rocky Mountain tributaries during this sampling time, and therefore yields a lower limit estimate of non-carbonate DIC in other Fraser basin samples. The choice of Cl concentration estimate for this sample is clearly important; however, within reasonable bounds, the exact value does not substantially alter the result and interpretation of the estimate of non-carbonate DIC. For instance, a Robson River medium discharge Cl concentration of 6 µmol L^{-1} yields a basin-wide mean proportion of non-carbonate DIC out of total DIC of 83-89% (the range of means for all three discharge conditions), while a Cl concentration of 2 µmol L^{-1} yields a basin-wide mean non-carbonate DIC proportion of 74-81%. Based on this, we estimate that the average non-carbonate-derived proportion of total DIC in the Fraser River is 75-90%.

Concentrations of non-carbonate DIC and DOC show a significant positive correlation (95% confidence interval) for all three discharge conditions (p-values 0.04, 0.002, and 0.005 for low, medium, and high discharge, respectively; Fig. 8). This suggests that respiration of DOC is a significant source of DIC in the Fraser River. According to this calculation, nearly every tributary and main stem site downstream of the McGregor River has >70% of its DIC derived from DOC respiration at all times of year, and 88-91% of DIC reaching the river mouth is non-carbonate-derived. The assumption that zero DIC derives from sources other than carbonate weathering and DOC respiration is imperfect. For instance, the DIC contributions from groundwater and precipitation are neglected, and DIC losses from CO_2 efflux or autotrophic uptake may also play a role. However, the significant correlation between non-carbonate-derived

DIC and DOC concentration clearly shows that DOC is an important source of DIC in this system. Furthermore, the fact that the slope of this relationship is >1 at most sites during low and medium discharge periods suggests that DOC-derived DIC is able to accumulate rather than escape entirely as CO_2. In contrast, during the spring freshet, the basin-wide average slope is ~0.5, meaning that the quantity of DOC entering the Fraser during this time is greater than the capacity of aquatic microbes to metabolize it to the same extent as during other times of year. Whether the controls on this microbial respiration are physiological (i.e. insufficient residence time for microbial growth) or biochemical (i.e. chemical nature of DOC inhibits complete metabolism), it is likely that a larger proportion of biologically labile DOC escapes degradation before it reaches the coastal ocean during the spring freshet. A physiological control is likely given that water temperatures during the spring freshet (3-10°C) are significantly colder than during late summer (15-25°C), which presumably exerts a significant control on microbial growth.

Because the DOC and DIC ^{13}C and ^{14}C dataset is limited to samples from the medium discharge sampling campaign, the following points may not apply equally for all seasons. The fact that the sites with relatively low DOC ^{14}C Fm (Robson and McGregor rivers and the Fraser at McBride) apparently correspond to the sites with low DIC ^{14}C Fm (Robson River; the McGregor River and Fraser River at McBride were not analyzed for DIC ^{14}C; Fig. 9) could be due to either interaction between these carbon pools, or to source materials that are distinct but similarly aged. These data provide an opportunity to independently test the estimates of non-carbonate weathering-derived DIC above based on dissolved major element composition. Assuming a simple mixture of carbonate weathering-derived DIC with DOC respiration-derived DIC, we can calculate a mass balance between the carbonate and DOC end-members for each

sample with both DOC and DIC isotope data. The carbonate end-member for ^{14}C is Fm = 0; that for ^{13}C could be somewhat variable, however a reasonable estimate for sedimentary carbonate is $\delta^{13}C$ = ~0 (Schulte et al., 2011). So long as DOC sources within individual tributary basins are not spatially variable, the ^{13}C and ^{14}C composition of DOC contributing to DIC through respiration can be derived from measured values of DOC $\delta^{13}C$ and Fm at a given site. Therefore, the fraction of DIC deriving from DOC respiration is calculated as the ratio of measured DIC $\delta^{13}C$ to DOC $\delta^{13}C$, and likewise for Fm. Applying this estimate to sites around the Fraser basin from the medium discharge summer campaign, we find that the ^{14}C-based estimates are of a similar magnitude to the major element-based estimates (predicting 75-96% of DIC derived from DOC respiration). However, the ^{13}C-based estimates predict a much smaller contribution from DOC to the DIC pool: 15-33%. Thus these estimates need to be further refined to account for influences such as exchange of CO_2 with the atmosphere and autotrophic conversion of DIC to POC. Additional measurements of DIC and DOC isotopes would also provide a more complete dataset, including multiple tributaries strongly influenced by carbonate weathering and samples from different flow conditions.

Combustion-derived aerosols are a major source of ancient OC in surface waters and soils globally (Jaffé et al., 2013). DOC in streams draining coastal and mountainous glaciers of western North America in particular have been shown to contain a significant aged component, most likely from aerosols derived from fossil fuel combustion (Hood et al., 2009; Stubbins et al., 2012). Though less directly impacted by air masses originating from east Asia (the predominant source for aerosols to the North American west coast), mountain glaciers of the Fraser River may be affected by deposition of such pre-aged anthropogenic OC. However, if this is the case, it is not clear why relatively old DOC would be restricted only to these headwater basins, given that

most major tributaries of the Fraser River have headwaters fed by glaciers (Thorne and Woo, 2011). The importance of glacial influence may be obscured by differences in residence time between tributaries given that the tributaries carrying ^{14}C-depleted DOC are smaller than most of the others analyzed. The aged DOC in larger basins may therefore have been respired before the DOC reached the sampling point. If the source of the aged DOC is truly combustion-derived, highly aromatic OC, however, it would likely persist in the aquatic system, as was observed by Stubbins et al. (2012). The source of aged DOC in the Fraser, in contrast, appears to be related to more than just the presence of glaciers.

As a test of the above hypothesis that DOC respiration is a major source of DIC in the Fraser River, it might be expected that DIC δ^{13}C composition would depend on DOC δ^{13}C composition. Since both DOC derived from leaching of C_3 plant material and DIC derived from weathering of carbonate-free lithologies have very negative δ^{13}C (-24‰ or lower), these abiotic, carbonate-free sources should contrast sharply with a carbonate weathering DIC signature (0 to -10‰). DOC δ^{13}C values in the Fraser are generally reflective of such a source, with values falling within a narrow range (-26.2 to -27.3‰). *In situ* production may also influence the δ^{13}C composition, and result in POC and DOC with more negative δ^{13}C values, and a residual DIC pool characterized by higher δ^{13}C values. Therefore both *in situ* production and carbonate weathering would cause higher δ^{13}C composition relative to a pure non-carbonate weathering source. A δ^{13}C value of POC in the Robson River that is lower than that of nearby main stem sites (Fitzwilliam, McBride, Hansard), however, suggests that the relatively low Fm value of DOC in the Robson River is due in part to fixation of carbonate-influenced aged DIC.

The influence of erosion of carbonate-rich lithologies on the sedimentary load of the Fraser River can be seen in the elevated Ca/Na and Mg/Na compositions and inorganic carbon

contents of flood sediments from the Robson and McGregor Rivers. The composition of sedimentary OC, particularly of POC, is highly variable in space and time (Fig. 4). Suspended sediments from across the basin define a strong correlation between total %OC and modern %OC (defined as ^{14}C Fm * %OC following Galy et al., 2008) over a very wide range of %OC values (Fig. 10). However, the basin-wide samples exhibit more scatter in this relationship ($r^2 = 0.994$) than the suite of sediment depth profiles collected near the Fraser River mouth ($r^2 = 0.999$; see Chapter 4), and thus the regression analysis for estimating the average petrogenic %OC contribution and biospheric OC residence time is very sensitive to the selection of samples included. This suggests that, even at different flow stages, the process of transport to the Fraser River mouth results in suspended sediments which integrate the basin in a consistent manner. Sediments collected farther upstream more closely resemble distinct source materials, which are clearly not uniform across the basin. The Quesnel River, for example, falls slightly below the line described by the other sites at high and low discharge. The Quesnel data alone predict a larger petrogenic %OC contribution (0.15%) than the depth profiles near the mouth (0.12%), indicating that this tributary is a significant source of petrogenic OC in the Fraser River. Conversely, using only data for the Blackwater River, a very small petrogenic OC contribution is predicted (0.01%), thus this tributary appears to deliver almost entirely biospheric POC. As petrogenic OC is determined by the OC content and erodability of the bedrock undergoing weathering (Copard et al., 2007), the variability in petrogenic OC contributions for different tributaries is not surprising given the geologic diversity in this basin.

The overall basin trend of highest POM C:N composition at high discharge and lowest at medium discharge may reflect the mobilization of distinct portions of soil OM and/or differential transformation of the POM that enters streams at different times of year. The fact that the C:N

composition of suspended sediments is lower during low flow conditions than during the freshet period, and %OC is higher, suggests that the additional OC carried during low flow is more degraded relative to fresh plant source material, as living plant tissue typically has C:N values of >20 while bacterial and fungal biomass C:N is typically ~4-10 (Hedges et al., 1997). It is possible that the lower C:N POM of low discharge periods represents older soil OM, relatively enriched in N through microbial degradation. Alternatively, if in-stream heterotrophy is significant, *in situ* degradation could reduce the C:N composition of POC. In stream heterotrophy is most likely strongest during the summer months when water temperature is high and turbidity is relatively low, which may partially explain the lowest C:N composition in the medium discharge samples.

The longer residence time of water and lower suspended sediment concentrations (i.e. greater light penetration) during low discharge periods may promote in situ production in the Fraser basin, particularly in tributaries with lakes. The very elevated δ^{13}C values (>-24‰) of POC samples collected during low discharge in the Chilcotin and Thompson rivers—which do contain large lakes in their basins—indicates that *in situ* production can be responsible for a significant portion of POC under certain conditions. Other tributaries with large lakes, however (e.g. Nechako, Quesnel, and Harrison rivers), do not exhibit such significant increases in POC δ^{13}C during low discharge. In the absence of additional DOC and DIC isotope composition data, it is difficult to surmise whether comparatively significant *in situ* production also occurs in these basins during low discharge periods.

3.5.3 Sedimentological controls on organic carbon transport

Mineral specific surface area is a potentially important indicator of OC preservation potential in near-shore marine sediments. In coastal settings, a hypothetical "monolayer equivalent" quantity of ~1 mg OC m^{-2} is often observed, indicating that further loss of OC is inhibited by physical or biochemical limits (Suess, 1973; Keil et al., 1994; Mayer, 1994; Keil et al., 1997; Ransom et al., 1997). The OC:surface area (OC:SA) composition of fluvial sediments is an important consideration as the source material for a significant portion of sediment delivered to coastal margins. The OC:SA values of Fraser River sediments generally increases with grain size, with the lowest values for suspended sediments (mean ± 1 s.d.: 0.6 ± 0.4 mg m^{-2}, n = 5), and increasing from the <63 μm flood sediments (0.8 ± 0.6 mg m^{-2}, n = 40) to the 63-150 μm flood sediments (1.7 ± 1.6 mg m^{-2}, n = 7) to the 150-250 μm flood sediments (3.1 ± 2.9 mg m^{-2}, n = 6) to the 250-1000 μm flood sediments (3.6 ± 2.6 mg m^{-2}, n = 6). The coarser-grained sediments therefore carry a greater loading of OC, which appears to be largely oxidized before they are physically broken down to particles which can be mobilized as suspended material. Further analysis of sediments travelling in the channel bed of the Fraser River should be undertaken in order to determine the OC:SA composition of material transported out of suspension which is also delivered to the delta and coastal ocean.

The age of OC is variable (Fm 0.48-1.10) for sediments with low OC:SA (Fig. 11); however, for sediments with OC:SA > ~0.6 mg m^{-2}, OC ^{14}C content (Fm 0.82-1.10) is much higher than that of some low OC:SA sediments (as low as Fm 0.48). The low proportion of petrogenic OC in high OC:SA sediments indicates that these sediments carry predominantly modern OC, regardless of their total OC content.

3.6 Conclusions

The sources of DIC, DOC, and POC in the Fraser basin are spatially decoupled. Carbonate weathering as a major source of DIC is restricted to certain headwater basins (Robson and McGregor rivers), as indicated by high DIC concentrations, relatively low DIC Fm values, high dissolved and sedimentary Ca/Na and Mg/Na ratios, and detectable inorganic C in sediments. Downstream of these basins, tributaries carrying a disproportionately high DOC load (Blackwater, Nechako, and Willow rivers) enter the Fraser. The brief pulse of DOC observed across the basin during the spring freshet is not synchronous from one tributary to the next. DOC respiration is a major source of DIC in non-carbonate influenced tributaries of the Fraser, accounting for up to 85% of the DIC reaching the river mouth. POC sources are driven primarily by suspended sediment concentration and secondarily by the OC content of the sediments. Higher sediment concentrations during the spring freshet compensate for the lower %OC, with the result that this period accounts for the majority of POC flux. The composition of POC changes under different flow conditions, with freshet sediments generally leaner in OC and exhibiting higher C:N relative to lower discharge periods. The $\delta^{13}C$ composition of POC in certain tributaries during low discharge indicates an influence from in situ production. Further ^{13}C and ^{14}C analyses of DIC and DOC will help assess the importance of this process.

The uneven distribution of POC export in the Fraser basin has important implications for the interpretation of material sampled near the river mouth or in proximal sedimentary deposits. These subbasins represent distinct biogeoclimatic zones with associated vegetation and geochemical signatures that do not represent the Fraser basin as a whole. Furthermore, the Nechako River, the second-largest tributary of the Fraser, is influenced by a major hydroelectric diversion which removes ~17% of its natural water discharge and presumably traps a significant

portion of its sediment load in the Kenney Dam reservoir. Hence the Nechako POC flux is likely much smaller than it was before the dam was installed in the 1950s.

The OC loading of sediments across the Fraser basin exhibit wide variability. OC:SA ratios of fine flood sediments and suspended sediments are generally lower than those of larger-grained flood sediments. Sediments with relatively high OC:SA (>0.6 mg m^{-2}) are associated with relatively modern OC, suggesting that modern OC is preferentially lost as sediments transition from immobile terrestrial deposits (e.g. soils, coarse flood deposits) to fine flood sediments and suspended material.

Site	Dist. (km)	Flow Stage	Parent IGSN	Concentrations (μmol L⁻¹)				C:N (mol mol⁻¹)		$\delta^{13}C$ (‰)			$\delta^{15}N$ (‰)	^{14}C Fm		
				DIC	DOC	POC	POC %OC	DOM	POM	DIC	DOC	POC	POM	DIC	DOC	POC
Fraser	50	low	GRO000027	803	117		1.64±0.18	67.6	13.8±1.8*			-26.83±0.30	1.3±0.4*			0.835
at Fitz-		med	GRO000009	506	44	30.4±12		13.2	8.6±2.6	-4.28	-26.18	-26.1±1.4	3.6±2.1	0.896	1.015	
william		high	GRO000073	719	189	20.8±1.7	0.67±0.10	46.8	13.3±1.5*			-25.94±0.30	1.4±0.4*			0.856
Fraser	230	low	GRO000030	1107	69			37.1								
at McBride		med	GRO000011	708	20	34±10		5.4	7.6±1.0		-26.66	-26.3±0.5	0.2±1.8		0.930	0.605
		high	GRO000070	891	161	33.6±0.8	0.53±0.10	77.9	11.4±0.9*			-25.80±0.30	1.6±0.4*			0.767
Fraser	480	low	GRO000038	2012	297	13.5±0.1	2.68±0.10	31.9	10.7±0.1*			-28.42±0.30	3.31*			0.891
at Hansard		med	GRO000012	1104	54	69±23		14.9	9.8±0.9			-27.3±1.3	1.1±0.4			0.779
		high	GRO000066	1066	233	13.3±0.2	0.97±0.10	53.1	10.9±0.2*			-26.43±0.30	2.1±0.4*			0.779
Fraser	615	low	GRO000041		243	25.1±1.6	2.98±0.19	80.3	9.8±0.7*			-26.68±0.30	-0.1±0.4*			0.973
at Stoner		med	GRO000018	983	199	47±14		31.4	8.9±0.8	-6.73	-26.87	-28.0±0.8	0.4±1.2	0.861	1.093	
Fraser	1050	low	GRO000045		235	21.3±0.8	2.00±0.10	24.2	9.9±0.4*			-26.32±0.30	1.4±0.4*			0.904
at Lillooet		med	GRO000022		156	15±25		25.8	3±10	-6.40	-26.69	-28.9±1.5	1.5±2.9	0.865	1.081	0.767
		high	GRO000058	1078	642			52.7			-27.58				1.020	
Fraser	1110	low	GRO000047		205											
at Lytton		med	GRO000008	955	145	62±29		21.0	10.4±1.2			-28.4±1.0	1.5±1.4			0.723
Fraser	1210	low	GRO000048		216	15.8±0.7	1.94±0.10	43.7	8.7±0.5*			-25.85±0.30	2.3±0.4*			0.875
at Hope		high	GRO000055	797	418	104±8	0.35±0.10	38.1	13.1±1.3*			-26.42±0.30	1.3±0.4*			0.660
Fraser	1315	low	GRO000051	1016	193	10.6±0.2	1.58±0.10	68.7	8.5±0.3*			-26.74±0.30	2.9±0.4*			0.822
at Fort		med	GRO000001	826		31±9			7.5±2.4	-6.26		-28.49±0.30	3.0±3.3	0.888		0.756
Langley		med	GRO000025	799	131	27±18		16.9	7.1±2.0		-26.67	-28.8±0.7	3.4±2.7		1.066	0.706
		high	GRO000073	894	386	123±4	0.62±0.10	49.8	13.1±0.7*			-26.83±0.30	1.8±0.3*			0.742
Delta 0.5 m	1336	low	GRO000052			24.1±0.6	1.66±0.10		10.0±0.6			-26.38±0.30	2.5±0.4			0.921
4.5 m		low	GRO000052			26.2±0.7	1.91±0.10		9.6±0.6*			-26.55±0.30	2.8±0.4*			0.935
8.0 m		low	GRO000052			22.0±0.8	1.71±0.10		10.0±0.4			-26.64±0.30	2.7±0.6			0.947
Delta 9.0 m	1340	med	GRO000002	674	132	44.7±20.9		16.4	14±9	-6.62		-26.7±1.4	1.2±1.9	0.877		0.741

0.5 m		med	GRO000002	662	130	27±13		15.7	8.1±0.9	-6.49	-26.82	-28.7±0.3	2.7±0.8	0.882	1.053	0.749
Delta 0.5 m	1336	high	GRO000075			103.7±0.5	0.67±0.10		12.4±0.6			-26.54±0.30	1.6±0.4			0.839
9.0 m		high	GRO000075			125±7	0.35±0.10		12.7±1.6*			-26.56±0.30	1.3±0.4*			0.813
12 m		high	GRO000075			134±4	0.28±0.10		13.2±0.7			-26.11±0.30	0.3±1.4			0.793
Robson	125	low	GRO000029	1417	31	3.2±0.1	0.65±0.10		6.3±0.3			-27.46±0.30	2.7±0.4			0.664
River		med	GRO000010	1212	17	4±15		3.0	6.7	-4.57	-26.82	-28.7±0.5	0.0±0. 4	0.711	0.945	0.659
		high	GRO000074	1594	62	2.0	1.75	43.3	9.4±0.1			-30.17	-0.28			0.765
Bowron	478	med	GRO000014	1563	108	4.2±2.0		26.4	6.6±0.9			-29.6±1.4	0.9±2.6			0.845
River		high	GRO000062	1084	365	18.9±0.3		62.3								
McGregor	500	low	GRO000037	1672	177	4.6±0.1	1.66±0.10	55.4	9.9±0.3			-27.62±0.30	2.5±0.5			0.806
River		med	GRO000013	1367	23	7±9		11.4	6±4		-27.02	-29.0±1.2	0.3±2.3		0.926	
		med	GRO000013		31			12.2								
		high	GRO000065	1126	211		0.80±0.10	29.4	12.7±0.5			-26.46±0.30	1.9±0.4			0.757
Willow	555	low	GRO000036	1043	289	5.7±0.6	4.94±0.51	51.1	13.3±1.4*			-28.62±0.30	1.8±0.4*			
River		med	GRO000015	1186	276	8.6±3.0		35.6	6.8±2.1			-29.5±0.8	5.7±6.4			0.924
		high	GRO000063	536	694			48.1								
Nechako	575	low	GRO000039	1124	437	4.5	4.35	46.3	9.3			-27.51	5.49			0.929
River		med	GRO000016	739	395	34±5		39.5	7.6±0.4	-6.38	-27.32	-29.5±0.6	3.7±1.0	1.003	1.090	0.934
Stuart	575	med	GRO000017	887	488	13±10		38.1	8.6±2.7			-29.4±1.1	-0.7±6.9			1.027
Lake		high	GRO000064	869	850	49±4	1.28±0.11	49.8	9.9±1.3			-27.77±0.30	2.6±0.4			0.899
Blackwater	705	low	GRO000040	1554	466	14.4±0.9	10.41±0.67	33.1	8.0±0.5*			-26.49±0.30	2.1±0.4*			0.873
River		med	GRO000019	1633	546	35±11		29.8	6.9±0.6	-8.74	-26.57	-27.1±0.6	1.9±0.4	0.950	1.070	0.971
		high	GRO000061	987	1479	332±38	0.63±0.10	51.7	12.1±1.8*		-27.16	-26.32±0.30	3.2±0.4*			0.859
Quesnel	770	low	GRO000042	1061	124	6.2±0.2	1.50±0.10	27.7	9.2±0.2			-26.93±0.30	2.3±0.4			0.734
River		med	GRO000020	984	88	17±12		11.6	10.2±2.1	-4.73	-26.36	-28.9±0.6	-0.6±2.8	0.871	1.060	0.544
		high	GRO000060	1125	268	43.6±0.8	0.51±0.10	73.1	11.4±0.4			-25.81±0.30	1.5±0.4			0.579
Chilcotin	805	low	GRO000043	733	90	9.3	3.84	58.0	8.7			-21.83	6.02			0.905
River		med	GRO000021	518	83	26±19		20.7	8±4	-3.80	-26.20	-28.0±1.1	0.2±1.9	0.981	1.019	0.868
		high	GRO000059	1397	1055	157±31	2.2±0.4	40.9	14±3		-27.10	-26.55±0.30	3.08±0.13		1.057	1.005

River			IGSN									δ¹³C	δ¹⁵N			
Bridge	1045	low	GRO000044	1684	70	12.7±2.8	5.0±1.1		13±3*			-27.51±0.30	1.2±0.5*			0.982
River		med	GRO000023		49	18±4		18.9	9.4±0.4			-27.2±0.5	0.5±2.7			0.853
		high	GRO000057		205			34.0								
Thompson	1111	low	GRO000046	734	172	10.6±1.3	5.3±0.6	109.8	8.6±1.1			-23.20±0.30	7.9±0.4			0.888
River		med	GRO000007	599	115	12±5		15.6	7.1±2.0	-5.36	-26.55	-28.0±1.2	2.7±1.5	0.935	1.063	0.864
		high	GRO000056	812	414	54±5	1.90±0.19	37.0	12.2±2.0			-26.36±0.30	3.5±0.4			0.978
Harrison	1265	low	GRO000049	397	127											
River		med	GRO000006	296	74	11±4		23.2	5.5±2.1		-26.38	-28.0±0.4	-0.3±2.6	1.024		0.915
		high	GRO000054	343	115	6.4±0.7		45.3								
Pitt	1335	low	GRO000050		118											
River		high	GRO000053	140	139			73.9								

Table 1. All bulk dissolved and suspended sediment organic matter data. IGSN codes refer to International GeoSample Numbers in the System for Earth Sample Registration (Sesar) database; sample metadata can be accessed at www.geosamples.org. C:N values marked with a * were not acidified. For sediment %OC, $\delta^{13}C$, and $\delta^{15}N$ data, if calculated uncertainties (1 s.d. of the mean of triplicate analyses) were less than instrumental uncertainty (0.1 for %OC, 0.3‰ for $\delta^{13}C$, and 0.4‰ for $\delta^{15}N$), instrumental uncertainties are shown.

POC Parameter	SPM Seasonal Trends	Sediment Type Trends
%OC	high < low	flood < SPM
C:N	med < low < high	SPM < flood*
δ^{13}C	med < low < high	SPM < flood
^{14}C Fm	med < high < low	no consistent trend

Table 2. Seasonal patterns of POC composition. Abbreviations are low = low discharge, fall; med = medium discharge, summer; high = high discharge, spring; "flood" refers to the <63 μm fraction of flood sediments. *During spring freshet, SPM > flood.

IGSN	Site	Flow Stage	Dist. (km)	Size Fraction (µm)	^{14}C Fm	FAMEs, C_{24-36} (µg/mg OC)	Alkanes, C_{12-36} (µg/mg OC)	%OC	$(C:N)_{unt.}$	$(C:N)_{acid.}$	δ^{13}C (‰)	$\delta^{15}N_{unt.}$ (‰)	$\delta^{15}N_{acid.}$ (‰)
GRO001047	Fraser at Fitzwilliam	low	50	<63		0.071	0.155	0.25±0.10	11.8±0.6		-24.5±0.3	2.1±0.5	
GRO001033	Fraser at Fitzwilliam	med	50	<63				0.24±0.10	7.3±0.3		-23.4±0.3	1.5±0.4	
GRO001078	Fraser at Fitzwilliam	high	50	<63	0.875			0.39±0.10	12.3±0.7	9.9±0.9	-24.6±0.3	1.6±0.4	2.05±1.1
	Fraser at Fitzwilliam	high	50	63-150				0.19±0.10	16.1±0.7	9.1±0.5	-24.4±0.3	1.5±0.4	-0.77±0.5
	Fraser at Fitzwilliam	high	50	150-250				0.33±0.10		16.3±4.5	-24.5±0.3		-0.32±1.7
	Fraser at Fitzwilliam	high	50	250-1000				4.79		24.9±4.2	-26.3		0.63±0.4
GRO001049	Fraser at McBride	low	230	<63	0.520	0.161	0.294	0.19±0.10	9.6±0.2		-23.8±0.3	1.0±0.5	
GRO001035	Fraser at McBride	med	230	<63				0.13±0.10	10.0±0.3		-23.3±0.3	1.7±0.4	
GRO001077	Fraser at McBride	high	230	<63				0.39±0.10	10.3±0.2	7.7±0.4	-24.8±0.3	1.4±0.4	0.92±0.7
	Fraser at McBride	high	230	63-150				0.33±0.10		10.4±0.5	-25.0±0.3		1.53±0.4
	Fraser at McBride	high	230	150-250				0.40±0.11		13.8±5.0	-25.5±0.3		0.89±1.0
	Fraser at McBride	high	230	250-1000				0.69±0.21		19.0±7.7	-26.7±0.3		0.84±0.8
GRO001053	Fraser at Hansard	low	480	<63		0.271	0.384	0.45±0.10	11.6±0.4		-25.9±0.3	1.3±0.4	
GRO001076	Fraser at Hansard	high	480	<63				0.58±0.10	11.4±0.4	10.3±0.4	-26.1±0.3	1.0±0.4	0.38±0.6
	Fraser at Hansard	high	480	63-150				1.00±0.10	13.5±0.4	13.1±0.8	-26.5±0.3	1.3±0.4	0.85±0.6
	Fraser at Hansard	high	480	150-250				2.58±0.20		18.0±2.6	-26.9±0.3		0.61±0.5
	Fraser at Hansard	high	480	250-1000				1.60±0.17		16.4±2.9	-27.0±0.3		0.41±0.4
GRO001056	Fraser at Stoner	low	615	<63		0.716	0.421	0.52±0.10	10.1±0.4		-26.0±0.3	1.4±0.4	
GRO001040	Fraser at Stoner	med	615	<63				0.50±0.10	11.6±0.6		-26.2±0.3	1.7±0.4	
GRO001060	Fraser at Lillooet	low	1050	<63		0.473	0.177	0.66±0.10	9.8±0.3		-24.1±0.3	-0.3±0.5	
GRO001044	Fraser at Lillooet	med	1050	<63				0.12±0.10	11.4±0.2		-25.4±0.3	0.7±1.3	
GRO001067	Fraser at Lillooet	high	1050	<150				0.10±0.10	10.3±0.3	4.8±0.6	-25.6±0.4	1.6±0.7	1.55±1.7
	Fraser at Lillooet	high	1050	150-250				0.07±0.10		8.2±0.7	-25.6±0.5		-2.37±3.2
	Fraser at Lillooet*	high	1050	150-250				0.08±0.10		8.9±0.6	-25.7±0.3		-2.01±1.0
	Fraser at Lillooet	high	1050	250-1000				0.16±0.14		18.9±17.6	-26.2±1.1		-3.38±3.7
	Fraser at Lillooet*	high	1050	250-1000				0.16±0.11		11.7±11.1	-26.7±0.3		-0.20±4.0
GRO001062	Fraser at Lytton	low	1110	<63				0.14±0.10	10.8±0.2		-25.2±0.3	1.0±0.4	
GRO001032	Fraser at Lytton	med	1110	<63				0.25±0.10	11.0±0.1		-24.7±0.3	3.0±0.4	
GRO001063	Fraser at Hope	low	1210	<63		0.888	0.281	0.68±0.10	11.0±0.3		-25.5±0.3	0.5±0.8	

GRO ID	Location												
GRO001065	Fraser at Hope	high	1210	<150				0.12±0.10	10.9±0.6	5.2±0.5	-25.8±0.3	0.4±0.5	2.87±0.5
	Fraser at Hope	high	1210	150-250				0.10±0.10		6.0±0.6	-25.2±1.1		0.22±3.2
	Fraser at Hope	high	1210	250-1000				0.10±0.10		8.2±1.3	-25.7±0.3		-0.67±2.5
GRO001028	Fraser at Fort Langley	med	1315	<63				0.80±0.10	13.5±0.1		-26.6±0.3	1.5±0.4	
GRO001029	Fraser at Fort Langley	med	1315	<63				0.62±0.10	13.5±0.3		-26.6±0.3	1.6±0.4	
GRO001081	Fraser at Fort Langley 11/9/11 flood		1315	<63				0.17±0.10	12.5±0.7		-26.0±0.3	0.7±0.4	
GRO001082	Fraser at Fort Langley 11/9/11 grab		1315	<63				0.15±0.10	11.2±0.2		-25.9±0.3	1.4±0.4	
GRO001083	Fraser at Fort Langley 9/19/11		1315	<63				0.39±0.10	12.4±0.4		-26.3±0.3	0.7±0.4	
GRO001084	Fraser at Fort Langley 10/26/11		1315	<63				0.42±0.10	11.6±0.2		-26.1±0.3	2.5±0.4	
GRO001085	Fraser at Fort Langley 10/31/11		1315	<63				0.17±0.10	10.8±0.4		-25.6±0.3	1.2±0.4	
GRO001024	Fraser at delta	med	1340	<63				0.62±0.10	14.6±0.4		-26.6±0.3	1.0±0.4	
GRO001025	Fraser at delta	med	1341	<63				0.43±0.10	15.8±0.6		-26.5±0.3	1.3±0.4	
GRO001026	Fraser at delta	med	1380	<63				0.56±0.10	12.4±0.3		-26.3±0.3	1.2±0.4	
GRO001027	Fraser at delta	med	1381	<63				0.34±0.10	10.6±0.6		-24.8±0.3	3.8±1.0	
GRO001048	Robson River	low	125	<63	0.952	0.109	0.098	0.53±0.10	9.5±0.2		-25.7±0.3	1.8±0.4	
GRO001034	Robson River	med	125	<63				0.83±0.10	12.9±0.4		-27.1±0.3	0.3±0.4	
GRO001079	Robson River	high	125	<63	1.087			0.42±0.10	9.4±0.2	7.9±0.7	-26.5±0.3	0.8±0.5	0.14±2.3
	Robson River	high	125	63-150				0.26±0.10		9.3±0.6	-26.3±0.3		1.10±0.9
	Robson River	high	125	150-250				0.17±0.10		7.8±1.3	-25.7±0.3		0.34±0.4
	Robson River	high	125	250-1000				0.74±0.10		16.5±1.7	-26.9±0.6		0.15±0.9
GRO001037	Bowron River	med	478	<63				0.72±0.10	13.1±0.3		-26.2±0.3	1.8±0.4	
GRO001071	Bowron River	high	478	<63	1.100			2.51±0.10	13.3±0.5	14.2±0.6	-25.8±0.3	3.4±0.4	4.06±0.4
	Bowron River	high	478	63-150				2.66±0.15	15.4±1.4	15.5±1.2	-25.9±0.3	2.6±0.4	3.37±0.4
	Bowron River	high	478	<150				1.19±0.10	12.6±0.7	12.1±1.1	-26.8±0.3	5.1±0.4	4.70±0.6
	Bowron River	high	478	150-250				0.28±0.10		9.6±1.9	-26.2±0.3		0.56±1.3
	Bowron River	high	478	150-250				4.15±1.10		19.2±7.7	-25.8±0.3		2.32±0.6
	Bowron River	high	478	250-1000				0.18±0.10		6.5±0.4	-25.7±0.3		-0.22±2.0
	Bowron River*	high	478	250-1000				1.01±0.23		18.1±5.2	-27.0±0.3		2.82±0.4
	Bowron River	high	478	250-1000				3.39±0.10		21.5±2.9	-26.0±0.3		2.38±0.4
GRO001052	McGregor River	low	500	<63		0.703	0.477	0.46±0.10	11.4±0.4		-26.5±0.3	-0.1±0.6	
GRO001036	McGregor River	med	500	<63				0.65±0.10	11.8±0.3		-27.2±0.3	0.1±0.4	

ID	River											
GRO001075	McGregor River	high	500	<63	0.986		0.29±0.10	11.3±0.2	8.3±0.3	-26.2±0.3	1.9±0.4	-0.24±1.3
	McGregor River	high	500	63-150			0.31±0.10		11.7±2.7	-26.0±0.3		1.39±0.8
	McGregor River	high	500	150-250			0.43±0.16		12.6±5.5	-26.2±0.3		1.05±0.4
	McGregor River	high	500	250-1000			0.53±0.10		14.0±0.6	-26.4±0.3		1.08±0.4
GRO001050	Willow River	low	555	<63	0.731	0.278	1.03±0.10	12.1±0.4		-27.7±0.3	1.3±0.4	
GRO001051	Willow River	low	555	<63	0.518	0.249	0.57±0.10	11.3±0.3		-26.0±0.3	1.2±0.4	
GRO001038	Willow River	med	555	<63			0.51±0.10	13.0±0.5		-26.1±0.3	2.3±0.4	
GRO001073	Willow River	high	555	<63			0.56±0.10	14.8±0.5	12.1±1.3	-26.1±0.3	1.9±0.8	0.78±0.8
	Willow River	high	555	63-150			0.13±0.10		10.9±1.2	-25.1±0.3		-2.55±0.6
	Willow River	high	555	150-250			0.12±0.10		10.2±1.1	-24.7±0.3		0.13±1.2
	Willow River	high	555	250-1000			0.13±0.10		10.3±1.7	-25.7±0.3		0.36±1.6
GRO001054	Nechako River	low	575	<63	1.546	0.303	1.02±0.10	12.7±0.3		-26.9±0.3	2.0±0.4	
GRO001039	Nechako River	med	575	<63			0.53±0.10	10.9±0.5		-26.3±0.3	3.6±0.5	
GRO001074	Nechako River	high	575	<63	0.928		0.43±0.10	13.0±0.3	8.2±1.5	-26.9±0.3	2.1±0.4	-1.27±2.7
	Nechako River	high	575	63-150			0.26±0.10	13.4±0.9	10.6±0.7	-26.9±0.3	1.6±0.4	0.31±1.3
	Nechako River	high	575	150-250			0.15±0.10		10.7±2.2	-26.9±0.3		-0.34±2.3
	Nechako River	high	575	250-1000			0.11±0.10		10.5±1.1	-26.5±0.3		-0.59±1.1
GRO001055	Blackwater River	low	705	<63	0.200	0.198	1.25±0.10	9.6±0.3		-26.3±0.3	3.1±0.4	
GRO001041	Blackwater River	med	705	<63			0.25±0.10	12.3±1.1		-25.9±0.3	1.5±0.4	
GRO001070	Blackwater River	high	705	<63			3.46±0.10	17.6±0.7	17.8±0.5	-25.6±0.3	3.5±1.0	3.11±0.4
	Blackwater River	high	705	63-150			2.00±0.11		18.7±1.8	-25.7±0.3		2.83±0.4
	Blackwater River	high	705	150-250			1.10±0.10		17.0±1.8	-25.7±0.3		2.13±1.0
	Blackwater River	high	705	250-1000			1.57±0.58		20.6±9.5	-25.7±0.3		1.97±0.5
	Blackwater River*	high	705	250-1000			2.26±0.12		21.0±1.2	-25.6±0.3		2.21±0.4
GRO001057	Quesnel River	low	770	<63	0.182	0.158	0.23±0.10	11.9±0.4		-24.8±0.3	-0.2±0.4	
GRO001042	Quesnel River	med	770	<63			0.23±0.10	12.1±0.2		-26.0±0.3	0.5±0.4	
GRO001069	Quesnel River	high	770	<63			0.67±0.10	10.8±0.3	9.4±0.5	-26.1±0.3	2.8±0.4	2.39±0.5
	Quesnel River	high	770	63-150			0.78±0.10	12.8±0.9	12.6±1.0	-26.7±0.3	2.2±0.5	2.52±0.5
	Quesnel River	high	770	150-250			0.53±0.10	8.2±3.8	11.7±2.9	-26.6±0.3	1.8±0.4	1.71±0.4
	Quesnel River	high	770	250-1000			0.83±0.10	13.7±2.1	13.5±0.8	-26.7±0.3	2.4±0.4	2.30±0.6
GRO000021	Chilcotin River	low	805	<63	0.804	0.417	0.61±0.10	9.4±0.3		-23.0±0.3	4.1±0.6	
GRO000043	Chilcotin River	med	805	<63			1.86±0.10	12.7±0.5		-26.0±0.3	5.3±0.4	

GRO000059	Chilcotin River	high	805	<63	1.100	1.32±0.10	12.2±0.4	11.1±0.9	-26.5±0.3	4.1±1.1	4.55±0.9
	Chilcotin River	high	805	63-150		1.31±0.10	13.2±0.9	13.0±1.2	-26.9±0.3	4.8±0.4	4.31±0.6
	Chilcotin River	high	805	150-250		2.54±0.38	17.9±4.1	15.9±3.2	-27.1±0.3	3.9±0.4	4.34±0.4
	Chilcotin River	high	805	250-1000		1.66±0.12	15.4±2.3	15.2±1.7	-26.6±0.3	3.8±0.6	4.60±0.4
GRO001059	Bridge River	low	1045	<63		0.18±0.10	9.2±0.3		-25.5±0.3	0.5±0.6	
GRO001045	Bridge River	med	1045	<63		0.60±0.10	10.4±0.2		-26.7±0.3	1.5±0.4	
GRO001059	Bridge River	low	1045	63-150		0.31±0.10	10.5±0.3		-25.8±0.3	1.6±0.4	
GRO001061	Thompson River	low	1111	<63	0.551	0.22±0.10	10.9±0.7		-25.6±0.3	1.5±0.4	
GRO001031	Thompson River	med	1111	<63		0.95±0.10	31.2±1.3		-24.6±0.3	3.4±0.4	
GRO001066	Thompson River	high	1111	<63		1.54±0.10	19.4±0.7	17.5±0.4	-25.5±0.3	6.2±0.4	4.83±0.5
	Thompson River	high	1111	63-150		1.56±0.15		19.0±1.8	-25.6±0.3		5.47±0.4
	Thompson River	high	1111	150-250		0.73±0.10		16.4±3.4	-26.0±0.3		4.28±0.9
	Thompson River	high	1111	250-1000		0.45±0.10		18.4±4.7	-25.6±0.3		3.97±1.0
GRO001064	Harrison River	low	1265	<63		0.18±0.10	8.2±0.3		-23.9±0.3	2.4±0.4	
GRO001030	Harrison River	med	1265	<63		0.72±0.10	11.1±0.6		-25.0±0.3	0.9±0.4	
GRO001046	Pitt River	med	1335	<63		0.63±0.10	15.5±0.2		-26.4±0.3	1.1±0.4	
GRO001112	Fraser at Hansard	low	480	susp.	0.891	2.68±0.10	10.7±0.1		-28.4±0.3	3.3	
GRO001114	Blackwater River	low	705	susp.	0.873	10.41±0.67	8.0±0.5		-26.5±0.3	2.1±0.4	
GRO001119	Fraser at Lillooet	low	1050	susp.	0.904	2.00±0.10	9.9±0.4		-26.3±0.3	1.4±0.4	
GRO001124	Fraser at delta mid	low	1336	susp.	0.935	1.91±0.10	9.6±0.6		-26.6±0.3	2.8±0.4	
GRO001126	Fraser at Hope	high	1210	susp.	0.660	0.35±0.10	13.1±1.3		-26.4±0.3	1.3±0.4	
GRO001127	Thompson River	high	1111	susp.	0.978	1.90±0.19		12.2±2.0	-26.4±0.3		3.51±0.4
GRO001128	Chilcotin River	high	805	susp.	1.005	2.24±0.44		13.7±3.1	-26.6±0.3		3.08±0.4
GRO001129	Quesnel River	high	770	susp.	0.579	0.51±0.10		11.4±0.4	-25.8±0.3		1.47±0.5
GRO001130	Blackwater River	high	705	susp.	0.859	0.63±0.10	12.1±1.8		-26.3±0.3	3.2±0.4	
GRO001131	Nechako River	high	575	susp.	0.899	1.28±0.11		9.9±1.3	-27.8±0.3		2.56±0.4
GRO001132	McGregor River	high	500	susp.	0.757	0.80±0.10		12.7±0.5	-26.5±0.3		1.87±0.4
GRO001133	Fraser at Hansard	high	480	susp.	0.779	0.97±0.10	10.9±0.2		-26.4±0.3	2.1±0.4	
GRO001134	Fraser at McBride	high	230	susp.	0.767	0.53±0.10	11.4±0.9		-25.8±0.3	1.6±0.4	
GRO001135	Fraser at Fitzwilliam	high	50	susp.	0.856	0.67±0.10	13.3±1.5		-25.9±0.3	1.4±0.4	
GRO001137	Fraser at delta deep	high	1336	susp.	0.793	0.28±0.10		13.2±0.7	-26.1±0.3		0.30±1.4
GRO001138	Fraser at delta mid	high	1336	susp.	0.813	0.35±0.10	12.7±1.6		-26.6±0.3	1.3±0.4	
GRO001139	Fraser at delta shallow	high	1336	susp.	0.839	0.67±0.10		12.4±0.6	-26.5±0.3		1.61±0.4
GRO001140	Fraser at Fort Langley	high	1315	susp.	0.742	0.62±0.10	13.1±0.7		-26.8±0.3	1.8±0.4	

| GRO001141 | Fraser at Fort Langley 11/9/11 | 1315 | susp. | 0.827 | | 2.55±0.11 | 8.9±0.5 | | -26.8±0.3 | 3.7±0.4 |

Table 3. All flood sediment (and SPM where available) organic carbon composition data (^{14}C Fm, %OC, C:N, δ^{13}C, δ^{15}N, and total FAME and alkane concentrations). Abbreviations: unt. = untreated (no sample pretreatment), acid. = acidified to remove inorganic carbonate, susp. = suspended sediment (bulk). Some SPM data duplicated from Table 2. IGSN codes refer to International GeoSample Numbers in the System for Earth Sample Registration (Sesar) database; sample metadata can be accessed at www.geosamples.org. For sediment %OC, δ^{13}C, and δ^{15}N data, if calculated uncertainties (1 s.d. of the mean of triplicate analyses) were less than instrumental uncertainty (0.1 for %OC, 0.3‰ for δ^{13}C, and 0.4‰ for δ^{15}N), instrumental uncertainties are shown. * indicates sediment was ground to a fine powder in an agate mortar and pestle.

IGSN	Site	Flow Stage	Dist. (km)	Size Fraction (μm)	Al/Si	Fe/Si	Mg/Na	Ca/Na	%IC	SA, ox ($m^2 g^{-1}$)	grain size D_{50}
GRO001047	Fraser at Fitzwilliam	low	50	<63	0.181	0.0498	0.821	0.232		4.37	84
GRO001033	Fraser at Fitzwilliam	med	50	<63	0.327	0.0721	1.444	0.146		4.33	177
GRO001078	Fraser at Fitzwilliam	high	50	<63	0.208	0.0549	0.861	0.213	0.07	2.59	80
	Fraser at Fitzwilliam	high	50	63-150					n.d.	1.98	
	Fraser at Fitzwilliam	high	50	150-250						2.07	
	Fraser at Fitzwilliam	high	50	250-1000						0.00	
GRO001049	Fraser at McBride	low	230	<63	0.238	0.0594	1.181	0.660		3.80	69
GRO001035	Fraser at McBride	med	230	<63							347
GRO001077	Fraser at McBride	high	230	<63	0.284	0.0763	1.253	0.838	0.41	3.99	60
	Fraser at McBride	high	230	63-150						2.65	
	Fraser at McBride	high	230	150-250						2.33	
	Fraser at McBride	high	230	250-1000						1.63	
GRO001053	Fraser at Hansard	low	480	<63	0.207	0.0591	1.040	0.776		3.92	85
GRO001076	Fraser at Hansard	high	480	<63	0.237	0.0608	1.082	0.841	0.52	5.28	31
	Fraser at Hansard	high	480	63-150					0.48	6.05	
	Fraser at Hansard	high	480	150-250						4.50	
	Fraser at Hansard	high	480	250-1000						6.38	
GRO001056	Fraser at Stoner	low	615	<63	0.209	0.0584	1.290	1.304		6.20	42
GRO001040	Fraser at Stoner	med	615	<63	0.208	0.0548	1.010	0.814		6.43	57
GRO001060	Fraser at Lillooet	low	1050	<63	0.213	0.0731	1.275	1.274		8.09	73
GRO001044	Fraser at Lillooet	med	1050	<63	0.199	0.0683	0.992	0.957		6.49	163
GRO001067	Fraser at Lillooet	high	1050	<150					0.23		308
GRO001062	Fraser at Lytton	low	1110	<63							244
GRO001032	Fraser at Lytton	med	1110	<63						7.14	254
GRO001063	Fraser at Hope	low	1210	<63	0.235	0.0667	1.353	1.260		9.92	36
GRO001065	Fraser at Hope	high	1210	<150	0.157	0.0701	1.053	1.018	0.18		198
GRO001028	Fraser at Fort Langley	med	1315	<63							63
GRO001029	Fraser at Fort Langley	med	1315	<63	0.178	0.0907	1.283	1.416		8.98	106
GRO001081	Fraser at Fort Langley 11/9/11 flood		1315	<63	0.173	0.0724	1.061	1.198		6.26	102
GRO001082	Fraser at Fort Langley 11/9/11 bed material		1315	<63							318
GRO001083	Fraser at Fort Langley 9/19/11 bed material		1315	<63	0.188	0.0584	0.941	0.929		8.43	234

ID	Name										
GRO001084	Fraser at Fort Langley 10/26/11 bed material		1315	<63	0.188	0.0607	0.978	0.956		7.85	234
GRO001085	Fraser at Fort Langley 10/31/11 bed material		1315	<63							243
GRO001024	Fraser at delta	med	1340	<63	0.199	0.0685	0.988	0.955		8.50	128
GRO001025	Fraser at delta	med	1341	<63						5.95	120
GRO001026	Fraser at delta	med	1380	<63	0.211	0.0639	0.868	0.702		8.27	70
GRO001027	Fraser at delta	med	1381	<63							318
GRO001048	Robson River	low	125	<63	0.280	0.0585	7.186	17.374		7.15	782
GRO001034	Robson River	med	125	<63	0.242	0.0538	7.722	24.731		3.72	45
GRO001079	Robson River	high	125	<63	0.221	0.0513	8.435	23.723	5.89	3.24	64
	Robson River	high	125	63-150						2.15	
GRO001037	Bowron River	med	478	<63							707
GRO001071	Bowron River	high	478	<63					0.27	6.66	94
	Bowron River	high	478	63-150					0.13	5.18	
	Bowron River	high	478	<150					0.34		351
	Bowron River	high	478	150-250						5.71	
	Bowron River	high	478	250-1000						6.13	
GRO001052	McGregor River	low	500	<63	0.146	0.0381	2.319	3.550		4.31	47
GRO001036	McGregor River	med	500	<63	0.189	0.0490	1.705	2.353		6.79	25
GRO001075	McGregor River	high	500	<63	0.135	0.0361	2.180	3.474	2.47	2.96	61
	McGregor River	high	500	63-150						2.67	
	McGregor River	high	500	150-250						2.36	
	McGregor River	high	500	250-1000						3.22	
GRO001050	Willow River	low	555	<63	0.192	0.0503	1.674	2.279		12.77	317
GRO001051	Willow River	low	555	<63							329
GRO001038	Willow River	med	555	<63	0.168	0.0486	0.749	0.800		9.52	265
GRO001073	Willow River	high	555	<63					0.14		231
GRO001054	Nechako River	low	575	<63	0.221	0.0635	0.531	0.677		14.42	550
GRO001039	Nechako River	med	575	<63	0.212	0.0640	0.461	0.661		12.02	680
GRO001074	Nechako River	high	575	<63					0.10	16.32	433
	Nechako River	high	575	63-150					0.06	8.70	
	Nechako River	high	575	150-250						5.38	
	Nechako River	high	575	250-1000						4.78	
GRO001055	Blackwater River	low	705	<63	0.226	0.0847	0.770	0.882		20.67	581
GRO001041	Blackwater River	med	705	<63							347
GRO001070	Blackwater River	high	705	<63					0.48	4.49	120

GRO001057	Quesnel River	low	770	<63	0.177	0.0572	0.903	1.087		8.01	55
GRO001042	Quesnel River	med	770	<63	0.171	0.0527	0.755	1.074		9.27	189
GRO001069	Quesnel River	high	770	<63					0.08	5.35	32
	Quesnel River	high	770	63-150					0.10		
	Quesnel River	high	770	150-250					0.55		
	Quesnel River	high	770	250-1000					0.13		
GRO000021	Chilcotin River	low	805	<63	0.261	0.0990	1.138	1.099		15.18	78
GRO000043	Chilcotin River	med	805	<63						14.09	436
GRO000059	Chilcotin River	high	805	<63	0.265	0.1001	1.120	1.185	0.26		38
	Chilcotin River	high	805	63-150					0.30		
	Chilcotin River	high	805	150-250					n.d.		
	Chilcotin River	high	805	250-1000					0.27		
GRO001059	Bridge River	low	1045	<63	0.200	0.1085	5.202	1.097			574
GRO001045	Bridge River	med	1045	<63	0.219	0.0808	2.254	1.788		15.22	62
GRO001061	Thompson River	low	1111	<63							242
GRO001031	Thompson River	med	1111	<63							636
GRO001066	Thompson River	high	1111	<63					0.33		322
GRO001064	Harrison River	low	1265	<63							179
GRO001030	Harrison River	med	1265	<63							672
GRO001046	Pitt River	med	1335	<63	0.214	0.0669	0.911	0.807		10.06	53
GRO001112	Fraser at Hansard	low	480	susp.							8
GRO001114	Blackwater River	low	705	susp.							14
GRO001119	Fraser at Lillooet	low	1050	susp.							11
GRO001124	Fraser at delta mid	low	1336	susp.						14.40	10
GRO001126	Fraser at Hope River	high	1210	susp.	0.177	0.0479	0.876	0.778		7.94	61
GRO001127	Thompson River	high	1111	susp.							9
GRO001128	Chilcotin River	high	805	susp.							11
GRO001129	Quesnel River	high	770	susp.	0.260	0.0836	1.268	1.097			10
GRO001130	Blackwater River	high	705	susp.	0.236	0.0766	0.892	0.759		19.65	24
GRO001131	Nechako River	high	575	susp.							13
GRO001132	McGregor River	high	500	susp.							11
GRO001133	Fraser at Hansard	high	480	susp.							12
GRO001134	Fraser at McBride	high	230	susp.							36
GRO001135	Fraser at Fitzwilliam	high	50	susp.							42
GRO001137	Fraser at delta deep	high	1336	susp.	0.166	0.0424	0.706	0.646			95
GRO001138	Fraser at delta mid	high	1336	susp.	0.175	0.0480	0.796	0.679		8.31	66

					Ca/Na	Mg/Na	Al/Si	Fe/Si		SA	D50
GRO001139	Fraser at delta shallow	high	1336	susp.	0.228	0.0677	1.016	0.882			14
GRO001140	Fraser at Fort Langley	high	1315	susp.						11.50	23
GRO001141	Fraser at Fort Langley 11/9/11		1315	susp.							9

Table 4. All flood sediment (and SPM where available) elemental abundance data from XRF (Ca/Na, Mg/Na, Al/Si, Fe/Si), inorganic carbon content (%IC, calculated as the different between total carbon analyses with and without acidification; n.d. = not detected), specific surface area (SA), and grain size (D_{50}, median grain size, shown). Abbreviation: susp. = suspended sediment (bulk). IGSN codes refer to International GeoSample Numbers in the System for Earth Sample Registration (Sesar) database; sample metadata can be accessed at www.geosamples.org.
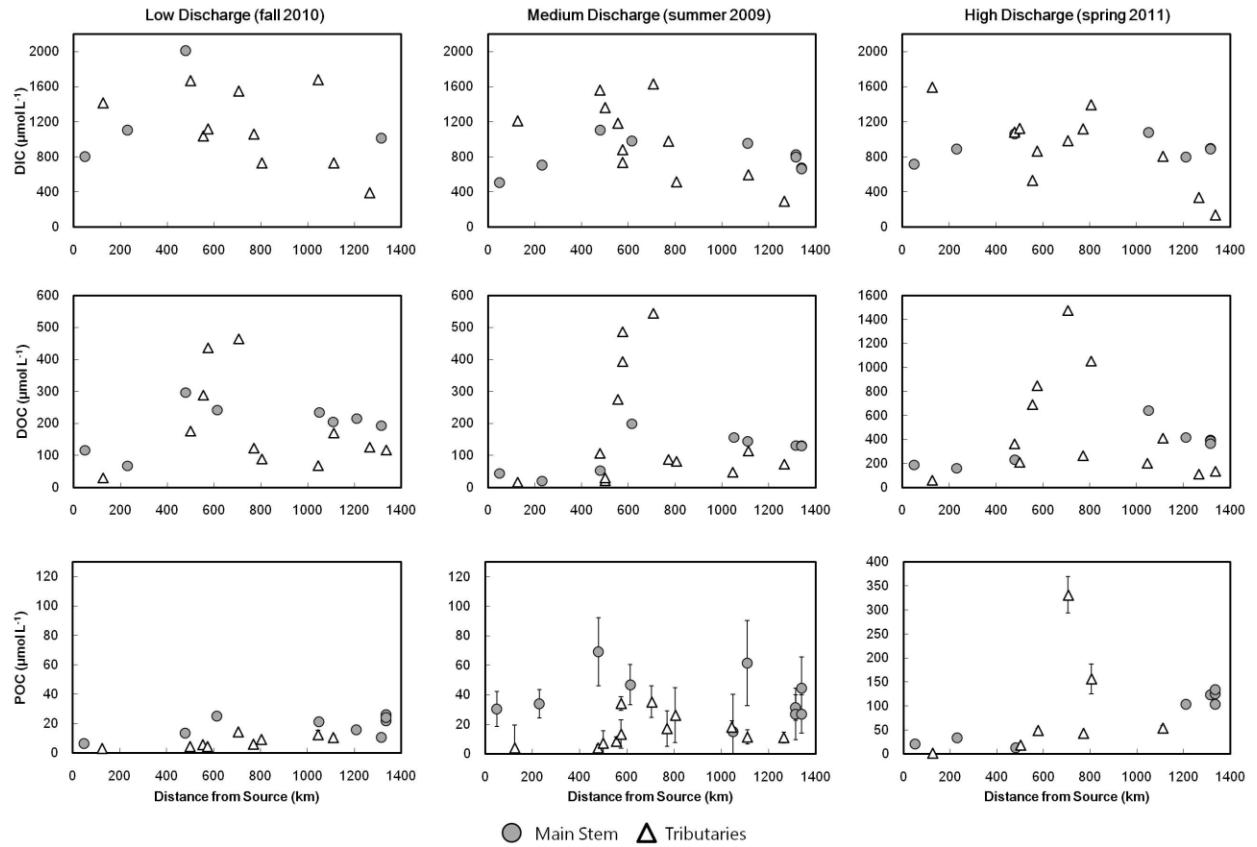
Figure 1. Concentrations of DIC (top row), DOC (middle row), and POC (bottom row) across the Fraser basin at low discharge (left column), medium discharge (center column), and high discharge (right column).
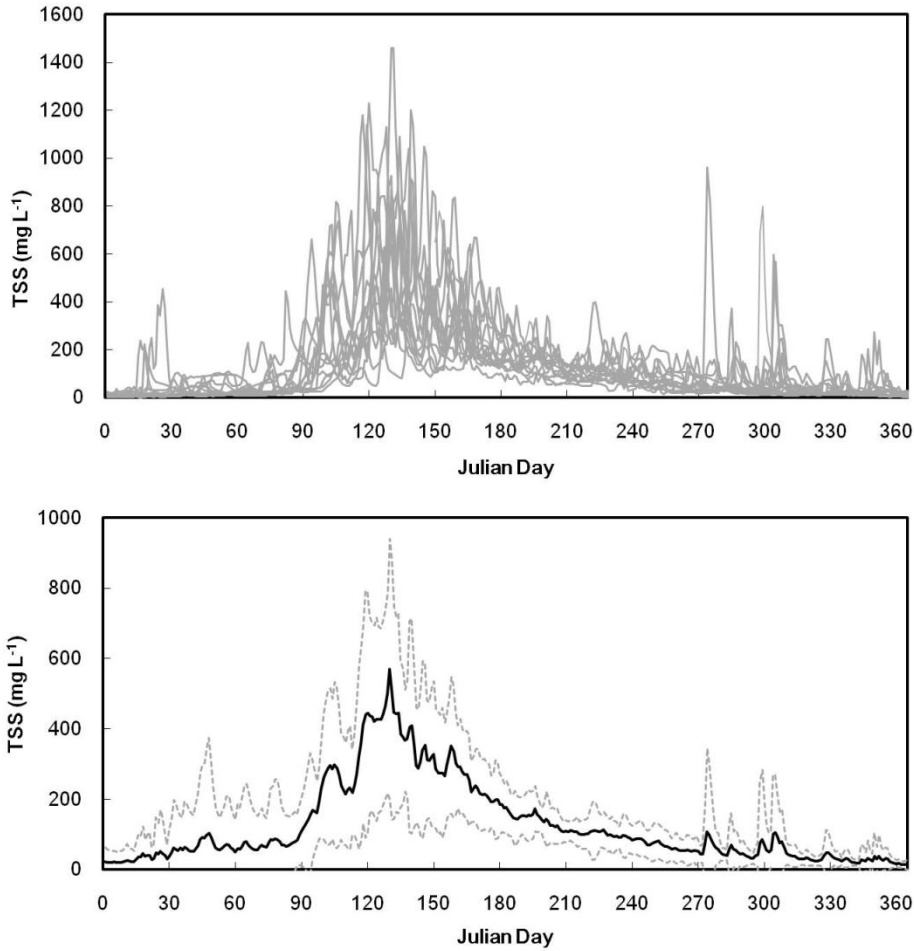
Figure 2. A ~15-year record (1965-1979) of daily suspended sediment sampling of the Fraser River at Hope by Environment Canada reveals a strong seasonal cycle of sediment concentrations dominated by the spring freshet. TSS is highly variable on shorter timescales as well. Top panel shows overlain annual records and bottom panel shows a daily mean annual cycle, with dotted lines indicating ±1 s.d. from the mean.
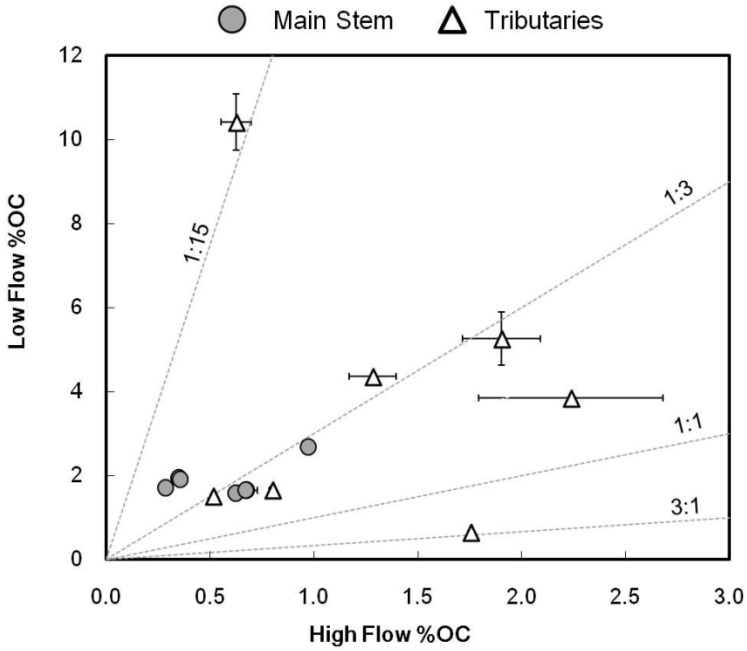
Figure 3. OC content of suspended sediments is almost universally higher under low discharge conditions relative to the spring freshet. Error bars indicate 1 s.d. of the mean of three analyses. For some samples, error bars are smaller than symbols.
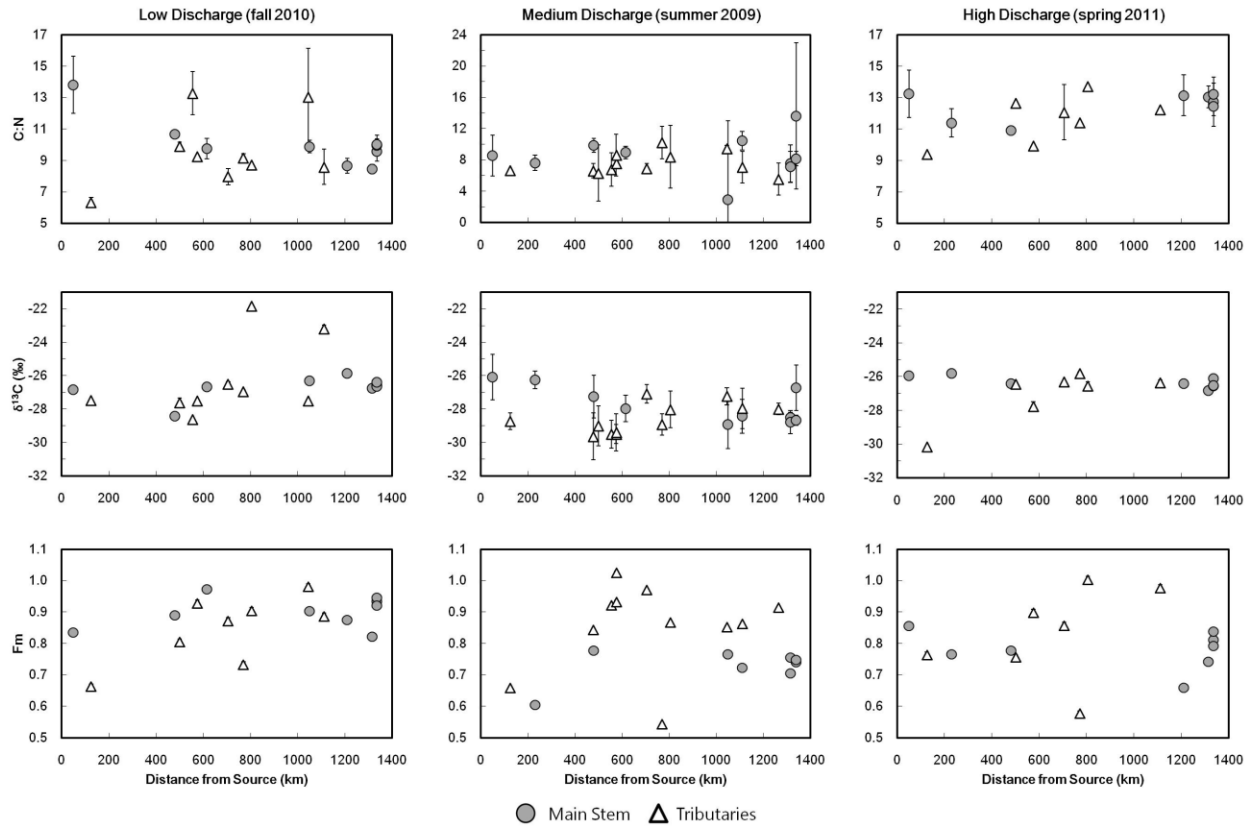
Figure 4. Bulk POC C:N (top row), δ^{13}C (middle row), and ^{14}C Fm (bottom row) compositions across the Fraser basin at low discharge (left column), medium discharge (center column), and high discharge (right column).
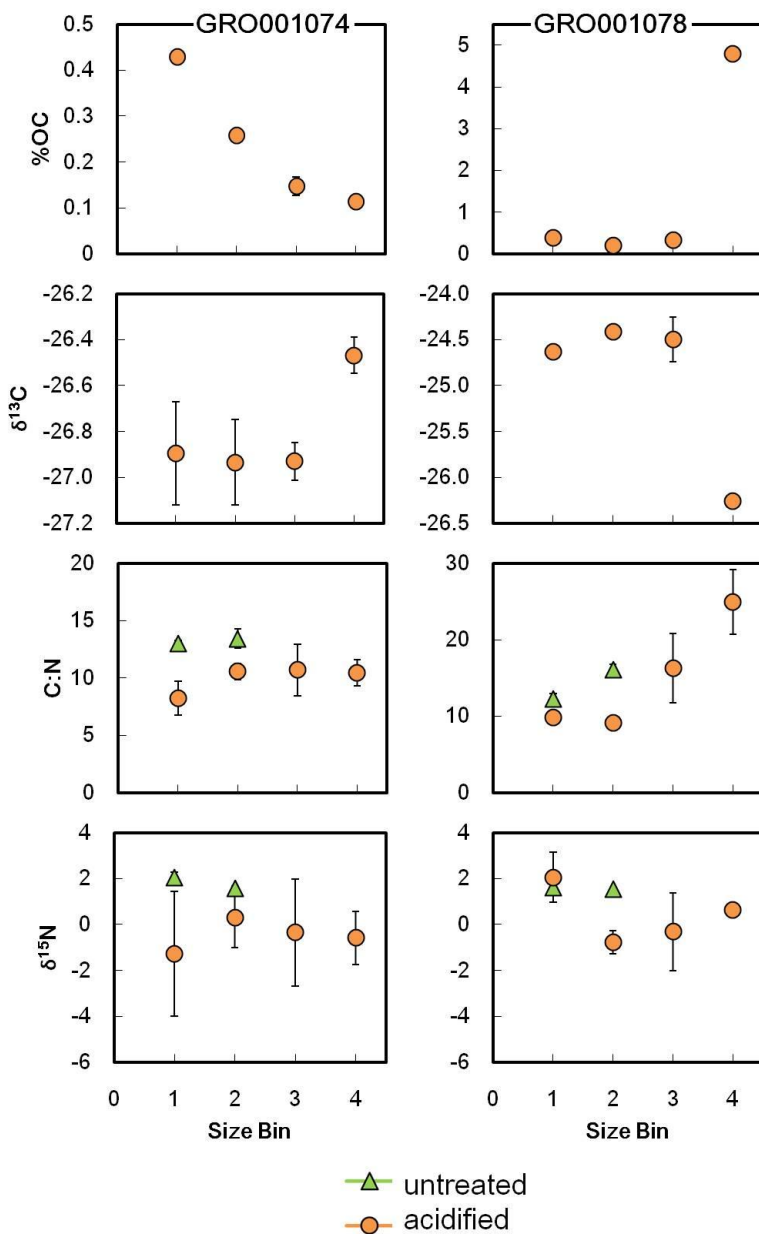
Figure 5. Variations in bulk OC and N properties were not systematic with grain size (size bins: 1 = <63 μm, 2 = 63-150 μm, 3 = 150-250 μm, 4 = 250-1000 μm). Shown here are two examples of samples with %OC decreasing with increasing grain size (GRO001074, Nechako River, freshet) and increasing with grain size (GRO001078, Fraser at Fitzwilliam, freshet). Orange circles represent samples which were acidified and green triangles those which were not. Error bars indicate ± 1 s.d. from triplicate analyses.
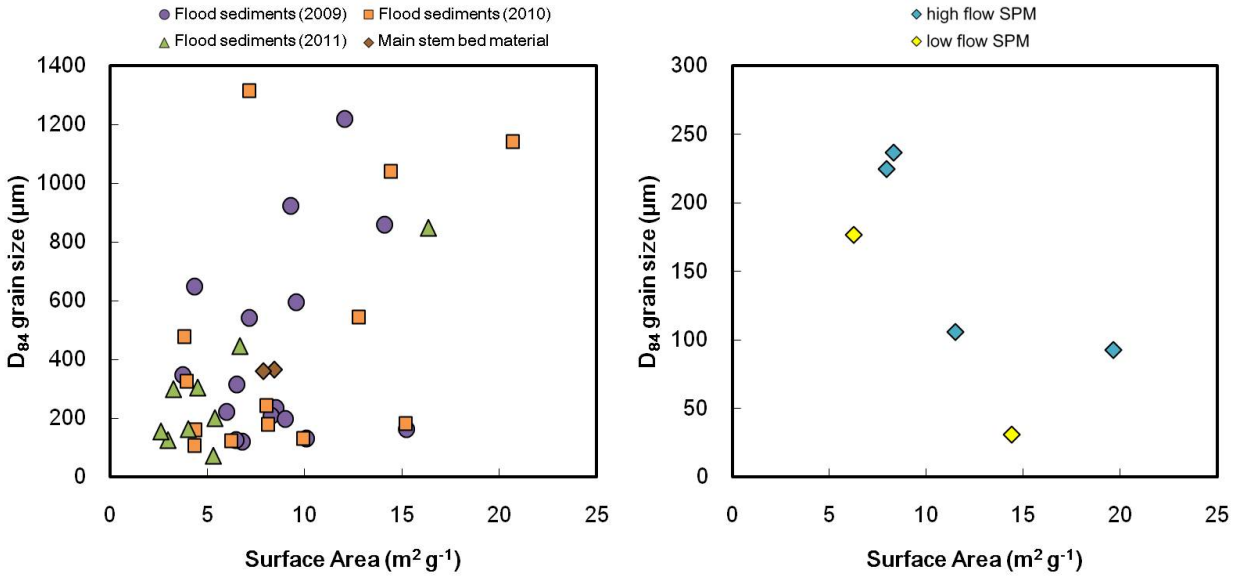
Figure 6. The non-uniform grain size distribution of flood sediments obscures the expected negative relationship between grain size and mineral surface area (left panel). Suspended sediments, however, have more uniform grain size distributions and do show a negative correlation with mineral surface area (right panel).
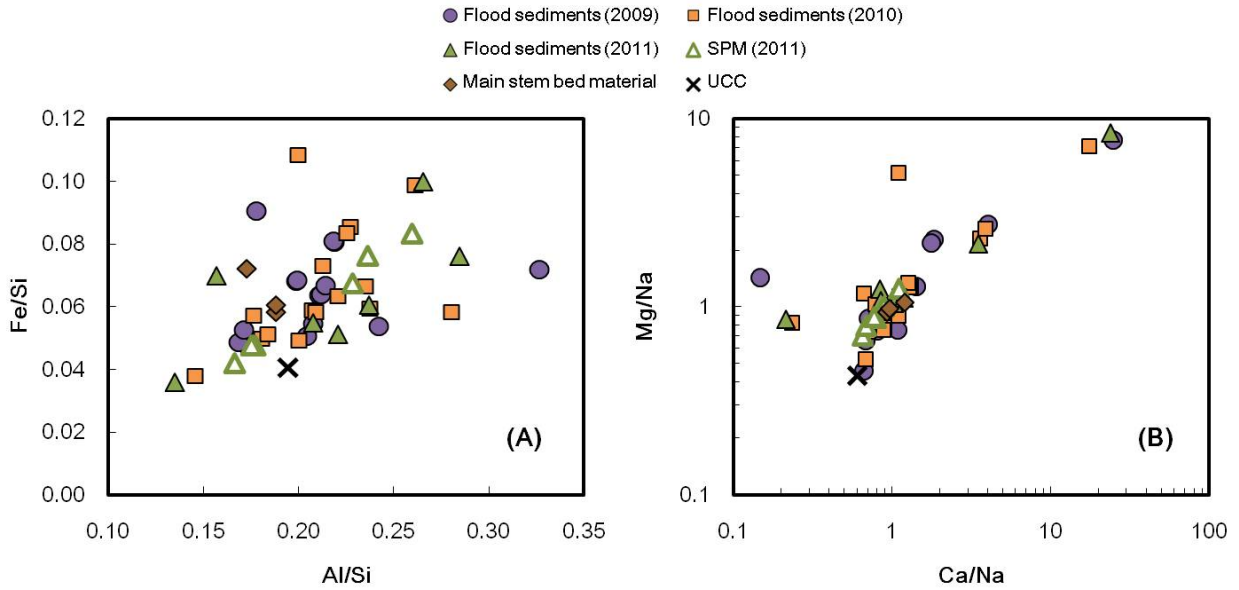
Figure 7. (A) Fe/Si and Al/Si ratios of Fraser River sediments show a range of degrees of chemical weathering. (B) High Mg/Ca and Ca/Na ratios highlight basins influenced by carbonate weathering (Robson and McGregor rivers; note log scale). UCC = Upper Continental Crust average from Taylor and McLennan (1995).
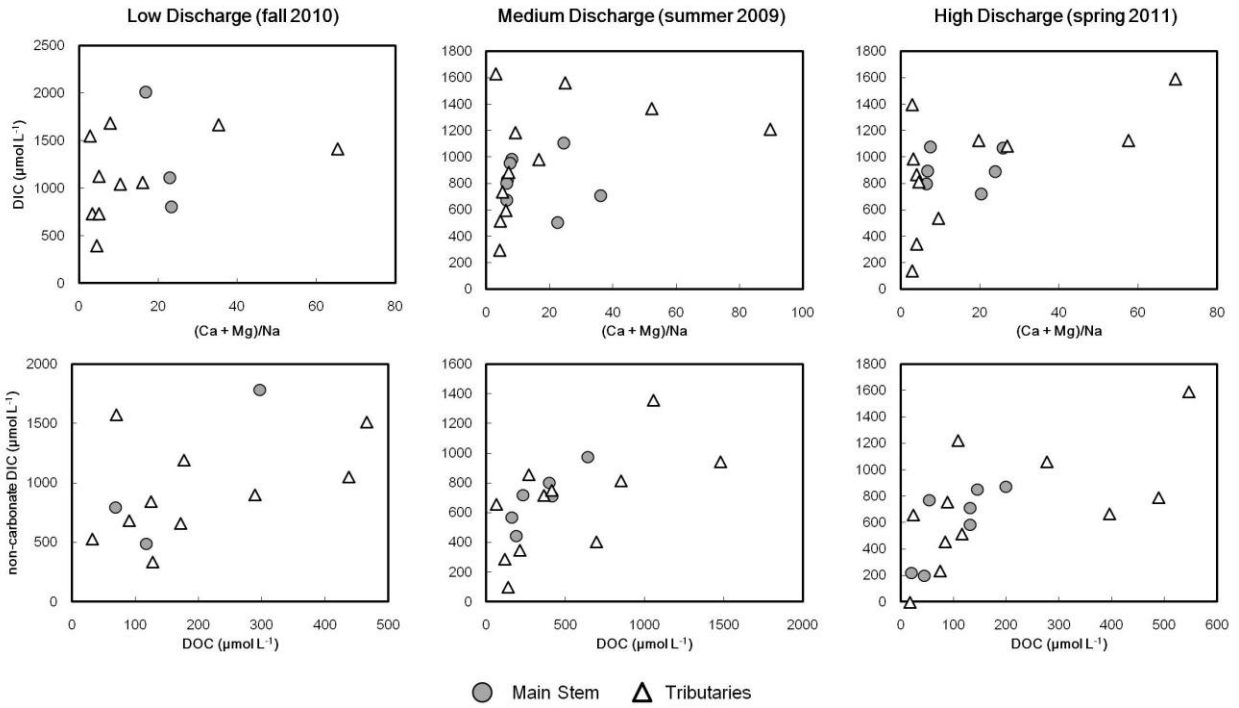
Figure 8. Using the dissolved (Ca+Mg)/Na composition of the Robson River, i.e. the highest (Ca+Mg)/Na values in the Fraser basin, as an end-member for carbonate weathering-derived DIC, the calculated "non-carbonate" DIC is positively correlated with DOC concentration. Dissolved Ca, Mg, and Na values are from Voss et al. (2014) (Chapter 2).
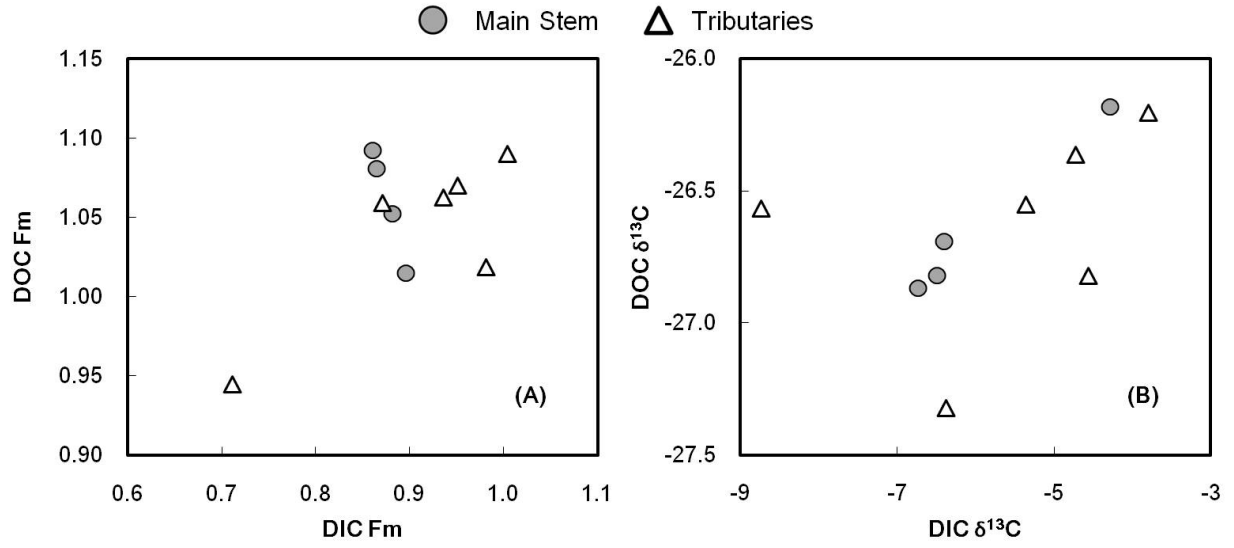
Figure 9. The ^{14}C content (Fm) (A) and δ^{13}C composition (B) of DIC and DOC are correlated (data from medium discharge conditions, summer 2009).
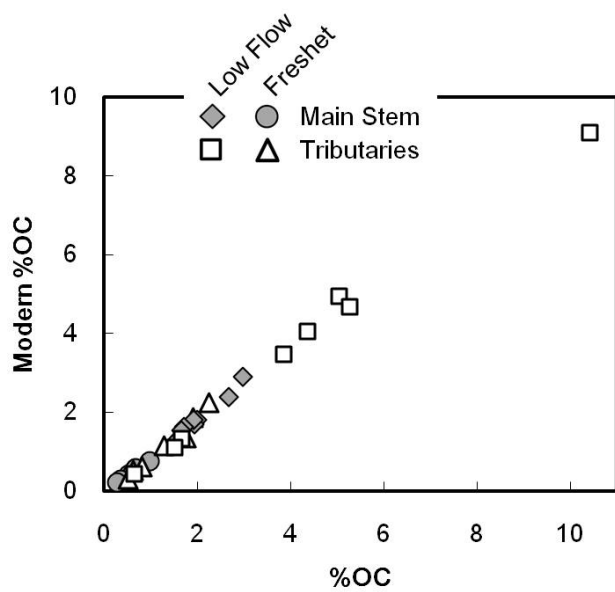
Figure 10. The diverse tributaries of the Fraser River exhibit generally consistent dilution of petrogenic OC with widely varying amounts of modern OC, although the petrogenic OC contribution is most likely not constant throughout the basin.
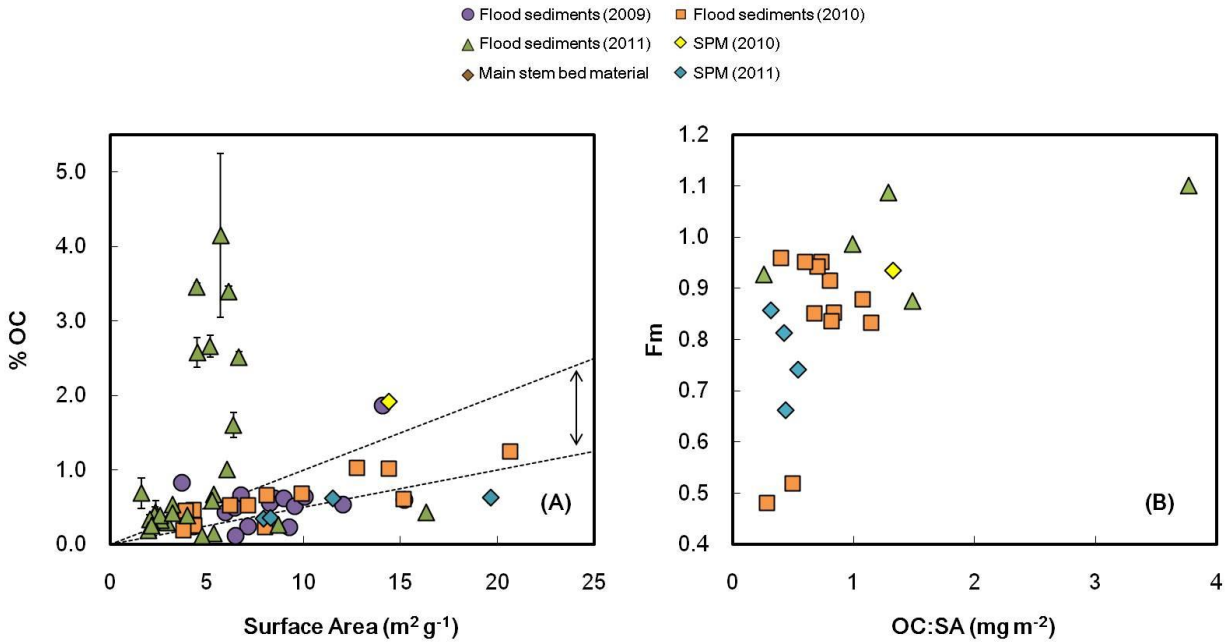
Figure 11. (A) Diverse sediments from the Fraser basin exhibit a wide range in OC loading. The area indicated by the arrow between the dotted lines in (A) represents the hypothetical "monolayer equivalent" OC loading range (Keil et al., 1994; Mayer, 1994). (B) While sediments with lower OC:SA (<0.6 mg m^{-2}) are associated with OC with a wide range of ages, those with higher OC:SA are associated only with relatively modern OC (Fm > 0.8).

References

Aufdenkampe A. K., Mayorga E., Raymond P. A., Melack J. M., Doney S. C., Alin S. R., Aalto R. E., and Yoo K. (2011) Riverine coupling of biogeochemical cycles between land, oceans, and atmosphere. *Front. Ecol. Environ.* **9**, 53-60. doi:10.1890/100014.

Battin T. J., Luyssaert S., Kaplan L. A., Aufdenkampe A. K., Richter A., and Tranvik L. J. (2009) The boundless carbon cycle. *Nat. Geosci.* **2**, 598-600. doi:10.1038/ngeo618.

Berner R. A., Lasaga A. C., and Garrels R. M. (1983) The carbonate–silicate geochemical cycle and its effect on atmospheric carbon dioxide over the past 100 million years. *Am. J. Sci.* **283**, 641-683.

Böhlke J. K., Gwinn C. J., and Coplen T. B. (1993) New reference materials for nitrogen-isotope-ratio measurements. *Geostand. Newsl.* **17**, 159-164.

Brearley F. Q. (2009) How does sample preparation affect the δ^{15}N values of terrestrial ecological materials? *J. Plant Nutr. Soil Sci.* **172**, 461-463. doi:10.1002/jpln.200900005.

Brodie C. R., Casford J. S. L., Lloyd J. M., Leng M. J., Heaton T. H. E., Kendrick C. P., and Yongqiang Z. (2011) Evidence for bias in C/N, δ^{13}C and δ^{15}N values of bulk organic matter, and on environmental interpretation, from a lake sedimentary sequence by pre-analysis acid treatment methods. *Quat. Sci. Rev.* **30**, 3076-3087. doi:10.1016/j.quascirev.2011.07.003.

Brunauer S., Emmett P. H., and Teller E. (1938) Adsorption of gases in multimolecular layers. *J. Am. Chem. Soc.* **60**, 309-319.

Cameron E. M. (1996) Hydrogeochemistry of the Fraser River, British Columbia: seasonal variation in major and minor components. *J. Hydrol.* **182**, 209-225.

Cameron E. M., Hall G. E. M., Veizer J., and Krouse H. R. (1995) Isotopic and elemental hydrogeochemistry of a major river system: Fraser River, British Columbia, Canada. *Chem. Geol.* **122**, 149-169.

Cameron E. M. and Hattori K. (1997) Strontium and neodymium isotope ratios in the Fraser River: a riverine transect across the Cordilleran orogen. *Chem. Geol.* **137**, 243-253.

Christl M., Vockenhuber C., Kubik P. W., Wacker L., Lachner J., Alfimov V., and Synal H. A. (2013) The ETH Zurich AMS facilities: Performance parameters and reference materials. *Nucl. Instrum. Methods Phys. Res., Sect. B* **294**, 29-38. doi:10.1016/j.nimb.2012.03.004.

Cole J. J. and Caraco N. F. (2001) Carbon in catchments: connecting terrestrial carbon losses with aquatic metabolism. *Mar. Freshwater Res.* **52**, 101-110.

Cooper L. W., McClelland J. W., Holmes R. M., Raymond P. A., Gibson J. J., Guay C. K., and Peterson B. J. (2008) Flow-weighted values of runoff tracers (δ^{18}O, DOC, Ba, alkalinity) from the six largest Arctic rivers. *Geophys. Res. Lett.* **35**. doi:10.1029/2008gl035007.

Copard Y., Amiotte-Suchet P., and Di-Giovanni C. (2007) Storage and release of fossil organic carbon related to weathering of sedimentary rocks. *Earth Planet. Sci. Lett.* **258**, 345-357. doi:10.1016/j.epsl.2007.03.048.

Coplen T. B., Brand W. A., Gehre M., Gröning M., Meijer H. A. J., Toman B., and Verkouteren R. M. (2006) New guidelines for δ^{13}C measurements. *Anal. Chem.* **78**, 2439-2441. doi:10.1021/ac052027c.

Dickson A. (2010) Standards for Ocean Measurements. *Oceanogr.* **23**, 34-47. doi:10.5670/oceanog.2010.22.

Dickson A. G., Sabine C. L., and Christian J. R. (2007) *Guide to Best Practices for Ocean CO$_2$ Measurements*. PICES Special Publication 3. 191 pp.

Ebelmen J. J. (1845) Sur les produits de la decomposition des espèces minérales de la famille des silicates. *Ann. Mines* **7**, 3-66.

France-Lanord C. and Derry L. A. (1997) Organic carbon burial forcing of the carbon cycle from Himalayan erosion. *Nature* **390**, 65-67. doi:10.1038/36324.

Gaillardet J., Dupré B., Louvat P., and Allègre C. J. (1999) Global silicate weathering and CO$_2$ consumption rates deduced from the chemistry of large rivers. *Chem. Geol.* **159**, 3-30.

Galy V., Beyssac O., France-Lanord C., and Eglinton T. (2008) Recycling of graphite during Himalayan erosion: A geological stabilization of carbon in the crust. *Science* **322**, 943-945. doi:10.1126/science.1161408.

Galy V., Eglinton T., France-Lanord C., and Sylva S. (2011) The provenance of vegetation and environmental signatures encoded in vascular plant biomarkers carried by the Ganges–Brahmaputra rivers. *Earth Planet. Sci. Lett.* **304**, 1-12. doi:10.1016/j.epsl.2011.02.003.

Garrels R. M., Lerman A., and Mackenzie F. T. (1976) Controls of atmospheric O_2 and CO_2: Past, present, and future. *Am. Sci.* **64**, 306-315.

Guo L., Cai Y., Belzile C., and Macdonald R. W. (2012) Sources and export fluxes of inorganic and organic carbon and nutrient species from the seasonally ice-covered Yukon River. *Biogeochemistry* **107**, 187-206. doi:10.1007/s10533-010-9545-z.

Hayes J. M. and Waldbauer J. R. (2006) The carbon cycle and associated redox processes through time. *Philos. Trans. R. Soc., B* **361**, 931-950. doi:10.1098/rstb.2006.1840.

Hedges J. I., Keil R. G., and Benner R. (1997) What happens to terrestrial organic matter in the ocean? *Org. Geochem.* **27**, 195-212.

Holmes R. M., McClelland J. W., Raymond P. A., Frazer B. B., Peterson B. J., and Stieglitz M. (2008) Lability of DOC transported by Alaskan rivers to the Arctic Ocean. *Geophys. Res. Lett.* **35**. doi:10.1029/2007gl032837.

Hood E., Fellman J., Spencer R. G. M., Hernes P. J., Edwards R., D'Amore D., and Scott D. (2009) Glaciers as a source of ancient and labile organic matter to the marine environment. *Nature* **462**, 1044-1047. doi:10.1038/nature08580.

IAEA (1995) Reference and intercomparison materials for stable isotopes of light elements, IAEA-TECDOC-825. Vienna.

Jaffé R., Ding Y., Niggemann J., Vähätalo A. V., Stubbins A., Spencer R. G. M., Campbell J., and Dittmar T. (2013) Global charcoal mobilization from soils via dissolution and riverine transport to the oceans. *Science* **340**, 345-347. doi:10.1126/science.1231476.

Jonkers L., Prins M. A., Brummer G.-J. A., Konert M., and Lougheed B. C. (2009) Experimental insights into laser diffraction particle sizing of fine-grained sediments for use in palaeoceanography. *Sedimentology* **56**, 2192-2206. doi:10.1111/j.1365-3091.2009.01076.x.

Keil R. G., Mayer L. M., Quay P. D., Richey J. E., and Hedges J. I. (1997) Loss of organic matter from riverine particles in deltas. *Geochim. Cosmochim. Acta* **61**, 1507-1511.

Keil R. G., Tsamakis E., Fuh C. B., Giddings J. C., and Hedges J. I. (1994) Mineralogical and textural controls on the organic composition of coastal marine sediments: Hydrodynamic separation using SPLITT-fractionation. *Geochim. Cosmochim. Acta* **58**, 879-893.

Kennedy P., Kennedy H., and Papadimitriou S. (2005) The effect of acidification on the determination of organic carbon, total nitrogen and their stable isotopic composition in algae and marine sediment. *Rapid Commun. Mass Spectrom.* **19**, 1063-1068. doi:10.1002/rcm.1889.

Mayer L. M. (1994) Surface area control of organic carbon accumulation in continental shelf sediments. *Geochim. Cosmochim. Acta* **58**, 1271-1284.

Mazumder D., Iles J., Kelleway J., Kobayashi T., Knowles L., Saintilan N., and Hollins S. (2010) Effect of acidification on elemental and isotopic compositions of sediment organic matter and macro-invertebrate muscle tissues in food web research. *Rapid Commun. Mass Spectrom.* **24**, 2938-2942. doi:10.1002/rcm.4729.

Meybeck M. (1986) Composition chimique des ruisseaux non pollués de France. *Sci. Géol., Bull.* **39**, 3-77.

Qi H., Coplen T. B., Geilmann H., Brand W. A., and Böhlke J. K. (2003) Two new organic reference materials for $\delta^{13}C$ and $\delta^{15}N$ measurements and a new value for the $\delta^{13}C$ of NBS 22 oil. *Rapid Commun. Mass Spectrom.* **17**, 2483-2487. doi:10.1002/rcm.1219.

Ransom B., Bennett R. H., Baerwald R., and Shea K. (1997) TEM study of in situ organic matter on continental margins - Occurrence and the "monolayer" hypothesis. *Mar. Geol.* **138**, 1-9.

Richey J. E., Brock J. T., Naiman R. J., Wissmar R. C., and Stallard R. F. (1980) Organic carbon: Oxidation and transport in the Amazon River. *Science* **207**, 1348-1351.

Roberts M. L., Burton J. R., Elder K. L., Longworth B. E., McIntyre C. P., Reden K. F. v., Han B. X., Rosenheim B. E., Jenkins W. J., Galutschek E., and McNichol A. P. (2010) A high-performance ^{14}C accelerator mass spectrometry system. *Radiocarbon* **52**, 228-235.

Rubey W. W. (1951) Geologic history of sea water: An attempt to state the problem. *Bull. Geol. Sci. Am.* **62**, 1111-1148.

Schlacher T. A. and Connolly R. M. (2014) Effects of acid treatment on carbon and nitrogen stable isotope ratios in ecological samples: a review and synthesis. *Methods Ecol. Evol.* **5**, 541-550. doi:10.1111/2041-210X.12183.

Schulte P., van Geldern R., Freitag H., Karim A., Négrel P., Petelet-Giraud E., Probst A., Probst J.-L., Telmer K., Veizer J., and Barth J. A. C. (2011) Applications of stable water and carbon isotopes in watershed research: Weathering, carbon cycling, and water balances. *Earth-Sci. Rev.* **109**, 20-31. doi:10.1016/j.earscirev.2011.07.003.

Spence J. and Telmer K. (2005) The role of sulfur in chemical weathering and atmospheric CO_2 fluxes: Evidence from major ions, $\delta^{13}C_{DIC}$, and $\delta^{34}S_{SO4}$ in rivers of the Canadian Cordillera. *Geochim. Cosmochim. Acta* **69**, 5441-5458. doi:10.1016/j.gca.2005.07.011.

Sperazza M., Moore J. N., and Hendrix M. S. (2004) High-resolution particle size analysis of naturally occurring very fine-grained sediment through laser diffractometry. *J. Sediment. Res.* **74**, 736-743.

Stubbins A., Hood E., Raymond P. A., Aiken G. R., Sleighter R. L., Hernes P. J., Butman D., Hatcher P. G., Striegl R. G., Schuster P., Abdulla H. A. N., Vermilyea A. W., Scott D. T., and Spencer R. G. M. (2012) Anthropogenic aerosols as a source of ancient dissolved organic matter in glaciers. *Nat. Geosci.* **5**, 198-201. doi:10.1038/ngeo1403.

Suess E. (1973) Interaction of organic compounds with calcium carbonate-II. Organo-carbonate association in recent sediments. *Geochim. Cosmochim. Acta* **37**, 2435-2447.

Taylor S. R. and McLennan S. M. (1995) The geochemical evolution of the continental crust. *Rev. Geophys.* **33**, 241-265.

Thorne R. and Woo M.-k. (2011) Streamflow response to climatic variability in a complex mountainous environment: Fraser River Basin, British Columbia, Canada. *Hydrol. Processes* **25**, 3076-3085. doi:10.1002/hyp.8225.

Tranvik L. J., Downing J. A., Cotner J. B., Loiselle S. A., Striegl R. G., Ballatore T. J., Dillon P., Finlay K., Fortino K., Knoll L. B., Kortelainen P. L., Kutser T., Larsen S., Laurion I., Leech D. M., McCallister S. L., McKnight D. M., Melack J. M., Overholt E., Porter J. A., Prairie Y., Renwick W. H., Roland F., Sherman B. S., Schindler D. W., Sobek S., Tremblay A., Vanni M. J., Verschoor A. M., Wachenfeldt E. v., et al. (2009) Lakes and reservoirs as regulators of carbon cycling and climate. *Limnol. Oceanogr.* **54**, 2298-2314. doi:10.4319/lo.2009.54.6_part_2.2298.

Voss B. M., Peucker-Ehrenbrink B., Eglinton T. I., Fiske G., Wang Z. A., Hoering K. A., Montluçon D. B., LeCroy C., Pal S., Marsh S., Gillies S. L., Janmaat A., Bennett M., Downey B., Fanslau J., Fraser H., Macklam-Harron G., Martinec M., and Wiebe B. (2014) Tracing river chemistry in space and time: Dissolved inorganic constituents of the Fraser River, Canada. *Geochim. Cosmochim. Acta* **124**, 283-308. doi:10.1016/j.gca.2013.09.006.

Wacker L., Fahrni S. M., Hajdas I., Molnar M., Synal H. A., Szidat S., and Zhang Y. L. (2013) A versatile gas interface for routine radiocarbon analysis with a gas ion source. *Nucl. Instrum. Methods Phys. Res., Sect. B* **294**, 315-319. doi:10.1016/j.nimb.2012.02.009.

Walker J. C. G., Hays P. B., and Kasting J. F. (1981) A negative mechanism for the long-term stabilization of Earth's surface temperature. *J. Geophys. Res.* **86**, 9776-9782.

SUPPLEMENTARY INFORMATION

Sample	IGSN	LOI wt.%	SiO$_2$ wt.%	TiO$_2$ wt.%	Al$_2$O$_3$ wt.%	Fe$_2$O$_3$ wt.%	MnO wt.%	MgO wt.%	CaO wt.%	Na$_2$O wt.%	K$_2$O wt.%	P$_2$O$_5$ wt.%	Cr$_2$O$_3$ wt.%	NiO wt.%
09FRA05B <63 µm	GRO001029	3.94	61.99	1.70	10.79	8.62	0.13	3.46	5.31	2.07	1.17	0.240	0.0419	0.0092
09FRA22 <63 µm	GRO001044	2.69	65.90	1.11	12.84	6.90	0.11	2.81	3.77	2.18	1.65	0.224	0.0231	0.0070
09FRA10 <63 µm	GRO001034	27.31	29.57	0.34	7.01	2.44	0.06	5.63	25.08	0.56	1.87	0.124	0.0051	0.0030
09FRA04 <63 µm	GRO001027	4.84	63.39	0.90	13.08	6.21	0.10	2.85	3.21	2.52	1.93	0.210	0.0189	0.0070
09FRA15 <63 µm	GRO001038	3.33	69.23	1.03	11.42	5.16	0.09	1.94	2.88	1.99	1.57	0.214	0.0179	0.0067
09FRA13 <63 µm	GRO001036	11.78	55.94	0.61	11.20	4.34	0.08	3.94	8.03	1.10	2.40	0.158	0.0095	0.0037
09FRA24 <63 µm	GRO001046	3.68	64.24	0.99	13.46	6.59	0.10	2.75	3.39	2.32	1.65	0.215	0.0222	0.0080
09FRA16 <63 µm	GRO001039	2.91	65.10	1.22	13.51	6.38	0.09	1.76	3.51	2.93	1.74	0.259	0.0220	0.0054
09FRA23 <63 µm	GRO001045	7.13	56.30	1.03	12.05	6.97	0.12	6.14	6.74	2.05	1.24	0.196	0.0501	0.0316
09FRA09 <63 µm	GRO001033	4.03	60.00	0.67	19.19	6.63	0.08	2.37	0.33	1.26	3.82	0.176	0.0115	0.0043
09FRA18 <63 µm	GRO001040	4.55	66.35	0.87	13.50	5.57	0.08	2.24	2.52	1.71	2.36	0.210	0.0149	0.0054
11FRA22 <63 µm	GRO001079	27.04	30.25	0.33	6.54	2.38	0.05	6.31	24.68	0.57	1.73	0.126	0.0046	0.0028
11FRA03 <63 µm	GRO001065	2.13	67.59	1.24	10.37	7.26	0.13	2.81	3.78	2.05	1.22	0.174	0.0334	0.0087
10FRA10M <63 µm	GRO001050	4.52	67.34	0.91	12.12	5.29	0.12	1.91	2.52	1.99	1.75	0.208	0.0164	0.0061
09FRA20 <63 µm	GRO001042	3.24	67.39	0.92	11.29	5.44	0.10	2.22	4.39	2.26	1.55	0.234	0.0213	0.0059
10FRA04 <63 µm	GRO001049	3.91	64.91	0.70	15.11	5.91	0.06	2.09	1.62	1.36	2.92	0.186	0.0133	0.0073
11FRA07 <63 µm	GRO001068	5.27	55.52	1.33	14.42	8.52	0.13	4.10	6.04	2.82	1.08	0.223	0.0294	0.0112
10FRA13 <63 µm	GRO001054	4.23	64.17	1.11	13.85	6.25	0.10	1.92	3.39	2.77	1.71	0.237	0.0207	0.0062
11FRA21 <63 µm	GRO001078	3.50	69.10	0.75	14.04	5.81	0.06	1.67	0.57	1.49	2.54	0.304	0.0085	0.0069
10FRA15 <63 µm	GRO001056	5.97	63.84	1.01	13.06	5.71	0.10	2.62	3.68	1.56	2.36	0.233	0.0196	0.0141
10FRA17 <63 µm	GRO001058	3.39	57.20	1.26	14.63	8.68	0.14	4.23	5.69	2.86	1.05	0.208	0.0272	0.0111
FL Nov 2011 <63 µm	GRO001081	2.55	65.04	1.42	10.99	7.21	0.11	2.93	4.60	2.12	1.25	0.251	0.0328	0.0076
10FRA18 <63 µm	GRO001059	6.65	52.37	0.84	10.25	8.71	0.13	13.33	3.91	1.97	0.77	0.108	0.2468	0.0782
TSFRA108 <63 µm	GRO001083	3.42	66.04	0.94	12.17	5.91	0.10	2.68	3.69	2.19	1.55	0.204	0.0216	0.0076
10FRA14-R <63 µm	GRO001055	2.42	62.28	1.60	13.74	7.99	0.18	2.74	4.44	2.79	1.53	0.339	0.0346	0.0102
TSFRA112 <63 µm	GRO001084	3.41	66.38	1.03	12.23	6.18	0.10	2.80	3.80	2.20	1.56	0.220	0.0228	0.0071
09FRA23-R <63 µm	GRO001045	6.07	56.54	1.05	12.08	7.02	0.12	6.12	6.79	2.14	1.24	0.308	0.0517	0.0303
10FRA10M-R <63 µm	GRO001050	2.40	62.34	0.67	12.21	4.71	0.09	4.36	8.98	1.29	2.60	0.285	0.0103	0.0049
09FRA13-R <63 µm	GRO001036	10.86	64.44	0.87	10.95	4.69	0.09	1.69	2.41	1.96	1.54	0.274	0.0151	0.0049
11FRA23M susp	GRO001138	2.95	70.27	0.71	12.04	5.17	0.09	2.34	2.78	2.26	1.55	0.160	0.0148	0.0075
11FRA23S susp	GRO001139	4.66	62.75	0.86	14.02	6.51	0.12	2.94	3.55	2.22	1.79	0.205	0.0165	0.0093

11FRA23D susp	GRO001137	2.76	70.61	0.62	11.49	4.59	0.09	2.17	2.77	2.37	1.49	0.143	0.0171	0.0076
11FRA08 susp	GRO001129	5.57	51.90	0.68	13.19	6.65	0.12	2.80	3.37	1.70	2.25	0.209	0.0170	0.0081
11FRA03 susp	GRO001126	3.72	68.51	0.66	11.86	5.03	0.09	2.39	2.95	2.10	1.66	0.156	0.0155	0.0078
11FRA09 susp	GRO001070	4.34	61.09	1.08	14.11	7.18	0.19	3.12	3.69	2.69	1.78	0.243	0.0250	0.0147
09FRA01 <63 μm	GRO001024	3.87	64.96	1.09	12.68	6.82	0.11	2.78	3.73	2.16	1.63	0.224	0.0222	0.0078
10FRA11 <63 μm	GRO001052	11.04	60.86	0.65	8.67	3.55	0.07	3.56	7.59	1.18	1.74	0.177	0.0082	0.0036
10FRA02 <63 μm	GRO001047	3.44	70.97	0.66	12.55	5.42	0.06	1.52	0.60	1.42	2.24	0.320	0.0078	0.0051
10FRA19 <63 μm	GRO001060	5.82	60.67	1.11	12.63	6.80	0.11	3.10	4.31	1.87	1.89	0.210	0.0249	0.0078
10FRA14 <63 μm	GRO001055	5.39	59.45	1.49	13.23	7.80	0.19	2.64	4.14	2.59	1.48	0.269	0.0305	0.0097
10FRA22 <63 μm	GRO001063	6.35	60.80	0.86	14.01	6.22	0.11	3.06	3.97	1.74	2.37	0.192	0.0186	0.0074
10FRA12 <63 μm	GRO001053	4.70	66.16	1.17	13.41	5.99	0.09	1.97	2.04	1.45	2.38	0.255	0.0128	0.0051
11FRA14 <63 μm	GRO001076	5.76	63.42	0.76	14.72	5.91	0.09	2.12	2.29	1.50	2.72	0.201	0.0127	0.0063
11FRA13 <63 μm	GRO001075	10.94	61.73	0.71	8.15	3.42	0.06	3.63	8.04	1.28	1.58	0.197	0.0078	0.0029
10FRA16 <63 μm	GRO001057	3.60	66.65	0.99	11.52	5.84	0.11	2.42	4.06	2.06	1.68	0.261	0.0218	0.0065
10FRA03 <63 μm	GRO001048	22.35	35.77	0.43	9.81	3.21	0.07	5.76	19.36	0.62	2.57	0.135	0.0072	0.0033
11FRA18 <63 μm	GRO001077	6.18	59.53	0.94	16.57	6.97	0.08	2.16	2.01	1.32	3.30	0.237	0.0145	0.0071

Table S1. XRF abundances of major elements in Fraser River sediments.

IGSN	Rb	Ba	Sr	Nb	Zr	Hf	Y	Ga	Zn	Cu	Ni	Co	Cr	V	Sc	La	Ce	Nd	Pb	Th	U
GRO001029	37.8	509	305	13.6	1058	50.8	51.2	33.8	95	44.9	72.4	22.2	287	195	18.1	46.3	140	52.1	57.7	13.8	(1.2)
GRO001044	56.2	617	291	11.0	492	24.7	33.7	35.6	133	36.8	55.1	21.3	158	151	16.2	40.5	85	35.3	61.2	9.2	<1.7
GRO001034	61.7	679	334	6.7	317	16.9	20.0	24.3	55	14.3	23.4	7.9	35	31	(3.6)	(10.1)	54	22.8	55.6	7.6	<1.9
GRO001027	67.1	622	267	9.7	304	16.2	30.0	34.1	74	36.3	55.3	19.0	129	130	15.5	33.8	64	28.1	56.1	6.7	<1.7
GRO001038	58.6	696	243	11.4	510	25.5	40.6	32.3	80	31.2	54.2	16.8	127	124	16.3	39.6	84	34.6	65.7	12.7	(1.0)
GRO001036	97.6	557	194	11.8	329	16.5	32.6	36.1	68	22.4	33.1	11.3	74	80	8.0	44.0	91	36.7	66.4	13.7	<1.7
GRO001046	57.5	671	318	9.5	286	15.4	29.8	36.5	97	44.7	65.1	18.8	158	141	19.0	23.3	50	23.5	65.0	6.8	(0.4)
GRO001039	53.7	766	395	10.1	409	22.4	30.2	36.8	90	19.1	43.7	15.7	155	153	17.1	19.3	52	25.0	63.1	4.7	<1.7
GRO001045	42.3	640	319	7.8	171	10.6	24.6	37.1	106	50.4	267.3	33.3	369	166	19.8	<10.0	25	16.5	60.7	2.4	<1.7
GRO001033	185.2	703	126	13.6	334	16.8	42.6	46.1	120	44.9	35.6	16.5	82	104	19.4	70.0	143	53.5	72.6	16.3	1.9
GRO001040	91.6	611	201	12.2	551	26.6	45.9	37.0	79	23.7	44.4	15.8	107	100	16.5	57.4	138	51.7	68.6	16.7	2.2
GRO001079	56.2	624	307	6.2	432	22.0	23.1	21.5	69	35.5	22.2	7.9	32	28	(0.8)	15.5	61	24.7	56.6	9.0	<1.9
GRO001065	38.2	493	268	12.8	459	23.8	36.9	30.5	82	35.4	68.0	18.1	229	157	16.3	32.5	96	38.3	60.1	5.8	<1.7
GRO001050	63.5	733	237	11.2	327	17.1	30.7	33.7	77	24.7	47.8	16.7	112	118	20.0	30.1	61	27.1	59.4	9.6	(0.3)
GRO001042	49.1	665	366	8.8	302	17.2	27.9	30.7	74	29.3	46.4	16.3	146	139	14.3	21.6	53	25.0	62.2	7.1	<1.7
GRO001049	117.5	609	155	11.7	404	20.5	43.6	41.8	95	62.5	59.4	15.0	95	89	12.8	61.3	143	53.3	72.5	18.5	(0.4)
GRO001068	30.8	443	425	8.8	204	13.0	22.4	35.8	103	50.3	93.2	29.9	212	190	18.8	(9.3)	32	18.7	56.5	2.1	<1.7
GRO001054	54.6	794	390	9.9	293	16.4	28.5	37.8	94	32.1	50.6	17.9	148	148	16.7	23.5	48	23.6	62.9	3.6	<1.7
GRO001078	120.6	462	106	14.5	455	22.2	63.4	36.4	108	71.5	56.6	23.8	60	76	11.5	106.7	236	82.6	65.8	23.0	5.9
GRO001056	93.1	599	198	14.6	847	41.7	58.8	37.8	93	40.6	117.5	13.1	143	102	12.7	76.2	184	65.8	69.0	21.6	2.3
GRO001058	31.4	462	420	6.2	197	12.7	22.2	39.8	99	41.8	90.1	28.1	193	185	18.7	(0.7)	26	16.6	59.8	(1.0)	<1.8
GRO001081	42.2	541	314	11.6	773	37.9	43.6	33.7	87	30.4	61.0	17.1	230	175	16.6	38.1	115	44.5	63.0	10.3	<1.7
GRO001059	27.4	321	193	3.7	96	5.4	19.5	31.7	110	52.1	658.7	46.9	1810	168	24.9	<9.9	15	13.0	55.6	(0.4)	<1.7
GRO001083	52.8	587	292	10.5	293	15.8	25.6	32.6	82	33.5	59.6	15.7	148	129	12.1	24.8	45	21.8	59.7	7.0	<1.7
GRO001055	45.4	680	418	13.3	308	17.6	25.7	36.1	101	36.5	80.4	21.7	237	172	17.7	16.4	42	21.4	58.4	3.5	<1.7
GRO001084	51.4	601	291	9.2	362	18.5	31.9	34.9	81	33.2	55.5	14.3	156	136	15.2	21.8	71	30.2	60.2	6.6	(0.6)
GRO001045	40.3	589	294	8.9	161	10.2	20.8	34.2	102	53.2	238.3	30.3	354	151	17.0	(7.2)	28	16.9	53.9	(1.2)	<1.7
GRO001050	94.3	558	195	13.1	327	16.3	31.6	37.0	71	31.8	39.2	11.2	72	75	6.9	38.8	80	33.0	63.1	12.9	(1.6)
GRO001036	62.4	735	250	12.6	351	19.1	31.0	32.4	79	35.0	43.2	16.4	116	115	13.6	33.8	74	31.6	59.5	11.2	(1.3)
GRO001138	51.1	631	300	8.6	148	9.9	18.7	32.8	81	57.7	60.5	17.7	104	113	10.9	14.0	31	18.1	54.5	5.3	<1.6
GRO001139	62.4	762	343	8.5	168	10.3	24.7	38.6	108	59.0	76.7	21.4	118	141	16.3	11.2	43	21.9	63.0	4.9	<1.7
GRO001137	48.6	638	297	6.3	131	8.5	18.1	33.4	74	34.3	61.2	14.6	121	104	10.5	(9.5)	19	14.3	59.8	5.3	<1.6
GRO001129	90.0	883	318	6.7	145	10.2	25.7	41.1	124	87.2	67.9	23.9	124	161	17.5	15.8	47	23.3	80.1	3.6	<1.8
GRO001126	57.5	683	273	9.8	133	7.9	20.2	32.8	81	41.2	63.3	16.7	110	112	12.5	17.8	19	14.0	54.2	5.8	(1.2)

GRO001070	56.9	815	402	10.7	179	11.0	25.8	37.4	105	49.0	120.4	26.6	179	148	12.1	11.8	47	23.5	62.3	2.9	<1.7
GRO001024	62.0	636	287	11.3	470	45.9	29.8	62.7	136	38.7	61.1	18.9	152	149	18.2	27.1	73	31.0	122.3	10.5	<1.8
GRO001052	66.3	364	164	8.7	451	34.8	32.3	48.3	53	17.3	28.4	9.2	56	56	7.7	43.8	102	39.3	105.3	15.3	<1.8
GRO001047	107.0	404	96	13.8	305	73.2	43.7	118.7	102	55.2	40.4	16.7	53	64	12.1	96.4	212	75.2	155.5	26.9	<1.9
GRO001060	71.9	574	260	13.1	455	82.5	29.2	111.7	99	33.8	61.6	17.7	171	139	12.4	39.0	84	34.0	153.8	9.1	<1.9
GRO001055	56.1	707	410	14.0	298	68.4	23.0	120.1	118	31.2	80.4	25.0	221	176	17.8	(4.1)	55	26.1	167.2	2.7	<2.0
GRO001063	96.3	682	250	12.1	289	46.4	25.5	102.9	106	34.5	61.9	20.2	136	128	12.2	34.4	76	32.3	159.0	13.5	<1.9
GRO001053	103.3	534	163	18.1	1539	199.9	77.3	89.6	90	31.8	42.2	15.6	92	88	15.2	122.5	306	104.3	158.0	40.5	3.2
GRO001076	120.2	650	185	13.9	441	65.4	44.0	93.9	96	31.2	52.7	17.0	92	91	16.2	65.6	144	53.4	159.7	20.0	<1.8
GRO001075	66.1	393	195	12.9	697	91.8	45.2	89.0	64	14.7	26.0	11.6	60	61	7.2	56.9	135	50.7	156.6	14.2	<1.9
GRO001057	67.7	647	334	12.5	430	62.9	32.7	87.1	90	37.6	53.3	16.1	155	141	16.0	34.8	92	37.4	156.7	10.1	<1.9
GRO001048	115.0	532	325	12.3	437	58.1	24.4	83.5	86	22.4	33.8	11.0	63	56	10.8	25.1	93	37.2	166.3	13.4	<2.0
GRO001077	144.2	681	185	15.3	813	94.9	63.5	90.3	104	40.9	59.5	21.4	106	100	14.6	97.3	243	84.8	160.2	27.1	(1.8)

Table S2. XRF Abundances of trace elements. All values in ppm by weight. For full sample names, see Table S1. Values in parentheses are approximate.

IGSN	Flow Stage	Site	Fraction	Crenarchaeol ng/g sed	Σ brGDGTs ng/g sed	iso/br	BIT	MBT	CBT	pH	MAT (°C)	MBT'	pH'	MAT' (°C)
GRO001029	med	Fraser at Fort Langley	<63 μm	7.72	249.2	0.23	0.97	0.29	0.75	6.80	1.58	0.30	6.43	5.80
GRO001040	med	Fraser at Stoner	<63 μm	2.04	159.8	0.12	0.99	0.25	0.66	7.03	0.09	0.25	6.60	4.90
GRO001044	med	Fraser at Lillooet	<63 μm	0.49	15.4	0.18	0.96	0.31	0.70	6.92	2.71	0.31	6.52	6.58
GRO001032	med	Fraser at Lytton	<63 μm	8.03	73.8	0.23	0.89	0.28	0.47	7.53	3.30	0.28	6.98	6.93
GRO001033	med	Fraser at Fitzwilliam	<63 μm	0.18	16.1	0.05	0.99	0.22	0.99	6.17	-4.46	0.22	5.96	2.02
GRO001056	low	Fraser at Stoner	<63 μm	2.88	175.6	0.14	0.98	0.24	0.63	7.09	-0.04	0.25	6.65	4.81
GRO001063	low	Fraser at Hope	<63 μm	3.93	209.3	0.11	0.98	0.26	0.65	7.05	0.59	0.26	6.62	5.21
GRO001060	low	Fraser at Lillooet	<63 μm	2.10	108.3	0.14	0.98	0.28	0.58	7.23	2.23	0.28	6.75	6.24
GRO001049	low	Fraser at McBride	<63 μm	0.39	15.5	0.10	0.97	0.20	0.83	6.57	-3.86	0.20	6.26	2.44
GRO001047	low	Fraser at Fitzwilliam	<63 μm	0.23	18.9	0.05	0.99	0.20	1.02	6.08	-5.50	0.21	5.89	1.38
GRO001053	low	Fraser at Hansard	<63 μm	1.61	122.6	0.07	0.99	0.19	0.70	6.92	-3.01	0.20	6.52	2.94
GRO001077	high	Fraser at McBride	<63 μm	1.71	50.7	0.11	0.96	0.19	0.72	6.87	-3.55	0.19	6.48	2.63
GRO001076	high	Fraser at Hansard	<63 μm	3.08	151.7	0.08	0.98	0.19	0.70	6.91	-3.34	0.19	6.51	2.75
GRO001042	med	Quesnel	<63 μm	3.68	58.3	0.19	0.93	0.20	0.48	7.51	-0.36	0.21	6.96	4.68
GRO001034	med	Robson	<63 μm	0.65	77.4	0.02	0.99	0.12	0.31	7.95	-2.83	0.13	7.29	3.02
GRO001046	med	Pitt	<63 μm	3.95	209.5	0.18	0.98	0.30	0.83	6.59	1.05	0.30	6.27	5.47
GRO001038	med	Willow	<63 μm	2.02	147.1	0.09	0.98	0.26	0.72	6.87	0.00	0.26	6.49	4.82
GRO001036	med	McGregor	<63 μm	2.50	150.9	0.10	0.98	0.23	0.66	7.03	-0.78	0.24	6.60	4.40
GRO001045	med	Bridge	<63 μm	1.87	58.5	0.16	0.97	0.12	0.57	7.26	-5.45	0.12	6.77	1.39
GRO001039	med	Nechako	<63 μm	3.60	363.4	0.05	0.99	0.29	0.65	7.06	2.12	0.29	6.63	6.08
GRO001058	low	Chilcotin	<63 μm	5.95	119.2	0.16	0.95	0.15	0.58	7.25	-4.06	0.15	6.77	2.26
GRO001057	low	Quesnel	<63 μm	2.80	31.3	0.29	0.90	0.36	0.68	6.97	5.29	0.37	6.56	8.30
GRO001048	low	Robson	<63 μm	0.60	38.4	0.03	0.98	0.07	0.07	8.59	-3.24	0.07	7.77	2.73
GRO001050	low	Willow	<63 μm	2.49	295.1	0.07	0.99	0.25	1.11	5.84	-4.01	0.25	5.71	2.40
GRO001051	low	Willow	<63 μm	2.14	159.7	0.08	0.98	0.25	0.63	7.10	0.57	0.26	6.65	5.19
GRO001052	low	McGregor	<63 μm	3.26	141.1	0.09	0.97	0.22	0.60	7.19	-0.92	0.22	6.72	4.29
GRO001055	low	Blackwater	<63 μm	10.98	963.3	0.10	0.99	0.16	0.61	7.17	-3.52	0.17	6.71	2.60
GRO001054	low	Nechako	<63 μm	10.12	728.4	0.07	0.98	0.25	0.67	7.00	-0.03	0.25	6.58	4.77
GRO001070	high	Blackwater	<63 μm	5.93	640.1	0.02	0.99	0.31	1.11	5.83	-0.99	0.31	5.71	4.17
GRO001081		Fraser at Fort Langley	<63 μm	1.65	43.8	0.17	0.96	0.28	0.65	7.06	1.59	0.28	6.62	5.85
GRO001065	high	Fraser at Hope	susp.	5.33	174.1	0.17	0.97	0.27	0.78	6.71	0.04	0.27	6.36	4.88
GRO001137	high	Fraser at delta deep	susp.	3.73	91.8	0.21	0.96	0.26	0.69	6.95	0.32	0.26	6.54	5.06
GRO001138	high	Fraser at delta mid	susp.	5.66	130.5	0.22	0.95	0.26	0.69	6.94	0.42	0.27	6.54	5.13

GRO001139	high	Fraser at delta shallow	susp.	10.23	236.3	0.20	0.95	0.25	0.69	6.94	-0.03	0.26	6.54	4.83
GRO001128	high	Chilcotin	susp.	7.80	282.8	0.14	0.97	0.15	0.46	7.56	-2.69	0.16	7.00	3.10
GRO001130	high	Blackwater	susp.	12.16	324.9	0.16	0.96	0.21	0.55	7.32	-0.89	0.21	6.82	4.29

Table S3. Concentrations of glycerol dialkyl glycerol tetraethers (GDGTs) and associated proxy values in Fraser River sediments.

MBT (MBT') = methylation of branched tetraether index; CBT = cyclization of branched tetraether index; MAT (MAT') = mean annual air temperature; iso = isoprenoid tetraether; br = branched tetraether; BIT = branched/isoprenoid tetraether index. MBT, CBT, pH, and MAT values calculated according to Weijers et al. (2007); MBT', pH', and MAT' calculated from Peterse et al. (2012).

Peterse F., van der Meer J., Schouten S., Weijers J. W. H., Fierer N., Jackson R. B., Kim J.-H., and Sinninghe Damsté J. S. (2012) Revised calibration of the MBT–CBT paleotemperature proxy based on branched tetraether membrane lipids in surface soils. *Geochim. Cosmochim. Acta* **96**, 215-229. doi:10.1016/j.gca.2012.08.011.
Weijers J. W. H., Schouten S., van den Donker J. C., Hopmans E. C., and Sinninghe Damsté J. S. (2007) Environmental controls on bacterial tetraether membrane lipid distribution in soils. *Geochim. Cosmochim. Acta* **71**, 703-713. doi:10.1016/j.gca.2006.10.003.
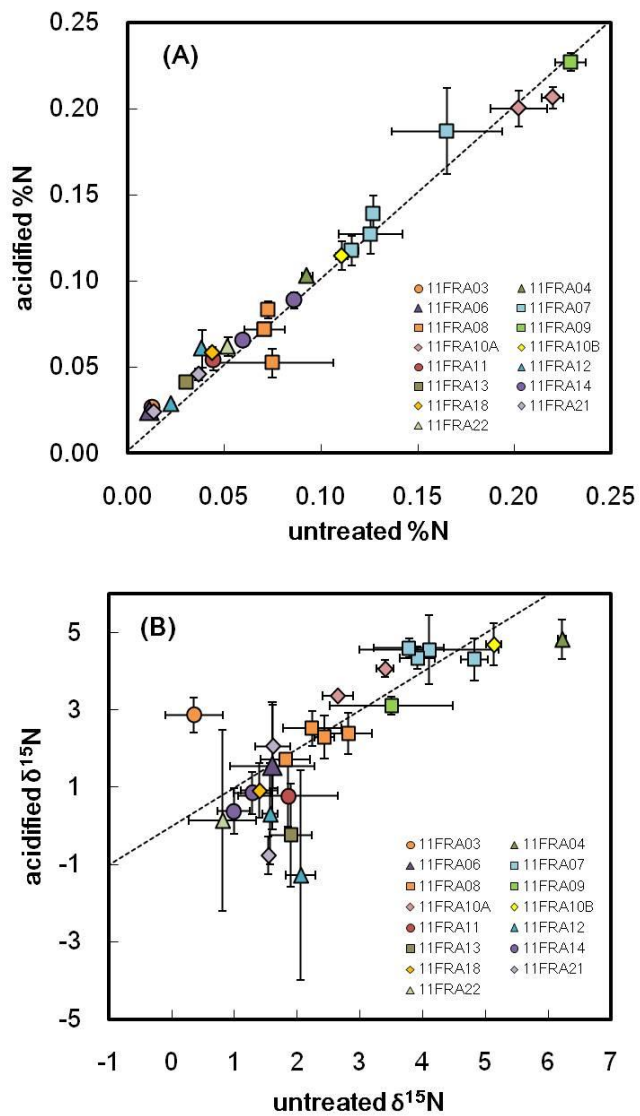
Figure S1. (A) The effect of sample acidification is minor for nitrogen abundance (%N). (B) Acidified samples, however, generally exhibited lower $\delta^{15}N$ values than corresponding unacidified samples. Shown here are different size fractions of individual sediment samples.

Figure S2. Removal of organic matter with H_2O_2 resulted in a slight increase in measured mineral surface area. The greatest disagreement occurred in samples with very low total measured surface area ($< 5 \, m^2$).

CHAPTER 4.

GEOCHEMICAL EVOLUTION OF THE SPRING FRESHET IN THE FRASER RIVER, CANADA

4.1 Abstract

Rapid changes in the volume and sources of discharge during the spring freshet lead to dramatic variations in biogeochemical properties in snowmelt-dominated river basins. We used high-frequency sampling duri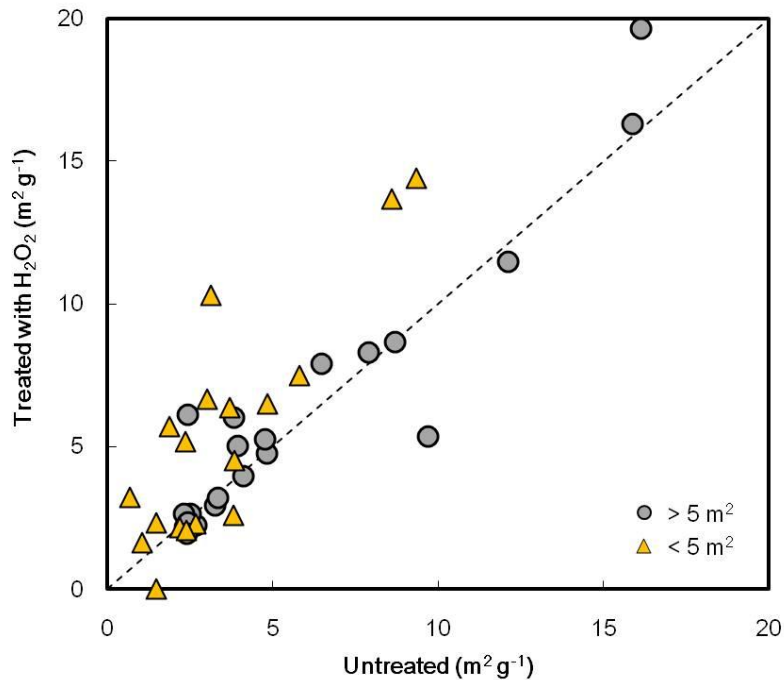ng the onset of the Fraser River (southwestern Canada) freshet in 2013 to identify rapid changes in the flux and composition of dissolved material, with a focus on dissolved organic carbon (DOC) and dissolved mercury dynamics. Previous time series sampling of dissolved inorganic species in the Fraser River has revealed smooth seasonal transitions in concentrations of major elements and runoff tracers between freshet and base flow periods. Daily sampling during the early portion of the 2013 spring freshet reveals a significant increase in DOC concentration occurring over a matter of days, accompanied by a shift towards higher molecular weight, more aromatic DOC composition. Further changes in DOC composition, but not concentration, occur at other times of year, underscoring the role of seasonal climatology in DOC cycling. Concentrations of mercury also varied during the spring freshet period, although dissolved mercury dynamics appear to be driven by factors beyond DOC dynamics. The time series records of DOC and POC indicate that the Fraser River exports a relatively large portion (~1%) of the basin net primary productivity annually.

4.2 Introduction

The present study was motivated by initial results from the observation in 2011 of a rapid pulse of DOC during the very early stages of the spring snowmelt period in the Fraser River. Such hydrologically driven seasonal patterns in DOC concentration have been observed in large Arctic rivers during the spring freshet (Holmes et al., 2011; Mann et al., 2012; Wickland et al., 2012), as well as in tropical catchments experiencing wet-season flushing of surface soils (Spencer et al., 2010; Laraque et al., 2013), and in small streams and headwater catchments dominated by episodic rain or snowmelt events (Carey, 2003; Wagner et al., 2008; Fellman et al., 2009; Raymond and Saiers, 2010; Jung et al., 2012; Lloret et al., 2013; Sandford et al., 2013; Pereira et al., 2014). In these scenarios, the composition of DOC is often observed to change significantly during such DOC pulses, as changing hydrologic flow paths draw upon different vegetation- and soil-derived DOC pools. The bulk concentration of DOC in the Fraser River has been investigated through water quality monitoring by Environment Canada in the past (Swain, 2004), however more detailed information about the composition of Fraser River DOC and its driving processes are unknown. The composition of sedimentary and particulate organic carbon (POC) also varies across the basin and between seasons (Chapter 3). DOC constitutes the larger pool of organic carbon delivered to the coastal ocean by the Fraser River, at concentrations ~5 times higher than POC during the spring freshet (when suspended sediment concentrations peak) and ~30 times higher during low discharge conditions. This ratio is high compared to global average rivers, which have an aggregate DOC/POC ratio of ~1.2, and more similar to Arctic Rivers with average ratios of ~4 (Ludwig et al., 1996).

The residence time in soils of OC derived from fresh litterfall varies tremendously, depending on its initial composition and environmental factors, between one year or less to

hundreds or thousands of years (Mills et al., 2014). DOC that enters stream channels under base flow conditions originates from deeper soil layers, where organic matter has been exposed to microbial degradation for a long time relative to fresh litter leachates in shallow soil layers (Hope et al., 1994). Freshet DOC, which derives largely from overland flow and more extensive soil inundation, is composed of organic matter that has been exposed to soil microbial communities for a shorter time than deep soil DOC (Wickland et al., 2007). This distinction is evident in the positive correlation between DOC radiocarbon content and discharge in large Arctic rivers (Raymond et al., 2007). This relatively fresh DOC has also been identified as more susceptible to microbial degradation (Holmes et al., 2008; Mann et al., 2012), and therefore a more potent source of metabolic fuel to coastal ocean ecosystems and a potential flux of CO_2 to the atmosphere.

Biogeochemical dynamics of DOC have not previously been investigated in the Fraser River, yet its distinct hydrologic regime and climatic setting suggest it may exhibit somewhat different behavior from the large Arctic river and small stream paradigms with respect to several characteristics: First, the hydrology of the Fraser River basin, a large, mountainous, mid-latitude system in southwestern Canada (Fig. 1), is dominated by a relatively protracted annual spring freshet. The freshet commences in late March to early May, when air temperatures rise to the point that snow accumulated over the winter months begins to melt, and lasts from one to three months in the mainstem Fraser (Fig. 2).

The mountainous headwaters of tributary basins supplying most of the freshet discharge lie to the north of the river mouth, and consequently, as spring warming migrates to higher latitudes, tributaries progressively reach their melting thresholds over a period of weeks. The elevation of the major mountain ranges in the Fraser basin (the Rocky Mountains in the

northeastern portion of the basin and the Coast Range in the southwest) are similar, with peaks of 3-4000 m. Large Arctic rivers, in contrast, have most of their headwater regions in the southern portions of their basins; therefore, the arrival of spring warming triggers sudden melting for the entire basin. The freshet hydrograph in the Fraser River is also often characterized by peaks and valleys caused by pauses in melting from cold intervals and/or to precipitation pulses from spring storms, which, due to the presence of major mountain ranges, can exert longitudinal differences across the basin. Thus, Arctic rivers typically experience a very rapid freshet, as melting, once commenced, quickly leads to the discharge peak. A stepwise freshet may lead to a more complex transition between base flow and freshet DOC. Furthermore, the lack of extensive permafrost in the Fraser basin excludes significant inputs from a potential pool of relatively degraded and aged soil DOC during late spring and summer months (Neff et al., 2006; Raymond et al., 2007; Wickland et al., 2007; O'Donnell et al., 2010), though this DOC is often found to be labile (Mann et al., 2012; Vonk et al., 2013). In small streams, on the other hand, storm-driven discharge events are short-lived and may deliver fresh DOC to stream channels more efficiently than the long, relatively gradual rising limb of the spring freshet in the Fraser. With snowpack in different tributary basins melting at different points throughout the rising limb of the freshet, the net effect on the composition of DOC in the main stem may be significantly buffered.

A consequence of variability in DOC concentration and composition in freshwaters is the potential for dynamic behavior of dissolved Hg. Due to the strong affinity of dissolved Hg for DOC, especially reduced sulfur moieties (Haitzer et al., 2002; Haitzer et al., 2003; Gerbig et al., 2011), concentrations of DOC and total dissolved Hg are generally observed to be positively correlated in natural waters (Schuster et al., 2008; Dittman et al., 2009; Dittman et al., 2010; Schuster et al., 2011; Burns et al., 2012a). We are not aware of any mercury monitoring in the

Fraser River by federal or provincial government agencies, despite multiple recommendations to establish such monitoring (MacDonald et al., 2011). Yet Hg—and in particular its monomethylated form which bioaccumulates in aquatic food webs—is an issue of concern for the health of Fraser River fisheries and individuals who subsist on diets rich in fish (Cohen Commission, 2012). Potential sources of Hg within the Fraser basin include urban and industrial point sources (e.g. sewage effluent, paper pulp mills), atmospheric deposition (particularly aerosols derived from coal combustion in east Asia), and mobilization of legacy Hg contamination from placer gold mining, which was widespread in the central portion of the basin in the 1850s-1910s. Hg-assisted gold mining in British Columbia, which involved the mobilization of ~58 x 10^6 m^3 of sediment in the central Fraser basin (Nelson and Church, 2012), has been proposed as the source of significant Hg deposits found in delta and lake sediments (Hales, 2000; Gallagher et al., 2003). Although the majority of the Hg contamination was most likely removed from the basin within decades due to preferential association with fine-grained (OC-rich) sediments, the ongoing transport of mining-mobilized sediment through the basin (Nelson and Church, 2012) creates the potential for continued contamination. Given the major role of rivers in global surface cycling of Hg (Amos et al., 2014), it is important to constrain the flux of Hg from this regionally-significant river basin.

Comprehensive time-series datasets for fluvial systems, including nutrients, dissolved major elements, water isotopes, and suspended sediments in addition to DOC properties are relatively rare, yet are necessary to establish a robust foundation for distinguishing biogeochemical from hydrologic and physical processes. We present here evidence for (1) rapid changes in water sources and DOC load during the early stages of the spring freshet, (2) hydrologically-driven changes in DOC flux and composition throughout the year, and (3)

implications of DOC and suspended sediment dynamics on the mercury load of the Fraser River. Given the anticipated changes in hydrology in the Fraser basin under a warming climate, particularly decreases in snowpack and an earlier onset to the spring freshet (Morrison et al., 2002; Déry et al., 2012), understanding freshet biogeochemical dynamics under present conditions is critical to predicting and preparing for the consequences of future changes.

4.3 Methods

Continuous discharge and water temperature data (5-minute frequency) were obtained from Environment Canada Water Office online real-time hydrologic data (http://www.wateroffice.ec.gc.ca). The record used was the station at Hope (08MF005; 49.381°N, -121.451°E), which is ~100 km upstream of our sampling location at Fort Langley (49.172°N,-122.577°E), and the furthest downstream station for which gauge height is not influenced by tides. Discharge at Fort Langley is 10-20% higher than at Hope (due mainly to input from the Harrison River), and water temperature is ~1.5°C higher.

Historical Fraser River DOC concentration data at Hope (1997-2014, station BC08MF0001) were obtained from the Environment Canada Pacific Yukon Freshwater Quality Monitoring and Surveillance online data (accessible at http://aquatic.pyr.ec.gc.ca/). A portion of this record is presented with sampling and analytical information by Swain (2004). Average DOC loads and discharge-weighted average DOC concentrations were calculated from time series records using the U.S. Geological Survey LoadEst program (Runkel et al., 2004).

Basic water properties were determined with a handheld multiparameter probe (YSI Professional Plus). The probe was equipped with sensors for water temperature, conductivity (μS

cm^{-1}), pH, and dissolved oxygen (DO, mg O$_2$ L^{-1}). DO and pH probes were calibrated according to manufacturer specifications approximately every 5 days.

Samples were collected from a floating dock, ~5 m from the river bank, where the water depth is ~6 m. All samples for concentrations of dissolved species were collected by in-line filtration (Pall AcroPak 500 Supor Membrane, 0.8/0.2 µm pore size) of surface water directly into pre-cleaned vials, which were rinsed three times with sample water before filling. Sampling and analytical methods for most types of samples are described in detail in Chapter 2 (Voss et al., 2014), therefore the following methods descriptions are abbreviated.

Nutrient samples were collected in pre-cleaned 20 mL polyethylene scintillation vials and stored frozen until analysis. Analyses were performed at the WHOI Nutrient Facility on an AutoAnalyzer (Lachat QuickChem 8000) with standard U.S. Environmental Protection Agency-certified spectrophotometric methods and calibrated using standard reference material MOOS-2 (National Research Council Canada).

Samples for dissolved major cations (Ca, Mg, Na, K) and anions (Cl, SO$_4$) were collected in pre-cleaned 125 mL high-density polyethylene bottles. Cation concentrations were determined using a Thermo Scientific Element2 single collector inductively-coupled plasma mass spectrometer, based on a standard curve of natural river water standard reference material SLRS-5 (National Research Council Canada). Anion concentrations were determined using a Dionex ion chromatograph with an anion column (AS15, 4 mm, with ASRS suppressor), based on a standard curve of a mixture of SpecPure ion chromatography standards (Alfa Aesar). No preservative was added to samples after collection, and samples were stored at room temperature until analysis.

Bicarbonate (HCO_3^-) concentration is assumed to be equivalent to total alkalinity concentration (for justification, see Voss et al., 2014). Total alkalinity samples were collected with care taken to ensure no air bubbles were entrapped in the sample water. Samples were collected in 250 mL borosilicate glass bottles, preserved with 60 μL of saturated $HgCl_2$ solution, and sealed with ground-glass stoppers (sealed with Apiezon M grease and secured with rubber bands) to prevent exchange with atmospheric CO_2. Samples were analyzed on an automated titrator (AS-ALK2, Apollo SciTech) using a modified Gran titration procedure (Wang and Cai, 2004).

An optical nephelometer (LaMotte, 2020-WE) was used to determine turbidity (measured in normalized turbidity units, NTU). The nephelometer was calibrated before each measurement with solutions of known turbidity (0, 1.0, and 10.0 NTU). A 20 mL surface water grab sample was collected in a glass vial and allowed to equilibrate to ambient air temperature. Vial walls were dried and wiped thoroughly with a Kimwipe before analysis. At least 6 readings were averaged for each sample to account for measurement variability.

To transform turbidity measurements into concentrations of total suspended solids (TSS), nephelometer readings were complemented with weighed sediment masses from filtered water samples. Large volume surface water grab samples (4 – 20 L) were filtered with specially designed filtration units onto 90 mm polyethersulfone membrane filters (Millipore, pore size 0.22 μm). The resulting sediments were rinsed from filters with purified water (Millipore, 18.2 $MΩ \, cm^{-1}$), freeze dried, and weighed. As there is some bias involved in sample processing due to retention of a small amount of sediment within the filters, rather than use these measured concentrations directly, we have used the linear correlation between turbidity and filtered-mass sediment concentration (Fig. 3) to calculate TSS based on nephelometer measurements. The TSS

values presented throughout the text are turbidity measurements converted to TSS using this relationship.

Fluorescent dissolved organic matter (FDOM) was measured in the field using a handheld probe (TurnerDesigns Cyclops-7 with DataBank). The probe was blank-calibrated with deionized water every 5 days. *In situ* FDOM was measured by lowering the probe from the dock at least 3 m below the river surface to eliminate possible interference from sunlight. For each sample, a second FDOM measurement was performed on filtered water (filtered with 0.2 μm pore size membrane filters as described above) in a shaded vessel. As *ex situ* FDOM measurements are affected by temperature, samples were filtered and analyzed as quickly as possible, with the FDOM measurement typically completed within 30 minutes of sample collection. The probe collected measurements every 30 seconds, and at least 20 values were averaged to account for measurement variability. Filtered FDOM values (539-1856 RFUB) correlated strongly with measured DOC concentrations, with an apparent approach towards a plateau in FDOM (~1800 RFUB) at high DOC (>~500 μmol L^{-1}; Fig. 4A). Such a plateau is likely due to light attenuation from increasing concentrations of colored dissolved material (Downing et al., 2012; Pereira et al., 2014). The suspended sediment concentration was found to account for most of the difference between *in situ* and filtered *ex situ* FDOM measurements (Fig. 4B).

Samples for the determination of dissolved organic carbon (DOC) concentration were collected in pre-combusted 40 mL amber glass vials. Concentrated HCl was added immediately to achieve a pH of 2, hindering biological activity and eliminating dissolved inorganic carbon as CO_2. Samples were stored at 4°C until analysis. DOC concentrations were determined by high-temperature catalytic oxidation on a Shimadzu TOC/TN-V instrument combined with a nitrogen

chemiluminescence detection unit (TNM-1). Concentrations are reported as the mean of 3-5 replicate injections with a coefficient of variation <2% (Mann et al., 2012).

Samples for the determination of DOC optical properties were collected in 20 mL polyethylene scintillation vials. Samples were stored at 4°C in the dark until analysis. UV-visible absorbance measurements were made at room temperature on a Shimadzu UV1800 dula-beam spectrophotometer using 10 mm path length quartz cuvettes. All samples were analyzed in triplicate and referenced to purified laboratory water (MilliQ, 18.2 MΩ cm^{-1}) (Mann et al., 2012). Naperian absorption coefficients were calculated at integer wavelengths between 200-800 nm from absorbance as follows:

$$a(\lambda) = 2.303 * A(\lambda)/l$$

where $A(\lambda)$ is the absorbance and l is the cell path length in meters (Del Vecchio and Blough, 2002).

For bulk carbon and nitrogen content and stable isotope analysis, suspended sediment samples were weighed in triplicate into combusted silver capsules. Samples were then acidified in concentrated HCl vapor under partial vacuum at 65°C to remove carbonate. Organic carbon and nitrogen concentrations (%OC and %N, by weight) and isotope values ($\delta^{13}C$) were measured on an Elemental Analyzer (Carlo Erba 1107) attached via a Finnigan-MAT Conflo II open split interface to a stable isotope ratio mass spectrometer (Delta^{Plus}) for measurement of $^{13}C/^{12}C$ (referenced to Pee Dee Belemnite). Sample %OC, %N, and $\delta^{13}C$ values were determined from standard reference materials NBS-19 limestone, IAEA-N-1 ammonium sulfate, USGS-40 glutamic acid, and a laboratory glycine standard. Analytical accuracy and precision of these measurements are 0.1 wt% for C and N abundance, 0.3‰ for $\delta^{13}C$, and 0.4‰ for $\delta^{15}N$.

Samples for stable isotope compositions of water were collected by filling 4 mL glass vials with filtered water without head space. Hydrogen (δD) and oxygen ($\delta^{18}O$) isotope compositions were measured on a Picarro L2120-I cavity ring-down spectrometer. Measured values were calibrated using secondary standards (mean $\pm$ 1 s.d.: Mediterranean Sea water, δD 8.12 $\pm$ 0.30 ‰, $\delta^{18}O$ 0.95 $\pm$ 0.05 ‰; Jungfrau water, δD -160.28 $\pm$ 0.21 ‰, $\delta^{18}O$ -22.50 $\pm$ 0.06 ‰; Zürich water, δD -75.57 $\pm$ 0.19 ‰, $\delta^{18}O$ -10.62 $\pm$ 0.04 ‰), which were calibrated to standard reference materials SLAP2, GISP, and VSMOW2 (International Atomic Energy Agency).

Samples for mercury concentrations were collected in pre-cleaned 250 mL glass bottles, that were double-bagged and handled using "clean hands-dirty hands" approaches (Patterson and Settle, 1976). Bottles were prepared following procedures outlined in Hammerschmidt et al. (2011); all materials were prepared in a class-100 cleanroom by Gretchen Swarr and Carl Lamborg at WHOI. Following established procedures (U.S. EPA, 2002), samples were preserved with BrCl (final concentration of 0.5% w/w) within 30 days of collection, then were stored in the dark at 4°C until analysis. Total dissolved mercury (TDHg) concentration represents samples filtered to 0.2 μm (as described above), while total mercury (THg) concentration represents unfiltered surface grab samples. Water sample bottles were stored in plastic bags after collection. In a clean laboratory, samples were oxidized with 100 μL saturated BrCl solution and left overnight to convert all Hg species to Hg^{2+}, then reduced with 100 μL each $NH_2OH \cdot HCl$ and $SnCl_2$ immediately before analysis to convert all species to Hg^0. Mercury concentrations were determined using a purge and trap/cold vapor atomic fluorescence spectrometry total mercury analyzer (Tekran 2600). A MilliQ water (18.2 MΩ cm^{-1}) blank was analyzed at the beginning of each day of analysis to ensure that background signal was sufficiently low (~0.5 pmol). A standard curve was generated from analyses of varying quantities of aqueous standard (NIST

SRM-3133), which was checked against vapor Hg^0 standard at 15°C. Samples were analyzed at least three times until standard deviations were <10% of the measured value, or until sample material was exhausted. Sediment total mercury concentration (SPM THg) was analyzed on material recovered from membrane filters. Sediments were analyzed on a DMA-80 mercury analyzer following established methods (U.S. EPA, 2007) at the U.S. Geological Survey in Woods Hole, MA. Concentrations were calibrated using standards MESS-3 and PACS-2 (marine sediments) and IAEA-SL-1(lake sediment). Blanks were analyzed as combusted (500°C, 1 hour) aluminum boats (the same as were used for samples). The total amount of Hg analyzed in samples ranged from 1.2-4.9 ng. The very low amounts of Hg reported here are detectable (3x standard deviation of blank = 0.6 ng), but in two of six samples were not quantifiable (10x standard deviation of blank = 2.0 ng). This limitation does not affect the conclusions drawn from the data.

4.4 Results

The data presented here include Fraser River samples collected during the early portion of the 2013 spring freshet (Table 1), and a DOC-specific dataset for samples collected between June 2011 and September 2013 (Table 3). During this period (March 26th-April 22nd 2013, hereafter referred to as the "2013 early freshet"), discharge (at Hope) increased from 950 to 3000 $m^3 s^{-1}$. In the same time period, water temperature (5.7-8.4°C), conductivity (109-136 $\mu S\ cm^{-1}$), DO (11.6-13.3 mg L^{-1}) and pH (7.53-7.90) were variable, but did not trend in a consistent direction. Total suspended sediment (TSS) concentrations were very low (3-9 mg L^{-1}) for the first ~10 days, then increased rapidly to high, but variable values (40-150 mg L^{-1}) (Fig. 4).

Nutrient concentrations varied somewhat during the early freshet period (NO_3+NO_2: 4-19 $\mu mol\ L^{-1}$, PO_4: 0.2-0.7 $\mu mol\ L^{-1}$; NH_4: 0.4-2.3 $\mu mol\ L^{-1}$; SiO_2: 83-113 $\mu mol\ L^{-1}$) (Fig. 5). Nitrate/nitrite and NH_4 concentrations showed a slight decreasing trend, continuing the decline from peak winter values, typical of the seasonal cycle in the Fraser River (Whitfield and Schreier, 1981; Cameron, 1996; Voss et al., 2014). Phosphate and dissolved SiO_2 concentrations did not show a clear trend. Nutrient concentrations were overall very variable, exhibiting a substantial portion of the total annual variation. Such large daily variability was not observed in the lower frequency time series sampling presented by Voss et al. (2014).

Dissolved major element concentrations are presented in supplementary Table S1. Concentrations of some major elements (Na, Cl, SO_4) decreased as discharge increased during the early freshet. Others decreased for the first two weeks, then increased (Mg, K) or remained relatively stable (Ca). The elements which exhibited a more systematic decrease in concentration throughout the early freshet are more significantly influenced by sea salt aerosols in precipitation relative to chemical weathering of rocks than those characterized by more variable behavior. All major elements except SiO_2 showed significant linear correlations ($p<0.01$, 95% confidence interval) with conductivity (a proxy for total dissolved solids).

The stable isotope composition of water (δD, $\delta^{18}O$) showed a steady shift to more negative values over the 2013 early freshet (Fig. 6). The change (>15‰ in δD over 27 days) is large and rapid compared to the total annual variability in this parameter (~40‰ in δD) (Voss et al., 2014). Deuterium excess (D excess = $\delta D - 8*\delta^{18}O$) (values not shown) decreased slightly during this period from ~8 to ~5‰.

A longer time series record of DOC properties is shown in Table 3 and Figures 7 and 8, including most of the 2011 and 2013 data. Insufficient sampling frequency in 2012 prevented a

thorough analysis of the key seasonal features. In both years of the record, DOC concentrations

rise rapidly during the early freshet period from fall/winter levels of ~200 μmol L^{-1} to a peak of

700-900 μmol L^{-1} (Fig. 7). This rise in DOC concentration occurs at the very early stages of the

rise in discharge, with peak DOC concentrations achieved when discharge had only reached 40%

of its maximum.

Optical properties of DOC reveal changes in the composition of dissolved organic matter

during the early freshet period, as well as at other times of year (Fig. 8). Decadal absorbance at

specific wavelengths is typically tightly correlated with total DOC concentration, while relative

absorbance at different wavelengths can be diagnostic of certain DOC properties: Normalizing

DOC concentrations to wavelength-specific absorbance (e.g. SUVA$_{254}$ = absorbance at 254 nm

divided by DOC concentration) allows the chromophoric character of DOC in different settings

to be compared, and the value of SUVA$_{254}$ is positively correlated with bulk aromaticity

(Weishaar et al., 2003); the absorbance ratio (a_{250}/a_{365}) represents the ratio of decadal absorbance

values at two wavelengths (250 and 365 nm), and is negatively correlated with molecular weight

and aromaticity of DOC (Peuravuori and Pihlaja, 1997); the slope ratio (S_R) represents the ratio

of the slopes of the absorbance-wavelength curve over two ranges (275-295 and 350-400 nm)

and is also negatively correlated with DOC molecular weight and aromaticity, as well as relative

vascular plant content (cf. Spencer et al., 2012 and sources therein).

During the early freshet of the Fraser River, values of a_{250}/a_{365} and S_R decrease, while

specific ultraviolet absorbance (SUVA$_{254}$) increases. These early freshet changes are part of a

larger seasonal cycle, shown in Figure 8 for a_{250}/a_{365} and S_R. While the values of these

parameters decrease during the early freshet DOC pulse, the values gradually rise throughout the

summer, peaking in early fall. In winter, values drop again before rising rather abruptly prior to

the early freshet. For the ~2-year record of these DOC optical properties, all three parameters show a consistent twice-yearly cycle between higher values in fall and early spring and lower values in winter and during the early freshet (the direction of these trends is reversed for $SUVA_{254}$).

In addition to DOC concentration, the POC concentration increases rapidly during the early freshet (Fig. 9). Although the organic carbon (OC) content of suspended sediments decreases during this time, the increase in TSS is so great that the POC concentration rises by an order of magnitude. The relative change in POC concentration is greater than that of DOC concentration, as the DOC:POC concentration ratio decreases from a value of 30 on March 26th to a minimum of 4.6 on April 8th, followed by a recovery to ~10 over the following two weeks. The C:N composition of POC also changes, with values before April 6th varying between 8.5 and <10 (excepting the value of 10.3 on March 31st), and then rising to values between 10-11 for the remainder of the sampling period. The POC $\delta^{13}C$ values also varied (-27.7 to -26.1‰), however no clear trends were apparent.

Total dissolved mercury (TDHg) concentrations varied between 5.9 and 15.2 pmol L^{-1}, with no distinct trend during the early freshet period (Fig. 10). Total mercury (THg, unfiltered) concentrations increased significantly in a matter of days during this period, with concentrations before April 7th at ~15 pmol L^{-1} and those on and after this date at ~50 pmol L^{-1}. The portion of the total (dissolved plus suspended) Hg load composed of dissolved Hg correspondingly decreased from 70-80% before April 7th to <25%.

4.5 Discussion

4.5.1 Rapid geochemical changes in the early freshet

The geochemical data presented here highlight the importance of the very early portion of the spring freshet to biogeochemical dynamics in the Fraser River. While discharge and basic water properties (temperature, DO, pH, conductivity, and major element concentrations) record only modest changes during this interval, the initial melting of snowpack manifests itself in a suite of geochemical shifts, including suspended sediment concentrations and certain properties of dissolved organic and inorganic matter.

The sudden change in water sources from different portions of the basin is demonstrated by the rapid decrease in δD and $\delta^{18}O$ values. As runoff from headwater areas and snowmelt with compositions more depleted in heavy isotopes begins to contribute a greater portion of the total discharge, the lower Fraser mainstem quickly records this transition at the whole basin-scale. Quantification of the proportional contributions of various water sources (particular snowpacks and tributaries) based on the observed changes in stable isotope composition is complicated due to insufficient knowledge of source water compositions. The δD and $\delta^{18}O$ values of individual tributaries are quite variable across the year (Voss et al., 2014). Furthermore, the isotope composition of snow and ice likely varies with altitude and water vapor source, causing the composition of the snow within a single tributary basin to vary as seasonal melting progresses. The isotope composition of precipitation in the Fraser basin is also poorly characterized. The magnitude of the change in isotope composition of the Fraser main stem, however, is sufficiently large that the transition to greater headwater and snowmelt influence during the early freshet is unequivocal.

A pronounced geochemical shift is recorded by the change in concentration and composition of DOC. DOC dynamics are driven by a combination of hydrological and biological processes. When discharge is low at "base flow" levels, hydrologic flow paths through soil are relatively deep and slow, drawing modest amounts of DOC from deeper soil layers (Townsend-Small et al., 2011). This DOC is likely older and more degraded from its initial plant source material as a result of exposure to soil microbiota (Gangloff et al., 2014), although a portion of soil DOC may also derive from soil biota, which may preferentially remineralized younger carbon sources. As discharge and, hence, overland flow, increase and soils become inundated across the basin, hydrologic flow paths change both laterally and vertically, drawing DOC from greater distances from stream channels and shallower soil horizons. This DOC is likely more concentrated, and exported to stream channels more efficiently than base flow DOC, explaining the pulse in DOC concentration.

The average total DOC flux of the Fraser River can be estimated from our three-year record, as well as from the sixteen-year record of water quality monitoring carried out by Environment Canada at the city of Hope. This site is ~100 km upstream of the sampling site used in this study, and notably excludes a large portion of the agricultural Fraser Valley and a large, DOC-poor Coast Range tributary, the Harrison River. Despite this distinction, the LoadEst estimates of total Fraser River DOC flux based on these two records (Table 4) agree within their uncertainties, with the longer Environment Canada record showing smaller uncertainty, as expected.

4.5.2 Annual cycles of DOC composition and sources

The composition of DOC during the freshet changes dramatically, as seen in the DOC optical properties. Lower a_{250}/a_{365} and S_R values, and higher $SUVA_{254}$ values, generally correspond to higher molecular weight, more aromatic, and more vascular plant-like composition (Weishaar et al., 2003; Helms et al., 2008). The fact that DOC concentrations peak and begin to fall before discharge reaches its freshet zenith indicates that this hydrologic flushing of DOC is limited by the size of the shallow soil DOC pool, and/or by different portions of the basin with distinct discharge timescales that contribute significantly different amounts of DOC during this period. Disentangling these effects would require extensive knowledge of seasonal changes in DOC flux and composition from individual tributary basins. If the spring freshet effectively strips the shallow soil DOC pool across the basin, this implies a decoupling from the deep DOC pool, as negligible shallow DOC is able to persist during high flow conditions, and transfer to deeper soil layers only occurs between late summer and the following spring. If, however, a portion of shallow soil DOC escapes mobilization into streams during the freshet, this material (which may not be representative of the bulk shallow DOC pool) has the opportunity to undergo aging and degradation in deeper soil layers and influence the flux and composition of DOC during non-freshet conditions. In addition, the magnitude of anthropogenic contributions to the OC load of the Fraser basin could potentially be investigated through measurement of tracers such as mammalian fecal markers (e.g., coprostanol) or phenolic flavor compounds (e.g. Writer et al., 1995; Keil et al., 2011).

Considering the full annual records of DOC concentration and composition, it is evident that DOC composition varies at other points in the seasonal hydrograph. Throughout the summer, as main stem DOC concentrations decrease to base flow levels, the DOC optical

properties gradually return to values similar to those of pre-freshet DOC (higher a_{250}/a_{365} and S_R, lower $SUVA_{254}$). In the late fall, while DOC concentrations remain low and stable, optical properties once again shift to freshet-like compositions (lower a_{250}/a_{365} and S_R, higher $SUVA_{254}$), and then return to pre-freshet composition in late winter/early spring, just before the DOC concentration pulse.

The twice-annual cycle in DOC composition is likely the result of hydrologic changes. As described above, the early freshet shift represents more rapid export of shallow soil DOC driven primarily by melting snowpack across the basin. The compositional change in the fall is likely driven by a similar flushing of shallow soil DOC derived from biomass accumulated over the growth season and liberated by episodic rain events, as has been observed in other non-snowmelt-driven systems such as the Mississippi River (Bianchi et al., 2013), as well as in the Yukon River (Wickland et al., 2012). The Fraser basin, particularly in areas east of the Coast Range, generally receives very little precipitation in the late summer months, which allows litter from fresh vegetation to accumulate and DOC export to revert to slower, deeper flow paths. Warmer temperatures in late summer relative to spring may also promote more rapid microbial degradation of soil DOC, thus diminishing the potential amount of DOC that can enter streams. In the winter, precipitation in much of the basin falls primarily as snow, which does not enhance surface runoff. Fall precipitation (rain), however, is capable of flushing shallow soil DOC into streams. This fall DOC has a more freshet-like composition, suggesting that it has a similarly short soil residence time and/or degradation history. The amount of DOC mobilized by this fall soil flushing is less than that of the spring freshet, presumably because the soil DOC pool has not yet recovered to its pre-freshet size, and the amount of runoff generated by fall rain storms is much less than that from spring snowmelt. Therefore, this relatively small input of lower

molecular weight, less aromatic DOC to the smaller base flow DOC load of the Fraser causes a change in DOC optical properties of a similar magnitude to that seen during the early freshet. The spatial extent and magnitude of fall rain events is also highly variable from year-to-year and across different tributary catchments, hence the fall and winter DOC composition changes are likely to be more variable than those during the freshet.

The average depth of the shallow soil horizon responsible for the freshet pulse of DOC can be estimated from the volume of water discharged during this pulse. In 2013, the freshet DOC pulse—from the point when DOC concentration began to rise rapidly until it returned to nearly pre-freshet values—lasted approximately from April 5th – June 7th. The end of the pulse occurred approximately at the midpoint of the peak in discharge. The cumulative discharge of the Fraser River during this time was 33 km^3. Given an average forest soil porosity of ~0.43 in British Columbia (Zhao et al., 2008), the actual soil volume represented by this volume of water is ~77 km^3. If this volume is distributed equally across the entire basin (228,776 km^2), this volume represents a soil depth of ~34 cm. Given that soil porosity varies considerably across the basin (as low as 0.15 in highly compacted fine-grained and agricultural soils, and as high as 0.70 in coarse-grained soils), depths of ca. 20-100 cm could be flushed in different localities. Furthermore, these values are presumably minimum depths, as some mountainous portions of the basin have essentially no soil cover and hence contribute negligibly to the DOC pulse. Total soil depth (above bedrock) is also highly variable across the basin, ranging from <0.5 m in rapidly-eroding mountainous areas to >3 m in flatter areas that have accumulated significant glaciofluvial sediments (Valentine et al., 1978; Vold, 1979). An estimate of a surface horizon of 0.2-1 m flushed during the freshet DOC pulse is therefore a reasonable first-order approximation of the spatial extent of this event.

In addition to hydrologic and soil microbial controls on DOC dynamics, in-stream and lacustrine biological activity may play a role in the observed changes in DOC concentration and composition. Throughout the spring freshet and summer, nutrient concentrations in the Fraser main stem also decrease. This trend is likely due in part to changes in the sources of nutrients from soil flushing, similar to DOC. However, nutrients are also consumed by autotrophic activity in some portions of the basin, particularly in tributary basins containing lakes. In these basins, such as the Thompson, Nechako, and Quesnel Rivers, lakes function as suspended sediment filters, allowing sunlight to penetrate more deeply in slow-flowing waters. Such basins are likely especially depleted in nutrients during this period, and may also contribute some DOC derived from autotrophic production. This DOC would have optical properties indicating a less aromatic, lower molecular weight composition. Aquatic autotrophic and heterotrophic DOC input would likely be strongest during summer, when discharge and river sediment concentrations are lower than during the peak freshet, and water temperatures are higher. More detailed data on seasonal and spatial variability in DOC concentration and composition within these basins, as compared with more mountainous tributaries, would be needed to better constrain this potential source of DOC to the main stem Fraser.

Using the concentrations and optical properties of DOC, we have estimated the contributions of "shallow" versus "deep" soil-derived DOC to the total DOC load of the Fraser River (Fig. 11). Assuming that the maximum and minimum values of the optical properties observed in our time series represent these hypothetical end-members, we have calculated the fractions of deep and shallow soil-derived DOC for each point in the time series, and generated discharge-weighted average values using LoadEst (Table 5). Both the slope ratios (S_R) and absorbance ratios (a_{250}/a_{365}) indicate that, on average, shallow soil-derived DOC constitutes

~60% of the total DOC flux. The fraction of total DOC derived from deep and shallow soils varies non-linearly with DOC concentration (Fig. 11). This reflects the observation from the time series record that DOC optical properties can change on the basin scale not only during the spring freshet, but also in response to relatively small hydrologic changes while the total DOC load remains constant.

Finally, the rapid increase in POC concentration is another noteworthy feature of the early freshet period. The high sediment %OC and variable C:N composition of the first two weeks of the sampling period may reflect biologically controlled conditions, meaning sediment transport time through the basin and initial OC substrate availability are sufficiently large to allow microbial and/or autotrophic influence on POC composition. In addition, the lower POC concentration may not be able to buffer relatively small contributions from POC sources with significantly different compositions. In contrast, the OC-lean, homogenous C:N ratios of the second portion of the early freshet reflects flux-controlled conditions in which material transport is too rapid for biogeochemical transformations to significantly influence POC composition.

The role of the Fraser River in transferring terrestrial OC to the coastal ocean can be assessed by comparing the fluxes of DOC and POC with total carbon fixation by land plants. Net primary productivity (NPP) in the Fraser basin is estimated at $\sim 210 \pm 79$ g C m^{-2} a^{-1} (mean value for British Columbia, which is comparable to 189 and 215 g C m^{-2} a^{-1} for the Pacific Maritime and Montane Cordillera ecozones, respectively, within the basin; Liu et al., 2002). Thus total terrestrial carbon fixation in the basin is $\sim 4.0 \times 10^{12}$ mol C a^{-1}. The DOC flux of 2.8×10^{10} mol C a^{-1} (Table 4) therefore represents 0.7% of NPP. Quantifying the annual POC flux is complicated by the very limited dataset available (n = 29, with 26 values from the 2013 early freshet period and 3 values during low discharge in 2010 and 2011); however, a first-order value based on these

data using LoadEst estimates a POC flux of ~1.1×10^{10} mol C a^{-1}. Therefore POC flux represents ~0.3% of annual net primary productivity. Together, annual DOC + POC fluxes transfer ~1% of total NPP in the Fraser basin to the coastal ocean. Based on NPP and DOC and POC flux data presented by Ludwig et al. (1996), the export of 1% of basin NPP as DOC+POC is relatively high, with most large rivers exporting only 0.3-0.5% (e.g. Rhine: 0.3%, Mississippi: 0.3%, St. Lawrence: 0.4%, Mackenzie: 0.5%, Yukon: 0.5%, Congo: 0.5%). The estimate of 1% of NPP exported in the Fraser basin is comparable to some rivers (Waikato: 1.0%, Orinoco: 1.1%, Amazon: 1.1%), and less than some rivers with high sediment yields (Ganges-Brahmaputra: 1.6%, Changjiang: 2.6%, Huanghe: 4.1%). Thus, relative to large rivers globally, the Fraser River appears to export terrestrial OC quite effectively. In addition to the export of biomass-derived OC, the work in Chapter 3 demonstrated that DOC respiration contributes a significant portion of the flux of dissolved inorganic carbon (DIC). The exact value of this proportion requires more detailed analysis to constrain; however, both major element- and radiocarbon-based calculations estimate that ~80% of the DIC delivered to the coastal ocean by the Fraser River (13.3×10^{10} mol C a^{-1}) is derived from DOC respiration, or ~10.7×10^{10} mol C a^{-1}. Thus the total flux of carbon (DIC+DOC+POC) derived from recently fixed atmospheric CO_2 in the Fraser River is ~14.6×10^{10} mol C a^{-1}, or ~3.6% of Fraser basin NPP.

4.5.3 Early freshet mercury dynamics

Finally, changes in dissolved and total Hg concentrations were examined as a possible consequence of the significant changes in DOC concentration during the early freshet period. Previous river DOC studies have identified a strong correlation between DOC concentration and TDHg concentration (e.g. Haitzer et al., 2002; Dittman et al., 2010; Schuster et al., 2011; Burns

et al., 2012b), resulting from the association of Hg with DOC functional groups, particularly reduced sulfur moieties (Gerbig et al., 2011). The TDHg concentrations in the Fraser River during the early freshet period, however, are not clearly correlated with DOC concentration (Fig. 12). While the size of this dataset is rather limited, the concentration changes are sufficiently large to indicate that processes in addition to changes in DOC concentration are likely required to explain the data. In small headwater tributaries of the Hudson River (Burns et al., 2012b), other streams in northern New England (Dittman et al., 2010), and the Yukon River (Schuster et al., 2011), the TDHg concentration observed for a given DOC concentration is generally lower than our observations for the Fraser. In particular, TDHg concentrations on March 30th (10.1 pmol L^{-1}) and April 3rd (13.3 pmol L^{-1}) are significantly higher than those predicted based on these previous studies.

The DOC optical property data demonstrated that the composition of DOC varies during the early freshet period, thus it is possible that distinct types of DOC bind dissolved Hg more or less strongly (Haitzer et al., 2003). While the relevant compositional characteristics may not be reflected in the optical property data, the lack of correlation between TDHg concentration and DOC optical properties casts doubt on this possibility. To properly investigate this hypothesis, the bulk sulfur content of DOC should be analyzed, or specific sulfur-bearing functional groups quantified via high-resolution mass spectrometry or X-ray spectroscopy.

The concentrations of total mercury (THg), including both dissolved and suspended material, may provide further insight. The marked increase in THg concentrations over the early freshet period corresponds to an increase in the suspended sediment concentration (Fig. 13), demonstrating that when suspended sediment concentrations rise above base flow levels, sediments contribute the majority of the total Hg load.

A final consideration regarding the TDHg concentration data is the possibility that at higher suspended sediment concentrations, a greater amount of sedimentary Hg is leached into the dissolved phase. The distribution coefficient (K_d) of Hg is defined as:

$$K_d = THg(SPM)/TDHg$$

and quantifies the proportion of Hg found in solid versus dissolved form. The calculated K_d values for the six time points sampled during the early freshet vary by over an order of magnitude ($2.2 \times 10^{-7} - 2.8 \times 10^{-8}$). Such variation indicates that either the exchange of Hg between particle-associated and dissolved phases is not at equilibrium, or that the concentration and/or composition of suspended sediments influences the affinity of Hg for the dissolved versus the solid phase. Although the Hg concentration of the sediments themselves (SPM THg, Table 1) does not change significantly during this period, the significant decrease in SPM organic carbon (OC) content during the early freshet may affect the affinity of Hg for dissolved versus solid phases, e.g. higher SPM OC content may enhance sorption of dissolved Hg. K_d values are strongly correlated with TSS ($r^2 = 0.75$) and POC ($r^2 = 0.69$), but not with DOC ($r^2 = 0.34$) or TDHg ($r^2 = 0.19$). TSS and POC are strongly related to each other in a nonlinear fashion (Fig. 14). A negative exponential relationship between suspended sediment concentration and POC concentration is a common feature of rivers globally, due to the tendency for sediment mobilization events (such as that experienced during the spring freshet) to erode particles from deeper soil horizons which are depleted in OC content by microbial activity, or coarser particles with lower capacity for OC loading (Mayer, 1994; Ludwig et al., 1996).

Given the general dependence of Hg distribution on associations with OC (Aiken et al., 2011), the concentration of POC is likely the relevant factor in the observed K_d behavior rather than TSS concentration. This influence may result in stronger adsorption of dissolved Hg onto

particles at higher POC concentration, causing a shallower slope in the TDHg-DOC relationship than if POC concentration were constant. Compared to previous studies investigating the relationship between DOC and dissolved Hg in rivers (Dittman et al., 2010; Schuster et al., 2011; Burns et al., 2012b), our Fraser River samples show generally higher TDHg concentrations for a given DOC concentration. Assuming that the slope of the relationship between DOC and TDHg seen in these rivers would apply to the Fraser River under stable POC conditions, this is the opposite offset that would be expected from POC-enhanced Hg sorption. Thus it appears that other processes (such as changes in the chemical composition of DOC or POC) are responsible for the trends observed in dissolved and particulate Hg during the Fraser River early freshet period. The most practical first step towards better understanding of Hg dynamics in this system is to generate a larger dataset of TDHg concentrations.

4.6 Conclusions

DOC concentration in the Fraser River peaks (>700 μmol L^{-1}) during the rising limb of the spring freshet and declines to base flow levels (~200 μmol L^{-1}) over the course of the summer. DOC optical properties show that during the early spring freshet, DOC shifts from a lower molecular weight, less aromatic composition, to a higher molecular weight, more aromatic composition. Such a contrast in optical composition has been associated with microbially-degraded sources of DOC (lower molecular weight, lower aromaticity) versus fresh plant-derived DOC (higher molecular weight, higher aromaticity; e.g. Wickland et al., 2007; Fellman et al., 2009; Fellman et al., 2010), as well as highly aromatic black carbon (Jaffé et al., 2013). After returning to the pre-freshet composition, DOC again shifts to a higher molecular weight, more aromatic composition in the fall, likely due to heavy rain events. POC concentration and

composition also change rapidly during the early freshet (from <10 to >90 µmol L^{-1} and C:N ratios ~9 to ~10.5, respectively). POC concentration is driven by the sudden rise in suspended sediment concentration, which compensates for the drop in sediment OC content. Dissolved mercury concentrations during the early freshet do not exhibit the expected strong correlation with DOC concentrations. The total mercury load of the Fraser is, however, strongly dependent on the concentration of suspended sediment; the concentration of Hg in the sediment is less important, as we found it to be relatively constant. More detailed work on the full annual cycle of mercury concentrations in the Fraser River, and the molecular composition of DOC, are required to fully characterize these processes. Despite its large size and less extreme hydrograph compared to Arctic rivers and small streams, DOC cycling in the Fraser basin is highly dynamic and warrants high-frequency sampling both on the main stem and its major tributaries in order to constrain the seasonal variability of DOC sources draining different biogeoclimatic zones. Such work could be carried out through the installation of a network of optical sensors (cf. Sandford et al., 2013; Wilson et al., 2013) to fully capture the seasonal and spatial variability in the flux and composition of DOC in this river. Compared to large rivers globally, the Fraser River exports a relatively high proportion (~1%) of annual basin net primary productivity as DOC and POC. This study demonstrates that significant changes in DOC flux and composition are possible not only in watersheds experiencing extreme temporal changes in climate and discharge, but also in large temperate basins with theoretically smaller intrinsic variability in DOC source contributions (relative to Arctic rivers) and greater capacity to buffer the impacts of seasonal changes in contributions from these sources (relative to small streams and headwater catchments). The relative lack of lakes and artificial reservoirs in the Fraser basin may be an important factor in transmitting these seasonal signals to the coastal ocean.

Date	Parent IGSN	Q_w at Hope ($m^3 s^{-1}$)	T (°C)	DO (mg L^{-1})	Cond. (µS cm^{-1})	pH	Turb. (NTU)	TSS (mg L^{-1})	δD (‰)	δ^{18}O (‰)	DOC (µmol L^{-1})	*in situ* FDOM (RFUB)	filtered FDOM (RFUB)
26.Mar.13	GRO000920	980	6.8	12.7	132.0	7.53	3.5±0.2	3.3	-115.68	-15.35	277	693	701
27.Mar.13	GRO000921	981	6.7	12.9	132.5	7.68	3.6±0.2	3.5	-120.68	-16.13	240	628	583
28.Mar.13	GRO000922	984	6.7	12.7	134.2	7.63	3.5±0.2	3.3	-118.74	-15.87	206	703	722
29.Mar.13	GRO000923	1015	7.2	13.3	135.6	7.66	4.0±0.3	4.2	-119.78	-15.99	198	647	596
30.Mar.13	GRO000178	1042	7.6	11.7	134.4	7.71	4.5±0.6	5.0	-120.68	-16.05	205	605	591
31.Mar.13	GRO000924	1085	7.8	12.3	132.5	7.79	4.5±0.6	5.0	-123.08	-16.38	198	570	593
01.Apr.13	GRO000925	1182	8.4	11.6	130.8	7.80	4.5±0.6	5.0	-122.66	-16.20	205	567	539
02.Apr.13	GRO000926	1294	8.4	12.3	122.2	7.67	4.5±0.6	5.0	-120.68	-16.02	189	555	546
03.Apr.13	GRO000179	1363	8.3	12.3	123.9	7.73	5.7±0.3	7.1	-120.87	-15.93	199	581	572
04.Apr.13	GRO000927	1485	8.2	12.4	122.3	7.71	6.7±0.4	8.6	-121.85	-16.08	205	626	624
05.Apr.13	GRO000928	1774	8.1	12.0	121.3	7.68	8.1±0.3	10.9	-122.19	-16.04	217	696	707
06.Apr.13	GRO000929	1861	8.0	12.2	117.2	7.69	12.6±0.4	18.5	-122.17	-16.02	234	791	825
07.Apr.13	GRO000180	1879	7.2	12.5	109.1	7.67	22.4±1.1	34.9	-120.13	-15.95	266	847	966
08.Apr.13	GRO000930	1936	6.8	12.5	109.2	7.66	39.5±1.4	63.4	-120.96	-15.78	286	844	1142
09.Apr.13	GRO000931	2158	6.8	12.7	118.1	7.70	38.0±1.3	60.8	-121.56	-16.07	343	951	1267
10.Apr.13	GRO000932	2354	7.0	13.0	124.1	7.77	53.0±1.3	85.9	-123.53	-16.32	415	1030	1539
11.Apr.13	GRO000933	2337	6.7	13.2	120.6	7.74	56.6±0.8	91.8	-125.50	-16.58	413	995	1553
12.Apr.13	GRO000181	2435	6.0	13.0	115.5	7.76	43.6±1.1	70.2	-125.33	-16.42	419	1114	1537
13.Apr.13	GRO000934	2511	5.7	12.9	118.1	7.74	38.6±1.1	61.9	-124.96	-16.21	435	1250	1663
14.Apr.13	GRO000935	2579	5.7	13.0	121.7	7.77	30.9±0.7	49.1	-127.26	-16.64	445	1339	1594
15.Apr.13	GRO000936	2479	6.0	13.0	127.4	7.90	81±4	132.9	-127.99	-16.77	458	929	1710
16.Apr.13	GRO000182	2475	6.6	12.9	124.1	7.81	44.1±0.9	71.0	-129.11	-16.89	558	1303	1776
17.Apr.13 09:00	GRO000937	2385	6.1	13.2	125.8	7.81	39.6±1.1	63.5	-130.21	-16.98	526	1421	1856
17.Apr.13 11:45	GRO000938	2357	6.6	13.3	126.2	7.81	40.6±1.2	65.2	-131.27	-17.12	522	1396	1836
17.Apr.13 14:30	GRO000939	2349	6.8	13.4	126.3	7.79	40.9±1.7	65.7	-130.92	-17.13	506		
17.Apr.13 17:45	GRO000940	2355	7.0	13.1	126.3	7.77			-130.30	-16.90	505		
18.Apr.13	GRO000941	2405	6.2	13.2	125.6	7.81	36.5±1.6	58.3	-131.37	-17.14	497		
19.Apr.13	GRO000942	2356	6.5	12.9	125.7	7.80	31.2±1.1	49.6	-129.59	-16.80	493		
20.Apr.13	GRO000183	2430	6.8	12.8	124.8	7.74	27.0±1.1	42.5	-127.80	-16.82	492		
21.Apr.13	GRO000943	2906	7.3	12.6	125.4	7.79	27.6±1.9	43.5	-127.51	-16.87	469		
22.Apr.13	GRO000945	3078	6.9	12.7	122.5	7.82	25.9±0.4	40.7	-128.35	-16.74	477		

Table 1. Basic water properties and geochemical data for the 2013 early freshet period. IGSN codes refer to International GeoSample

Numbers in the System for Earth Sample Registration (Sesar) database; sample metadata can be accessed at www.geosamples.org.

Date	NO$_2$+NO$_3$ (μmol L^{-1})	PO$_4$ (μmol L^{-1})	NH$_4$ (μmol L^{-1})	SiO$_4$ (μmol L^{-1})	SPM %OC	SPM C/N	SPM δ^{13}C (‰)	SPM δ^{15}N (‰)	SPM Fm	TDHg (pmol L^{-1})	THg (pmol L^{-1})	SPM THg (pmol kg^{-1})
26.Mar.13	15.10	0.36	1.46	95	3.32±0.1	9.7±0.3	-27.7±0.3	1.6±0.7	0.834			
27.Mar.13	11.75	0.33	1.86	104	2.79±0.1	10.5±0.9	-28.1±0.4	1.1±0.4				
28.Mar.13	19.40	0.32	1.85	107								
29.Mar.13	6.87	0.34	2.29	92	3.03±0.1	9.61±0.1	-27.1±0.3	2.2±0.4	0.840			
30.Mar.13	13.82	0.24	1.48	102	3.05±0.1	9.0±0.4	-27.3±0.3	2.0±0.5	0.755	10.1±0.1	14.5±1.6	0.44
31.Mar.13	11.22	0.23	1.23	101	4.53±0.1	10.3±0.7	-27.2±0.3	2.0±0.4	0.868			
01.Apr.13	9.96	0.22	0.38	97	4.49±0.2	8.9±0.4	-27.3±0.3	1.4±0.4	0.828			
02.Apr.13	6.55	0.23	1.79	88	3.56±0.1	8.5±0.4	-27.2±0.3	2.0±0.4				
03.Apr.13	9.64	0.29	1.33	90	2.91±0.1	9.3±0.1	-26.4±0.3	2.1±0.4	0.838	13.3±0.8	16.4±1.0	0.46
04.Apr.13	4.24	0.35	0.98	83	2.76±0.1	9.4±1.0	-27.6±0.6	2.0±0.4	0.831			
05.Apr.13	9.64	0.34	1.71	95	2.89±0.1	9.29±0.2	-26.1±0.3	2.4±0.4	0.849			
06.Apr.13	7.44	0.31	1.10	92	1.82±0.1	9.9±0.8	-27.3±0.4	2.3±0.5	0.835			
07.Apr.13	12.23	0.29	0.98	93	1.43±0.1	10.0±0.6	-26.9±0.3	2.3±0.6	0.794	5.9±0.5	41.7±1.6	0.46
08.Apr.13	10.43	0.40	2.12	88	1.19±0.1	10.5±1.2	-26.9±0.3	2.1±0.6	0.788			
09.Apr.13	7.60	0.34	0.82	96	1.16±0.1	10.7±0.9	-26.8±0.3	2.0±0.4	0.774			
10.Apr.13	13.85	0.48	1.15	107	1.03±0.1	10.3±0.8	-27.0±0.5	2.7±0.4	0.771			
11.Apr.13	7.74	0.37	0.87	100	1.08±0.1	11.0±1.0	-27.1±0.4	1.9±1.0	0.796			
12.Apr.13	12.17	0.38	0.92	104	0.92±0.1	10.9±1.1	-26.9±0.3	1.7±0.7	0.700	10.6±1.2	44.3±2.7	0.43
13.Apr.13	11.85	0.45	1.15	103	1.22±0.1	10.7±0.9	-27.1±0.3	1.8±0.5	0.780			
14.Apr.13	7.10	0.28	0.70	94	1.20±0.1	10.8±1.2	-26.8±0.3	1.9±0.5	0.785			
15.Apr.13	11.18	0.38	0.87	108	0.80±0.1	10.9±0.7	-26.4±0.3	1.9±0.6	0.657			
16.Apr.13	11.69	0.38	0.95	107	1.06±0.1	10.9±1.1	-26.9±0.3	2.3±0.8	0.784	11.8±0.3	50.1±1.8	0.43
17.Apr.13 09:00	11.64	0.36	0.79	113	1.12±0.1	10.7±0.7	-26.7±0.3	2.1±0.6				
17.Apr.13 11:45	10.19	0.36	1.21	111								
17.Apr.13 14:30	7.77	0.35	0.87	110								
17.Apr.13 17:45	8.24	0.33	0.88	108								
18.Apr.13	7.83	0.34	1.24	84	1.25±0.1	11.1±1.3	-26.8±0.3	2.2±0.8	0.802			
19.Apr.13	11.22	0.38	0.91	108	1.24±0.1	10.8±1.2	-27.5±0.4	2.2±0.4	0.790			
20.Apr.13	12.01	0.65	0.88	111	1.50±0.1	10.9±0.8	-27.6±0.3	1.9±0.4	0.781	15.2±1.7	69±13	0.46
21.Apr.13	6.78	0.36	0.64	105	1.30±0.1	11.1±0.9	-27.7±0.4	2.0±0.6	0.796			
22.Apr.13	10.05	0.25	0.79	105								

Table 2. Concentrations of dissolved nutrients, bulk suspended sedimentary matter (SPM) composition, and mercury concentrations for the 2013 early freshet period. TDHg = total dissolved mercury; THg = total mercury (unfiltered water). For sediment %OC, δ^{13}C, and δ^{15}N data, if calculated uncertainties (1 s.d. of the mean of triplicate analyses) were less than instrumental uncertainty (0.1 for %OC, 0.3‰ for δ^{13}C, and 0.4‰ for δ^{15}N), instrumental uncertainties are shown. For parent IGSN codes, see Table 1.

Date	IGSN	DOC $(\mu mol\ L^{-1})$	a_{254} (m^{-1})	$SUVA_{254}$ $(L\ mgC^{-1}\ m^{-1})$	a_{250}/a_{365}	S_R
28.Jun.2011	GRO000140	265	19.37	2.64	6.45	0.98
08.Jul.2011	GRO000142	282	20.90	2.68	6.38	0.95
15.Jul.2011	GRO000143	364	28.18	2.80	5.92	0.87
19.Jul.2011	GRO000144	339	28.32	3.02	6.06	0.95
29.Jul.2011	GRO000145	335	26.91	2.90	5.91	0.95
26.Sep.2011	GRO000155	193	12.65	2.37	6.60	1.11
14.Oct.2011	GRO000156	242	17.43	2.61	6.03	1.02
25.Oct.2011	GRO000157	256	16.69	2.36	6.89	0.97
26.Oct.2011	GRO000158	250	16.87	2.44	6.58	1.04
31.Oct.2011	GRO000159	275	17.15	2.25	7.91	0.86
15.Nov.2011	GRO000160	318	18.28	2.08	8.12	0.87
28.Nov.2011	GRO000161	254	19.88	2.83	5.98	0.92
11.Jan.2012	GRO000163	237	22.52	3.43	6.38	0.93
10.Feb.2012	GRO000165	217	20.13	3.35	6.53	1.01
18.May.2012	GRO000168	352	35.67	3.67	5.50	0.92
13.Jun.2012	GRO000220	299	28.89	3.49	5.84	0.89
22.Jun.2012	GRO000207	280	26.92	3.47	5.78	0.88
29.Jun.2012	GRO000169	207	19.26	3.37	6.45	0.94
05.Jul.2012	GRO000170	200	18.28	3.30	6.54	0.96
13.Jul.2012	GRO000171	176	16.33	3.35	6.56	0.98
13.Jul.2012	GRO000171	176	16.63	3.42	6.75	0.99
27.Jul.2012	GRO000222		14.87		6.15	1.10
27.Jul.2012	GRO000222		13.85		6.67	0.90
17.Aug.2012	GRO000239		13.34		7.05	1.11
07.Sep.2012	GRO000172		14.48		6.46	1.17
21.Sep.2012	GRO000221		14.97		6.64	1.11
05.Oct.2012	GRO000223		13.33		6.67	1.11
18.Oct.2012	GRO000173		17.40		5.72	1.00
12.Jan.2013	GRO000218		23.58		5.49	0.85
02.Feb.2013	GRO000174	266	21.02	2.85	5.82	0.92
09.Feb.2013	GRO000175	248	22.55	3.28	5.46	0.89
16.Mar.2013	GRO000176	242	23.97	3.59	5.21	0.86
23.Mar.2013	GRO000177	209	17.69	3.06	5.88	0.92
27.Mar.2013	GRO000921	240	17.02	2.56	5.98	1.04
28.Mar.2013	GRO000922	206	18.76	3.29	5.80	0.94
29.Mar.2013	GRO000923	198	19.56	3.57	5.62	0.96
29.Mar.2013	GRO000923	198				
30.Mar.2013	GRO000178	205	18.66	3.29	5.73	0.99
30.Mar.2013	GRO000178	205				
31.Mar.2013	GRO000924	198	18.47	3.37	5.72	0.98
31.Mar.2013	GRO000924	198				
01.Apr.2013	GRO000925	205	17.70	3.13	5.98	0.98
02.Apr.2013	GRO000926	189	20.60	3.94	5.34	1.07
03.Apr.2013	GRO000179	199	19.92	3.62	5.58	1.04
04.Apr.2013	GRO000927	205	25.96	4.58	5.49	1.11
05.Apr.2013	GRO000928	217	21.23	3.54	5.51	0.99
05.Apr.2013	GRO000928	217				
06.Apr.2013	GRO000929	234	25.40	3.93	5.38	1.02

Date	IGSN					
07.Apr.2013	GRO000180	266	32.65	4.44	5.30	1.06
08.Apr.2013	GRO000930	286	29.12	3.68	5.48	0.89
09.Apr.2013	GRO000931	343	34.35	3.62	5.52	0.88
10.Apr.2013	GRO000932	415	41.05	3.58	5.64	0.87
11.Apr.2013	GRO000933	413	52.53	4.60	4.94	0.99
12.Apr.2013	GRO000181	419	47.00	4.05	5.18	0.93
13.Apr.2013	GRO000934	435	51.81	4.31	5.08	0.94
14.Apr.2013	GRO000935	445	44.52	3.62	5.42	0.86
15.Apr.2013	GRO000936	458	49.14	3.88	5.28	0.90
16.Apr.2013	GRO000182	558	49.82	3.23	5.48	0.85
17.Apr.2013	GRO000937	526	54.12	3.72	5.36	0.84
17.Apr.2013	GRO000938	522	52.39	3.63	5.44	0.83
17.Apr.2013	GRO000939	506	53.43	3.81	5.39	0.84
17.Apr.2013	GRO000940	505	52.23	3.74	5.41	0.83
18.Apr.2013	GRO000941	497	48.68	3.54	5.51	0.83
19.Apr.2013	GRO000942	493	51.40	3.77	5.40	0.83
20.Apr.2013	GRO000183	492	49.91	3.66	5.27	0.96
21.Apr.2013	GRO000943	469	48.29	3.73	5.30	0.90
22.Apr.2013	GRO000945	477	51.46	3.90	5.31	0.85
01.May.2013	GRO000184		79.94		5.46	0.81
17.May.2013	GRO000946		38.33		5.70	0.84
07.Jun.2013	GRO000949		25.20		5.87	0.91
22.Jun.2013	GRO000947		20.10		5.92	0.95
24.Jul.2013	GRO000948		15.37		6.56	1.10
24.Jul.2013	GRO000948		15.16		6.54	1.10
24.Jul.2013	GRO000948		14.14		6.71	1.05
20.Sep.2013	GRO000950		9.26		7.11	1.07

Table 3. Two-year record of DOC concentration and optical properties of the Fraser River main stem at Fort Langley. IGSN codes refer to International GeoSample Numbers in the System for Earth Sample Registration (Sesar) database; sample metadata can be accessed at www.geosamples.org.

	Environment Canada record at Hope (1998-2013)	This study (2011-2013)
DOC flux (mol C a^{-1})	$2.74 \pm 0.38 \times 10^{10}$	$2.8 \pm 1.0 \times 10^{10}$
DOC yield (mol C km^{-2} a^{-1})	1.20×10^5	1.2×10^5
Discharge-weighted average DOC concentration (μmol L^{-1})	277 ± 14	270 ± 71

Table 4. Discharge-weighted fluxes and concentrations of DOC in the Fraser River. Environment

Canada data were accessed online at http://aquatic.pyr.ec.gc.ca.

	S_R	a_{250}/a_{365}
shallow soil end-member	0.81	4.94
deep soil end-member	1.17	8.12
shallow soil DOC fraction	0.611 ± 0.018	0.638 ± 0.014
deep soil DOC fraction	0.459 ± 0.036	0.364 ± 0.015

Table 5. Soil DOC sources LoadEst results. Uncertainties represent 1 s.d. of the average for the three years of the record (2011 – 2013).
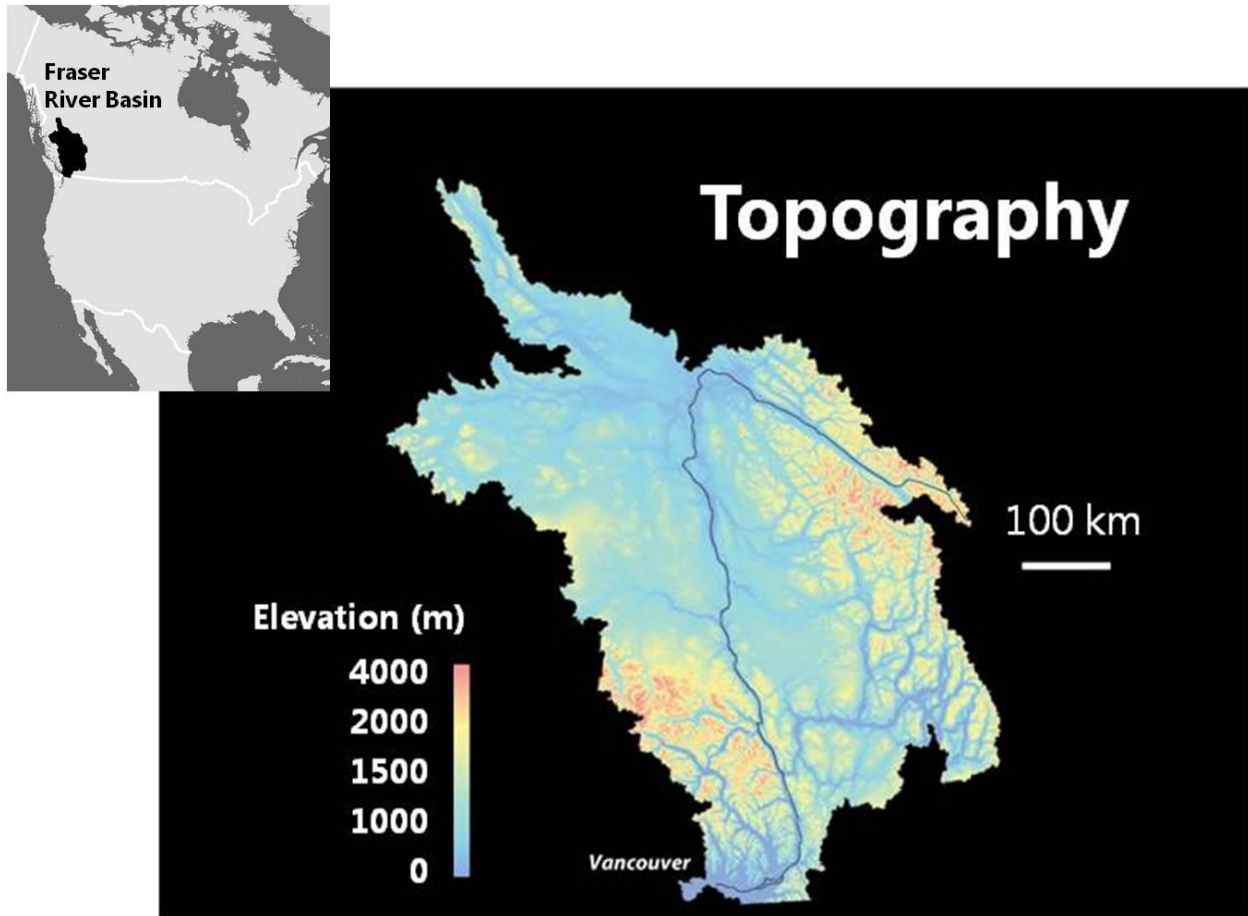
Figure 1. Topography of the Fraser River Basin features the Coast Range in the southwestern portion of the basin and the Cariboo and Rocky Mountains in the eastern portion (map courtesy of S. Adam Soule, WHOI). Inset map of North America highlighting the Fraser River Basin provided by Gregory Fiske (Woods Hole Research Center).
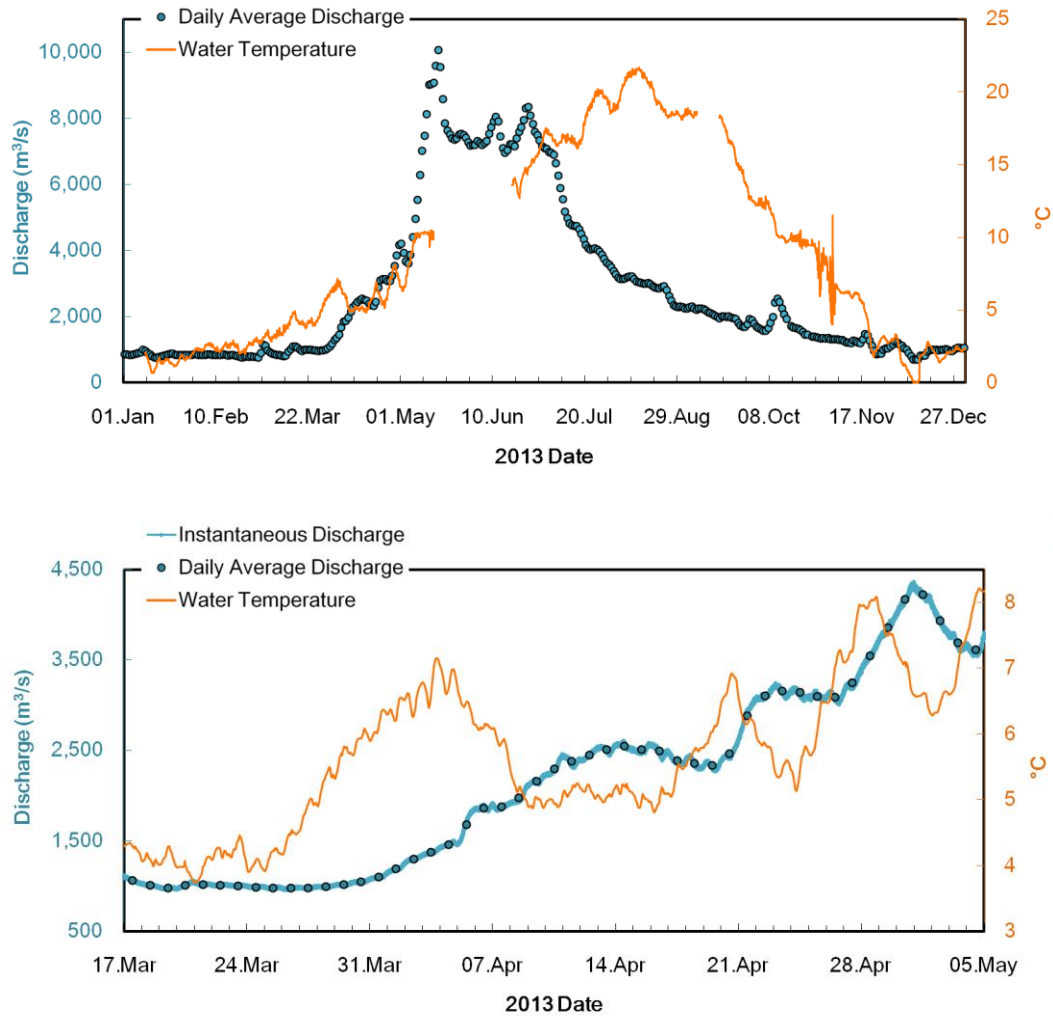
Figure 2. Water discharge and temperature during the study year 2013 from Environment Canada real-time records of the Fraser River at Hope. "Instantaneous" discharge is derived from gauge height measurements at 5-minute frequency; water temperature measurements are hourly. (A) Full year, showing the relationship between seasonal warming and water discharge; (B) Inset of the early freshet period, when daily fluctuations in water temperature create diurnal discharge pulses.
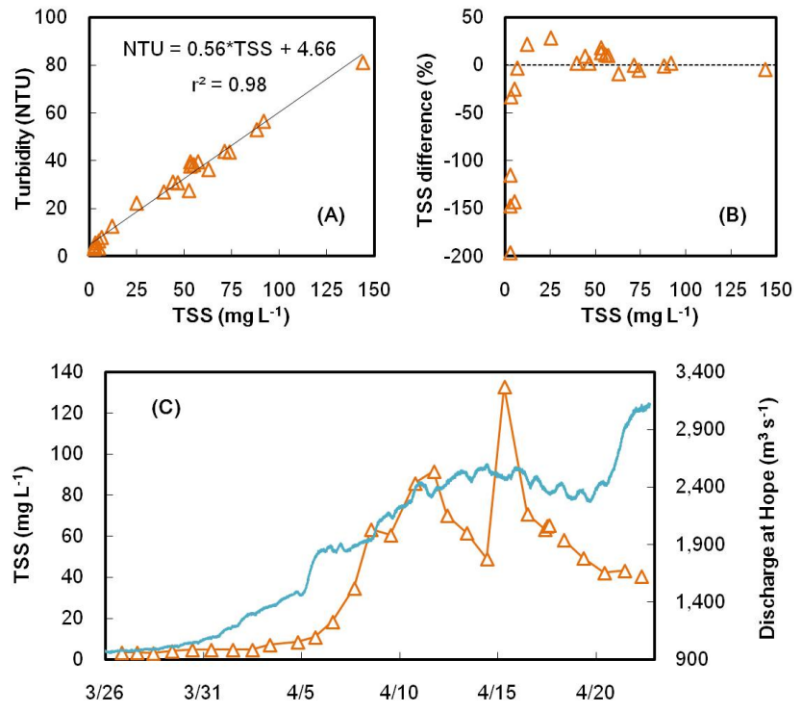
Figure 3. (A) Measured suspended sediment concentration (SS) correlated strongly with turbidity (measured with a nephelometer). (B) The difference between the two measurements was most pronounced at very low sediment concentrations. Turbidity values were considered more reliable as sample processing for measured TSS values likely biases results due to loss of material. (C) Suspended sediment concentrations increased rapidly during the early freshet period.
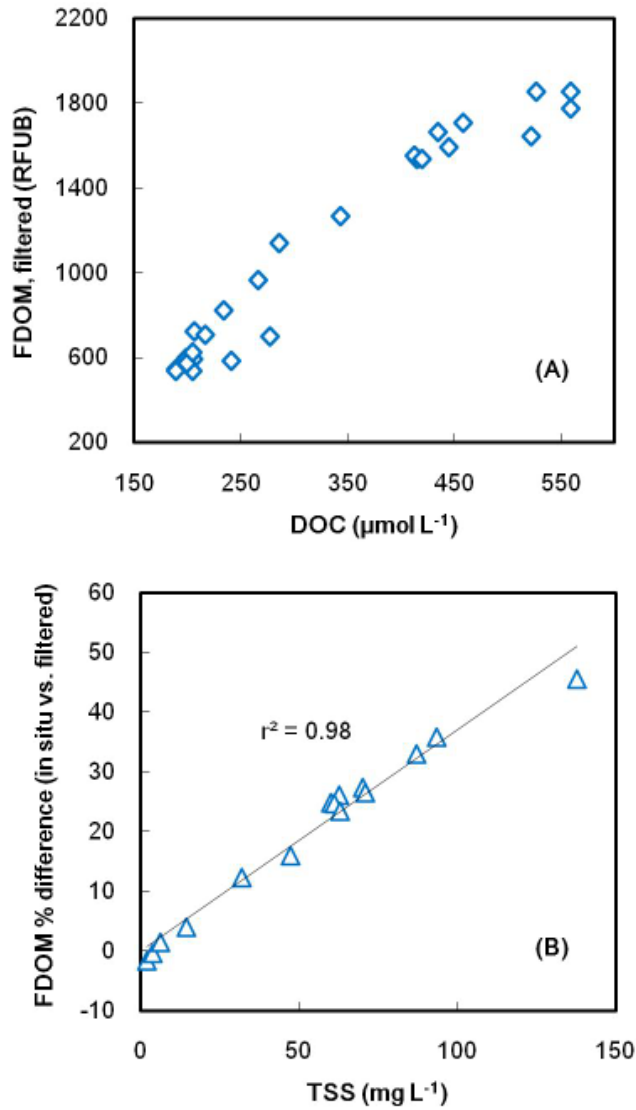
Figure 4. (A) Filtered FDOM (fluorescent dissolved organic matter) was positively correlated with DOC concentration. (B) The difference between filtered and *in situ* FDOM values was strongly dependent on suspended sediment concentration (TSS).
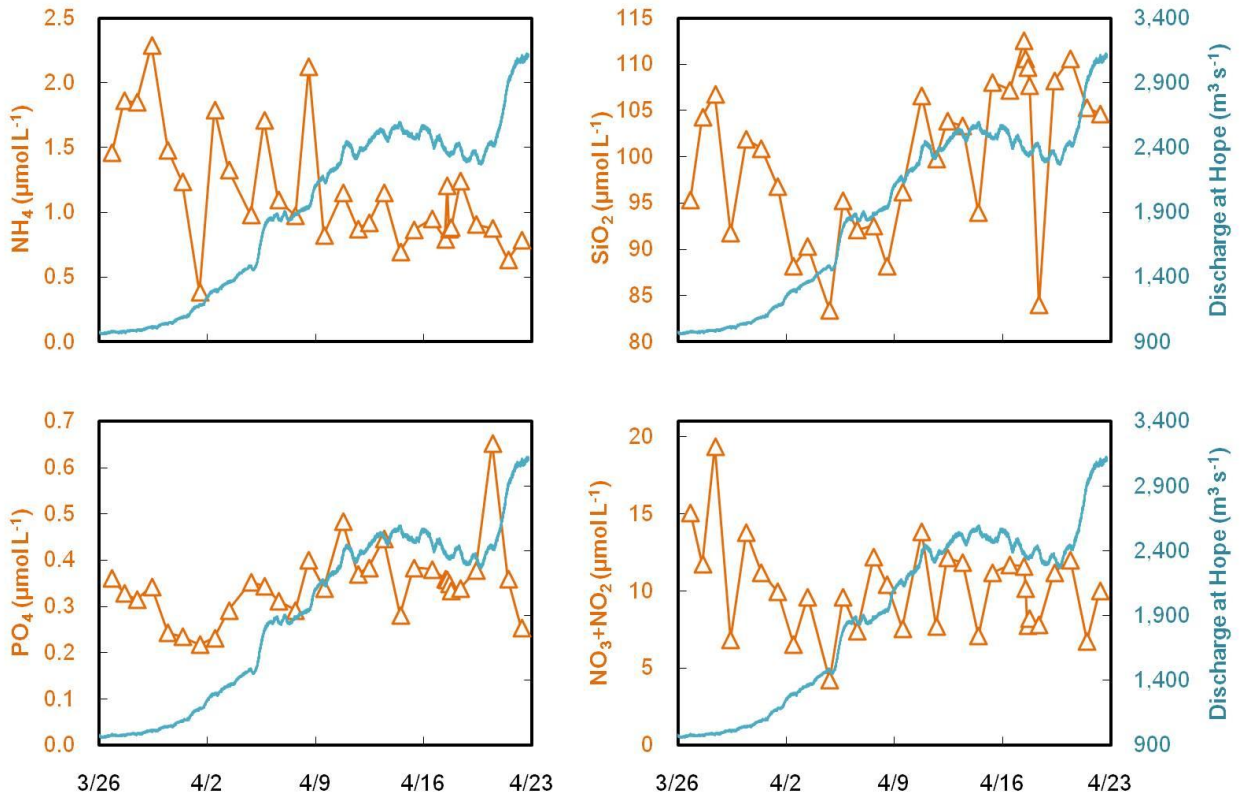
Figure 5. Concentrations of nutrients in the Fraser River during the early freshet in 2013 showed significant day-to-day variability.
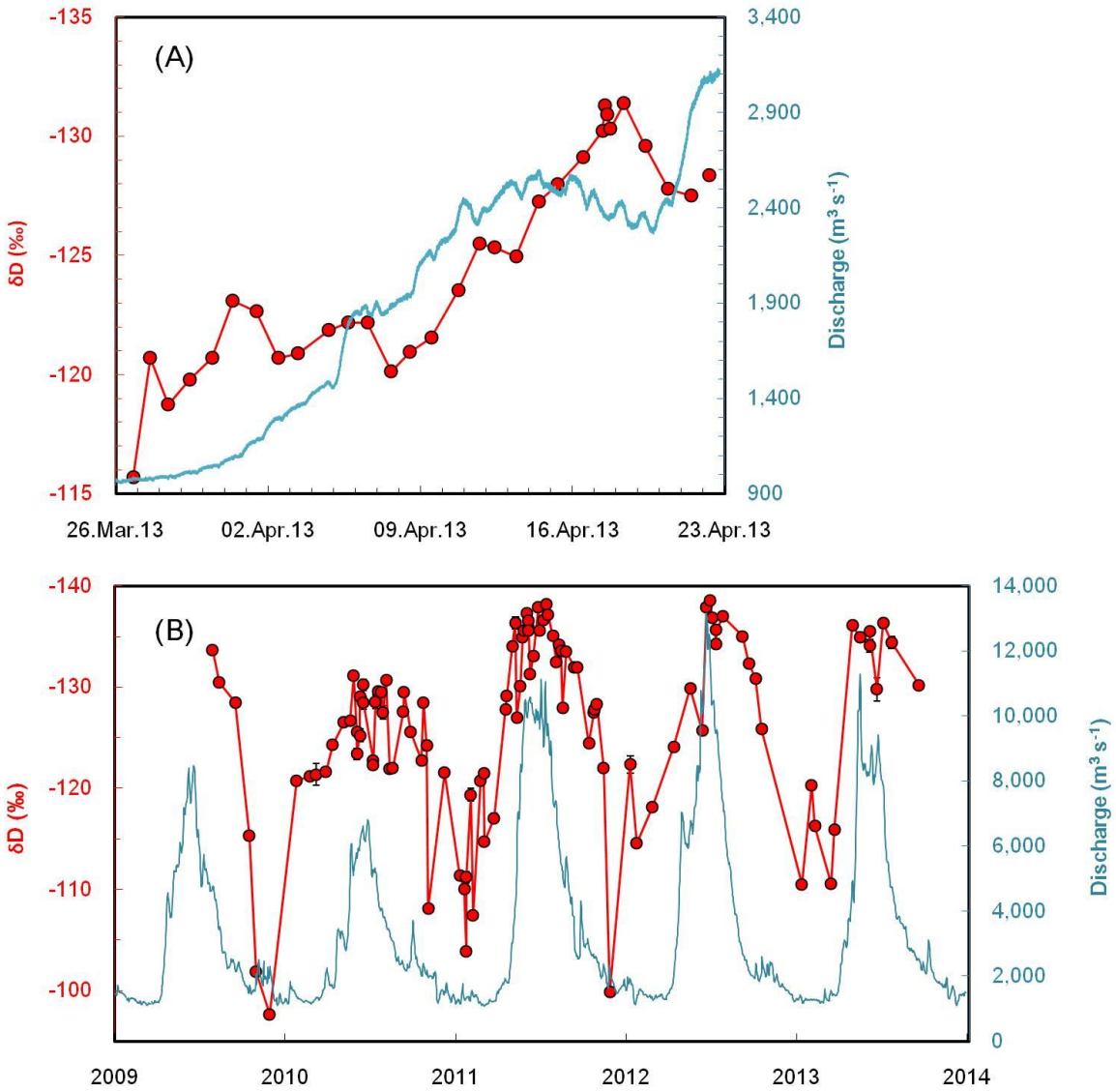
Figure 6. (A) During the early freshet period (2013), the stable isotope composition of Fraser River water becomes lighter as discharge increases due to a shift from precipitation and groundwater sources towards snowmelt-dominated runoff sources. (B) In the context of the 4-year record of δD in the Fraser River (total variability ~40 ‰), the change observed during the 1-month period of the early freshet (~16 ‰) is very rapid.
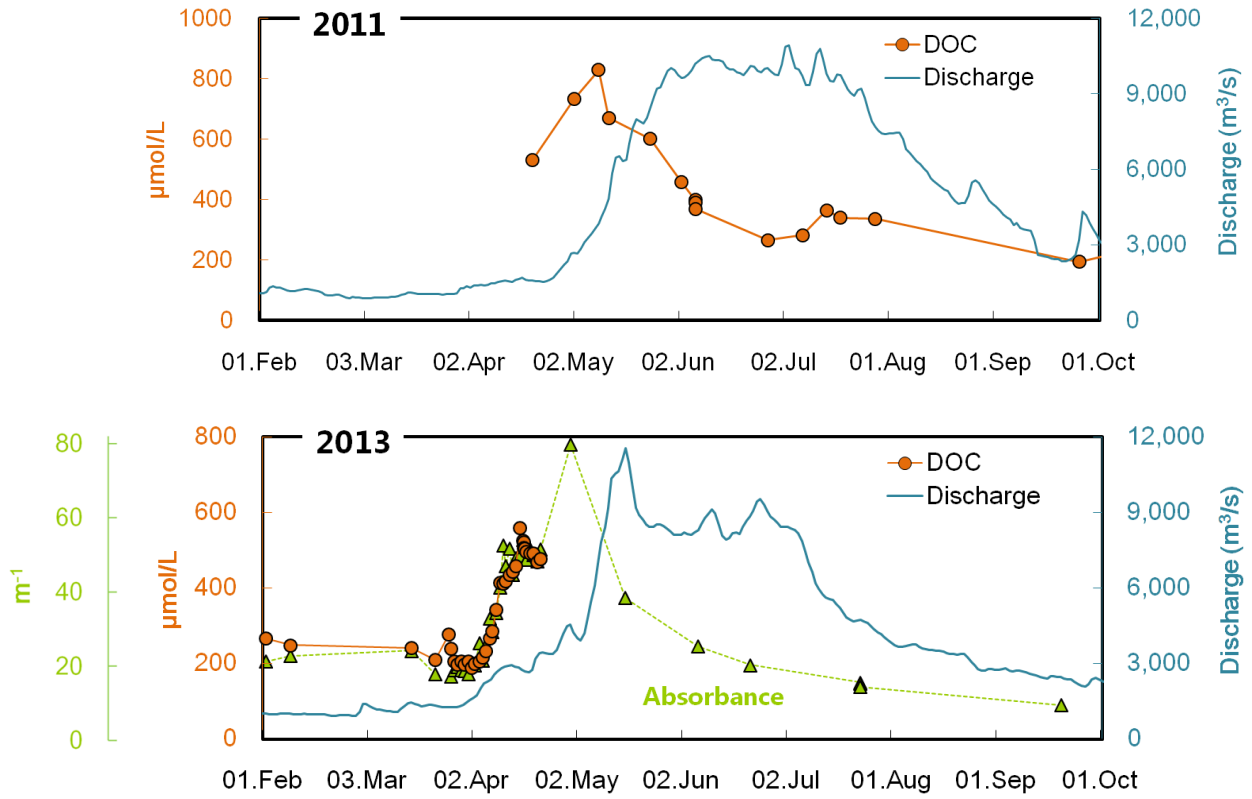
Figure 7. Concentrations of dissolved organic carbon (DOC) peak during the early stages of the spring freshet and decrease over the course of the summer.
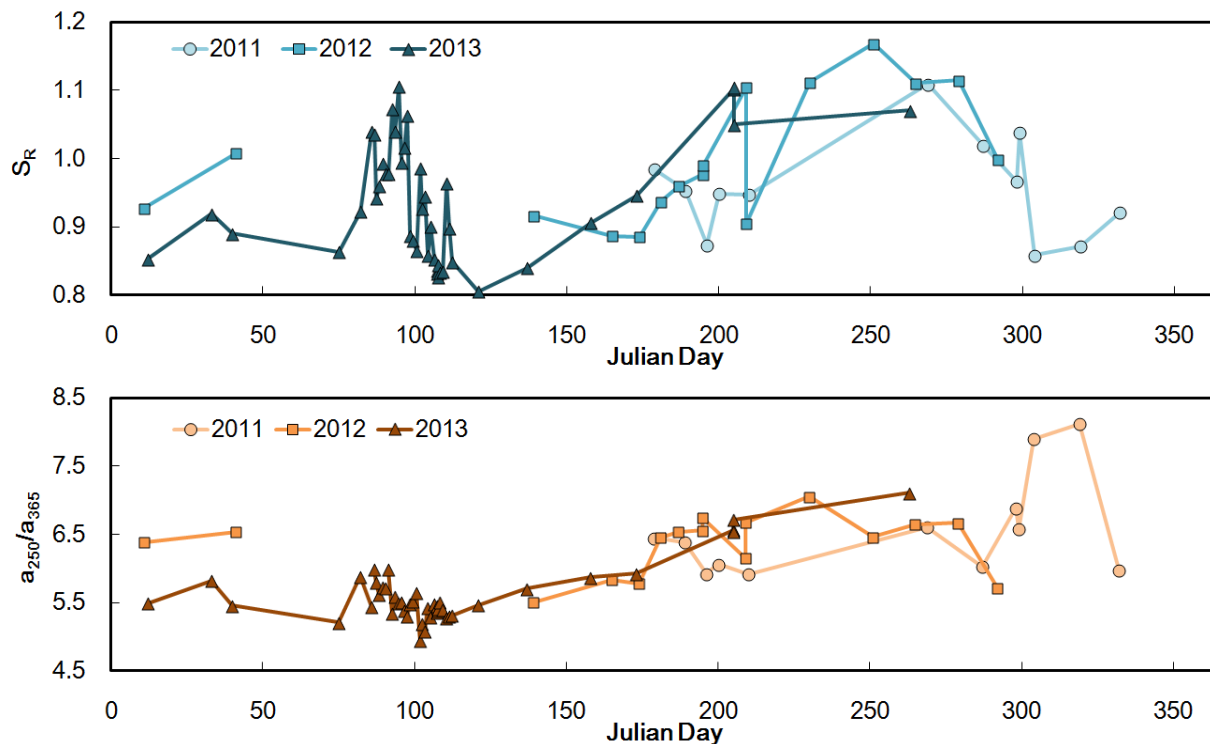
Figure 8. Optical properties of DOC show rapid changes in DOC composition during early freshet DOC pulse, shifting towards more aromatic, high molecular weight, vascular plant-like material. A more gradual return to lower molecular weight, less aromatic composition follows throughout the summer. A second cycle occurs in late winter, likely associated with soil flushing during fall rain events.
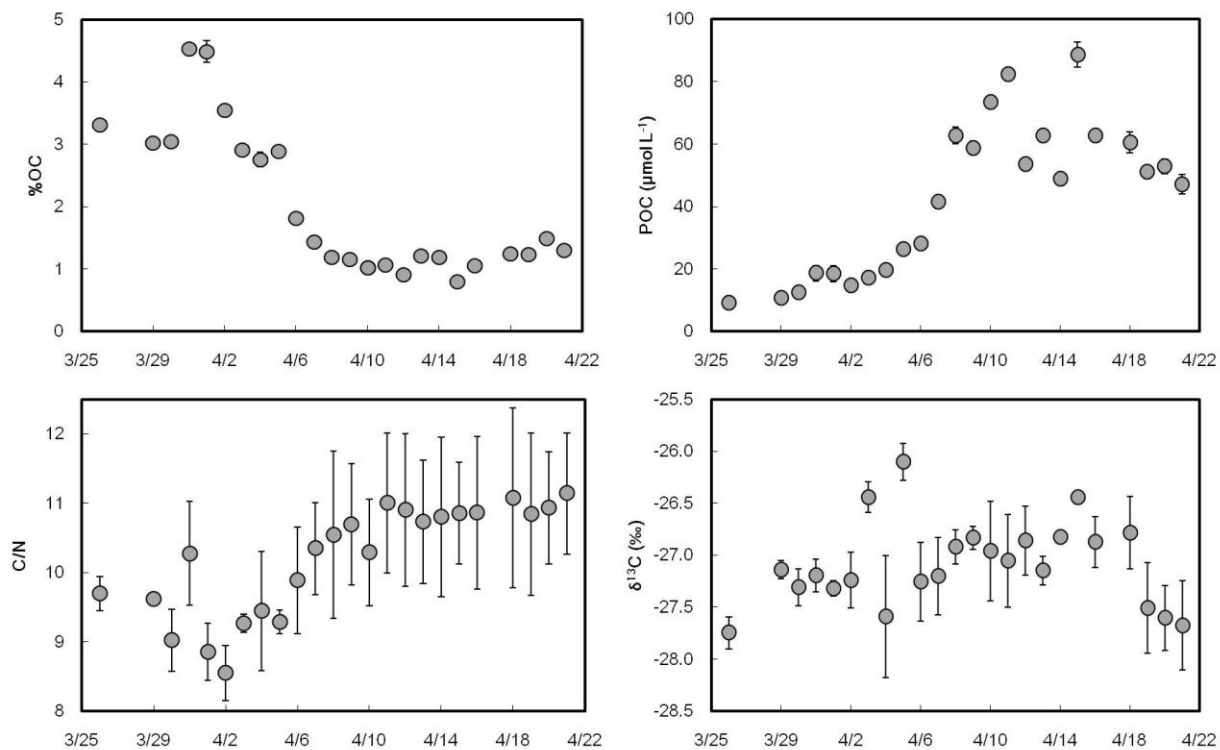
Figure 9. The abundance and composition of POC shifted during the early freshet period towards relatively lower %OC (but higher POC concentration due to increased sediment concentration) and higher C:N. Error bars represent 1 s.d. of triplicate measurements.
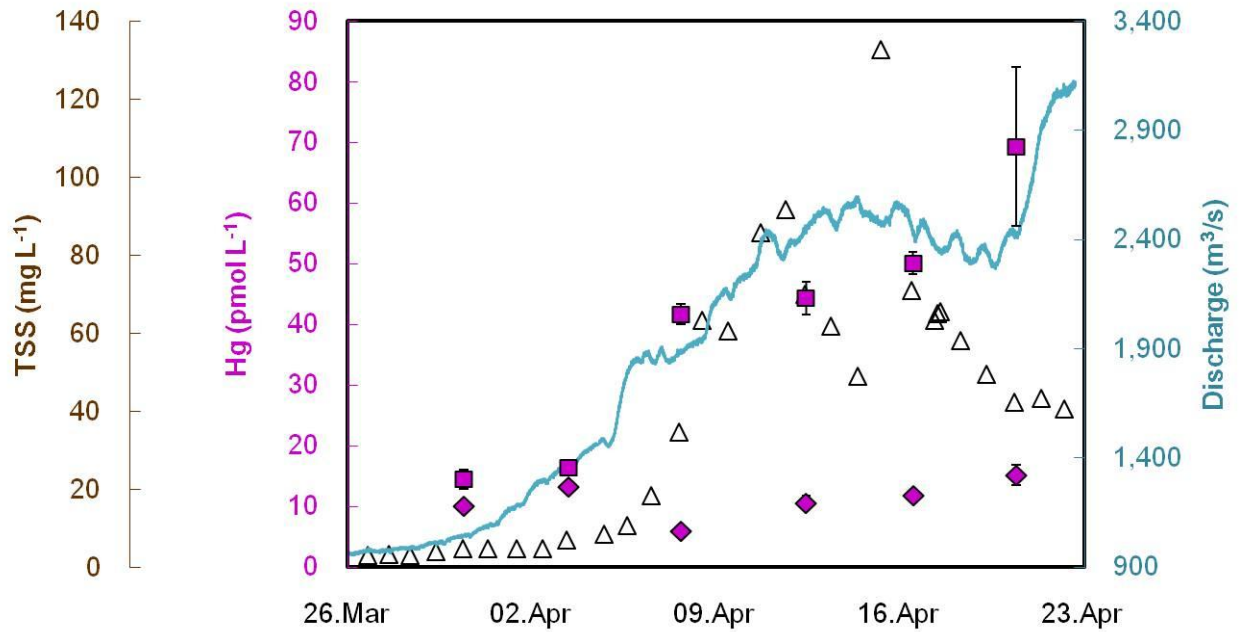
Figure 10. Total mercury concentrations in filtered (diamonds) and unfiltered (squares) water samples during the 2013 early freshet period. Error bars represent 1 s.d. of repeated measurements. Suspended sediment concentration (TSS) shown in triangles.
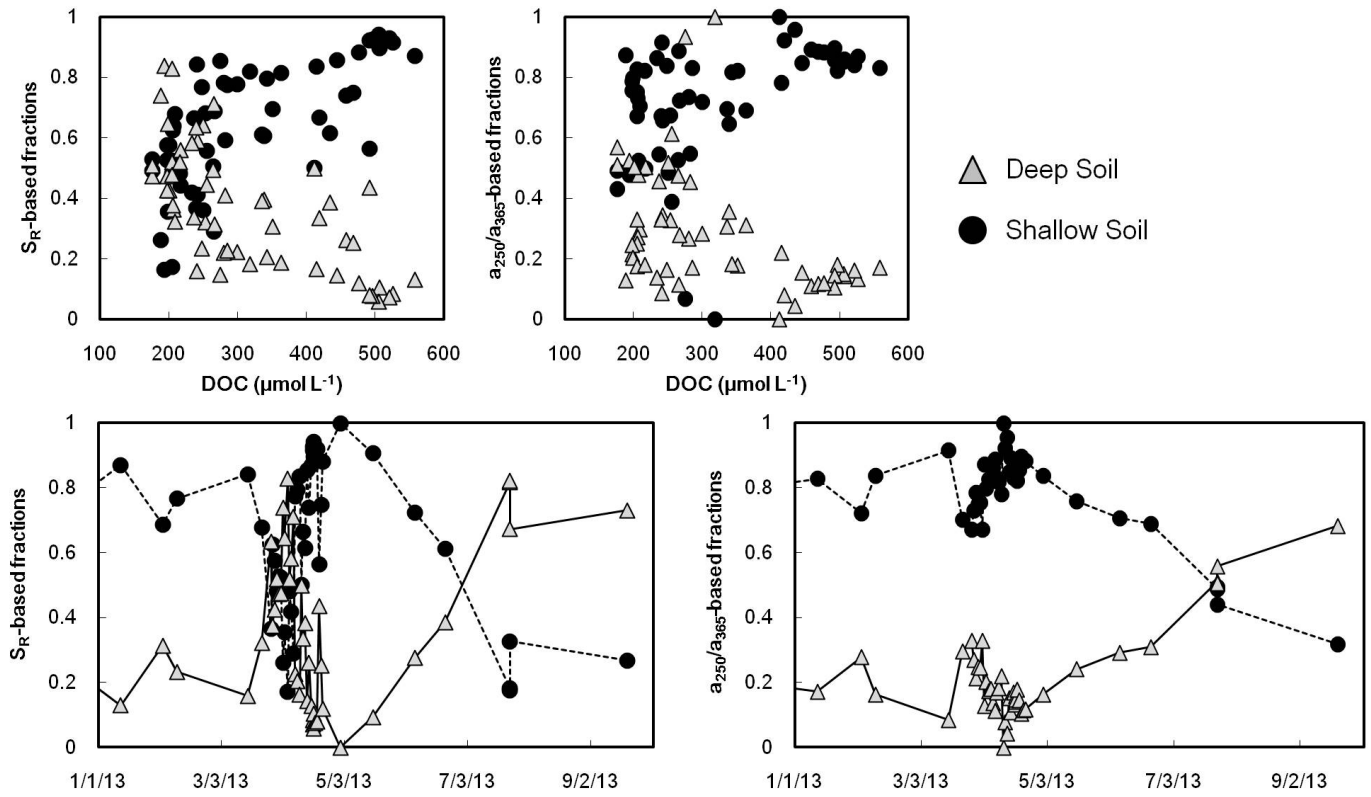
Figure 11. The contributions of deep and shallow soil DOC to total Fraser DOC were estimated based on the observed maximum and minimum values of DOC optical properties (spectral slope ratio, S_R, and absorbance ratio, a_{250}/a_{365}).
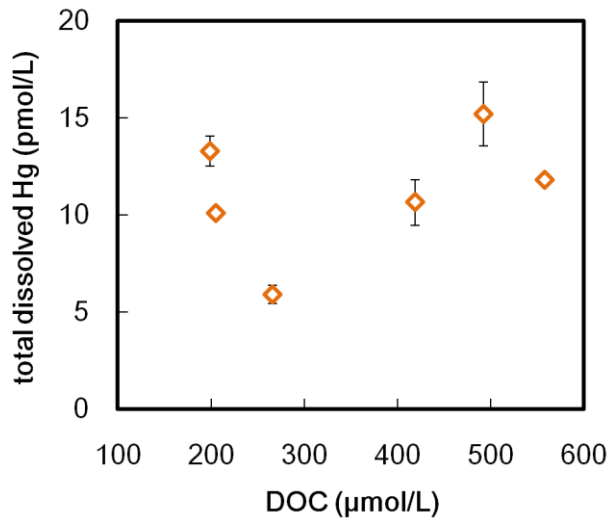
Figure 12. The relationship between total dissolved mercury (TDHg) and DOC concentrations is
not as strong as has been observed in other systems (Dittman et al., 2010; Schuster et al., 2011;
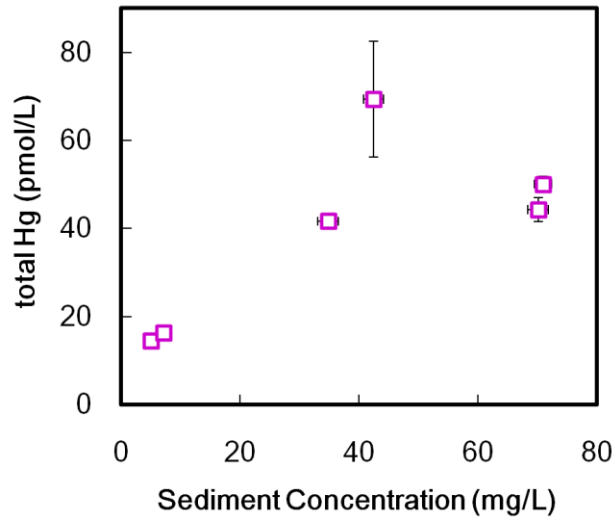Burns et al., 2012b).

Figure 13. THg concentration is positively correlated with suspended sediment concentration.
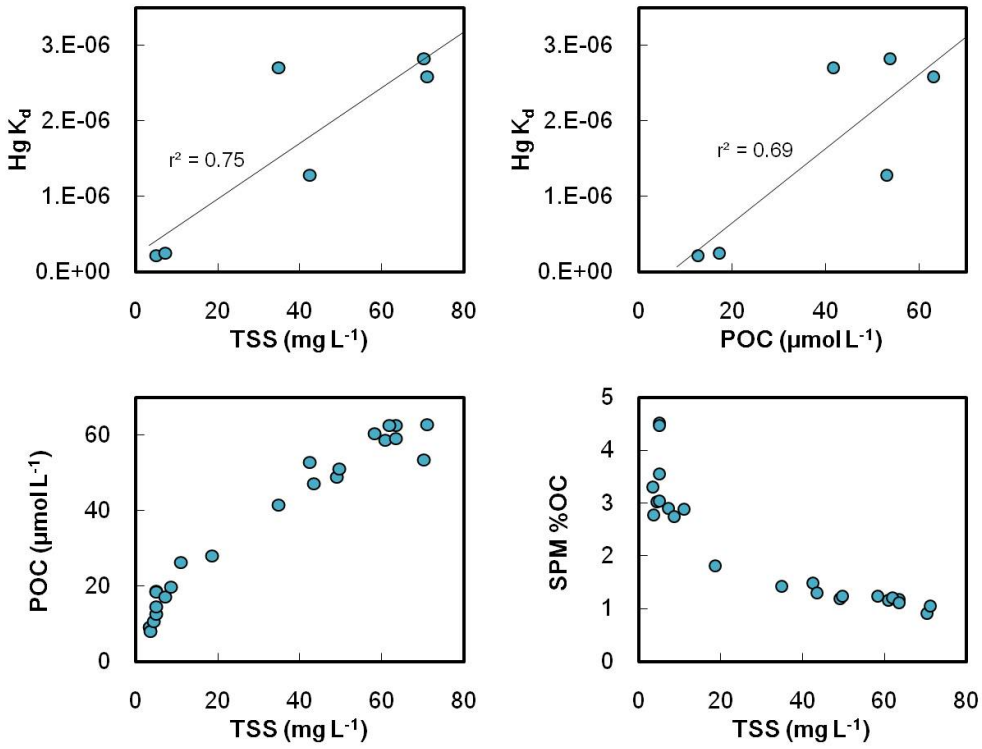
Figure 14. The distribution coefficient (K_d) of Hg is strongly dependent on suspended sediment and POC concentration (top panels), which are in turn related to each other (bottom panels).

References

Aiken G. R., Hsu-Kim H., and Ryan J. N. (2011) Influence of dissolved organic matter on the environmental fate of metals, nanoparticles, and colloids. *Environ. Sci. Technol.* **45**, 3196-3201. doi:10.1021/es103992s.

Amos H. M., Jacob D. J., Kocman D., Horowitz H. M., Zhang Y., Dutkiewicz S., Horvat M., Corbitt E. S., Krabbenhoft D. P., and Sunderland E. M. (2014) Global biogeochemical implications of mercury discharges from rivers and sediment burial. *Environ. Sci. Technol.* doi:10.1021/es502134t.

Bianchi T. S., Garcia-Tigreros F., Yvon-Lewis S. A., Shields M., Mills H. J., Butman D., Osburn C., Raymond P., Shank G. C., DiMarco S. F., Walker N., Reese B. K., Mullins-Perry R., Quigg A., Aiken G. R., and Grossman E. L. (2013) Enhanced transfer of terrestrially derived carbon to the atmosphere in a flooding event. *Geophys. Res. Lett.* **40**, 116-122. doi:10.1029/2012gl054145.

Burns D. A., Aiken G. R., Bradley P. M., Journey C. A., and Schelker J. (2012a) Specific ultra-violet absorbance as an indicator of mercury sources in an Adirondack River basin. *Biogeochemistry* **113**, 451-466. doi:10.1007/s10533-012-9773-5.

Burns D. A., Riva-Murray K., Bradley P. M., Aiken G. R., and Brigham M. E. (2012b) Landscape controls on total and methyl Hg in the upper Hudson River basin, New York, USA. *J. Geophys. Res.* **117**. doi:10.1029/2011jg001812.

Cameron E. M. (1996) Hydrogeochemistry of the Fraser River, British Columbia: seasonal variation in major and minor components. *J. Hydrol.* **182**, 209-225.

Carey S. K. (2003) Dissolved organic carbon fluxes in a discontinuous permafrost subarctic alpine catchment. *Permafrost Periglacial Processes* **14**, 161-171. doi:10.1002/ppp.444.

Cohen Commission (2012) Chapter 2: Recommendations. *The Cohen Commission of Inquiry into the Decline of Sockeye Salmon in the Fraser River*. 64 p.

Del Vecchio R. and Blough N. V. (2002) Photobleaching of chromophoric dissolved organic matter in natural waters: kinetics and modeling. *Mar. Chem* **78**, 231-253.

Déry S. J., Hernández-Henríquez M. A., Owens P. N., Parkes M. W., and Petticrew E. L. (2012) A century of hydrological variability and trends in the Fraser River Basin. *Environ. Res. Lett.* **7**, 024019. doi:10.1088/1748-9326/7/2/024019.

Dittman J. A., Shanley J. B., Driscoll C. T., Aiken G. R., Chalmers A. T., and Towse J. E. (2009) Ultraviolet absorbance as a proxy for total dissolved mercury in streams. *Environ. Pollut.* **157**, 1953-1956. doi:10.1016/j.envpol.2009.01.031.

Dittman J. A., Shanley J. B., Driscoll C. T., Aiken G. R., Chalmers A. T., Towse J. E., and Selvendiran P. (2010) Mercury dynamics in relation to dissolved organic carbon concentration and quality during high flow events in three northeastern U.S. streams. *Water Resour. Res.* **46**. doi:10.1029/2009wr008351.

Downing B. D., Pellerin B. A., Bergamaschi B. A., Saraceno J. F., and Kraus T. E. C. (2012) Seeing the light: The effects of particles, dissolved materials, and temperature on in situ measurements of DOM fluorescence in rivers and streams. *Limnol. Oceanogr.: Methods* **10**, 767-775. doi:10.4319/lom.2012.10.767.

Fellman J. B., Hood E., Edwards R. T., and D'Amore D. V. (2009) Changes in the concentration, biodegradability, and fluorescent properties of dissolved organic matter during stormflows in coastal temperate watersheds. *J. Geophys. Res.* **114**. doi:10.1029/2008jg000790.

Fellman J. B., Spencer R. G. M., Hernes P. J., Edwards R. T., D'Amore D. V., and Hood E. (2010) The impact of glacier runoff on the biodegradability and biochemical composition of terrigenous dissolved organic matter in near-shore marine ecosystems. *Mar. Chem* **121**, 112-122. doi:10.1016/j.marchem.2010.03.009.

Gallagher L., Macdonald R. W., and Paton D. W. (2003) The historical record of metals in sediments from six lakes in the Fraser River Basin, British Columbia. *Water, Air, Soil Pollut.* **152**, 257-278.

Gangloff S., Stille P., Pierret M.-C., Weber T., and Chabaux F. (2014) Characterization and evolution of dissolved organic matter in acidic forest soil and its impact on the mobility of major and trace elements (case of the Strengbach watershed). *Geochim. Cosmochim. Acta* **130**, 21-41. doi:10.1016/j.gca.2013.12.033.

Gerbig C. A., Ryan J. N., and Aiken G. R. (2011) The effects of dissolved organic matter on mercury biogeochemistry. In *Environmental Chemistry and Toxicology of Mercury* (eds. G. Liu, Y. Cai, and N. O'Driscoll). John Wiley & Sons, Inc. 259-292.

Haitzer M., Aiken G. R., and Ryan J. N. (2002) Binding of mercury(II) to dissolved organic matter: The role of the mercury-to-DOM concentration ratio. *Environ. Sci. Technol.* **36**, 3564-3570. doi:10.1021/es025699i.

Haitzer M., Aiken G. R., and Ryan J. N. (2003) Binding of mercury(II) to aquatic humic substances: Influence of pH and source of humic substances. *Environ. Sci. Technol.* **37**, 2436-2441. doi:10.1021/es026291o.

Hales W. J. (2000) Impact of human activity on deltaic sedimentation, marshes of the Fraser River delta, British Columbia, University of British Columbia.

Hammerschmidt C. R., Bowman K. L., Tabatchnick M. D., and Lamborg C. H. (2011) Storage bottle material and cleaning for determination of total mercury in seawater. *Limnol. Oceanogr.: Methods* **9**, 426-431. doi:10.4319/lom.2011.9.426.

Helms J. R., Stubbins A., Ritchie J. D., Minor E. C., Kieber D. J., and Mopper K. (2008) Absorption spectral slopes and slope ratios as indicators of molecular weight, source, and photobleaching of chromophoric dissolved organic matter. *Limnol. Oceanogr.* **53**, 955-969.

Holmes R. M., McClelland J. W., Peterson B. J., Tank S. E., Bulygina E., Eglinton T. I., Gordeev V. V., Gurtovaya T. Y., Raymond P. A., Repeta D. J., Staples R., Striegl R. G., Zhulidov A. V., and Zimov S. A. (2011) Seasonal and annual fluxes of nutrients and organic matter from large rivers to the Arctic Ocean and surrounding seas. *Estuaries Coasts* **35**, 369-382. doi:10.1007/s12237-011-9386-6.

Holmes R. M., McClelland J. W., Raymond P. A., Frazer B. B., Peterson B. J., and Stieglitz M. (2008) Lability of DOC transported by Alaskan rivers to the Arctic Ocean. *Geophys. Res. Lett.* **35**. doi:10.1029/2007gl032837.

Hope D., Billett M. F., and Cresser M. S. (1994) A review of the export of carbon in river water: Fluxes and processes. *Environ. Pollut.* **84**, 301-324.

Jaffé R., Ding Y., Niggemann J., Vähätalo A. V., Stubbins A., Spencer R. G. M., Campbell J., and Dittmar T. (2013) Global charcoal mobilization from soils via dissolution and riverine transport to the oceans. *Science* **340**, 345-347. doi:10.1126/science.1231476.

Jung B.-J., Lee H.-J., Jeong J.-J., Owen J., Kim B., Meusburger K., Alewell C., Gebauer G., Shope C., and Park J.-H. (2012) Storm pulses and varying sources of hydrologic carbon export from a mountainous watershed. *J. Hydrol.* **440-441**, 90-101. doi:10.1016/j.jhydrol.2012.03.030.

Keil R., Salemme K., Forrest B., Neibauer J., and Logsdon M. (2011) Differential presence of anthropogenic compounds dissolved in the marine waters of Puget Sound, WA and Barkley Sound, BC. *Mar. Pollut. Bull.* **62**, 2404-2411. doi:10.1016/j.marpolbul.2011.08.029.

Laraque A., Castellanos B., Steiger J., Lòpez J. L., Pandi A., Rodriguez M., Rosales J., Adèle G., Perez J., and Lagane C. (2013) A comparison of the suspended and dissolved matter dynamics of two large inter-tropical rivers draining into the Atlantic Ocean: the Congo and the Orinoco. *Hydrol. Processes* **27**, 2153-2170. doi:10.1002/hyp.9776.

Liu J., Chen J. M., Cihlar J., and Chen W. (2002) Net primary productivity mapped for Canada at 1-km resolution. *Global Ecol. Biogeogr.* **11**, 115-129. doi:10.1046/j.1466-822X.2002.00278.x.

Lloret E., Dessert C., Pastor L., Lajeunesse E., Crispi O., Gaillardet J., and Benedetti M. F. (2013) Dynamic of particulate and dissolved organic carbon in small volcanic mountainous tropical watersheds. *Chem. Geol.* **351**, 229-244. doi:10.1016/j.chemgeo.2013.05.023.

Ludwig W., Probst J.-L., and Kempe S. (1996) Predicting the oceanic input of organic carbon by continental erosion. *Global Biogeochem. Cycles* **10**, 23-41.

MacDonald D., Sinclair J., Crawford M., Prencipe H., and Meneghetti M. (2011) Technical Report 2: Potential effects of contaminants on Fraser River sockeye salmon. *The Cohen Commission of Inquiry into the Decline of Sockeye Salmon in the Fraser River*. Nanaimo, BC. 603 p.

Mann P. J., Davydova A., Zimov N., Spencer R. G. M., Davydov S., Bulygina E., Zimov S., and Holmes R. M. (2012) Controls on the composition and lability of dissolved organic matter in Siberia's Kolyma River basin. *J. Geophys. Res.* **117**. doi:10.1029/2011jg001798.

Mayer L. M. (1994) Relationships between mineral surfaces and organic carbon concentrations in soils and sediments. *Chem. Geol.* **114**, 347-363.

Mills R. T. E., Tipping E., Bryant C. L., and Emmett B. A. (2014) Long-term organic carbon turnover rates in natural and semi-natural topsoils. *Biogeochemistry* **118**, 257-272. doi:10.1007/s10533-013-9928-z.

Morrison J., Quick M. C., and Foreman M. G. G. (2002) Climate change in the Fraser River watershed: flow and temperature projections. *J. Hydrol.* **263**, 230-244.

Neff J. C., Finlay J. C., Zimov S. A., Davydov S. P., Carrasco J. J., Schuur E. A. G., and Davydova A. I. (2006) Seasonal changes in the age and structure of dissolved organic carbon in Siberian rivers and streams. *Geophys. Res. Lett.* **33**. doi:10.1029/2006gl028222.

Nelson A. D. and Church M. (2012) Placer mining along the Fraser River, British Columbia: The geomorphic impact. *Geol. Soc. Am. Bull.* **124**, 1212-1228. doi:10.1130/b30575.1.

O'Donnell J. A., Aiken G. R., Kane E. S., and Jones J. B. (2010) Source water controls on the character and origin of dissolved organic matter in streams of the Yukon River basin, Alaska. *J. Geophys. Res.* **115**. doi:10.1029/2009jg001153.

Patterson C. C. and Settle D. M. (1976) The reduction of orders of magnitude errors in lead analyses of biological material and natural waters by evaluating and controlling the extent and sources of industrial lead contamination introduced during sample collection, handling and analysis. In *Accuracy in Trace Analysis: Sampling, Sample Handling, and Analysis* (ed. P. D. LaFleur). U.S. National Bureau of Standards Special Publication 422, Washington, D.C. 321-351.

Pereira R., Isabella Bovolo C., Spencer R. G. M., Hernes P. J., Tipping E., Vieth-Hillebrand A., Pedentchouk N., Chappell N. A., Parkin G., and Wagner T. (2014) Mobilization of optically invisible dissolved organic matter in response to rainstorm events in a tropical forest headwater river. *Geophys. Res. Lett.* **41**, 1202-1208. doi:10.1002/2013gl058658.

Peuravuori J. and Pihlaja K. (1997) Molecular size distribution and spectroscopic properties of aquatic humic substances. *Anal. Chim. Acta* **337**, 133-149.

Raymond P. A., McClelland J. W., Holmes R. M., Zhulidov A. V., Mull K., Peterson B. J., Striegl R. G., Aiken G. R., and Gurtovaya T. Y. (2007) Flux and age of dissolved organic carbon exported to the Arctic Ocean: A carbon isotopic study of the five largest arctic rivers. *Global Biogeochem. Cycles* **21**. doi:10.1029/2007gb002934.

Raymond P. A. and Saiers J. E. (2010) Event controlled DOC export from forested watersheds. *Biogeochemistry* **100**, 197-209. doi:10.1007/s10533-010-9416-7.

Runkel R. L., Crawford C. G., and Cohn T. A. (2004) Load Estimator (LOADEST): A FORTRAN program for estimating constituent loads in streams and rivers. U.S. Geological Survey techniques and methods Book 4, chapter A5. Reston, VA. http://water.usgs.gov/software/loadest.

Sandford R. C., Hawkins J. M. B., Bol R., and Worsfold P. J. (2013) Export of dissolved organic carbon and nitrate from grassland in winter using high temporal resolution, in situ UV sensing. *Sci. Total Environ.* **456-457**, 384-391. doi:10.1016/j.scitotenv.2013.02.078.

Schuster P. F., Shanley J. B., Marvin-Dipasquale M., Reddy M. M., Aiken G. R., Roth D. A., Taylor H. E., Krabbenhoft D. P., and DeWild J. F. (2008) Mercury and organic carbon dynamics during runoff episodes from a Northeastern USA watershed. *Water, Air, Soil Pollut.* **187**, 89-108. doi:10.1007/s11270-007-9500-3.

Schuster P. F., Striegl R. G., Aiken G. R., Krabbenhoft D. P., Dewild J. F., Butler K., Kamark B., and Dornblaser M. (2011) Mercury export from the Yukon River Basin and potential response to a changing climate. *Environ. Sci. Technol.* **45**, 9262-9267. doi:10.1021/es202068b.

Spencer R. G. M., Butler K. D., and Aiken G. R. (2012) Dissolved organic carbon and chromophoric dissolved organic matter properties of rivers in the USA. *J. Geophys. Res.* **117**. doi:10.1029/2011jg001928.

Spencer R. G. M., Hernes P. J., Ruf R., Baker A., Dyda R. Y., Stubbins A., and Six J. (2010) Temporal controls on dissolved organic matter and lignin biogeochemistry in a pristine tropical river, Democratic Republic of Congo. *J. Geophys. Res.* **115**. doi:10.1029/2009jg001180.

Swain L. G. (2004) Water quality assessment of the Fraser River at Hope (1979 – 2004). B.C. Ministry of Environment and Environment Canada. 74 pp. http://www.env.gov.bc.ca/wat/wq/quality/hope/wq_fraser_riv_hope_2004.pdf.

Townsend-Small A., McClelland J. W., Max Holmes R., and Peterson B. J. (2011) Seasonal and hydrologic drivers of dissolved organic matter and nutrients in the upper Kuparuk River, Alaskan Arctic. *Biogeochemistry* **103**, 109-124. doi:10.1007/s10533-010-9451-4.

U.S. EPA (2002) Method 1631, Revision E: Mercury in water by oxidation, purge, and trap, and cold vapor atomic fluorescence spectrometry. U.S. EPA Office of Science and Technology, Washington, D.C.

U.S. EPA (2007) Method 7473, Mercury in solids and solutions by thermal decomposition, amalgamation, and atomic absorption spectrophotometry, Revision 0. U.S. EPA Office of Science and Technology, Washington, D.C.

Valentine K. W. G., Sprout P. N., Baker T. E., and Lawkulich L. M. E. (1978) *The Soil Landscapes of British Columbia*. BC Ministry of Environment, Resource Analysis Branch.

Vold T. (1979) Soils in the Cariboo River Valley, B.C., with selected engineering interpretations. B.C. Ministry of Environment, Victoria, B.C. 22 pp.

Vonk J. E., Mann P. J., Davydov S., Davydova A., Spencer R. G. M., Schade J., Sobczak W. V., Zimov N., Zimov S., Bulygina E., Eglinton T. I., and Holmes R. M. (2013) High biolability of ancient permafrost carbon upon thaw. *Geophys. Res. Lett.* **40**, 2689-2693. doi:10.1002/grl.50348.

Voss B. M., Peucker-Ehrenbrink B., Eglinton T. I., Fiske G., Wang Z. A., Hoering K. A., Montluçon D. B., LeCroy C., Pal S., Marsh S., Gillies S. L., Janmaat A., Bennett M., Downey B., Fanslau J., Fraser H., Macklam-Harron G., Martinec M., and Wiebe B. (2014) Tracing river chemistry in space and time: Dissolved inorganic constituents of the Fraser River, Canada. *Geochim. Cosmochim. Acta* **124**, 283-308. doi:10.1016/j.gca.2013.09.006.

Voss B. M., Peucker-Ehrenbrink B., Eglinton T. I., and Galy V. (in prep) Tracing river chemistry in space and time 4. Organic carbon cycling in the Fraser River.

Wagner L. E., Vidon P., Tedesco L. P., and Gray M. (2008) Stream nitrate and DOC dynamics during three spring storms across land uses in glaciated landscapes of the Midwest. *J. Hydrol.* **362**, 177-190. doi:10.1016/j.jhydrol.2008.08.013.

Wang Z. A. and Cai W.-J. (2004) Carbon dioxide degassing and inorganic carbon export from a marsh-dominated estuary (the Duplin River): A marsh CO_2 pump. *Limnol. Oceanogr.* **49**, 341-354.

Weishaar J. L., Aiken G. R., Bergamaschi B. A., Fram M. S., Fujii R., and Mopper K. (2003) Evaluation of specific ultraviolet absorbance as an indicator of the chemical composition and reactivity of dissolved organic carbon. *Environ. Sci. Technol.* **37**, 4702-4708. doi:10.1021/es030360x.

Whitfield P. H. and Schreier H. (1981) Hysteresis in relationships between discharge and water chemistry in the Fraser River basin, British Columbia. *Limnol. Oceanogr.* **26**, 1179-1182.

Wickland K. P., Aiken G. R., Butler K., Dornblaser M. M., Spencer R. G. M., and Striegl R. G. (2012) Biodegradability of dissolved organic carbon in the Yukon River and its tributaries: Seasonality and importance of inorganic nitrogen. *Global Biogeochem. Cycles* **26**. doi:10.1029/2012gb004342.

Wickland K. P., Neff J. C., and Aiken G. R. (2007) Dissolved organic carbon in Alaskan boreal forest: Sources, chemical characteristics, and biodegradability. *Ecosystems* **10**, 1323-1340. doi:10.1007/s10021-007-9101-4.

Wilson H. F., Saiers J. E., Raymond P. A., and Sobczak W. V. (2013) Hydrologic drivers and seasonality of dissolved organic carbon concentration, nitrogen content, bioavailability, and export in a forested New England stream. *Ecosystems* **16**, 604-616. doi:10.1007/s10021-013-9635-6.

Writer J. H., Leenheer J. A., Barber L. B., Amy G. L., and Chapra S. C. (1995) Sewage contamination in the upper Mississippi River as measured by the fecal sterol, coprostanol. *Water Res.* **29**, 1427-1436.

Zhao Y., Krzic M., Bulmer C. E., and Schmidt M. G. (2008) Maximum Bulk Density of British Columbia Forest Soils from the Proctor Test: Relationships with Selected Physical and Chemical Properties. *Soil Sci. Soc. Am. J.* **72**, 442. doi:10.2136/sssaj2007.0075.

Date	Parent IGSN	Q_w at Hope ($m^3 s^{-1}$)	Cond. ($\mu S\ cm^{-1}$)	SiO_4 ($\mu mol\ L^{-1}$)	Ca ($\mu mol\ L^{-1}$)	Mg ($\mu mol\ L^{-1}$)	Na ($\mu mol\ L^{-1}$)	K ($\mu mol\ L^{-1}$)	Cl ($\mu mol\ L^{-1}$)	SO_4 ($\mu mol\ L^{-1}$)
26.Mar.13	GRO000920	980	132.0	95	414	161	215	28.3	80.7	100
27.Mar.13	GRO000921	981	132.5	104	433	167	198	25.0	61.6	105
28.Mar.13	GRO000922	984	134.2	107	421	165	211	26.8	75.5	103
29.Mar.13	GRO000923	1015	135.6	92	434	172	222	28.0	75.2	104
30.Mar.13	GRO000178	1042	134.4	102	431	164	198	25.6	70.4	104
31.Mar.13	GRO000924	1085	132.5	101	428	173	211	25.5	60.0	104
01.Apr.13	GRO000925	1182	130.8	97	433	175	210	24.9	56.6	102
02.Apr.13	GRO000926	1294	122.2	88	406	154	187	22.5	54.3	97
03.Apr.13	GRO000179	1363	123.9	90	401	150	170	22.0	51.6	97
04.Apr.13	GRO000927	1485	122.3	83	390	151	181	22.0	52.1	92
05.Apr.13	GRO000928	1774	121.3	95	396	153	187	23.6	55.4	90
06.Apr.13	GRO000929	1861	117.2	92	385	146	174	23.9	52.2	85
07.Apr.13	GRO000180	1879	109.1	93	317	122	143	20.0	45.6	73
08.Apr.13	GRO000930	1936	109.2	88	371	140	158	25.1	45.8	71
09.Apr.13	GRO000931	2158	118.1	96	393	150	161	24.4	47.9	75
10.Apr.13	GRO000932	2354	124.1	107	408	158	165	27.1	51.1	77
11.Apr.13	GRO000933	2337	120.6	100	398	159	164	26.5	48.6	78
12.Apr.13	GRO000181	2435	115.5	104	391	148	151	24.9	45.1	74
13.Apr.13	GRO000934	2511	118.1	103	383	154	155	26.7	49.9	75
14.Apr.13	GRO000935	2579	121.7	94	400	163	158	27.3	46.9	76
15.Apr.13	GRO000936	2479	127.4	108	425	163	156	26.5	45.6	76
16.Apr.13	GRO000182	2475	124.1	107	416	162	154	27.0	58.9	73
17.Apr.13 09:00	GRO000937	2385	125.8	113	423	172	165	28.4	46.2	73
17.Apr.13 11:45	GRO000938	2357	126.2	111	426	176	168	28.8	65.7	78
17.Apr.13 14:30	GRO000939	2349	126.3	110	426	175	167	28.2	49.1	77
17.Apr.13 17:45	GRO000940	2355	126.3	108	422	172	163	28.5	47.3	75
18.Apr.13	GRO000941	2405	125.6	84	427	171	158	26.8	47.8	78
19.Apr.13	GRO000942	2356	125.7	108	410	165	160	27.8	47.0	73
20.Apr.13	GRO000183	2430	124.8	111	411	169	162	28.3	49.7	77
21.Apr.13	GRO000943	2906	125.4	105	421	170	162	28.1	49.8	74
22.Apr.13	GRO000945	3078	122.5	105	409	164	154	25.9	43.6	72

Table S1. Concentrations of dissolved major elements during the 2013 early freshet period. IGSN codes refer to International

GeoSample Numbers in the System for Earth Sample Registration (Sesar) database; sample metadata can be accessed at

www.geosamples.org.

CHAPTER 5.

SEASONAL VARIABILITY IN SEDIMENT SOURCES AND TERRESTRIAL ORGANIC CARBON

EXPORT IN THE FRASER RIVER, CANADA

5.1 Abstract

Burial of terrestrial organic carbon (OC) in marine sediments is controlled by physical weathering rates, the balance between recently fixed and ancient OC in river sediments and biogeochemical processing and temporary storage of this organic matter during fluvial transport, and in the coastal ocean. Constraining the contribution from rock-derived (i.e. radiocarbon-dead, or "petrogenic") versus vegetation-derived ("biospheric") OC is critical to assessing the importance of terrestrial POC burial in the context of regional carbon budgets. The lack of sediment impoundments, seasonality of flow, and diverse bedrock lithology of the Fraser River basin make it a prime target for deconstructing weathering versus biogeochemical impacts on sediment and OC transport in a large river system. By combining tracers of both inorganic and organic sedimentary material, this study demonstrates the tight coupling between seasonally-varying sediment sources and biospheric OC export in the Fraser River basin. Relative to freshet conditions, sediments during low discharge in the Fraser exhibit relatively unradiogenic Sr isotope signatures (low ^{87}Sr/^{86}Sr ratios), and are rich in relatively young OC. Correcting for a constant petrogenic OC contribution (0.12 wt%), we estimate the average residence time of

biospheric OC in the Fraser basin to be ~650 years. The much older age of terrestrial plant-derived long-chain n-alkanoic acids (~3700 years) shows that a portion of the biospheric OC pool is significantly aged, likely due to mobilization and export of old soil OC.

5.2 Introduction

Riverine export of terrestrial organic carbon represents a significant flux of recently fixed atmospheric carbon to the coastal ocean, where a portion of the carbon is buried on geologic timescales (Burdige, 2007; Galy et al., 2008a; Kao et al., 2014). The amount of riverine particulate organic carbon (POC) derived from recent terrestrial photosynthesis versus aquatic productivity and weathering of petrogenic organic carbon is controlled by a range of tectonic, climatic, geomorphologic, and biogeochemical processes (Blair et al., 2004; Leithold et al., 2006; Longworth et al., 2007; Hilton et al., 2010; Galy and Eglinton, 2011; Hovius et al., 2011; Hilton et al., 2012; Bouchez et al., 2014), which differ significantly across river basins.

A key tool in tracing the biospheric versus rock-derived components of river sediments is the ability to associate the organic carbon composition of the sediments with their mineralogical hosts. Inorganic features of sediments can be used to distinguish the sources of sediments within a basin based on the spatial distribution of different bedrock lithologies (e.g. Cameron and Hattori, 1997; Huh et al., 2004; Chung et al., 2009; Bouchez et al., 2011a; Padoan et al., 2011). By assessing the degree to which the composition of POC is simply controlled by the sediment provenance, as opposed to biological modification of source material, we aim to elucidate how efficiently the river exports the portion of its OC load derived from recently fixed atmospheric CO_2. This efficiency has significant implications for the importance of riverine POC export in the long-term evolution of Earth's climate via the transfer of carbon from the rapidly cycling surface reservoirs to the slowly cycling lithosphere.

The Fraser River basin in southwestern Canada (Fig. 1) is an ideal setting for studying sedimentary processes in a large basin due to its lack of main stem sediment impoundments, either natural or anthropogenic. The main stem has only one small lake (Moose Lake), which is

very near the headwaters, so sediments entering the Fraser main stem throughout the basin have the potential to reach the mouth. There is, however, some potential for sediment storage within the basin, particularly in the northern peneplain region (including the Nechako and Willow rivers) and within the narrow floodplain of the Fraser Valley downstream of Hope. Furthermore, anthropogenic influences that could modify the flux and composition of POC (e.g. agriculture, logging, mining activities, and urban development) are relatively minor.

The diverse bedrock geology (rock type and age) of the Fraser basin creates large contrasts in inorganic radioisotope compositions (Cameron and Hattori, 1997; Peucker-Ehrenbrink et al., 2010), allowing these to serve as sensitive sediment provenance tracers. The biogeoclimatic variability across the Fraser basin (Pojar et al., 1987) also creates the potential for distinct sources of organic matter. Through a combined investigation of organic and inorganic sedimentary composition, we aim to evaluate the extent to which export of mineral and vegetation material is coupled in the Fraser River. The results of this study have implications for the natural geomorphic and biogeochemical processes controlling carbon cycling between land plants and marine sediments, and how these processes may be impacted by anthropogenic activities.

5.3 Methods

5.3.1 Sample Collection

This study includes samples of riverbank flood deposit sediments and suspended sediments (Table 1). Flood sediments from sites across the Fraser basin were collected under low discharge conditions from October 14th-27th, 2010. This sampling occurred during the falling limb of a brief rise in discharge (2130-3750 m^3 s^{-1} between Sept. 25th-Oct. 2nd) caused by a

significant basin-wide precipitation event; hence, some riverbank material was presumably recently deposited by this event. A large amount (>1 kg) of sediment was collected in plastic Whirl-Pak bags from exposed banks near the water's edge and frozen immediately. The sediment was freeze dried, divided using a micro-splitter, and dry sieved to yield <63 μm size fractions.

Suspended sediment samples were collected from the Fraser River main stem, mid-channel, near the city of Mission, BC, Canada (49.1256°N, 122.2975°W; Fig. 2). The river channel is ~500 m wide at this site and maximum water depth varies seasonally between ~10-15 m (Attard, 2012). The two sampling times (22 June 2013 and 2 October 2013) represent freshet (high flow) and low flow periods, respectively, of the annual hydrograph.

Suspended particulate matter (SPM) was collected using a depth-specific water sampler lowered from a small boat using an E-reel (Fig. 3). The water sampler, a horizontal cylinder with pressure-activated pistons to close doors at the head and tail, was mounted below a 90-kg USGS P-63 isokinetic point-integrating water sampler. The weight of the sampler apparatus was sufficient to keep the samplers hanging vertically in the water column, therefore depths were determined from the length of cable released. The deepest sample collected during the low flow sampling period appeared (visually) to contain bed material distinct from the suspended load present in other samples collected at that time (which is supported by geochemical data below). Although it is uncertain whether the sampler was in close enough proximity to the true bed of the channel to collect material travelling out of suspension, either topographic heterogeneity of the bed or a discrete unit of coarse sediment travelling near the bed caused this sample to contain visually and geochemically distinct sediment material. This sample is therefore referred to as "bed material" throughout the manuscript. Water samples (~10 L) were recovered in pre-cleaned plastic carboys and stored overnight at ambient outdoor temperature (6-15°C).

Sediments were recovered onto 90 mm polyethersulfone membrane filters (Millipore, pore size 0.22 μm) using specially-designed filtration units. The resulting sediments were rinsed from filters, freeze dried, and ground to a fine powder using an agate mortar and pestle. This trap-type water sampler and filtration procedure has been used in previous studies for collecting relatively large volumes (5-10 L) of river water at specific depths for SPM geochemical analyses (e.g. Galy and Eglinton, 2011; Lupker et al., 2012).

5.3.2 Strontium isotope analysis

For inorganic isotopic analysis, an aliquot of the sediments was subjected to a two-step digestion procedure to ensure complete dissolution of solids. First, 50-100 mg of sediment was weighed out into 17 mL acid-cleaned Teflon beakers, followed by addition of 3 mL sub-boiling distilled HNO_3 (16.8 N) and 1 mL HF (SeaStar, 25 N). Beakers were sealed and heated to 180°C for 48 hours, then dried at 80°C. When the vessels reached near-dryness, 4 mL of sub-boiling distilled HCl (12 N) was added to each beaker and samples were refluxed at 180°C for 48 hours. After this first digestion step, the majority of samples were fully dissolved. These samples were heated to near-dryness and transferred to storage vessels in 10% sub-boiling distilled HCl.

For samples with solids remaining (03 October 2013, depths 0.2, 0.4, and 0.6), a second digestion step was carried out in a High-Pressure Asher (Anton Paar HPA-S). Before treating samples, 100 mL quartz vessels were pre-cleaned with 2 mL sub-boiling distilled HNO_3, reacted at 150°C for 30 minutes. Waste acid from the cleaning step was discarded and the vessel rinsed with Milli-Q H_2O (18.2 MΩ cm^{-1}). Sample material in Teflon beakers was gently heated to dryness (to eliminate HF) and transferred to the clean quartz vessels in 1 mL sub-boiling distilled HCl, and 2 mL sub-boiling distilled HNO_3 was added. Samples were reacted at 280°C for 90

minutes. The resulting material, fully dissolved, was transferred to clean Teflon beakers, heated to near-dryness, and transferred to storage vessels in 10% sub-boiling distilled HCl.

Approximate strontium concentrations were measured by calibration curves of standard reference material SLRS-5 (Natural Research Council Canada) on a single-collector inductively-coupled plasma mass spectrometer (ThermoScientific Element2). Target volumes of each sample were transferred to clean Teflon beakers for isotope analysis. Details of the strontium isotope analysis are given in Voss et al. (2014). Briefly, strontium was isolated by ion chromatography using Sr Spec resin (Eichrom) and eluted with 7 mL Milli-Q water. Column eluents were analyzed on a multicollector inductively-coupled plasma mass spectrometer (ThermoScientific Neptune). Raw $^{87}Sr/^{86}Sr$ for all samples and standards was corrected for instrumental mass bias with a power law and corrected for ^{86}Kr and ^{87}Rb interferences. Sample results were normalized to the average measured value of standard SRM 987 (U.S. National Institute of Standards and Technology). The certified value of the standard is $^{87}Sr/^{86}Sr = 0.710240$; the average measured value was 0.710236 (n = 18, 2 s.d. = 0.000069).

5.3.3 Bulk organic carbon and nitrogen content and stable isotopes

Sediments were weighed in triplicate into combusted silver capsules and acidified in concentrated HCl vapor under partial vacuum at 65°C to remove carbonate. Organic carbon and nitrogen concentrations (%OC and %N, by weight) and isotope values ($\delta^{13}C$) were measured by Carl Johnson at WHOI on an Elemental Analyzer (Carlo Erba 1107) attached via a Finnigan-MAT Conflo II open split interface to a stable isotope ratio mass spectrometer (Delta^{Plus}) for measurement of $^{13}C/^{12}C$ (referenced to Pee Dee Belemnite). Sample %OC, %N, and $\delta^{13}C$ values were determined from standard reference materials NBS-19 limestone, IAEA-N-1 ammonium

sulfate, USGS-40 glutamic acid, and a laboratory glycine standard. Analytical accuracy and precision of these measurements are 0.1 wt% for C and N abundance, 0.3‰ for δ^{13}C, and 0.4‰ for δ^{15}N.

5.3.4 Bulk organic carbon radiocarbon content

Bulk radiocarbon sample processing and analysis took place at ETH-Zürich. Sediments were weighed into silver capsules (pre-combusted at 450°C for 5 hours) and placed inside quartz inserts (pre-combusted at 850°C for 5 hours). Inserts were acidified in a desiccator in concentrated HCl vapor under partial vacuum at 65°C to remove inorganic carbonate. After acidification, the HCl dish was replaced with a dish of NaOH pellets to eliminate acid residue. Inserts were transferred to pre-combusted quartz tubes and a small amount of pre-combusted granular CuO was added. Tubes were evacuated and flame-sealed on a vacuum line, then combusted at 850°C for 5 hours. Evolved CO_2 gas was cryogenically purified, quantified on the vacuum line, and transferred to Pyrex tubes before analysis. Standard reference materials of oxalic acid II (NIST SRM-4990C) and lab anthracite coal (ETH #48160) were prepared in the same manner as samples (excepting the acidification step for oxalic acid). Samples were analyzed as CO_2 using the Micadas gas ion source accelerator mass spectrometer at the ETH-Zürich Laboratory for Ion Beam Physics. Samples were corrected for instrumental fractionation using oxalic acid II and coal reference gases.

5.3.5 Fatty acid extraction and compound-specific radiocarbon analysis

One flood sediment sample (<63 μm fraction) was selected for compound-specific radiocarbon analysis. This sample was collected at the Fraser River main stem at Hope

(49.381°N, -121.451°E) on Oct. 24th, 2010, which integrates 95% of the total basin drainage

area, excluding only the floodplain of the lower Fraser Valley. Approximately 15 g of sediment

was extracted in 9:1 dichloromethane (DCM):methanol in a Teflon vessel at 100°C for 20

minutes using a CEM microwave accelerated reaction system. The extract was purified by

gravity column containing 1 g aminopropyl silica gel (Sigma Aldrich Supelclean[TM] LC-NH$_2$).

After elution of less polar fractions, fatty acids were eluted with 14 mL of 2% formic acid in

DCM and dried to <1 mL under N$_2$. Fatty acids were converted to their corresponding methyl

esters (FAMEs) by reacting in 15 mL 5% hydrochloric acid in methanol under N$_2$ headspace at

70°C for 12 hours. The reaction was terminated by adding ~15 mL MilliQ water. FAMEs were

isolated by liquid-liquid extraction in 4:1 hexane:DCM and dried over combusted Na$_2$SO$_4$.

FAMEs were further purified by elution over 1 g aminopropyl silica gel in 7 mL 4:1

hexane:dichloromethane, followed by elution over 0.5 g silver nitrate silica gel in 18 mL 5:1

hexane:DCM. Compounds were analyzed on a gas chromatograph with flame ionization detector

(GC-FID) and quantified using an external standard mixture of n-C$_{16:0}$, n-C$_{20:0}$, n-C$_{23:0}$, and n-C$_{28:0}$ methyl esters.

Individual FAMEs were isolated using a preparative capillary gas chromatography

system at WHOI (HP 5890 GC-FID coupled to a HP 7673 autoinjector and Gerstel cooled

injection system), following Eglinton et al. (1996). After ~100 injections, 5-25 μg of each FAME

was isolated, transferred in DCM to pre-combusted quartz tubes, dried down, and a small amount

of pre-combusted granular CuO was added. Tubes were evacuated and flame-sealed on a vacuum

line at WHOI and combusted at 850°C for 5 hours. Evolved CO$_2$ gas was cryogenically purified,

quantified on the vacuum line, transferred to Pyrex tubes, and brought to ETH-Zürich for

analysis. AMS analysis was identical to that described above for bulk samples. Measured FAME

[14]C values were corrected for methyl carbon and for vacuum line and combustion blanks following Santos et al. (2010). Data are presented as fraction modern (Fm) and/or conventional ^{14}C ages relative to 1950 (Stuiver and Polach, 1977).

5.4 Results

5.4.1 Strontium isotope composition

The Sr isotope composition of flood sediment fine fractions (<63 μm; Table 1) shows a distinct trend toward less radiogenic values (lower $^{87}Sr/^{86}Sr$ ratios) moving from the headwaters to the river mouth (Fig. 4). The most radiogenic sediments are represented by main stem sites in the Rocky Mountains; less radiogenic Rocky Mountain tributaries (Robson and McGregor rivers) are noticeably influenced by erosion of carbonate lithologies. The main stem samples record incorporation of upstream material, as the initially radiogenic composition in the Rocky Mountains becomes gradually less radiogenic due to contributions from unradiogenic Coast Range tributaries. This trend is also observed in the dissolved and surface SPM loads of the Fraser River (Cameron and Hattori, 1997; Voss et al., 2014).

Depth profiles of suspended sediment concentrations and SPM geochemical properties for samples collected during freshet (June 20) and low flow (October 3) conditions at Mission in 2013 are presented in Figure 5. Suspended sediment concentrations at low flow (7-15 mg L^{-1}) are very low compared to those during the freshet (185-327 mg L^{-1}). The changes in sediment concentration with depth are minor relative to this seasonal difference; however, the freshet profile shows a slight decrease between the 1.5-4.4 m, followed by an increase to the deepest point at 9.2 m. While suspended sediment concentration in river channels is often observed to increase with depth (e.g. Bouchez et al., 2011b; Lupker et al., 2011), the mid-depth minimum in

the Fraser River freshet samples may be caused by transient pulses of sediment which travel within defined depth ranges. Grain size data for these sediments will further inform the relationship between the depth segregation of sediment mass and the geochemical properties presented below. The depth trends of the concentration of particulate organic carbon (POC; Fig. 5B) mirror those of sediment concentration, with the exception of the deepest sample collected during low flow (which includes bed material), for which the exceptionally low OC content (0.22%) results in very low POC concentration (2 μmol L^{-1}). The other low flow samples exhibit POC concentrations of 8-20 μmol L^{-1}, while freshet POC is 98-117 μmol L^{-1}.

The SPM depth profiles show relatively little variation in ^{87}Sr/^{86}Sr ratios with depth (Table 2, Fig. 5C). In the Amazon River, for example, a depth profile of suspended sediment ^{87}Sr/^{86}Sr composition ranged from 0.716047-0.722395 (Bouchez et al., 2011b). In contrast, the flux-integrated average values for the Fraser River June and October profiles are markedly different, with SPM during low flow conditions being substantially more radiogenic than that during freshet conditions (flux-weighted average ^{87}Sr/^{86}Sr = 0.7117 $\pm$ 0.0005 and 0.70701 $\pm$ 0.00025, respectively; mean $\pm$ 1 s.d., n = 11). Furthermore, bed material during low flow conditions is even less radiogenic (0.705314) than the freshet SPM.

5.4.2 Organic carbon composition

The trends in bulk OC composition in the SPM depth profiles mirror those of the ^{87}Sr/^{86}Sr composition (Fig. 5D, E, and F). Freshet SPM is leaner in OC, has higher δ^{13}C values, and is older in ^{14}C age than SPM during low flow. Higher δ^{13}C values may indicate organic matter influenced by aquatic production or microbial processing, while lower values indicate a more vascular plant-like composition, although the picture is likely significantly more complex

than a binary mixture of inputs (Hedges and Mann, 1979; Goñi et al., 2003; Galy et al., 2008c). The range in $\delta^{13}C$ values for both freshet and low flow samples, however, is small, and all values fall within the range expected for a predominantly C_3 plant source (Deines, 1980; Collister et al., 1994). As in the case of $^{87}Sr/^{86}Sr$ composition, the OC composition of bed material sampled during low flow is more similar to freshet SPM than to the SPM flowing above it, suggesting that petrogenic OC influences both bulk ^{14}C and ^{13}C composition, particularly in sediments with low OC content.

The strong even-over-odd carbon number preference among the long-chain fatty acid homologs, together with a dominance of the C_{24} fatty acid in the main stem flood sediment sample from Hope (Table 3), suggests a significant vascular plant contribution to the organic matter (Drenzek et al., 2007; Medeiros and Simoneit, 2008; Vonk et al., 2010). The radiocarbon composition of these fatty acids (Fig. 6) exhibits the commonly observed trend of older age with increasing chain length (Ohkouchi et al., 2003; Drenzek et al., 2007; Matsumoto et al., 2007). The abundance-normalized radiocarbon age of C_{24}-C_{32} fatty acids in this sample is 4680 ± 1600 years (1 s.d.; Fm: 0.63 ± 0.12).

5.5 Discussion

5.5.1 $^{87}Sr/^{86}Sr$ constraints on sediment provenance

The fact that the $^{87}Sr/^{86}Sr$ ratios of main stem flood sediments in the Fraser River follows the same downstream evolution as the dissolved load is a testament to the lack of natural or anthropogenic sediment traps in the Fraser River main stem. The only main stem lake, Moose Lake, lies in the extreme headwaters of the basin, and therefore exerts little influence on the sediment load of the river. Certain large tributaries, including the Nechako, Thompson, and

Quesnel rivers, contain large lakes in their watersheds, and their sediment fluxes to the main stem Fraser relative to total sediment mobilization are likely somewhat diminished and regionally biased (e.g. most of the sediment delivered by the Thompson River derives from areas downstream of Kamloops Lake, only ~100 km from the confluence with the main stem Fraser). By and large, however, tributary sediments are capable of influencing the main stem composition throughout the basin.

The seasonal dynamics in SPM ^{87}Sr/^{86}Sr ratios are, in contrast, very different from the dissolved load (Fig. 7). Dissolved ^{87}Sr/^{86}Sr responds to changing hydrologic sources throughout the freshet, with radiogenic contributions from headwater snowmelt rising in the spring and remaining high throughout the summer and early fall (Voss et al., 2014). In contrast, the SPM profiles show a transition from relatively unradiogenic composition during the early portion of the freshet to more radiogenic composition in the fall. That is, during the early freshet period, the sedimentary load remains relatively unradiogenic while the dissolved load already exhibits more radiogenic characteristics. The total range in the two-year time series of ^{87}Sr/^{86}Sr ratios for the dissolved load is 0.0051, while the difference between the average freshet and low flow sediment ^{87}Sr/^{86}Sr ratios is 0.0047.

It is possible that the freshet SPM samples represent a midpoint during the radiogenic-to-unradiogenic transition, as the beginning of this shift is not constrained by these observations. This would require that the Sr isotope composition of pre-freshet SPM is even less radiogenic than the values observed in our freshet samples, and therefore that the seasonal variability in ^{87}Sr/^{86}Sr composition is even greater than that recorded thus far. It is also possible that the low flow sampling point represents a pulse of sedimentary material with sources unrepresentative of average low flow conditions. This sample was taken within days of a significant basin-wide rain

event, which may have mobilized sediments from areas that do not typically contribute significant amounts of SPM during the fall.

The low flow SPM profile likely represents background sediment levels that are maintained regardless of the season, whereas the freshet profile represents a supplement of these sediments with less radiogenic material. SPM during low flow is characterized by fine-grained particles that remain in suspension even under less energetic conditions. The freshet sample presumably contains the same fine sediment, augmented by coarser material which can only enter and be maintained in the suspended load under high flow conditions (flow velocities during the freshet sampling were 1.40-1.84 m s^{-1}; those during the low flow sampling were 0.78-0.98 m s^{-1}; Table 2). Given the general contrast between the sedimentary Rocky Mountain lithologies of the headwaters and the intrusive, metamorphic, and volcanic lithologies of the Interior Plateau and Coast Range, this coarser-grained material may be derived from more local sources than the fine sediment, as evidenced by its composition approaching the unradiogenic Coast Range tributary sediments. This coarse fraction is also apparent in the less radiogenic "bed material" sample from the low discharge sampling period. However, there may also be coarse-grained lithologies within the headwater region (which may be significantly physically abraded during downstream transport) and/or fine-grained sediment sources derived from the middle and lower reaches of the basin. These nuances should be further investigated with mineralogical and Sr isotope analyses of various grain size fractions of the bulk suspended sediments.

5.5.2 Seasonality of OC age and composition

Such a supplement of the more radiogenic, fine-grained SPM with less radiogenic, coarser-grained sediment during the freshet is supported by the bulk OC data. Plots of the bulk

OC characteristics against $^{87}Sr/^{86}Sr$ composition show a clear mixing between a more radiogenic end-member enriched with young organic matter, and a less radiogenic end-member that is OC-poor, and bears older organic matter (Fig. 8).

The age of the OC is also related to the OC content (Fig. 9). Galy et al. (2008a) used the apparent binary mixing relationship between the modern portion of POC and corresponding %OC to estimate a constant contribution of OC from a rock-derived (i.e. radiocarbon-dead) end-member. Following this approach (based on the *x*-axis intercept of the linear correlation in Fig. 9), we estimate that the average rock-derived OC content of Fraser River SPM is 0.12 wt%. The slope of this relationship, which represents the increase in radiocarbon content for a given addition of non-petrogenic OC, can be interpreted as the average apparent age of biospheric organic matter in the watershed. Remarkably, for both freshet and low flow sediments, the calculated apparent age is 650 years. This implies that the significantly older age of bulk POC during the freshet (ca. 1500 years older than for low flow sediments) thus results from dilution of biospheric OC by petrogenic OC entrained with the mineral load.

The contribution from rock-derived OC in the Fraser River is large in comparison to the Ganges-Brahmaputra and Amazon rivers (0.025% and 0.06%, respectively), but smaller than that of the small mountainous rivers draining Taiwan (0.35%) (Galy et al., 2008a; Hilton et al., 2010; Bouchez et al., 2014). These differences are driven by both the OC content of the bedrock being weathered in these basins, as well as the efficiency of petrogenic OC mineralization during riverine transport. The average age (or residence time) of biospheric OC in the Fraser (650 years) is also much younger the larger basins: 1400 years in the Amazon and 2500 years in the Ganges-Brahmaputra. In each of these rivers, the non-petrogenic biospheric OC is likely composed of at least two distinct pools: modern vegetation material and aged soil OC, and the relative

proportions of these pools determine the residence time predicted by the spread in modern OC contents.

5.5.3 Biomarker constraints on OC residence time

The age of individual organic compounds offers insight to the cycling of distinct components of the bulk organic carbon pool (Eglinton et al., 1996; Ohkouchi et al., 2003). In particular, the ages of vascular plant biomarkers such as long-chain fatty acids can also be used to assess the terrestrial residence time of biospheric organic carbon (Galy and Eglinton, 2011). Leaf wax-derived long-chain fatty acids serve as useful tracers of vascular plant-derived material as they are generally not synthesized by bacteria, fungi, or aquatic primary producers, and their hydrophobic nature allows them to persist in soils (e.g. Eglinton and Hamilton, 1967; Eglinton et al., 1968; Schnitzer and Neyroud, 1975; Volkman et al., 1998; Saliot et al., 2002).

The fact that these vascular plant biomarkers in the Fraser River are so much older (~3700 years) than the bulk biospheric OC (~650 years) indicates a highly diverse sedimentary organic carbon pool. This difference stands in contrast to the few other large river systems for which this analysis has been performed. Through SPM samples collected from downstream areas of the Ganges-Brahmaputra basin, Galy and Eglinton (2011) showed that the ^{14}C age of terrestrial plant biomarkers (50-1000 years) is consistently younger than that of bulk biospheric OC (1600-4800 years). The Ganges-Brahmaputra is a large low-latitude system with extensive floodplains in which significant compositional changes in terrestrial OC from upstream portions of the basin take place (Galy et al., 2008b). The authors propose that sources of long-chain fatty acids and bulk biospheric OC may be spatially decoupled in this basin, with young fatty acids deriving from recent vegetation in the floodplains and significant quantities of fatty-acid poor

organic matter deriving from pre-aged soils on the Tibetan plateau (Galy and Eglinton, 2011). A study of six large Arctic rivers by Gustafsson et al. (2011) showed a trend of increasing bulk POC ages moving eastward across Siberia, driven by the increasing areal extent of permafrost, while long-chain fatty acid ages show no distinct trend (note that, in this study, bulk OC ages are not corrected for the input of petrogenic OC to these basins, and hence biospheric OC would be even younger than the bulk OC). Consequently, the age difference between the younger bulk OC and the fatty acids in these rivers generally decreases from west to east across Siberia. In this context, the Fraser River appears to behave more analogously to Arctic rivers, particularly those with little permafrost coverage, by exporting relatively young bulk OC and aged long-chain plant wax lipids.

An average biospheric OC residence time of 650 years in Fraser basin soils substantiates a recent vegetation source for the bulk of this material, particularly in light of the fact that this reservoir also contains some considerably older material (represented by the long-chain fatty acids). Fatty acids, as well as long-chain *n*-alkanes and other recalcitrant leaf wax constituents, are themselves likely derived from a spectrum of sources ranging in age from fully modern to thousands of years. The source of such aged terrestrial OC in the Fraser basin is suggested by the work of Smittenberg et al. (2006), who observed a significant difference between the depositional age and the age of long-chain *n*-alkanes (corrected for an estimated petrogenic contribution) in a sediment core from Saanich Inlet, proximal to the Fraser River mouth. The age difference begins at ~0 at a sediment depositional age of 12,000 years b.p. and increases to ~5000 years for surface sediments. The authors attribute this growing offset to persistent post-glacial mobilization of aged Holocene soils, such that modern plant waxes carried by river sediments are continuously diluted by highly aged soil-derived organic matter. These authors'

observation of *n*-alkanes ~5000 years older than sediment deposition age is comparable to the ~3000-year age difference between Fraser River long-chain fatty acids and bulk biospheric OC. Thus it appears that Fraser River sediments are composed of a heterogeneous mixture of not only petrogenic OC and modern vegetation material, but also a significant component of pre-aged soil OC.

The proportion of pre-aged versus modern OC in Fraser River sediments can be estimated from the age distribution of the long-chain fatty acids. In addition to the trend towards increasing age with increasing chain length, the ages of the homologs appear to approach a constant value with decreasing abundance (Fig. 10), suggesting that as the abundance of fatty acids approaches zero, the age of these compounds reaches a constant value representing the age of the relict soil OC pool. Given the age distribution of these compounds, the longer chain length homologs clearly have a stronger influence from aged material, as would be expected from the increasing hydrophobicity of longer fatty acids. Therefore, the age of the oldest long-chain fatty acid (n-C$_{32:0}$) is an appropriate estimate for the age of the aged soil OC pool. Using this value, the proportion of the aged and modern biospheric OC pools can be calculated as follows:

$$Fm_{bulk} * \%OC_{bulk} = Fm_{petro} * \%OC_{petro} + Fm_{aged} * \%OC_{aged} + Fm_{mod} * \%OC_{mod}$$

$$\%OC_{bulk} = \%OC_{petro} + \%OC_{aged} + \%OC_{mod}$$

As determined above, $\%OC_{foss} = 0.12$, and Fm_{aged} is estimated to be 0.367. Since $Fm_{foss} = 0$, the equations simplify to:

$$Fm_{bulk} * \%OC_{bulk} = Fm_{aged} * \%OC_{aged} + Fm_{mod} * \%OC_{mod}$$

$$\%OC_{bulk} - 0.12 = \%OC_{aged} + \%OC_{mod}$$

These equations can be solved for each depth profile suspended sediment sample to determine $\%OC_{aged}$ and $\%OC_{mod}$. The deepest sample from the low flow sampling is excluded, as it

contains bed material and its old bulk age results in a negative calculated aged component. When normalized to %OC$_{bulk}$, the average aged fraction for all samples is 0.11 ± 0.04. The calculated modern and petrogenic components are 0.73 ± 0.08 and 0.16 ± 0.08, respectively. This analysis assumes that the bulk age distribution of the aged biospheric OC pool is identical to that of the long-chain fatty acids. This assumption could be tested with other techniques such as ramped pyrolysis ^{14}C analysis (Rosenheim and Galy, 2012; Rosenheim et al., 2013).

Hydrophobic biomarkers such as long-chain fatty acids preferentially associate with fine-grained soil particles, hence they are likely to be retained for long periods of time in soils; in contrast, less hydrophobic material (such as lignin, which makes up a much larger fraction of the total OC carried by river sediments than plant wax lipids), would likely mobilize from soils into aquatic systems more rapidly and hence have a younger age (Feng et al., 2013). Therefore the ~11% contribution from the soil OC pool estimated from long-chain fatty acid ages is most likely a lower bound on the proportion of OC derived from this pre-aged soil OC source. Further compound-specific radiocarbon analyses of samples from across the basin, as well as diverse biospheric compound classes (e.g. lignin) could further inform the spatial extent and age distribution of this reservoir.

5.6 Conclusions

The Sr isotopic characteristics of fine-grained (<63 μm) riverbank material, considered flood deposits and referred to here as "flood sediments" (see Chapter 3), trace the bedrock lithology of the Fraser River basin. The composition of suspended sediments collected near the mouth reflect temporal changes in the relative contributions of these source regions, with greater inputs from Coast Range regions during the spring freshet. Similarly, freshet bulk SPM is OC-

poor and old relative to SPM during low flow conditions. The close correspondence between $^{87}Sr/^{86}Sr$ ratios and bulk OC composition in these sediments suggests that the Fraser SPM load contains a constant fine-grained component with a high proportion of young OC and a larger contribution from the radiogenic Rocky Mountain headwaters. During the spring freshet, this material is augmented by an influx of coarser-grained sediment derived from the Coast Range, bearing a low concentration of relatively old OC. This apparently simple mixing behavior of both mineral sediments and POC suggests that OC is transported through the Fraser basin with minimal biogeochemical processing.

Deconvolution of OC components of these sediments indicate a constant rock-derived OC component in Fraser River SPM of 0.12% and an average residence time of 650 years for bulk biospheric OC. The old ^{14}C age of long-chain fatty acids derived from plant wax lipids (3700 years) indicates that a significant portion (~11%) of the OC stored in Fraser basin soils is highly aged, supporting the concept of sustained post-glacial mobilization of pre-aged OC in this basin.

Acknowledgements

IGSN	Fraction	Site	Region	^{87}Sr/^{86}Sr
GRO001049	<63 μm	Fraser River at McBride	main stem	0.748042
GRO001053	<63 μm	Fraser River at Hansard	main stem	0.736543
GRO001062	<63 μm	Fraser River at Lytton	main stem	0.709984
GRO001063	<63 μm	Fraser River at Hope	main stem	0.715700
GRO001048	<63 μm	Robson River	Rockies	0.715844
GRO001052	<63 μm	McGregor River	Rockies	0.721780
GRO001050	<63 μm (muddy)	Willow River	Cariboo	0.710696
GRO001051	<63 μm (sandy)	Willow River	Cariboo	0.710424
GRO001061	<63 μm	Thompson River	Cariboo	0.706413
GRO001054	<63 μm	Nechako River	Coast	0.704748
GRO001055	<63 μm	Blackwater River	Coast	0.704344
GRO001058	<63 μm	Chilcotin River	Coast	0.703975
GRO001064	<63 μm	Harrison River	Coast	0.706890

Table 1. ^{87}Sr/^{86}Sr compositions of 2010 flood sediments (<63 μm). Analytical errors (1 s.d.) for Sr isotope measurements are <0.000013. IGSN codes refer to International GeoSample Numbers in the System for Earth Sample Registration (Sesar) database; sample metadata can be accessed at www.geosamples.org.

Date	IGSN	Depth (fraction)	Depth (m)	velocity (m s^{-1})	TSS (mg L^{-1})	Point Q$_s$ (m^2 s^{-1})	^{87}Sr/^{86}Sr	%OC	C/N	δ^{13}C (‰)	^{14}C Fm	^{14}C Age (yrs)
20.Jun.13	GRO001297	0.1	2.0	1.6	255	4.2×10^{-4}	0.706884 (013)	0.52	11.7 ± 1.2	-26.0 ± 0.3	0.700 ± 0.008	2870 ± 33
	GRO001298	0.2	3.3	1.8	224	3.1×10^{-4}	0.707070 (005)	0.55	11.5 ± 2.0	-26.0 ± 0.3	0.743 ± 0.008	2384 ± 27
	GRO001299	0.4	5.9	1.5	185	2.8×10^{-4}	0.707330 (006)	0.64	12.2 ± 1.3	-26.1 ± 0.3	0.697 ± 0.008	2904 ± 33
	GRO001300	0.6	8.6	1.4	199	2.8×10^{-4}	0.707297 (013)	0.61	11.8 ± 1.0	-26.4 ± 0.3	0.728 ± 0.008	2555 ± 28
	GRO001301	0.8	11.2	1.4	273	2.9×10^{-4}	0.706889 (007)	0.50	12.1 ± 1.3	-26.2 ± 0.3	0.679 ± 0.007	3112 ± 33
	GRO001302	0.9	12.5	1.4	327	2.2×10^{-4}	0.706519 (007)	0.43	13.2 ± 1.2	-26.1 ± 0.3	0.684 ± 0.008	3056 ± 34
		1.0	13.1									
	Freshet Average						0.707006 (255)	0.54 ± 0.06	12.0 ± 0.5	-26.1 ± 0.1	0.706 ± 0.023	2805 ± 256
03.Oct.13	GRO001303	0.1	1.5	0.9	9.63	6.7×10^{-6}	0.712458 (009)	1.74	10.4 ± 1.0	-27.0 ± 0.3	0.848 ± 0.009	1321 ± 13
	GRO001304	0.2	2.5	0.9	7.13	3.7×10^{-6}	0.711389 (011)	1.37	10.1 ± 0.9	-26.7 ± 0.4	0.873 ± 0.009	1092 ± 12
	GRO001305	0.4	4.4	1.0	9.50	6.7×10^{-6}	0.711474 (006)	1.47	9.7 ± 1.3	-26.6 ± 0.7	0.863 ± 0.009	1185 ± 12
	GRO001306	0.6	6.3	0.8	14.15	7.0×10^{-6}	0.711197 (009)	1.44	9.8 ± 0.9	-26.6 ± 0.4	0.855 ± 0.009	1257 ± 13
	GRO001307	0.8	7.7	0.8	15.31	6.5×10^{-6}	0.711796 (005)	1.54	9.7 ± 1.0	-26.8 ± 0.5	0.827 ± 0.009	1522 ± 16
	GRO001308	0.9*	9.2	0.9	12.01	4.9×10^{-6}	0.705314 (007)	0.22	11.6 ± 0.5	-26.1 ± 0.3	0.518 ± 0.006	5289 ± 58
		1.0	9.5									
	Low Flow Average*						0.711684 (457)	1.53 ± 0.12	10.0 ± 0.3	-26.7 ± 0.1	0.852 ± 0.015	1292 ± 138

Table 2. ^{87}Sr/^{86}Sr and OC compositions of Mission SPM depth profiles. Averages are weighted by point sediment fluxes at each depth. *October flux-weighted averages exclude the deepest sample, as it contains bed material. TSS, velocity, and Q$_s$ values provided by Daniel Haught. For sediment δ^{13}C, if calculated uncertainties (1 s.d. of the mean of triplicate analyses) were less than instrumental uncertainty (0.3‰), instrumental uncertainties are shown; for all %OC values, calculated uncertainties were less than the instrumental uncertainty of 0.1%. Uncertainties for Fm represent propagated errors for standard normalization, instrumental fractionation, and blank correction.

| Fatty Acid	$\mu g / g$ OC	^{14}C Fm	^{14}C Age (years)
n-$C_{16:0}$	6639		
n-$C_{17:0}$	36		
n-$C_{18:0}$	309		
n-$C_{19:0}$	12		
n-$C_{20:0}$	115		
n-$C_{21:0}$	27		
n-$C_{22:0}$	244	0.877 ± 0.021	1059 ± 191
n-$C_{23:0}$	56		
n-$C_{24:0}$	308	0.717 ± 0.012	2676 ± 134
n-$C_{25:0}$	45		
n-$C_{26:0}$	185	0.723 ± 0.019	2608 ± 214
n-$C_{27:0}$	31		
n-$C_{28:0}$	154	0.547 ± 0.014	4841 ± 203
n-$C_{29:0}$	22		
n-$C_{30:0}$	90	0.407 ± 0.013	7230 ± 252
n-$C_{31:0}$	9		
n-$C_{32:0}$	34	0.367 ± 0.021	8055 ± 461
n-$C_{33:0}$	3		
n-$C_{34:0}$	8		
n-C_{24-32} (even) weighted mean		0.63 ± 0.12	3700 ± 1600

Table 3. Fraser at Hope (49.381°N, -121.451°E; IGSN GRO001063) flood sediment (<63 μm; collected Oct. 24th, 2010) fatty acid concentrations and ^{14}C composition. Radiocarbon uncertainties represent propagated errors for standard normalization, instrumental fractionation, and blank correction.
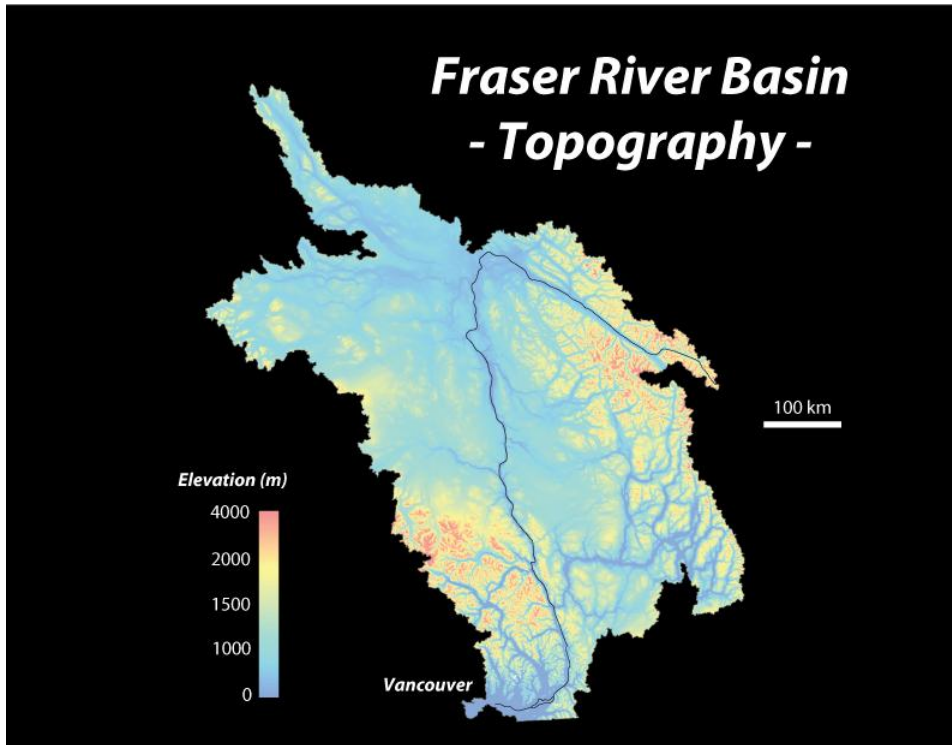
Figure 1. A topographic map of the Fraser basin highlights two main physiographic features: the

Rocky Mountains in the northeast, through which the upper portion of the river flows, and the

Coast Range in the southwest, through which the Fraser carves its outlet to the Pacific Ocean.

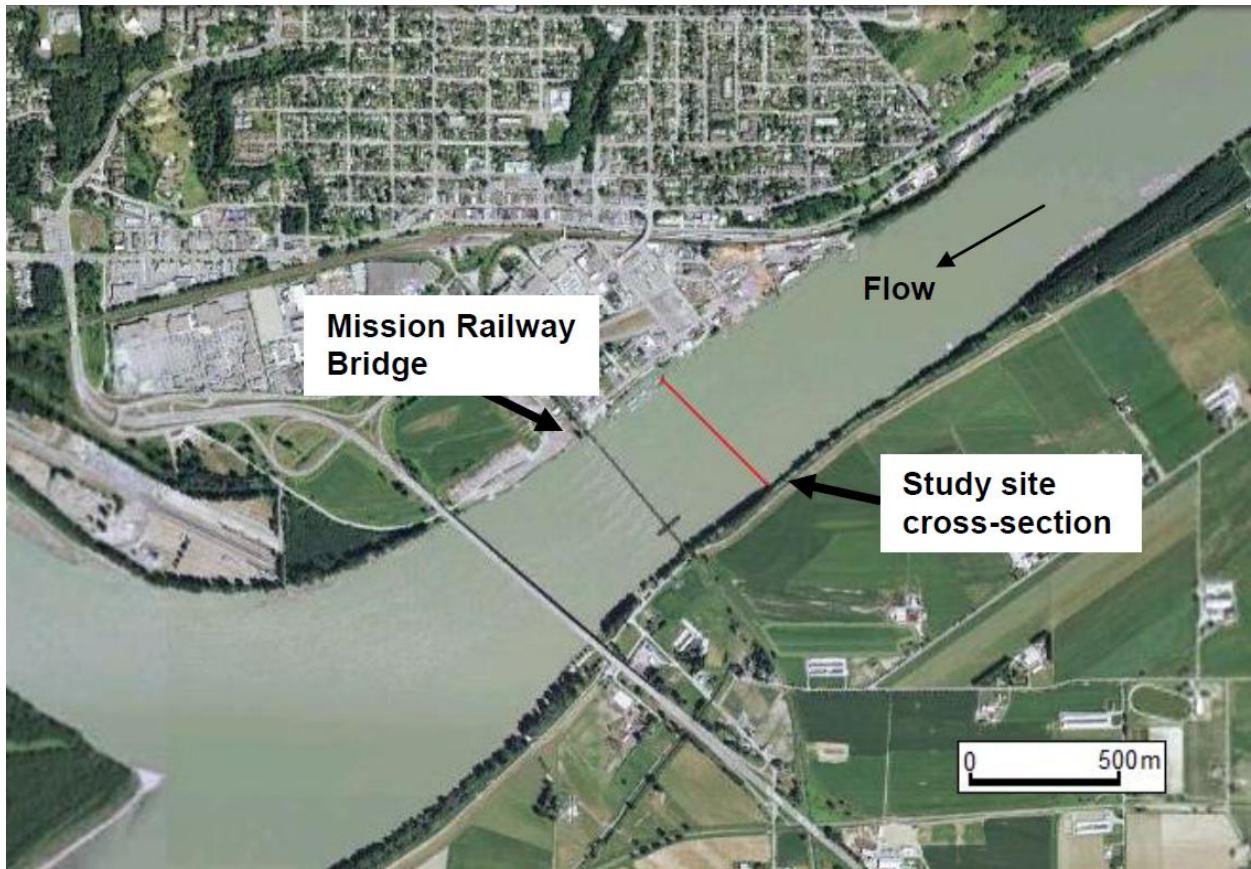Map provided by Adam Soule (WHOI).

Figure 2. Aerial view of the sampling location of suspended sediment depth profiles at Mission (49.1256°N, 122.2975°W). Samples presented in this study were collected in the center of the river channel along the transect indicated by the red line. Image from Attard (2012).
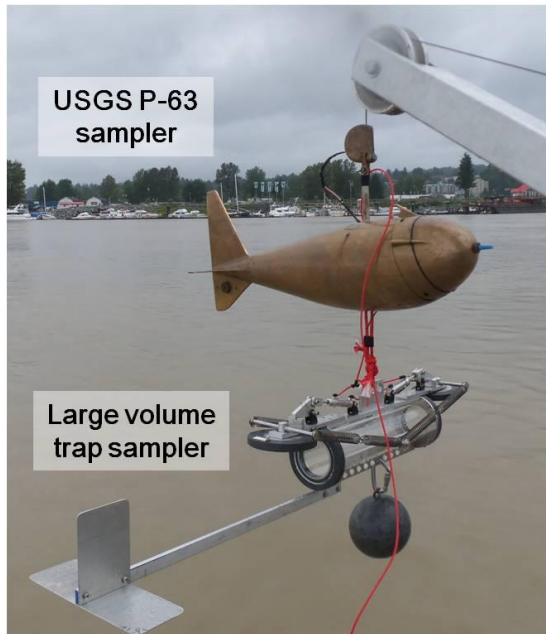
Figure 3. Configuration of water samplers for collecting 5-10 L samples ("trap" sampler) for geochemical analyses simultaneously with ~1 L samples (P-63 sampler) for sediment concentration and grain size measurements.
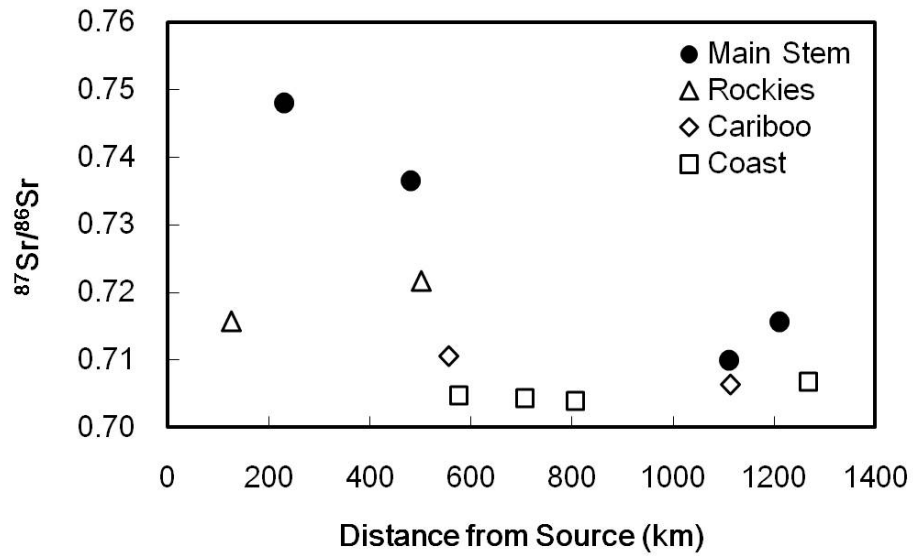
Figure 4. Radiogenic Sr isotope compositions of flood sediments reflect the bedrock geology of the Fraser basin, with old Rocky Mountain lithologies generating high $^{87}Sr/^{86}Sr$ values in the headwaters and young Coast Range lithologies the low $^{87}Sr/^{86}Sr$ values of downstream tributaries.
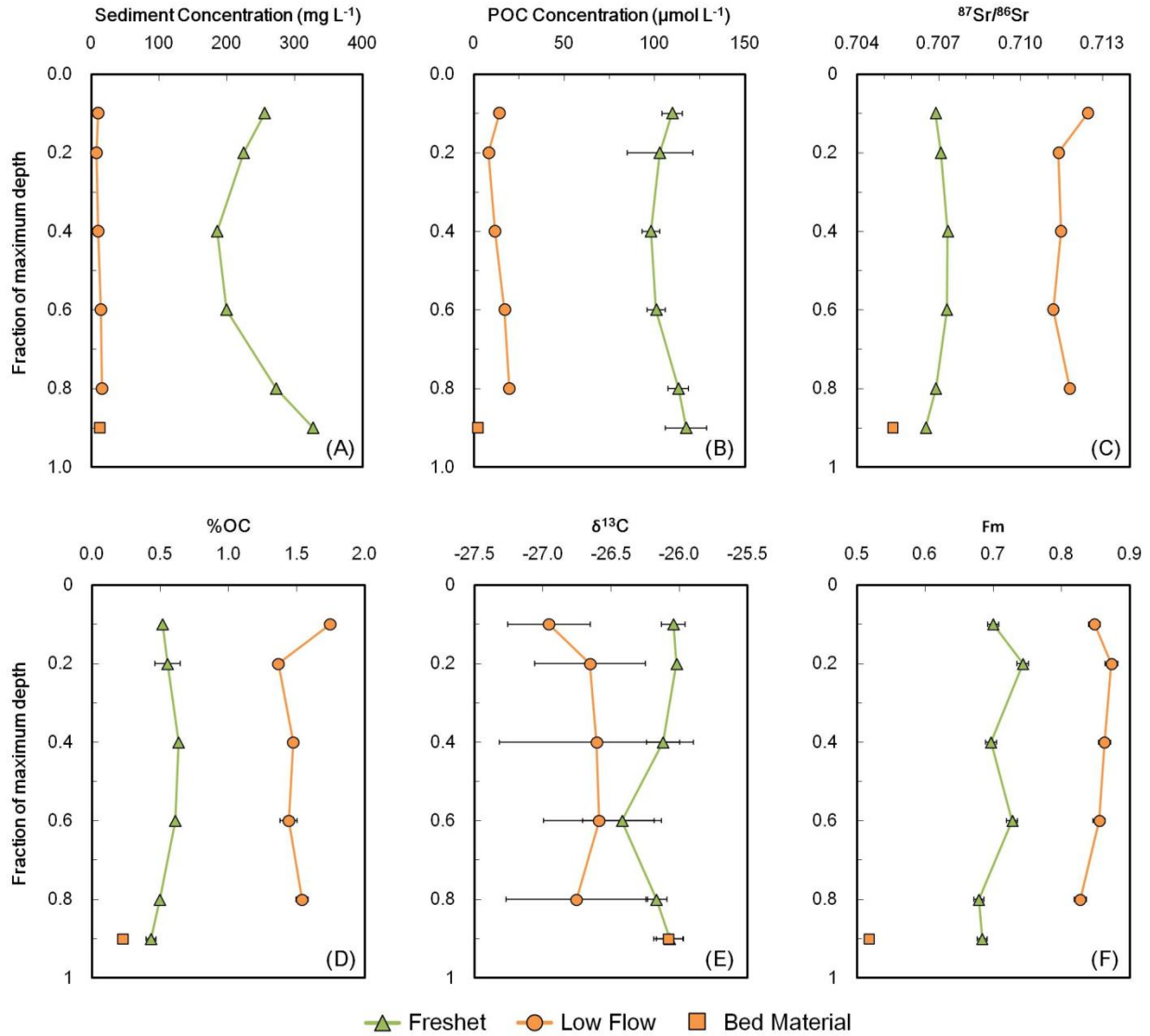
Figure 5. Depth profiles of (A) SPM concentrations, (B) particulate organic carbon (POC) concentrations, (C) Sr isotope composition, (D) total OC content of SPM, (E) bulk stable isotope composition of OC, and (F) bulk ^{14}C fraction modern (Fm) composition of SPM during freshet and low flow conditions in 2013. Samples labeled "bed material" (squares) represent a mixture of suspended material and bed material collected in October 2013 (low flow). Error bars represent ±1 s.d. of the mean of triplicate measurements; analytical uncertainties in ^{87}Sr/^{86}Sr are smaller than the symbols.
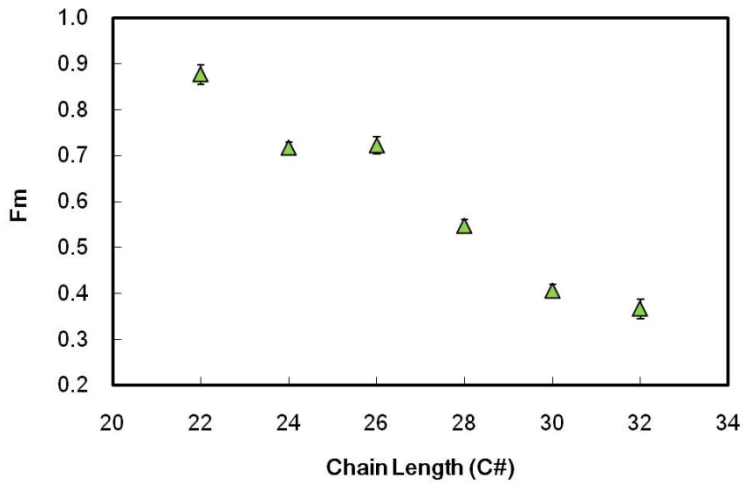
Figure 6. Radiocarbon composition of individual long-chain fatty acids exhibit a characteristic decreasing fraction modern (Fm) with increasing chain length. Error bars (representing propagated errors for standard normalization, instrumental fractionation, and blank correction) are approximately the size of the symbols.
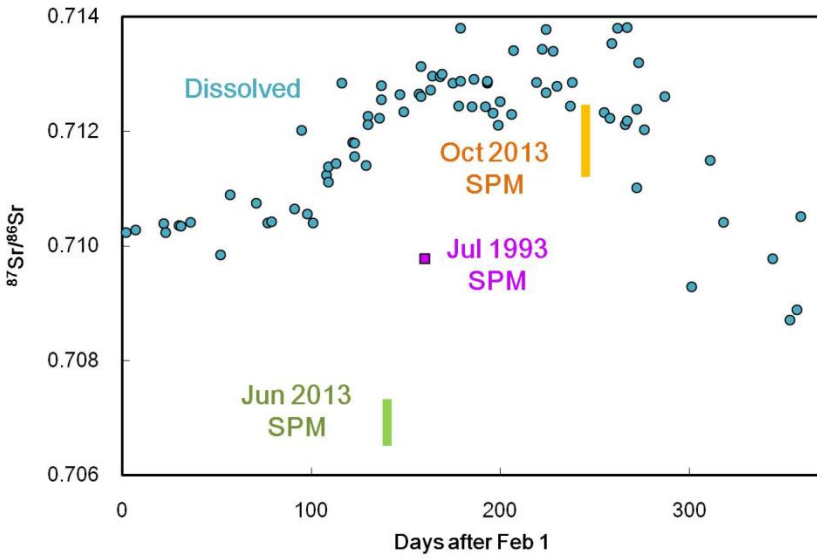
Figure 7. Sediment ^{87}Sr/^{86}Sr compositions from freshet (Jun) and low flow (Oct) conditions collected in 2013 (represented as the full range of values for all depths) bracket a single surface SPM value from July 1993 reported by Cameron and Hattori (1997) for the Fraser main stem at Hope. Blue circles represent the 2-year record of dissolved ^{87}Sr/^{86}Sr values for the Fraser River at Fort Langley reported by Voss et al. (2014).
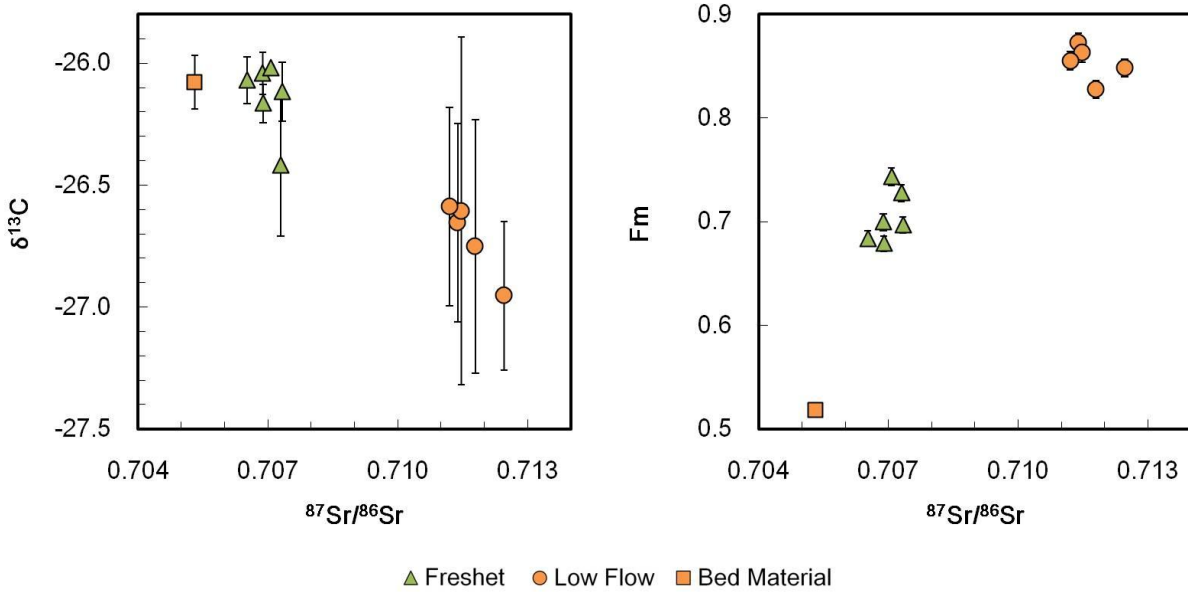
Figure 8. The bulk C isotope composition of Fraser River SPM is coupled to sediment sources, represented by ^{87}Sr/^{86}Sr. Error bars for δ^{13}C data indicate 1 s.d. of the mean of triplicate measurements, and those for ^{14}C Fm represent propagated errors for standard normalization, instrumental fractionation, and blank correction; analytical error for Fm and ^{87}Sr/^{86}Sr values are smaller than the symbols.
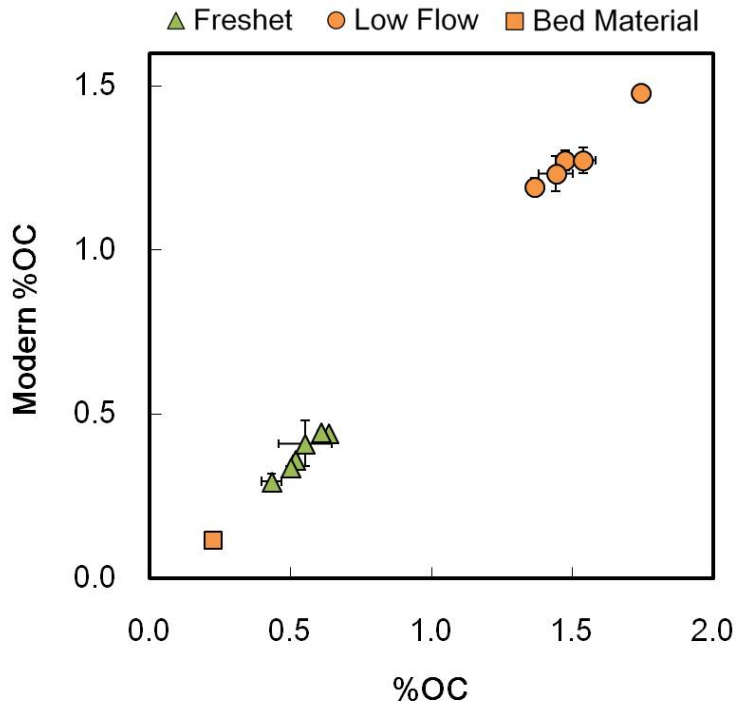
Figure 9. The mixing curve between an OC-poor, aged end-member and OC-enriched, relatively young end-member estimates an average terrestrial residence time for biospheric OC of 650 years and a petrogenic OC contribution of 0.12%.
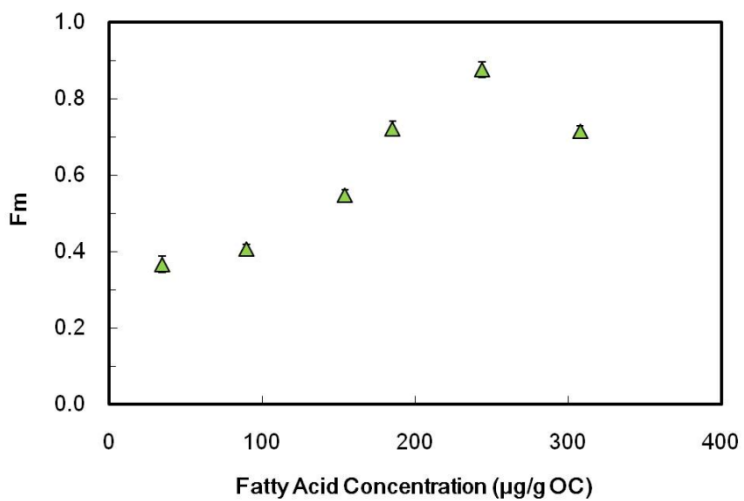
Figure 10. The ages of long-chain fatty acids approach a constant value with decreasing abundance.

References

Attard M. E. (2012) Evaluation of aDcps for suspended sediment transport monitoring, Fraser River, British Columbia, Simon Fraser University.

Blair N. E., Leithold E. L., and Aller R. C. (2004) From bedrock to burial: the evolution of particulate organic carbon across coupled watershed-continental margin systems. *Mar. Chem* **92**, 141-156. doi:10.1016/j.marchem.2004.06.023.

Bouchez J., Gaillardet J., France-Lanord C., Maurice L., and Dutra-Maia P. (2011a) Grain size control of river suspended sediment geochemistry: Clues from Amazon River depth profiles. *Geochem., Geophys., Geosyst.* **12**. doi:10.1029/2010gc003380.

Bouchez J., Galy V., Hilton R. G., Gaillardet J., Moreira-Turcq P., Pérez M. A., France-Lanord C., and Maurice L. (2014) Source, transport and fluxes of Amazon River particulate organic carbon: Insights from river sediment depth-profiles. *Geochim. Cosmochim. Acta* **133**, 280-298. doi:10.1016/j.gca.2014.02.032.

Bouchez J., Lupker M., Gaillardet J., France-Lanord C., and Maurice L. (2011b) How important is it to integrate riverine suspended sediment chemical composition with depth? Clues from Amazon River depth-profiles. *Geochim. Cosmochim. Acta* **75**, 6955-6970. doi:10.1016/j.gca.2011.08.038.

Burdige D. J. (2007) Preservation of organic matter in marine sediments: Controls, mechanisms, and an imbalance in sediment organic carbon budgets? *Chem. Rev.* **107**, 467-485.

Cameron E. M. and Hattori K. (1997) Strontium and neodymium isotope ratios in the Fraser River: a riverine transect across the Cordilleran orogen. *Chem. Geol.* **137**, 243-253.

Chung C.-H., You C.-F., and Chu H.-Y. (2009) Weathering sources in the Gaoping (Kaoping) river catchments, southwestern Taiwan: Insights from major elements, Sr isotopes, and rare earth elements. *J. Mar. Syst.* **76**, 433-443. doi:10.1016/j.jmarsys.2007.09.013.

Collister J. W., Rieley G., Stern B., Eglinton G., and Fry B. (1994) Compound-specific δ^{13}C analyses of leaf lipids from plants with differing carbon dioxide metabolisms. *Org. Geochem.* **21**, 619-627.

Deines P. (1980) The isotopic composition of reduced organic carbon. In *Handbook of Environmental Isotope Geochemistry* (eds. P. Fritz and J. C. Fontes). Elsevier. 329-406.

Drenzek N. J., Montluçon D. B., Yunker M. B., Macdonald R. W., and Eglinton T. I. (2007) Constraints on the origin of sedimentary organic carbon in the Beaufort Sea from coupled molecular ^{13}C and ^{14}C measurements. *Mar. Chem* **103**, 146-162. doi:10.1016/j.marchem.2006.06.017.

Eglinton G. and Hamilton R. J. (1967) Leaf epicuticular waxes. *Science* **156**, 1322-1335.

Eglinton G., Hunneman D. H., and Douraghi-Zadeh K. (1968) Gas chromatographic—mass spectrometric studies of long chain hydroxy acids—II: The hydroxy acids and fatty acids of a 5000-year-old lacustrine sediment. *Tetrahedron* **24**, 5929-5941.

Eglinton T. I., Aluwihare L. I., Bauer J. E., Druffel E. R. M., and McNichol A. P. (1996) Gas chromatographic isolation of individual compounds from complex matrices for radiocarbon dating. *Anal. Chem.* **68**, 904-912.

Feng X., Vonk J. E., van Dongen B. E., Gustafsson O., Semiletov I. P., Dudarev O. V., Wang Z., Montlucon D. B., Wacker L., and Eglinton T. I. (2013) Differential mobilization of terrestrial carbon pools in Eurasian Arctic river basins. *Proc. Natl. Acad. Sci.* **110**, 14168-14173. doi:10.1073/pnas.1307031110.

Galy V., Beyssac O., France-Lanord C., and Eglinton T. (2008a) Recycling of graphite during Himalayan erosion: A geological stabilization of carbon in the crust. *Science* **322**, 943-945. doi:10.1126/science.1161408.

Galy V. and Eglinton T. (2011) Protracted storage of biospheric carbon in the Ganges–Brahmaputra basin. *Nat. Geosci.* **4**, 843-847. doi:10.1038/ngeo1293.

Galy V., France-Lanord C., and Lartiges B. (2008b) Loading and fate of particulate organic carbon from the Himalaya to the Ganga–Brahmaputra delta. *Geochim. Cosmochim. Acta* **72**, 1767-1787. doi:10.1016/j.gca.2008.01.027.

Galy V., François L., France-Lanord C., Faure P., Kudrass H., Palhol F., and Singh S. K. (2008c) C_4 plants decline in the Himalayan basin since the Last Glacial Maximum. *Quat. Sci. Rev.* **27**, 1396-1409. doi:10.1016/j.quascirev.2008.04.005.

Goñi M. A., Teixeira M. J., and Perkey D. W. (2003) Sources and distribution of organic matter in a river-dominated estuary (Winyah Bay, SC, USA). *Estuarine, Coastal Shelf Sci.* **57**, 1023-1048. doi:10.1016/s0272-7714(03)00008-8.

Gustafsson Ö., van Dongen B. E., Vonk J. E., Dudarev O. V., and Semiletov I. P. (2011) Widespread release of old carbon across the Siberian Arctic echoed by its large rivers. *Biogeosciences* **8**, 1737-1743. doi:10.5194/bg-8-1737-2011.

Hedges J. I. and Mann D. C. (1979) The lignin geochemistry of marine sediments from the southern Washington coast. *Geochim. Cosmochim. Acta* **43**, 1809-1818.

Hilton R. G., Galy A., Hovius N., Horng M. J., and Chen H. (2010) Efficient transport of fossil organic carbon to the ocean by steep mountain rivers: An orogenic carbon sequestration mechanism. *Geology* **39**, 71-74. doi:10.1130/g31352.1.

Hilton R. G., Galy A., Hovius N., Kao S.-J., Horng M.-J., and Chen H. (2012) Climatic and geomorphic controls on the erosion of terrestrial biomass from subtropical mountain forest. *Global Biogeochem. Cycles* **26**. doi:10.1029/2012gb004314.

Hovius N., Galy A., Hilton R. G., Sparkes R., Smith J., Shuh-Ji K., Hongey C., In-Tian L., and West A. J. (2011) Erosion-driven drawdown of atmospheric carbon dioxide: The organic pathway. *Appl. Geochem.* **26**, S285-S287. doi:10.1016/j.apgeochem.2011.03.082.

Huh Y., Birck J.-L., and Allègre C. J. (2004) Osmium isotope geochemistry in the Mackenzie River basin. *Earth Planet. Sci. Lett.* **222**, 115-129. doi:10.1016/j.epsl.2004.02.026.

Kao S. J., Hilton R. G., Selvaraj K., Dai M., Zehetner F., Huang J. C., Hsu S. C., Sparkes R., Liu J. T., Lee T. Y., Yang J. Y. T., Galy A., Xu X., and Hovius N. (2014) Preservation of terrestrial organic carbon in marine sediments offshore Taiwan: mountain building and atmospheric carbon dioxide sequestration. *Earth Surf. Dyn.* **2**, 127-139. doi:10.5194/esurf-2-127-2014.

Leithold E. L., Blair N. E., and Perkey D. W. (2006) Geomorphologic controls on the age of particulate organic carbon from small mountainous and upland rivers. *Global Biogeochem. Cycles* **20**. doi:10.1029/2005gb002677.

Longworth B. E., Petsch S. T., Raymond P. A., and Bauer J. E. (2007) Linking lithology and land use to sources of dissolved and particulate organic matter in headwaters of a temperate, passive-margin river system. *Geochim. Cosmochim. Acta* **71**, 4233-4250. doi:10.1016/j.gca.2007.06.056.

Lupker M., France-Lanord C., Galy V., Lavé J., Gaillardet J., Gajurel A. P., Guilmette C., Rahman M., Singh S. K., and Sinha R. (2012) Predominant floodplain over mountain weathering of Himalayan sediments (Ganga basin). *Geochim. Cosmochim. Acta* **84**, 410-432. doi:10.1016/j.gca.2012.02.001.

Lupker M., France-Lanord C., Lavé J., Bouchez J., Galy V., Métivier F., Gaillardet J., Lartiges B., and Mugnier J.-L. (2011) A Rouse-based method to integrate the chemical composition of river sediments: Application to the Ganga basin. *J. Geophys. Res.* **116**. doi:10.1029/2010jf001947.

Matsumoto K., Kawamura K., Uchida M., and Shibata Y. (2007) Radiocarbon content and stable carbon isotopic ratios of individual fatty acids in subsurface soil: Implication for selective microbial degradation and modification of soil organic matter. *Geochem. J.* **41**, 483-492.

Medeiros P. M. and Simoneit B. R. T. (2008) Multi-biomarker characterization of sedimentary organic carbon in small rivers draining the Northwestern United States. *Org. Geochem.* **39**, 52-74. doi:10.1016/j.orggeochem.2007.10.001.

Ohkouchi N., Eglinton T. I., and Hayes J. M. (2003) Radiocarbon dating of individual fatty acids as a tool for refining Antarctic margin sediment chronologies. *Radiocarbon* **45**, 17-24.

Padoan M., Garzanti E., Harlavan Y., and Villa I. M. (2011) Tracing Nile sediment sources by Sr and Nd isotope signatures (Uganda, Ethiopia, Sudan). *Geochim. Cosmochim. Acta* **75**, 3627-3644. doi:10.1016/j.gca.2011.03.042.

Peucker-Ehrenbrink B., Miller M. W., Arsouze T., and Jeandel C. (2010) Continental bedrock and riverine fluxes of strontium and neodymium isotopes to the oceans. *Geochem., Geophys., Geosyst.* **11**. doi:10.1029/2009gc002869.

Pojar J., Klinka K., and Meidinger D. V. (1987) Biogeoclimatic ecosystem classification in British Columbia. *For. Ecol. Manage.* **22**, 119-154.

Rosenheim B. E. and Galy V. (2012) Direct measurement of riverine particulate organic carbon age structure. *Geophys. Res. Lett.* **39**. doi:10.1029/2012gl052883.

Rosenheim B. E., Roe K. M., Roberts B. J., Kolker A. S., Allison M. A., and Johannesson K. H. (2013) River discharge influences on particulate organic carbon age structure in the Mississippi/Atchafalaya River System. *Global Biogeochem. Cycles* **27**, 154-166. doi:10.1002/gbc.20018.

Saliot A., Parrish C. C., Sadouni N. m., Bouloubassi I., Fillaux J., and Cauwet G. (2002) Transport and fate of Danube Delta terrestrial organic matter in the Northwest Black Sea mixing zone. *Mar. Chem* **79**, 243-259.

Santos G. M., Southon J. R., Drenzek N. J., Ziolkowski L. A., Druffel E., Xu X., Zhang D., Trumbore S., Eglinton T. I., and Hughen K. A. (2010) Blank assessment for ultra-small radiocarbon samples: chemical extraction and separation versus AMS. *Radiocarbon* **52**, 1322-1335.

Schnitzer M. and Neyroud J. A. (1975) Alkanes and fatty acids in humic substances. *Fuel* **54**, 17-19.

Smittenberg R. H., Eglinton T. I., Schouten S., and Damsté J. S. S. (2006) Ongoing buildup of refractory organic carbon in boreal soils during the Holocene. *Science* **314**, 1283-1286. doi:10.1126/science.1129376.

Stuiver M. and Polach H. R. (1977) Reporting of ^{14}C data. *Radiocarbon* **19**, 355-363.

Volkman J. K., Barrett S. M., Blackburn S. I., Mansour M. P., Sikes E. L., and Gelin F. (1998) Microalgal biomarkers: A review of recent research developments. *Org. Geochem.* **29**, 1163-1179.

Vonk J. E., Sánchez-García L., Semiletov I., Dudarev O., Eglinton T., Andersson A., and Gustafsson Ö. (2010) Molecular and radiocarbon constraints on sources and degradation of terrestrial organic carbon along the Kolyma paleoriver transect, East Siberian Sea. *Biogeosciences* **7**, 3153-3166. doi:10.5194/bg-7-3153-2010.

Voss B. M., Peucker-Ehrenbrink B., Eglinton T. I., Fiske G., Wang Z. A., Hoering K. A., Montluçon D. B., LeCroy C., Pal S., Marsh S., Gillies S. L., Janmaat A., Bennett M., Downey B., Fanslau J., Fraser H., Macklam-Harron G., Martinec M., and Wiebe B. (2014) Tracing river chemistry in space and time: Dissolved inorganic constituents of the Fraser River, Canada. *Geochim. Cosmochim. Acta* **124**, 283-308. doi:10.1016/j.gca.2013.09.006.

CHAPTER 6. CONCLUSIONS

As described in Chapter 1, the Fraser River is a unique research setting because of its intrinsic geologic and climatic diversity, as well as its relatively limited anthropogenic disturbance, particularly when compared to other large mid-latitude river basins (e.g. Mississippi, Rhine, Columbia, St. Lawrence, Danube, and Colorado rivers). Exploiting these attributes, we have been able to reveal how different pools of carbon respond to spatial differences in climate and lithology and seasonal changes in discharge and temperature under primarily natural conditions. In Chapter 2, we examined the seasonal dynamics of a suite of dissolved inorganic runoff tracers to elucidate the response of chemical weathering to hydrological changes in the basin. This study utilized data from tributaries and main stem sites around the basin at different flow conditions together with a two-year time series record near the river mouth to assess the relative contributions of different source areas to basin-integrated fluxes. New estimates of discharge-weighted average concentrations of dissolved nutrients and major and trace elements, and runoff tracers (δD, ^{87}Sr/^{86}Sr) were determined, which in many cases were significantly different from values published in popular global compilations (Durum et al., 1960; Livingstone, 1963; Berner and Berner, 1996; Meybeck and Ragu, 2012). Changes in the δD composition of water reflected the shift towards snowmelt-derived runoff during the spring freshet versus precipitation- and groundwater-fed runoff during baseflow conditions. Dissolved major ion composition (Ca/Na, Mg/Na) revealed that different tributary basins span a wide range of silicate- versus carbonate-dominated chemical weathering domains. The seasonal trends in these values showed that the seasonally changing water sources are also associated with a shift in the balance of carbonate versus silicate weathering influence, with greater carbonate weathering influence in spring and summer relative to fall and winter. A consistent, large seasonal change in dissolved ^{87}Sr/^{86}Sr ratios (0.709-0.714) demonstrates that specific portions of the drainage basin contribute varying proportions of total dissolved weathering products throughout the year. These observations reveal that (1) dissolved fluxes from chemical weathering, and its associated CO_2 consumption, vary throughout the year as the volume and spatial distribution of discharge respond to seasonal changes in temperature and precipitation; and (2) basin-average values of weathering tracers such as δD and ^{87}Sr/^{86}Sr must account for flow-weighted seasonal variability. In light of previously published values of ^{87}Sr/^{86}Sr for the

Fraser (Wadleigh et al., 1980; Cameron and Hattori, 1997; Allègre et al., 2010), neglecting to account for such variability on regional and global scales has the potential to significantly bias estimates of world average values and the interpretations drawn from them. The capacity of the Fraser River Sr isotope composition to change significantly based simply on the amount of discharge derived from different regions within the basin calls into question the assumption of a constant global continental runoff value through time. This assumption is the foundation for interpretations of the long-term rise in marine $^{87}Sr/^{86}Sr$ ratios as an indication of increasing continental weathering, and hence increased atmospheric CO_2 drawdown and global cooling (e.g. Hodell et al., 1990; Raymo and Ruddiman, 1992). Our results for the Fraser River highlight the strong dependence of the value of this runoff tracer on the distribution of different lithologies undergoing chemical weathering.

Chapter 3 investigates the seasonal and spatial patterns of carbon export in the Fraser basin, examining interactions between various pools of carbon and the association of mineral particles with organic carbon. Certain portions of the basin were found to dominate DOC and POC sources to the main stem, and the differences in DOC and POC concentrations between seasons at most sites were proportionally much greater than for concentrations of DIC. The influence of carbonate weathering on the dissolved load of certain headwater basins was exploited to estimate the amount of carbonate- versus non-carbonate-derived DIC. Non-carbonate-derived DIC was found to dominate the DIC load of nearly all tributaries, resulting in DIC exported at the river mouth that is >80% non-carbonate-derived throughout the year. As the proportion of non-carbonate DIC correlates with DOC concentration, it is hypothesized that the main source of non-carbonate DIC is DOC respiration. Since the DIC in tributaries (sampled just upstream of their confluence with the main stem of the Fraser) is already predominantly non-carbonate-derived, it appears that the majority of this respiration occurs in relatively small streams or even in soil water, before the material reaches the larger channels. Interaction between DOC and DIC is also indicated by lower ^{14}C content of both DIC and DOC in tributaries influenced by carbonate weathering. Seasonal changes in POC composition are attributed to the mobilization of different fractions of soils and bank sediments under different flow conditions, as well as autotrophic production in some tributaries during low discharge. Bulk ^{14}C contents of sediments show that POC in sediments with higher specific surface area is consistently modern

(Fm >0.7), suggesting that this portion of the sedimentary load is the most important for burial of recently fixed terrestrial OC in the ocean.

In Chapter 4, daily samples near the Fraser River mouth collected during the early portion of the spring freshet demonstrate the extremely rapid rise in DOC concentration that occurs as soon as runoff across the basin beings to increase. Such a freshet DOC pulse has been extensively documented in Arctic rivers (e.g. Cooper et al., 2008; Spencer et al., 2008; Mann et al., 2012), but not in a large temperate river such as the Fraser. The fact that such a major portion of the total DOC flux escapes respiration within the basin during this period suggests that the input of DOC to streams during the spring freshet exceeds the aquatic microbial community's capacity to fully metabolize this pulse, or that high turbidity inhibits photochemical degradation. The freshet pulse of DOC is also associated with a shift toward higher molecular weight, more aromatic DOC composition, as indicated by DOC optical properties (Helms et al., 2008), which may also influence its potential for photochemical degradation (Stubbins et al., 2010). The seasonal cycle of DOC optical properties also shifts in the fall, although DOC concentrations are relatively stable. If DOC lability is linked to its chemical structure, as has been demonstrated in Arctic rivers (Spencer et al., 2008; Mann et al., 2012), then DOC released during fall rain events is likely also relatively labile.

The final chapter focuses on depth-specific samples of suspended sediments near the Fraser River mouth. These depth profiles, collected at peak freshet discharge and fall low discharge, reveal significant changes in sediment composition between these extreme hydrologic conditions. The sediment $^{87}Sr/^{86}Sr$ composition, serving as a tracer of spatial provenance, shows a magnitude of variability between these two time points (0.707-0.712) comparable to that of the full range of the two-year dissolved $^{87}Sr/^{86}Sr$ time series record. The ^{14}C content of suspended sediments is much greater in the relatively OC-rich low flow sediments compared to the freshet sediments. Using the approach of Galy et al. (2008), we predict a ^{14}C-dead petrogenic OC contribution of 0.12% of total sediment weight and an average terrestrial residence time for non-petrogenic OC of 650 years. However, "non-petrogenic" OC is likely composed of a very heterogeneous mixture of fully modern to highly aged (1000s of years) OC. The old ^{14}C ages of vascular plant wax biomarkers in the Fraser basin (1000-8000 years) support the existence of a very old biospheric OC component, as proposed by Smittenberg et al. (2006) based on a nearby sediment deposit in Saanich Inlet. The large range in biomarker ages indicates that even at the

molecular level, OC is derived from material exhibiting a spectrum of ages. This has important implications for sedimentary archives, which might be probed for information about past climate conditions in the Fraser River basin, as the distinct sources of biospheric OC may be difficult to disentangle.

The results of this work will be applicable to future investigations of sedimentary archives in the Pacific Northwest region of North America, for which other large modern river systems (specifically the Columbia River) do not provide information relevant to pre-industrial conditions. The significant seasonal variations in the quantity, composition and provenance of dissolved and suspended material, organic and inorganic, serves as a caution against overly simplistic interpretations of material delivered to the ocean by rivers in general. These findings help to set a framework for acquiring a comprehensive understanding of such river systems. First, multiple samples across a seasonal cycle are required in order to quantify discharge-weighted average fluxes and concentrations for large-scale assessments; second, heterogeneity in source materials within a basin gives rise to the potential for changes in basin-integrated geochemical composition that are not due purely to general changes in climate and/or weathering intensity. Therefore, terrestrially-influenced sedimentary archives must account for the possibility that the relative contributions from distinct portions of the basin may alter the basin-integrated composition of sediments through non-climatic mechanisms such as changes in basin morphology (e.g. through erosion, landslides, or stream capture) or exposure of previously buried lithologies.

Apportionment of the primary sources of DIC, DOC, and POC among fixation by land plants or aquatic algae, transformation by heterotrophic microbes and fungi, and weathering of carbonate and silicate minerals is critical to assessing the role of large rivers to regional carbon balances and global atmospheric CO_2 exchange. In this work, we estimated that, in the Fraser River, fluxes of carbon originating from terrestrial autotrophic production total ~14.6×10^{10} mol C a^{-1}, of which ~73% is in the form of DIC, ~19% is DOC, and ~8% is POC. Assuming that at least a portion of this carbon is transferred to a sedimentary deposit and buried before being completely metabolized to CO_2, on the time scales of this burial process (presumably decades to millennia, depending on the rate of sediment accumulation and the pH and oxidative status of the deposition site, which determine whether mineral carbonate is able to accumulate and the amount of time required to isolate the carbon from biological oxidation), the Fraser River itself is a net

sink of atmospheric CO_2. The magnitude of the sink depends on the proportion of this carbon retained in sediment deposits or the ocean interior over the timescale of interest. The portion of the Fraser River carbon flux most amenable to tracking is that already in sedimentary form, which must simply escape biological oxidation in floodplain, deltaic, or marine sediments. Typical terrestrial OC burial efficiencies for continental margin sediments overlain by oxygenated waters (such as the Strait of Georgia into which the Fraser River flows) are ~1-40% (Burdige, 2007; Blair and Aller, 2012). Using a median estimate of 20% burial efficiency, we can estimate that ~0.2×10^{10} mol C a^{-1} of Fraser River POC is effectively buried in nearshore sediment deposits. The fate of terrestrial DOC in the marine environment is a subject of considerable debate. Assuming that negligible amounts of DOC are aggregated and/or adsorbed to particles dense enough to sink and accumulate in sediments, the only method for long-term preservation of terrestrial DOC in the ocean is to escape microbial degradation and photooxidation. Photochemical oxidation is typically a significant sink of terrestrial DOC in marine waters, as lower turbidity exposes DOC to higher levels of irradiation than in rivers, and the highly aromatic structure of terrestrial DOC makes it inherently absorbant of radiation and hence susceptible to photodegradation. Given that terrestrial biochemical markers are scarcely detectable in pelagic marine DOC (e.g. Opsahl and Benner, 1997), it is unlikely that significant quantities of terrestrial DOC remain in the ocean for centuries or longer. However, this remains an open discussion, as the composition of terrestrial DOC may be considerably modified by *partial* biological and photochemical oxidation such that the portion remaining is not readily distinguishable as "terrestrial." However, in the absence of evidence supporting the persistence of terrestrial DOC in general or Fraser River DOC in particular in the marine environment, a reasonable conservative estimate is that it is completely mineralized within decades to centuries. The fate of DIC in the coastal ocean can only be discussed generally, as the minimal isotopic distinction between DIC of terrestrial and marine origin and the lack of distinctive structural features prevent tracking terrestrial DIC across the land-ocean transition. We must therefore assume that a similar proportion of terrestrially-derived DIC as marine-derived DIC is buried as sedimentary carbonate in the coastal ocean. Given that, in the global ocean, ~4×10^{12} mol C a^{-1} is converted into biogenic carbonate from a total reservoir of ~3.16×10^{18} mol C of DIC (i.e. ~0.000126%), and that preservation of carbonate in coastal marine sediments is typically ~25% of carbonate produced (Milliman, 1993), and given that bottom waters in the Strait of Georgia do

allow for the preservation of sedimentary carbonate (Guilbault et al., 2003), we may estimate that ~0.000126% of Fraser River DIC is converted to biogenic carbonate annually, of which ~25% of is buried in marine sediments. We therefore estimate that ~34×10^3 mol C a^{-1} of Fraser River DIC is buried for thousands of years or more in marine sediments. This is most likely a conservative estimate, as Fraser River DIC likely does not mix completely throughout the global ocean, but rather is converted to biogenic carbonate at a higher-than-global-average rate on account of generally higher calcareous plankton production in the coastal zone relative to the pelagic ocean. This burial flux of DIC is insignificant compared to the estimated burial flux of POC from the Fraser River. Therefore, the estimated burial flux of terrestrial productivity-derived carbon in the Fraser River (assumed to be dominated by POC) constitutes an atmospheric carbon sink of ~0.2×10^{10} mol C a^{-1} (or ~1.5% of the flux of carbon derived from terrestrial production from the Fraser River).

Future studies on the biogeochemistry of the Fraser River would benefit from more measurements of plant biomarker ^{14}C ages at multiple sites across the basin in order to constrain the ages of various components of the biospheric OC pool and determine whether pre-aged material is sourced equally throughout the basin. For instance, a combination of long-chain fatty acids and alkanes and lignin phenols would provide information about components of the biospheric OC pool with different turnover timescales (Feng et al., 2013). The δD composition of plant biomarkers may also be a valuable means of quantifying POC source contributions on account of the large range of precipitation δD across the basin.

Studies of DOC cycling and stream metabolism may provide further insight into the importance of DOC respiration to the DIC load of the Fraser River. A time series of microbial incubation and UV irradiation experiments of DOC could test the hypothesis that relatively labile DOC escapes degradation during the spring freshet. Detailed studies of DOC lability and composition in headwater catchments in different parts of the basin would elucidate the rate of DOC turnover from the point of mobilization into the aquatic system. Additional measurements of dissolved Hg, especially during times or at sites experiencing variable DOC and suspended sediment concentrations, would also greatly benefit the understanding of Hg cycling in the Fraser basin.

An intriguing comparison could be made between the estimate of biospheric OC residence time of 650 years (or the ages of various terrestrial biomarker compound classes) and

the sediment transport time within the basin using the abundance of cosmogenic ^{10}Be in sediments (Balco et al., 2008; Lupker et al., 2012; von Blanckenburg et al., 2012). Such an assessment would potentially allow a comparison to be made between basin transport patterns of mineral particles versus biospheric OC. With additional samples of suspended sediments from major tributaries (either through depth profile sampling or surface samples collected at varying flow conditions), modern OC-total OC plots would place constraints on biospheric OC ages in different portions of the basin (expanding on the basin-average estimate presented in Chapter 5). Cosmogenic ^{10}Be data for the mineral fraction of these sediments would provide an estimate of the surface exposure age (i.e. the time since the mineral has been within a given distance of the Earth surface) of sediments. Although not necessarily an exact reflection of the age since the mineral was first mobilized from its parent rock, the relative ages of sediments from across the basin would indicate relative transport times among subbasins. Caution in applying this method to the Fraser basin must be exercised given that post-glacial erosion may have stored sufficient volumes of sediment in some areas to temporarily halt accumulation of cosmogenic nuclides in buried sediments. This issue could be evaluated by analyzing sediments along a transect starting upstream of and continuing downstream of a major former sediment impoundment, such as across the outflow of Kamloops Lake in the Thompson River basin. If the approach is found to be robust (i.e. no significant change in exposure age across such features), and biospheric OC ages are found to be strongly correlated with mineral surface exposure ages, it could be inferred that biospheric OC transport is primarily controlled by sediment transport with minimal loss due to biological degradation or addition from non-sediment-associated material (e.g. vegetation detritus). Such processes could be further probed to understand subbasins which deviate from a basin-wide trend between biospheric OC age and sediment exposure age. If particular regions are identified to have exceptionally old biospheric OC ages relative to corresponding sediment exposure ages, this analysis may put important constraints on the spatial distribution of pre-aged biospheric OC within the Fraser basin.

Finally, a detailed investigation of variations in sediment ^{87}Sr/^{86}Sr with grain size and mineral fraction would significantly extend the work presented in this thesis. In addition to the areas of abundant carbonate bedrock lithologies in the Rocky Mountain portion of the Fraser River basin (e.g. Robson River drainage), carbonate minerals are likely present in a range of abundances throughout the basin, in some cases likely as disseminated grains within primarily

silicate lithologies. Though relatively low in abundance, such carbonates can exert a significant influence on the elemental and isotope composition of riverine dissolved material (on account of more rapid reaction kinetics of carbonate dissolution than dissolution of silicate minerals) and— if the carbonate mineral composition is distinct from that of the dominant silicate minerals—on that of river sediments (e.g. Jacobson and Blum, 2000). In order to quantify the importance of chemical weathering to the long-term drawdown of atmospheric CO_2 in the Fraser basin, accurate lithological end-member compositions must be established so that the geochemical signals presented here can be more quantitatively ascribed to carbonate versus silicate sources. This will allow for a better assessment of contemporary erosion and weathering fluxes, as well as past changes in sediment sources recorded in Fraser River-influenced floodplain or marine deposits. Likewise, a study of the grain size dependence of elemental and isotope compositions of Fraser River sediments will aide in the interpretation of the seasonal patterns observed in the $^{87}Sr/^{86}Sr$ composition of suspended sediment depth profiles by testing the hypothesis that the addition of coarse-grained material during the spring freshet causes the less radiogenic $^{87}Sr/^{86}Sr$ values. Furthermore, data on the mineralogical differences between various grain size fractions in Fraser River sediments will support a better understanding of the relationship between suspended sediments and riverbank material. The nature of this relationship has important practical implications for the potential to use abundant bank material as a proxy for suspended sediments, which are difficult to collect in large quantities.

References

Allègre C. J., Louvat P., Gaillardet J., Meynadier L., Rad S., and Capmas F. (2010) The fundamental role of island arc weathering in the oceanic Sr isotope budget. *Earth Planet. Sci. Lett.* **292**, 51-56. doi:10.1016/j.epsl.2010.01.019.

Balco G., Stone J. O., Lifton N. A., and Dunai T. J. (2008) A complete and easily accessible means of calculating surface exposure ages or erosion rates from [10]Be and [26]Al measurements. *Quat. Geochronol.* **3**, 174-195. doi:10.1016/j.quageo.2007.12.001.

Berner E. K. and Berner R. A. (1996) *Global Environment: Water, Air, and Geochemical Cycles.* Prentice Hall. 172-235.

Blair N. E. and Aller R. C. (2012) The fate of terrestrial organic carbon in the marine environment. *Annu. Rev. Mar. Sci.* **4**, 401-423. doi:10.1146/annurev-marine-120709-142717.

Burdige D. J. (2007) Preservation of organic matter in marine sediments: Controls, mechanisms, and an imbalance in sediment organic carbon budgets? *Chem. Rev.* **107**, 467-485.

Cameron E. M. and Hattori K. (1997) Strontium and neodymium isotope ratios in the Fraser River: a riverine transect across the Cordilleran orogen. *Chem. Geol.* **137**, 243-253.

Cooper L. W., McClelland J. W., Holmes R. M., Raymond P. A., Gibson J. J., Guay C. K., and Peterson B. J. (2008) Flow-weighted values of runoff tracers ($\delta^{18}O$, DOC, Ba, alkalinity) from the six largest Arctic rivers. *Geophys. Res. Lett.* **35**. doi:10.1029/2008gl035007.

Durum W. H., Heidel S. G., and Tison L. J. (1960) Worldwide run-off of dissolved solids. XII General Assembly of the International Union of Geodesy and Geophysics, 25 July - 9 August 1960, Helsinki. 618-628.

Feng X., Vonk J. E., van Dongen B. E., Gustafsson O., Semiletov I. P., Dudarev O. V., Wang Z., Montlucon D. B., Wacker L., and Eglinton T. I. (2013) Differential mobilization of terrestrial carbon pools in Eurasian Arctic river basins. *Proc. Natl. Acad. Sci.* **110**, 14168-14173. doi:10.1073/pnas.1307031110.

Galy V., Beyssac O., France-Lanord C., and Eglinton T. (2008) Recycling of graphite during Himalayan erosion: A geological stabilization of carbon in the crust. *Science* **322**, 943-945. doi:10.1126/science.1161408.

Guilbault J.-P., Barrie J. V., Conway K., Lapointe M., and Radi T. (2003) Paleoenvironments of the Strait of Georgia, British Columbia during the last deglaciation: microfaunal and microfloral evidence. *Quat. Sci. Rev.* **22**, 839-857. doi:10.1016/s0277-3791(02)00252-4.

Helms J. R., Stubbins A., Ritchie J. D., Minor E. C., Kieber D. J., and Mopper K. (2008) Absorption spectral slopes and slope ratios as indicators of molecular weight, source, and photobleaching of chromophoric dissolved organic matter. *Limnol. Oceanogr.* **53**, 955-969.

Hodell D. A., Mead G. A., and Mueller P. A. (1990) Variation in the strontium isotopic composition of seawater (8 Ma to present): Implications for chemical weathering rates and dissolved fluxes to the oceans. *Chem. Geol.* **80**, 291-307.

Jacobson A. D. and Blum J. D. (2000) Ca/Sr and $^{87}Sr/^{86}Sr$ geochemistry of disseminated calcite in Himalayan silicate rocks from Nanga Parbat. *Geology* **28**, 463-466.

Livingstone D. A. (1963) Chemical composition of rivers and lakes. (ed. M. Fleischer). *Data of Geochemistry*. 148 p.

Lupker M., Blard P.-H., Lavé J., France-Lanord C., Leanni L., Puchol N., Charreau J., and Bourlès D. (2012) [10]Be-derived Himalayan denudation rates and sediment budgets in the Ganga basin. *Earth Planet. Sci. Lett.* **333-334**, 146-156. doi:10.1016/j.epsl.2012.04.020.

Mann P. J., Davydova A., Zimov N., Spencer R. G. M., Davydov S., Bulygina E., Zimov S., and Holmes R. M. (2012) Controls on the composition and lability of dissolved organic matter in Siberia's Kolyma River basin. *J. Geophys. Res.* **117**. doi:10.1029/2011jg001798.

Meybeck M. and Ragu A. (2012) GEMS-GLORI world river discharge database. Université Pierre et Marie Curie, Paris. doi:10.1594/PANGAEA.804574.

Milliman J. D. (1993) Production and accumulation of calcium carbonate in the ocean: Budget of a nonsteady state. *Global Biogeochem. Cycles* **7**, 927-957.

Opsahl S. and Benner R. (1997) Distribution and cycling of terrigenous dissolved organic matter in the ocean. *Nature* **386**, 480-482.

Raymo M. E. and Ruddiman W. F. (1992) Tectonic forcing of late Cenozoic climate. *Nature* **359**, 117-122.

Smittenberg R. H., Eglinton T. I., Schouten S., and Damsté J. S. S. (2006) Ongoing buildup of refractory organic carbon in boreal soils during the Holocene. *Science* **314**, 1283-1286. doi:10.1126/science.1129376.

Spencer R. G. M., Aiken G. R., Wickland K. P., Striegl R. G., and Hernes P. J. (2008) Seasonal and spatial variability in dissolved organic matter quantity and composition from the Yukon River basin, Alaska. *Global Biogeochem. Cycles* **22**. doi:10.1029/2008gb003231.

Stubbins A., Spencer R. G. M., Chen H., Hatcher P. G., Mopper K., Hernes P. J., Mwamba V. L., Mangangu A. M., Wabakanghanzi J. N., and Six J. (2010) Illuminated darkness: Molecular signatures of Congo River dissolved organic matter and its photochemical alteration as revealed by ultrahigh precision mass spectrometry. *Limnol. Oceanogr.* **55**, 1467-1477. doi:10.4319/lo.2010.55.4.1467.

von Blanckenburg F., Bouchez J., and Wittmann H. (2012) Earth surface erosion and weathering from the ^{10}Be (meteoric)/^{9}Be ratio. *Earth Planet. Sci. Lett.* **351-352**, 295-305. doi:10.1016/j.epsl.2012.07.022.

Wadleigh M. A., Veizer J., and Brooks C. (1980) Strontium and its isotopes in Canadian rivers: Fluxes and global implications. *Geochim. Cosmochim. Acta* **49**, 1727-1736.